Transition endommagement-fissuration par une formulation eikonale pour les modèles d'endommagement avec et sans plasticité

Florian Marconi

▶ **To cite this version:**

Florian Marconi. Transition endommagement-fissuration par une formulation eikonale pour les modèles d'endommagement avec et sans plasticité. Mechanics of materials [physics.class-ph]. Université Paris-Saclay, 2022. English. NNT : 2022UPAST096 . tel-04194160

HAL Id: tel-04194160

https://theses.hal.science/tel-04194160v1

Submitted on 2 Sep 2023

HAL is a multi-disciplinary open access archive for the deposit and dissemination of scientific research documents, whether they are published or not. The documents may come from teaching and research institutions in France or abroad, or from public or private research centers.

L'archive ouverte pluridisciplinaire **HAL**, est destinée au dépôt et à la diffusion de documents scientifiques de niveau recherche, publiés ou non, émanant des établissements d'enseignement et de recherche français ou étrangers, des laboratoires publics ou privés.

université
PARIS-SACLAY

Damage-fracture transition by an Eikonal-based gradient-type formulation for damage (-plastic) models.

Transition endommagement-fissuration par une formulation eikonale pour les modèles d'endommagement avec et sans plasticité

Thèse de doctorat de l'université Paris-Saclay

École doctorale n°579 : sciences mécaniques et énergétiques, matériaux et géosciences (SMEMaG)
Spécialité de doctorat: Mécanique des matériaux
Graduate School : Sciences de l'ingénierie et des systèmes, Réferent : ENS Paris-Saclay

Thèse préparée dans l'unité de recherche Laboratoire de Mécanique Paris-Saclay (Université Paris-Saclay, CentraleSupélec, ENS Paris-Saclay, CNRS) et la Czech Tecnical University in Prague, sous la direction d'Emmanuel BARANGER, Chargé de Recherche CNRS (ENS Paris-Saclay), la co-direction de Rodrigue DESMORAT, Professeur des Universités (ENS-Paris-Saclay), et le co-encadrement de Milan JIRÁSEK, Professor, (CTU Prague).

Thèse soutenue à Paris-Saclay, le 11 juillet 2022, par

Florian MARCONI

Composition du jury

Gilles PIJAUDIER-CABOT Professeur, ISA BTP	Président
Frédéric DUFOUR Professeur, Grenoble INP	Rapporteur & Examinateur
Nicolas MOËS Professeur, École Centrale de Nantes	Rapporteur & Examinateur
Rodrigue DESMORAT Professeur, ENS Paris-Saclay	Examinateur
Emmanuel BARANGER Chargé de Recherche CNRS, ENS Paris-Saclay	Directeur de thèse

THESE DE DOCTORAT

NNT : 2022UPAST096

université PARIS-SACLAY

ÉCOLE DOCTORALE
Sciences mécaniques et énergétiques, matériaux et géosciences (SMEMAG)

Titre: Transition endommagement-fissuration par une formulation eikonale pour les modèles d'endommagement avec et sans plasticité

Mots clés: Endommagement, Plasticité, Localisation, Nonlocal, Eikonal, Régularisation

Résumé: Modéliser la ruine des matériaux nécessite d'être capable de prédire pour un chargement donné l'initiation et la possible propagation de fissures. En dehors de la mécanique linéaire de la rupture qui ne traite que des fissures existantes, ceci peut être réalisé en utilisant la mécanique continue de l'endommagement qui permet également de prendre en compte la perte de rigidité associée. Cependant, malgré leurs avantages ces modèles présentent un certain nombre de défauts, notamment en ce qui concerne la localisation des déformations. En effet, alors que les modèles d'endommagement locaux présentent une dépendance pathologique au maillage, les modèles non locaux développés pour résoudre ce problème ne parviennent pas à rendre une zone fortement endommagée équivalente à une fissure.

Une formation non locale basée sur une approche eikonale avec des interactions dépendantes de l'endommagement s'est avérée adaptée pour palier ces défauts, même si elle conserve les inconvénients inhérents aux approches intégrales. Après avoir proposé une définition de ce qu'on qualifiera ici de « bon » modèle d'endommagement, ce travail se concentre sur une nouvelle formulation de type gradient qui dérive de cette approche, et dont on peut espérer qu'elle résolve les problèmes associés aux modèles locaux et non locaux.

Cette thèse présente dans un premier temps l'implémentation non-intrusive dans Abaqus de la formulation associée à un modèle d'endommagement isotrope qui est utilisée pour étudier ses propriétés dans un cas unidirectionnel. Il est ainsi démontré que cette formulation a des propriétés similaires à celles d'une formulation basée sur les approches de type champs de phase, et que malgré un comportement plutôt fragile les deux formulations sont à même de gérer la transition endommagement-fissuration.

Elle traite ensuite de l'introduction de plasticité, i.e. de l'utilisation d'un modèle couplant endommagement et plasticité au lieu d'un modèle d'endommagement pur, et de la manière dont elle pourrait être utilisée pour résoudre le problème de la fragilité tout en conservant les propriétés de l'approche dite eikonale. Une étude unidimensionnelle se concentrant sur les réponses théoriques obtenues avec une zone de localisation fixe ou se rétrécissant est donc menée, et les résultats obtenus avec les deux modèles comparés. Les observations ainsi réalisées permettent de conclure que l'introduction de déformations permanentes réduirait la fragilité liée au rétrécissement de la zone de localisation et au déchargement associé.

Les deux formulations associées aux modèles d'endommagement avec et sans plasticité sont ensuite implémentées dans le code éléments finis OOFEM qui est utilisé pour confirmer ces observations dans le cas de la flexion trois points. On peut ainsi montrer que les deux formulations peuvent être utilisées pour modéliser la ruine d'une structure en fournissant des résultats indépendants du maillage où une zone fortement endommagée est bien équivalente à une fissure. De plus, alors que la réponse associée au modèle d'endommagement pur reste relativement fragile, ce problème est résolu par l'utilisation du modèle couplant endommagement et plasticité.

université PARIS-SACLAY

ÉCOLE DOCTORALE
Sciences mécaniques et énergétiques, matériaux et géosciences (SMEMAG)

Title: Damage-fracture transition by an Eikonal-based gradient-type formulation for damage (-plastic) models

Keywords: Damage, Plasticity, Localization, Nonlocal, Eikonal, Regularization

Abstract: To properly handle material failure, one needs to be able to predict, for a given loading, the possible initiation and propagation of cracks. Aside from the Linear Elastic Fracture Mechanics, which only deals with existing cracks, this can be achieved through continuum damage mechanics, which also accounts for the associated progressive loss of stiffness. However, despite their advantages, those models suffer from a certain number of deficiencies, especially when handling strain localization. As it is, while local damage models suffer from spurious mesh dependency, the nonlocal ones, which were developed to address this issue, fail to make a highly damaged zone equivalent to a crack.

A nonlocal Eikonal-based formulation with damage-dependent interactions has been shown to successfully address these issues, though it still suffers from the drawbacks inherent to integral-type formulations. After proposing a definition of what is called here a "good" damage model, this work focuses on a new gradient-type formulation that derives from this approach and can thus be expected to address the issues associated with both local and nonlocal models.

This work first presents the non-intrusive implementation in Abaqus of the formulation associated with an isotropic damage model, which is used to study its properties in a one-dimensional setting. This formulation is shown to have properties similar to those of a phase-field-based formulation, both successfully addressing the damage-fracture transition though they exhibit a rather brittle behaviour.

It then deals with the introduction of plasticity, i.e. using a damage-plastic model instead of a pure damage one, and how it could be used to address the brittleness issue while keeping the properties of the Eikonal-based approach. A one-dimensional study is thus conducted, focusing on the theoretical responses obtained with both models associated with either fixed or shrinking localization area. Based on its results, one can conclude that introducing permanent strains would reduce the brittleness linked to the shrinking of the localization area and the associated unloading.

Both damage and damage-plastic formulations are then implemented in the finite element code OOFEM, which is used to confirm these preliminary observations in a three-point-bending setting. It is then shown that both formulations can be used to model structural failure by providing mesh-independent results where a highly damaged zone is equivalent to a crack. Moreover, while the response associated with the pure damage model remains somewhat brittle, the issue is addressed by the damage-plastic one.

Contents

List of Figures

Remerciements

En préambule de cette thèse, je tiens à remercier toutes les personnes qui m'ont aidé et soutenu pendant ces années, et sans qui elle n'aurait pas été possible.

Je tiens tout d'abord à remercier les membres de mon jury d'avoir accepté d'évaluer mon travail. Je remercie en particulier Frédéric Dufour et Nicolas Moës d'avoir pris le temps de lire ce manuscrit afin de rapporter cette thèse, et Gilles Pijaudier-Cabot d'avoir accepté de présider ce jury. Je remercie également l'ensemble du jury pour nos discussions très enrichissantes lors de la soutenance.

Je remercie maintenant mes encadrants Emmanuel, Rodrigue et Milan de m'avoir confié ce sujet de thèse et de m'avoir accompagné jusqu'au bout. Merci également de m'avoir transmis votre rigueur et votre envie d'aller jusqu'au bout des choses. Je remercie en particulier Milan pour son accueil à Prague, son aide et sa disponibilité malgré la distance à mon retour en France.

Je remercie également l'ensemble des doctorants et des permanents du LMT pour l'environnement agréable dans lequel j'ai eu l'occasion de travailler pendant 3 ans. Merci en particulier à Amélie, Fabrice et Federica pour leurs précieux conseils lors de la préparation de ma soutenance. Merci également au département de Génie Civil et à son équipe pédagogique de m'avoir confié une mission d'enseignement, ce fut une expérience très enrichissante. Je remercie également Adam, Magalie, Claire, Pierre, Thibault, Flavien, Pierre-Jean, Boubou, Jean-Baptiste, Yannis, Philippe, Florian, Léonard et Jordan pour ces bons moments passés ensembles et pour nos discussions plus ou moins scientifiques au bar du LMT ou autour d'un verre.

Merci aux gens de l'Université Technique de Prague de m'avoir accueilli, et merci à Martin, Claudio, Vasco, Lorenzo et Emma pour nos échanges scientifiques et footballistiques, au bureau et autour d'une bière. Merci en particulier à Martin pour son aide avec OOFEM.

Merci à mes collègues du CEA de m'avoir soutenu pendant les deux dernières années de ma thèse. Merci en particulier à Mireille, Romain et Arnaud d'avoir cru en moi, et merci à Paul, Fabien et Tommaso pour toutes nos discussions parfois trop scientifiques au café comme autour d'une bière. Merci également à Bruno, Thomas, Jérôme et Fabien pour leurs précieux conseils lors de la préparation de ma soutenance de thèse.

Merci à ma famille et mes amis de m'avoir soutenu jusqu'au bout, notamment dans les moments difficiles de ces presque 5 années de thèse. Merci en particulier à Papi, Mamie Arlette, Mamie Jeannette, Maman, Papa, Loïc, Pierre, Aurélie, Hugo, Nathalie, Thierry, Manon, Micka, TD et Alexis pour leur soutien sans faille.

Merci enfin à ma compagne Audrey qui m'a accompagné jusqu'au bout pour son aide et son soutien permanent et inconditionnel.

Résumé en français

0.1 Introduction et cadre de l'étude

0.1.1 Contexte général

Bien que la plupart des systèmes soient conçus de façon à prévenir l'apparition de tout phénomène de dégradation, en particulier en fonctionnement nominal, la modélisation des mécanismes de ruine des matériaux reste un enjeu majeur.

En effet, pour de nombreuses applications, les règles de conception imposent des marges de sécurité conséquentes pour s'assurer que le système étudié reste largement dans son domaine élastique, y compris lors de situations incidentelles. C'est notamment le cas pour les systèmes de levage où la prise en compte des différents scénarios correspondant aux situations nominales et incidentelles se fait à travers différentes marges sur des critères spécifiques [ANO, 1998].

Malgré leur robustesse, ces méthodes n'apportent pas de compréhension des phénomènes en jeu lors des différentes sollicitations subies par un système donné au cours de sa vie, ce qui peut s'avérer insuffisant. En effet, si le système vient à subir une sollicitation imprévue, une modélisation purement élastique associée à des marges prédéfinies ne permettra pas d'évaluer le risque d'apparition de fissures. De surcroît, si pour des systèmes complexes comme des barrages ou des avions l'apparition de fissure ne peut pas être synonyme de ruine totale, il est toutefois nécessaire d'évaluer leur dangerosité, et notamment le risque de propagation.

La modélisation de la dégradation progressive des matériaux en vue d'évaluer le risque d'apparition de fissures et de prédire leur éventuelle propagation. Cela permettrait en effet d'améliorer les marges de sécurité tout en optimisant les conceptions, permettant ainsi une réduction des coûts associés.

0.1.2 Modélisation de la ruine des matériaux

Il existe historiquement deux grandes familles de méthodes permettant de traiter de la dégradation des matériaux : les approches discrètes basées sur la mécanique de la rupture, et celles continues basées sur la mécanique de l'endommagement.

Là où les premières traitent essentiellement de la propagation de fissures existantes décrites explicitement dans la géométrie, les secondes proposent une modélisation continue de la dégradation du matériau. Cette dernière est modélisée au travers d'une variable d'endommagement qui peut être assimilée à une densité de micro-défauts (microfissures et microporosités), ce qui permet de prendre en compte la perte progressive de rigidité du matériau.

Bien qu'ils semblent plus adaptés à la modélisation de la dégradation progressive d'un matériau, les modèles basés sur la mécanique de l'endommagement continu souffrent d'un certain nombre de défauts intrinsèques. On observe en particulier une perte d'ellipticité liée au fait que la taille de la zone de localisation dans laquelle l'endommagement apparait, et donc l'énergie dissipée par la rupture, n'est pas fixée. Lors de simulations numériques avec de tels modèles, ce problème se traduit par une forte dépendance au maillage avec une énergie dissipée qui tend vers zéro avec la taille de maille [Pijaudier-Cabot and Bažant, 1987].

Des approches dites non-locales ont été développées pour résoudre ce problème en introduisant une longueur interne via une moyenne spatiale [Pijaudier-Cabot and Bažant, 1987] ou une équation du second degré [Peerlings et al., 1996]. Bien que ces approches permettent de fixer la taille de la zone de localisation, et ainsi de rendre les problèmes associés bien posés, elles ne permettent pas de gérer la transition endommagement-fissuration. En effet, on n'observe pas de coupure des interactions ni de saut de déplacement au travers des zones fortement endommagées qui ne peuvent de fait pas reproduire un comportement de fissure.

0.1.3 Propriétés attendues d'un modèle d'endommagement

Avant de présenter les modèles étudiés dans cette thèse, il convient d'établir une liste des propriétés permettant de caractériser ce qui sera appelé ici un "bon" modèle d'endommagement. On notera que cette définition est spécifique au cadre de ce travail, et n'est en particulier pertinente que pour des modèles ayant un comportement élastique jusqu'à la contrainte maximale. On peut ainsi considérer qu'un tel modèle est caractérisé par :

- Un comportement réaliste avant et après le pic [Jirásek, 1998]
  - pré-pic : pas de modification de la réponse élastique
  - post-pic : allure de courbe réaliste avec une chute de contrainte
- La convergence et l'indépendance des résultats vis-à-vis du maillage [Pijaudier-Cabot and Bažant, 1987]
  - convergence vers une solution à énergie dissipée non-nulle en raffinant le maillage
  - endommagement réparti sur une zone de largeur non-nulle
  - faible sensibilité au maillage pour une taille d'éléments suffisamment petite
- Une zone fortement endommagée se comportant comme une fissure [Desmorat and Gatuingt, 2007]
  - contrainte finale nulle
  - localisation dans un unique élément quand l'endommagement vaut 1
  - pas d'interaction à travers une zone où l'endommagement est égal à 1

  - existence d'une solution avec un saut en déplacement lorsque l'endommagement est égal à 1

- La possibilité d'être implémenté de façon non-intrusive dans un code de calcul commercial [Azinpour et al., 2018].

On notera que d'autres critères pourraient également être envisagés comme la prise en compte des conditions aux limites [Bažant et al., 2010] et la gestion de l'initiation de l'endommagement [Eringen et al., 1977].

0.1.4 Régularisation et méthodes non-locales

De nombreuses formulations ont été développées pour modéliser la dégradation progressive des matériaux tout en évitant les défauts intrinsèques aux modèles d'endommagement locaux.

On retrouve parmi elles les approches dites non-locales qui visent à fixer la taille de la zone de localisation en introduisant une longueur interne dans le modèle. L'idée ici est de remplacer la variable gouvernant l'évolution de l'endommagement $\mathcal{V}$ par sa contrepartie régularisée dite non-locale $\bar{\mathcal{V}}$. Ce traitement non-local consiste généralement en une moyenne spatiale [Pijaudier-Cabot and Bažant, 1987, Giry et al., 2011] ou une équation du second degré en espace [Peerlings et al., 1996, Geers et al., 1998] où les longueurs peuvent être pondérées par les variables d'état du système [Geers et al., 1998, Giry et al., 2011]. Les formulations de type intégral et gradient s'écrivent respectivement

$$\bar{\mathcal{V}}(\boldsymbol{x}) = \frac{1}{V_0(\boldsymbol{x})} \int_\Omega \mathcal{V}(\boldsymbol{\xi}) \alpha(\boldsymbol{x}, \boldsymbol{\xi}) \, \mathrm{d}\boldsymbol{\xi} \tag{1}$$

$$V_0(\boldsymbol{x}) = \int_\Omega \alpha(\boldsymbol{x}, \boldsymbol{\xi}) \, \mathrm{d}\boldsymbol{\xi} \tag{2}$$

et

$$\bar{\mathcal{V}} - \nabla \cdot \left(b \, \nabla \bar{\mathcal{V}} \right) = \mathcal{V} \tag{3}$$

où α est une fonction de poids qui décroit avec la distance entre les points $\boldsymbol{x}$ et $\boldsymbol{\xi}$, et a et b sont des fonctions dont le produit est homogène à une distance au carré. On notera que α, a et b peuvent dépendre de l'état du matériau.

Les principaux avantages de ce type d'approches viennent du fait qu'elles sont a priori compatibles avec n'importe quel modèle d'endommagement. De surcroît, alors que le calcul de la moyenne spatiale empêche l'implémentation non intrusive des modèles de type intégral, ce n'est pas le cas des approches de type gradient qui s'y prêtent bien [Azinpour et al., 2018]. Pour cette raison, c'est ce type d'approche qui sera étudiée dans la suite de ce travail.

Une alternative aurait pu être d'utiliser les approches de type Thick Level Set [Moës et al., 2011] et Lip Field [Moës and Chevaugeon, 2021] qui visent à obtenir des propriétés similaires en imposant directement la régularité de l'endommagement.

D'autres formulations auraient également pu être envisagées comme les approches énergétiques de type Phase Field [Miehe et al., 2010b] ou l'approche variationnelle de la rupture [Francfort and Marigo, 1998]. Elles visent à modéliser la

dégradation progressive d'un matériau en lien avec la mécanique de la rupture, mais n'ont de fait pas vocation à être associées à des modèles d'endommagement.

Des approches visant à régulariser l'endommagement en limitant sa vitesse d'évolution ont également été développées [Dubé et al., 1996, Allix and Deü, 1997], mais elles sont surtout adaptées aux chargements dynamiques.

0.1.5 Les approches de type eikonales

Comme évoqué précédemment, un des principaux défauts des approches dites non-locales vient du fait qu'elles ne rendent pas forcément une zone fortement endommagée équivalente à une fissure. Des formulations où le traitement non-local dépend de l'état du matériau (déformation, contraintes, endommagement) ont ainsi été proposées pour pallier ce défaut.

On retrouve parmi ces approches les formulations dites eikonales dont l'idée originale [Desmorat and Gatuingt, 2007] était d'utiliser des temps de propagation au lieu de distances dans le calcul des traitements non-locaux. Ainsi, la fonction de poids α ne dépend plus de la distance $\|\boldsymbol{x} - \boldsymbol{\xi}\|$, mais du temps $\tau_{x\xi}$ que mettrait une onde mécanique pour relier les deux points. L'un des intérêts de cette approche vient du fait que dans ce cas une fissure aurait le même impact sur le traitement non-local qu'une zone fortement endommagée que les ondes ne peuvent pas traverser.

Cependant, l'un des principaux défauts de cette approche vient de la nécessité de calculer les temps de propagation entre tous les points à chaque pas de temps. Une formulation alternative considérant un espace courbé par l'endommagement a ensuite été proposée et associée à différents modèles d'endommagement avec et sans plasticité [Jirásek and Desmorat, 2019]. Il a ainsi pu être montré qu'en plus d'assurer un comportement réaliste et l'indépendance vis-à-vis du maillage [Rastiello et al., 2018a], elle rendait une zone fortement endommagée équivalente à une fissure. Malgré ces avantages, le temps de calcul associé à l'évaluation des distances effectives restait très élevé, et cette approche souffrait toujours des défauts associés aux approches intégrales en termes d'implémentation.

Pour toutes les raisons évoquées ci-dessus, il a été décidé dans cette thèse de travailler avec une approche de type gradient qui dérive de cette formulation dite eikonale [Desmorat et al., 2015].

Le travail présenté dans cette thèse vise donc à évaluer les propriétés de cette nouvelle approche dite eikonale de type gradient, et notamment à évaluer sa capacité à gérer la transition endommagement-fissuration en étant couplée à des modèles d'endommagement avec et sans plasticité. Pour ce faire, le travail présenté dans la thèse a comporté différents volets :

- Vérification de la possibilité d'implémenter la formulation de façon non-intrusive dans un code commercial : conduite en 1D dans Abaqus ;
- Étude des propriétés de régularisation : conduite en 1D dans Abaqus et sur des essais de flexion 3 points dans OOFEM ;

- Comparaison avec des formulations non-locales classiques : conduite en 1D dans Abaqus, comparaison avec l'approche classique de type Peerlings et une formulation basée sur les champs de phase ;
- Association avec différents modèles d'endommagement : modèle isotrope sans plasticité utilisé dans Abaqus et dans OOFEM, et modèle avec plasticité uniquement dans OOFEM après une étude analytique préliminaire visant à évaluer l'apport potentiel de la plasticité.

La suite de ce document va présenter les principaux résultats issus de cette thèse, et s'articule donc comme suit :

◊ Modèles d'endommagement non-locaux avec et sans plasticité

◊ Implémentation non-intrusive et propriétés dans un cadre unidimensionnel

◊ Introduction de la plasticité et analyse de localisation

◊ Simulations numériques en flexion 3-points avec OOFEM

0.2 Modèles d'endommagement non-locaux avec et sans plasticité

Cette partie va présenter les modèles d'endommagement avec et sans plasticité utilisés dans cette thèse, ainsi que les formulations non-locales associées.

0.2.1 Modèle d'endommagement isotrope sans plasticité

Le premier modèle considéré dans cette thèse est un modèle d'endommagement isotrope sans plasticité avec adoucissement exponentiel, et où l'évolution de l'endommagement est gouverné par la déformation équivalente de Mazars $\hat{\varepsilon}$.

Le modèle local s'écrit ainsi :

$$\boldsymbol{\sigma} = \tilde{\mathbb{C}} : \boldsymbol{\varepsilon} = (1-D)\,\mathbb{C} : \boldsymbol{\varepsilon} \tag{4}$$

$$\hat{\varepsilon} = \sqrt{\langle\varepsilon_1\rangle_+^2 + \langle\varepsilon_2\rangle_+^2 + \langle\varepsilon_3\rangle_+^2} \tag{5}$$

$$\kappa(t) = \max_{\tau\leq t} \hat{\varepsilon}(\tau) \tag{6}$$

$$D = g(\kappa) = \begin{cases} 0 & \text{if } \kappa < \varepsilon_0 \\ 1 - \dfrac{\varepsilon_0}{\kappa}\exp\left(-\dfrac{\kappa-\varepsilon_0}{\varepsilon_f-\varepsilon_0}\right) & \text{if } \kappa \geq \varepsilon_0 \end{cases} \tag{7}$$

Le modèle non-local associé est obtenu en conservant les équations (4), (5) et (7), et en remplaçant la déformation équivalente $\hat{\varepsilon}$ dans l'équation (6) par sa version non-locale $\bar{\varepsilon}$ calculée via :

$$\bar{\varepsilon} - a\,\nabla\cdot(b\,\nabla\,\bar{\varepsilon}) = \hat{\varepsilon} \tag{8}$$

On notera que dans le cas de l'approche eikonale étudiée ici, les fonctions a et b sont définies comme $a = c^2(1-D)^{1/2}$ et $b = (1-D)^{1/2}$.

0.2.2 Modèle d'endommagement isotrope avec plasticité

Il a été montré que pour prendre en compte les frottements à l'intérieur des fissures, la modélisation de certains matériaux comme le béton nécessitait l'introduction de déformations permanentes [Mazars et al., 1990]. Il a donc été décidé d'étudier un second modèle où l'évolution de l'endommagement est cette fois gouvernée par la déformation plastique cumulée. Ce modèle s'écrit ainsi :

$$\boldsymbol{\sigma} = \tilde{\mathbb{C}} : (\boldsymbol{\varepsilon} - \boldsymbol{\varepsilon}^p) = (1 - D)\ \mathbb{C} : (\boldsymbol{\varepsilon} - \boldsymbol{\varepsilon}^p) \tag{9}$$

$$\dot{p} = \sqrt{\frac{2}{3}\ \dot{\boldsymbol{\varepsilon}}^p : \dot{\boldsymbol{\varepsilon}}^p} \tag{10}$$

$$\kappa(t) = p(t) = \int_0^t \dot{p}(\tau)\mathrm{d}\tau \tag{11}$$

$$\tag{12}$$

où la déformation cumulée est calculée en utilisant le critère de Rankine ci-après

$$f\left(\tilde{\boldsymbol{\sigma}}, p\right) = \max\left(\tilde{\sigma}_I, \tilde{\sigma}_{II}, \tilde{\sigma}_{III}\right) - \sigma_y(p) \tag{13}$$

$$f\ \dot{p} = 0, \quad f \leq 0, \quad \dot{p} \geq 0 \tag{14}$$

où la contrainte seuil est définie comme

$$\sigma_y(p) = \sigma_0 + R(p) = \sigma_0 + H\ p \tag{15}$$

ce qui traduit un écrouissage isotrope. On notera que ce critère est basé sur la contrainte effective $\tilde{\boldsymbol{\sigma}}$ définie comme

$$\tilde{\boldsymbol{\sigma}} = \frac{\boldsymbol{\sigma}}{1 - D} = \mathbb{C} : (\boldsymbol{\varepsilon} - \boldsymbol{\varepsilon}^p) \tag{16}$$

pour prendre en compte la présence d'endommagement.

Enfin, pour en vue de faciliter la comparaison entre les deux modèles, l'évolution de l'endommagement a été choisie de façon à ce que les deux modèles aient des lois de contrainte-déformation équivalentes, ce qui donne :

$$D = g(\kappa) = 1 - \frac{\sigma_0}{\sigma_0 + H\kappa} \exp\left(-\frac{(1 + H/E)\kappa}{\varepsilon_f - \varepsilon_0}\right) \tag{17}$$

Là encore, la formulation non-locale est obtenu à partir du modèle local en introduisant la variable non-locale dans a loi d'évolution de l'endommagement. Dans le cadre de ce modèle, on conserve ainsi les équations (9) à (16), et on remplace p dans l'équation (17) par la variable κ définie comme :

$$\kappa = m\ \bar{p} + (1 - m)p \tag{18}$$

La déformation plastique cumulée non-locale est ici déterminée en résolvant

$$\bar{p} - a\ \nabla \cdot (b\ \nabla\ \bar{p}) = p \tag{19}$$

où a et b sont toujours définies comme $a = c^2(1 - D)^{1/2}$ et $b = (1 - D)^{1/2}$.

0.3 Implémentation non-intrusive et propriétés dans un cadre unidimensionnel

La première étude menée sur la formulation eikonale visait à valider la faisabilité d'une implémentation non-intrusive dans le logiciel commercial Abaqus. Cette étude a été menée dans un cadre unidimensionnel en se concentrant sur le modèle sans plasticité pour en évaluer les propriétés de régularisation. Les résultats ainsi obtenus ont également été comparés à ceux obtenus avec la formulation classique de Peerlings et avec une formulation basée sur une approche de type Phase Field.

L'implémentation non-intrusive dans Abaqus a été conduite en utilisant les similitudes entre l'équation de la chaleur et l'équation de type gradient (8). Cette analogie a permis de résoudre de façon monolithique le problème mécanique couplé au non-local en utilisant le solveur thermomécanique d'Abaqus ainsi que les éléments finis associés.

Le problème ainsi étudié est celui d'une barre en traction encastrée à une extrémité et où le chargement est imposé via un élément spécifique (UEL) . Ce choix a permis d'utiliser une méthode de pilotage global en dissipation, ce qui a permis de mener à bien les simulations présentant des instabilités de type snap-back en calculant la courbe de réponse associée.

Cette étude a notamment permis de montrer qu'en plus de pouvoir être implémentée de façon non-intrusive, l'approche eikonale permet d'avoir un comportement réaliste et indépendant vis-à-vis du maillage. Il a également été montré qu'une zone fortement endommagée se comportait comme une fissure avec un saut de déplacement et un profil d'endommagement qui se rétrécit lorsque l'endommagement tend vers 1 comme on peut le voir sur la Figure 1.

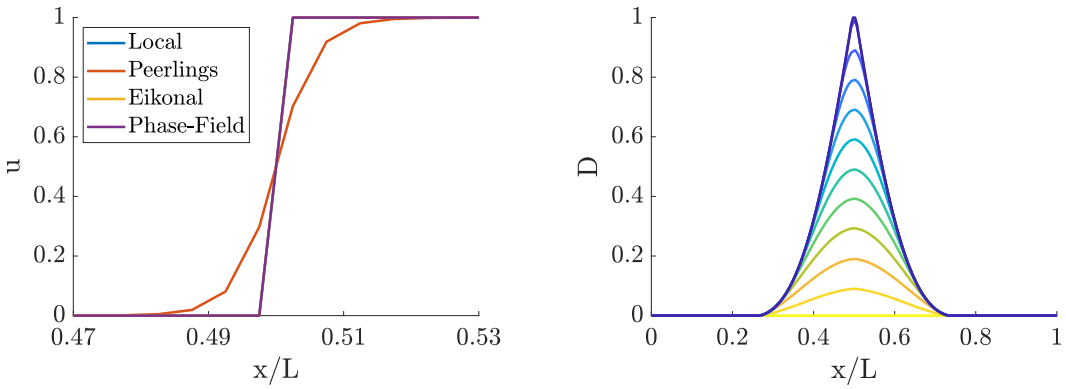

(a) Saut de déplacement en milieu de barre. (b) Évolution du profil d'endommagement

Figure 1: Saut de déplacement et évolution du profil d'endommagement.

Cette première étude a ainsi permis de confirmer que l'approche dite eikonale de type gradient possède toutes les propriétés identifiées comme caractéristiques d'un "bon" modèle d'endommagement.

0.4 Introduction de la plasticité et analyse de localisation

Après avoir validé les propriétés de l'approche eikonale associée au modèle d'endommagement sans plasticité, une étude théorique a été menée pour évaluer l'apport potentiel de l'introduction de la plasticité.

Un première analyse de localisation a ainsi permis de confirmer que les deux modèles (avec et sans plasticité) fixent la taille de la zone dans laquelle l'endommagement se localise. Elle a notamment permis de montrer que la taille des zones de localisation initiales associées aux deux modèles diffèrent et dépendent des paramètres associés aux lois gouvernant l'évolution de l'endommagement.

Une seconde étude théorique unidimensionnelle a ensuite été menée pour évaluer l'influence de la plasticité sur la réponse lorsque la localisation se fait dans une zone de taille fixe ou qui tend vers un point.

Il a ainsi pu être montré que la plasticité n'a pas d'influence sur la réponse globale tant que la taille de la zone de localisation n'évolue pas. En revanche, lorsque taille de la zone de localisation diminue, la présence de déformations permanentes limite l'ampleur de la décharge élastique et donc la fragilité de la réponse. Il a également pu être montré que la fragilité de la réponse associée au modèle d'endommagement avec plasticité peut être ajustée via le paramètre d'écrouissage H.

0.5 Simulations numériques en flexion 3-points avec OOFEM

Après avoir montré dans un cadre unidimensionnel que l'approche eikonale avait toutes les propriétés attendues d'un bon modèle d'endommagement, il est nécessaire de passer à des chargements plus complexes comme la flexion 3-points. Cette étude, conduite dans le code élément fini OOFEM à l'occasion de deux séjours de recherche à la Czech Technical University de Prague où il est développé a également été l'occasion d'évaluer les propriétés du modèle avec plasticité.

L'étude menée avec le modèle sans plasticité a permis de montrer que malgré la fragilité de la réponse, les résultats obtenus étaient bien indépendants vis-à-vis du maillage. On notera toutefois que le pilotage en déplacement utilisé pour ces simulations n'a pas permis d'obtenir les courbes de réponse complètes en raison de l'occurrence de snap-backs. En outre, il a pu être vérifié que la localisation a lieu dans des zones de plus en plus étroites lorsque l'endommagement tend vers 1.

Pour ce qui est du modèle avec plasticité, il a pu être montré que les résultats associés étaient indépendant du maillage et que la zone fortement endommagée se comportait comme une fissure avec une localisation dans une bande de plus en plus étroite. Comme on peut le voir dans la Figure 2, une fois apparue, cette zone

s'est propagée au travers de la barre en flexion, reproduisant ainsi la propagation d'une fissure et la perte de rigidité associée.

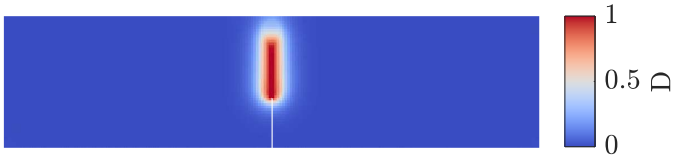

(a) Endommagement.

(b) Déformation plastique cumulée.

Figure 2: Cartes finales d'endommagement et de déformation plastique cumulée.

Les études menées dans OOFEM ont donc permis de confirmer que l'approche eikonale de type gradient avait bien les propriétés attendues, et ce, qu'elle soit associée à des modèles d'endommagement avec ou sans plasticité.

0.6 Conclusion

Après avoir détaillé les principaux défauts des modèles d'endommagement locaux et non-locaux, cette thèse a tout d'abord proposé une liste de propriétés pouvant caractériser un bon modèle d'endommagement. Une nouvelle formulation de type gradient dite eikonale a ensuite été proposée et étudiée de façon à démontrer qu'elle pouvait être utilisée pour gérer la transition endommagement-fissuration.

Pour ce faire, la formulation obtenue en couplant cette approche à un modèle d'endommagement isotrope a été implémentée de façon non-intrusive dans Abaqus en utilisant une analogie thermomécanique et un pilotage en dissipation globale. Une étude uni-dimensionnelle a ensuite été menée dans Abaqus pour vérifier que cette approche avait bien toutes les propriétés attendues d'un "bon" modèle.

Une étude théorique a ensuite été menée, toujours dans le cas unidimensionnel, pour s'assurer analytiquement que les formulations obtenues en couplant l'approche dite eikonale à deux modèles d'endommagement avec et sans plasticité imposaient bien la taille de la zone de localisation. Ces études ont également permis d'évaluer l'apport de l'introduction de la plasticité, notamment en ce qui concerne la fragilité de la réponse du matériau.

Enfin, ces formulations ont été implémentées dans le code de calcul OOFEM. Cela a permis de confirmer les propriétés de cette approche lors de la simulation d'essais de flexion 3-points avec deux modèles différents, et notamment le fait qu'elle permet de rendre une zone fortement endommagée équivalente à une fissure.

On peut donc en conclure qu'il est possible d'utiliser l'approche de type gradient dite eikonale pour gérer la transition endommagement fissuration.

Introduction

While most systems are designed in a way that should prevent the occurrence of any degradation phenomenon under nominal loading, one still needs to be able to accurately model material failure.

As it is, to prevent dramatic events, critical systems are usually designed with huge margins to ensure that they remain well within the elastic domain, which induces additional costs and restrictions. This tendency concerns a wide range of applications from planes to nuclear power plants, including bridges and hydroelectric dams, but also more conventional applications such as cranes and hoisting systems.

For example, when following the rules set by the European material handling federation (FEM) [ANO, 1998] to design a hoisting system, one needs to ensure that it matches a certain number of requirements. These requirements mainly consist of having certain margins regarding the elastic limit for different loading cases corresponding to different scenarios. Based on empiric results, this approach is supposed to ensure that the system will not suffer any degradation due to fatigue or specific incidents like wire failure.

However, it does not provide any knowledge about what happens on the material level, especially in the presence of defects. It thus cannot give any hindsight regarding the possible failure mechanisms. Those shortcomings can be pretty problematic, namely on the occurrence of an unexpected event or when the system does not behave as expected. In such cases, especially for critical and expensive systems, one needs to know whether degradation phenomena did or will occur and how likely they are to induce a system failure.

Aeronautics applications illustrate this phenomenon well since small cracks can always be found on aeroplanes. This well-known phenomenon raises the question of damage tolerance: levels of microcracking are inevitable and acceptable, but one needs to know how and when they will become problematic. Then, the question is not to determine whether cracks will appear but rather where and how dangerous they will be. The same can be said about hydroelectric dams that cannot be replaced whenever a crack appears and for which specific fracture studies had to be conducted [Linsbauer et al., 1989a, Linsbauer et al., 1989b]. Proper material modelling is also crucial when optimising critical systems, especially when designing their maximum load and lifespan. As an example, despite the 7.2 billion passengers expected in 2035 [IAT, 2016], the Advisory Council for Aviation Research and Innovation in the EU (ACARE) aims to cut the CO_2 and NOx emissions by 75% [ACA, 2014]. To achieve this goal, one would need to use more efficient materials and technologies that will have to be precisely validated. Accurate modelling of

the material's behaviour, including its possible failure, is thus critical to optimise the design and reduce the cost by replacing experimental testing with numerical testing at structural load.

The consideration regarding replacing experimental testing with numerical simulations is particularly relevant in fields where few to no experimental results are available. Apart from the aeronautic applications, this is also true for the nuclear field, where one cannot always reproduce the exact conditions corresponding to an accidental situation to see what would happen. However, for safety reasons, one still has to know what would happen if one of the systems fails. This insight is usually achieved using models representing the physics of the material and calibrated using dedicated experimental testing. Provided that the models are accurate enough, they can then be used to correctly understand what happens during both incidental and accidental situations.

As pointed out, this general concern is especially relevant in the nuclear field. Accident situations such as Loss of Cooling Accidents (LOCA) and Reactivity Initiated Accidents (RIA) can have dramatic consequences and need to be correctly understood. For example, Pellet-Cladding Mechanical Interactions, which can occur during an RIA and compromise the fuel's structural integrity, involve many mechanisms, including cracking, that must be accurately modelled.

It is worth noting that those considerations apply not only to new systems but also to existing ones, namely when changing their loading conditions or increasing their lifespan. While the latter mainly deals with the detection and the propagation prediction of existing cracks, the former might include completely different solicitations linked to the emergence of new threats such as tsunamis or plane crashes. In such cases, one can wonder whether the system would withstand the new load and how it would behave since it was not designed accordingly. A precise understanding of the failure mechanisms is thus mandatory to assess the risks induced by a potential local failure of the system. For example, apart from their capacity to produce electricity, the potential failure of hydroelectric dams and nuclear power plants can have dramatic consequences, such as the release of radioactivity or vast amounts of water, which would induce substantial losses both human and material.

One can thus conclude that the proper and physical modelling of material failure is critical for designing and studying both new and existing systems. Due to the variety of concerned applications, this issue needs to be addressed for a wide range of materials (e.g. concrete, metallic and composites) and solicitations (e.g. fatigue, quasi-static and dynamic loadings).

The most classical way to answer the question of whether a crack will propagate is to use the Linear Elastic Fracture Mechanic. This approach, based on the pioneering works of Griffith [Griffith, 1921], Irwin [Irwin, 1957], and Rice and Tracey [Rice and Tracey, 1969], uses propagation criteria based on stress intensity factors and elastic energy release rate.

Despite the maturity acquired by its long history, this approach still suffers from several deficiencies, the most problematic one being the need for a priori knowledge regarding the crack location. As it is, one can only use it to handle

existing cracks and to predict whether they will propagate, but not to predict crack initiation. Moreover, the need to work with existing discontinuities embedded in an elastic material can be problematic in finite element applications since one cannot accurately model crack propagation either. A direct consequence of these drawbacks is that it does not model the progressive loss of material properties inherent to the progressive nucleation and coalescence of voids and micro-defects.

Part of this issues can be addressed by using the so-called extended (XFEM [Belytschko and Black, 1999, Moës et al., 1999]) and generalized (GFEM [Strouboulis et al., 2000, Strouboulis et al., 2001]) Finite Element Methods, based on the partition of unity [Melenk and Babuška, 1996], along with fracture mechanics. Such methods, using additional degrees of freedom defined with enrichment functions, allow the representation of evolving discontinuities through finite elements without a priori knowledge regarding their location. Though such models were initially designed for the sole geometrical description of discontinuities, they can be coupled with material laws to bring additional knowledge regarding crack behaviour.

Another option would be to use Cohesive Zone Models [Dugdale, 1960, Barenblatt, 1962] which allow the definition of a stress-displacement law across a cracked element but requires a priori knowledge of the crack path to position the cohesive elements accordingly.

Finally, an alternative way to model the progressive degradation of materials up to failure is to use the Continuum Damage Mechanics formalism [Marigo, 1981, Mazars, 1984, Lemaitre and Chaboche, 1994], which will be done here. The main advantage of such formulations is that they allow continuous modelling of failure, including crack initiation and propagation, without any initial knowledge regarding the crack.

In addition to these considerations, other properties can be expected from a model handling material failure and that are compatible with the Continuum Damage Mechanics framework.

First, one could expect such a model to take into account crack closure and the associated partial stiffness recovery [Ladeveze and Lemaitre, 1984, Ladeveze, 1990, Mazars et al., 1990, Chaboche et al., 1994, Cantournet et al., 2009]. While this comes naturally with the LEFM approach, it is not a standard feature of isotropic damage models and thus requires specific attention. In some cases, such as the phase-Field models [Miehe et al., 2010b], this is achieved through the isotropic degradation of the "positive" elastic energy while the "negative" part remains unaffected [Ladeveze, 1983]. One can note that, while these approaches allow for the modelling of crack closure, the LEFM only considers existing cracks, i.e. it does not consider micro-cracking. Moreover, isotropic modelling, even with crack closure, does not consider the micro-cracks orientations. Thus, a tensile loading in a given direction can induce material degradation in orthogonal directions.

This issue could be addressed, taking into account the anisotropy of the micro-cracking path, by using tensorial damage [Suaris and Shah, 1984, Chaboche, 1981, Cordebois and F., 1982, Ladeveze, 1983, Mazars et al., 1990, Papa and Taliercio, 1996, Murakami and Kamiya, 1997, Halm and Dragon, 1996, Fichant et al., 1997, Lemaitre et al., 2000, Badel et al., 2007]. To remain thermodynamically consistent,

those models should use a single variable per degradation mechanism to represent damage, which can be either an eighth order tensor [Chaboche, 1978, Chaboche, 1979], a fourth-order tensor [Chaboche, 1978, Chaboche, 1979, Chaboche, 1984, Leckie and Onat, 1981, Andrieux et al., 1986, Ju, 1989, Kachanov, 1993, Zheng and Collins, 1998, Ladeveze, 2002, Cormery and Welemane, 2010, Dormieux and Kondo, 2016], or a symmetric second-order tensor [Vakulenko and Kachanov, 1971, Murakami and Ohno, 1978, Cordebois and F., 1982, Ladeveze, 1983, Murakami, 1988]. It is worth noting that some formulations use a scalar damage variable associated with a single vector to describe pre-existing cracks (e.g. [Andrieux et al., 1986]) and can thus only account for a single crack orientation.

Besides, while there exists a wide range of models using a second-order damage tensor [Murakami, 1988, Kattan and Voyiadjis, 1990, Ramtani et al., 1992, Papa and Taliercio, 1996, Halm and Dragon, 1998, Steinmann and Carol, 1998, Lemaitre et al., 2000, Carol et al., 2001, Menzel and Steinmann, 2001, Menzel et al., 2002, Brünig, 2003, Lemaitre and Desmorat, 2005, Desmorat et al., 2007a, Badel et al., 2007, Desmorat and Otin, 2008, Desmorat, 2015], which can be partially unified in a single model [Ladeveze, 1983, Ladeveze, 1995], a new general micro-mechanics based framework was recently introduced in [Desmorat et al., 2018]. Moreover, the physical consideration of induced anisotropy [Desmorat, 2004, Desmorat et al., 2007a, Desmorat, 2015] allows for the reduction of the otherwise prohibitive number of material parameters while remaining thermodynamically consistent [Desmorat, 2006].

A common shortcoming of the so-called pure damage models lies in their inability to capture the fact that some materials, such as concrete, exhibit permanent strain [Terrien, 1980, Mazars et al., 1989, Mazars et al., 1990] due both to dissipation linked to crack friction and to imperfect crack closure. This issue, first addressed with models involving only plasticity [William and Warnke, 1975, Ortiz, 1985, Voyiadjis and Abu-Lebdeh, 1994, Feenstra and Borst, 1996], can be addressed with the so-called damage-plastic models [Lemaitre, 1985, Lemaitre and Chaboche, 1985, Andrieux et al., 1986, Simo and Ju, 1987b, Ju, 1989, Govindjee et al., 1995, Feenstra and Borst, 1996, Meschke et al., 1998, Burlion et al., 2000, Nechnech et al., 2002, Gatuingt and Pijaudier-Cabot, 2003, Lemaitre and Desmorat, 2005, Jason et al., 2006, Grassl and Jirásek, 2006, Grassl and Jirásek, 2005, Desmorat et al., 2007b, Matallah and Borderie, 2009, Lemaitre et al., 2009], using the plasticity framework coupled with damage. Following the work done by [Herrmann and Kestin, 1988], one could also consider handling the permanent strain issue by using damage-driven permanent strain [La Borderie, 1991, Halm and Dragon, 1998, Desmorat, 2004, Lebon, 2011, Matallah and Borderie, 2009] instead of plasticity-driven damage. It is worth noting that, while dedicated models using plasticity without damage were historically developed to handle these phenomenons in concrete, one can also stick to the elasto-damage framework [Mazars, 1984] for the sake of simplicity and efficiency.

The last specificity of concrete that should be modelled is the rate dependency of its behaviour, namely the increase of material's strength with the strain rate

[Bischoff and Perry, 1991, Brara et al., 1997, Brara and Klepaczko, 1997], which was first handled by introducing dynamics within the continuum damage framework [Taylor et al., 1986]. Delay (or visco) damage was successfully used to reproduce such a behaviour [Simo and Ju, 1987a, Simo and Ju, 1987b, Pontiroli, 1995, Dubé et al., 1996, Allix and Deü, 1997, Sercombe et al., 1998, Gatuingt and Pijaudier-Cabot, 2001, Allix et al., 2003, Pedersen et al., 2008, Häußler-Combe and Kitzig, 2009], but also to reproduce the effect of dynamics on fragmentation [Denoual and Hild, 2000]. It is worth noting that a side effect of such models is the fact that they introduce additional dissipation and could thus have a spurious stabilising effect.

It thus seems that most of these properties can be obtained using a dedicated damage model. However, as discussed in [Bažant, 1976, Bažant and Belytschko, 1985, Pijaudier-Cabot and Bažant, 1987], these so-called local damage models suffer from the same deficiency, namely the fact that the size of the area where damage localises is not well fixed. When implementing such models in classical finite elements codes, one can thus observe that localisation occurs in a single element. This phenomenon induces a spurious mesh dependency and convergence toward a physically unrealistic solution with zero dissipated energy when the element size tends to zero.

Starting with [Pijaudier-Cabot and Bažant, 1987], and as detailed in the review [Bažant and Jirásek, 2002], nonlocal models were thus introduced to address this issue, the idea being to impose the size of the localisation area by introducing an internal length in the damage evolution law. This was initially done by replacing a damage driving variable with its nonlocal counterpart, i.e. its weighted average over a finite zone. Such formulations, physically motivated [Bažant, 1991, Bažant, 1994, Bažant and Jirásek, 1994, Pijaudier-Cabot et al., 2004], allow convergence toward solutions with a finite and non-zero dissipated energy [Pijaudier-Cabot and Benallal, 1993]. However, their implementation might not be practical in commercial finite element software due to the computation of the weighted average over the numerical neighbourhood. Gradient-type formulations [Aifantis, 1987, Frémond and Nedjar, 1996, Peerlings et al., 1996] deriving from the original formulation [Pijaudier-Cabot and Bažant, 1987] were thus proposed, and the implicit ones were shown to have similar properties to those of the original nonlocal model [Peerlings et al., 2001].

It is worth noting that, while such formulations offer a proper way to handle the spurious mesh dependency under quasi-static loading, rate-dependent models could provide similar regularisation properties in the case of dynamic loading. As it is, it was shown that introducing a time dependency in the degradation mechanism of both plastic [Needleman, 1988] and damage [Taylor et al., 1986, Dubé et al., 1996, Ladeveze, 1991, Eibl and Schmidt-Hurtienne, 1999, Hervé et al., 2005] models was equivalent to introducing an internal length and thus helped to handle the mesh sensitivity when taking into account the inertial term. Similar regularisation properties were also obtained by introducing a saturation (bounding) effect in damage evolution rate [Allix and Deü, 1997, Allix et al., 2003].

Nonlocal treatments were successfully applied to anisotropic damage models

[Desmorat and Gatuingt, 2007], damage-plastic models [Jirásek and Desmorat, 2019], and even bounded rate anisotropic damage models [Desmorat et al., 2010a]. The resulting formulations, namely nonlocal anisotropic damage models, nonlocal damage-plastic models, and nonlocal anisotropic bounded-rate damage models, were shown to exhibit the properties associated with each of their constitutive models.

Thus, continuum damage associated with nonlocal treatment might be an excellent way to handle material failure, especially when associated with anisotropy, plasticity, and rate dependency.

The goal of this thesis was thus to work on the implementation and analysis of a new eikonal-based gradient-type formulation and to compare it with classical gradient-type formulations.

Despite their advantages, the so-called nonlocal formulations usually suffer from certain deficiencies linked to boundary conditions [Borino et al., 2003, Krayani et al., 2009, Bažant et al., 2010, Pijaudier-Cabot and Dufour, 2010, Giry et al., 2011], size effect [Bažant, 1976, Jirásek et al., 2004, Krayani et al., 2007], and initiation and propagation of damage [Simone et al., 2004]. Moreover, when applied to models where the nonlocal equivalent strain drives damage, the standard approaches [Pijaudier-Cabot and Bažant, 1987, Peerlings et al., 1996] exhibit a spurious expansion of the damage profile at the late stages of failure. Another problematic issue associated with these damage models is linked to the fact that, physically, no interaction should exist between two points located on opposite sides of a crack. However, while this requirement can be met with gradient-type formulations, it does not come naturally with the standard averaging, and some specific care needs to be taken. One way to do so is to change how the interaction distances are computed by choosing the shortest path that does not cross the crack. Such a method, called visibility check [Belytschko et al., 1996], was used successfully with the element-free Galerkin method [Belytschko et al., 1994, Lu et al., 1994, Belytschko et al., 1995], which is beyond the scope of this thesis.

To address those issues, nonlocal damage models with evolving internal length based on stress [Giry et al., 2011, Vandoren and Simone, 2018], strain [Geers et al., 1998, Pijaudier-Cabot et al., 2004, Saroukhani et al., 2013] and damage [Simone et al., 2003, Pijaudier-Cabot et al., 2004, Pijaudier-Cabot and Dufour, 2010, Desmorat et al., 2010b, Nguyen, 2011] were proposed by a number of authors. Variational approaches [Francfort and Marigo, 1998, Bourdin et al., 2000, Bourdin et al., 2008], shown to converge toward Griffith theory [Bourdin et al., 2000], and Phase Field models [Miehe et al., 2010b, Miehe et al., 2010a, Miehe et al., 2015] were also introduced with the same purpose. Such models could work as efficient localisation limiters by successfully bridging the gap between continuum damage and fracture mechanics, matching the physical expectation that interactions tend to vanish when the damage gets close to 1.

A new type of nonlocal formulation was introduced in [Desmorat and Gatuingt, 2007, Desmorat and Gatuingt, 2010], replacing the interaction distance in [Pijaudier-Cabot and Bažant, 1987] with a propagation time. The idea was to use

the reduction of the elastic wave speed in a damaged material to create damage-dependent interactions, making a highly damaged zone equivalent to a crack. An equivalent formulation, using effective distance instead of propagation time, was then proposed in [Desmorat et al., 2015] and used with different damage models [Rastiello et al., 2018a, Rastiello et al., 2018b, Jirásek and Desmorat, 2019]. Those effective lengths are computed as a geometric distance between two points in a space curved by damage through a Riemannian metric up to complete material failure. Following the work done in [Peerlings et al., 1996], the gradient-type formulation studied here was also proposed in [Desmorat et al., 2015] to avoid the drawbacks associated with integral formulations and is expected to have comparable properties.

Other formulations such as the crack-band theory [Bažant and Oh, 1983] and the Thick-Level-Set method [Moës et al., 2011, Moës et al., 2014] were also developed by a certain number of authors to handle damage evolution but were not studied in this work which focuses on gradient-type nonlocal models. It is worth noting that an equivalent formulation of the Thick-Level-Set approach, using a differential equation, was also proposed [Frémond and Stolz, 2017] but will not be treated here. One can also note that, following this work, a more straightforward approach was also proposed in [Moës and Chevaugeon, 2021], the idea being to impose a Lipschitz condition on the damage field to prevent sharp discontinuities. Another way to handle fracture from continuous modelling could be, following the work presented in [Legrain et al., 2007, Dufour et al., 2008, Dufour et al., 2010], to locate a crack from an internal variable field and then estimate its opening.

As pointed out before, the implementation of nonlocal damage models usually raises numerical issues, linked either to the averaging process or to the need for solving an additional differential equation. The latter usually requires the creation of dedicated elements with additional, nonlocal degrees of freedom and corresponding numerical solvers ([Molnár and Gravouil, 2017]). To facilitate the implementation, it was proposed in [Azinpour et al., 2018] to use the thermo-mechanical solver embedded in the Abaqus software to solve this nonlinear problem, using the degrees of freedom associated with temperature for the nonlocal variable. It is worth noting that while the non-intrusive implementation allows the use of all the standard features coming with commercial software, the use of a dedicated one allows the creation of dedicated tools that might be more efficient and more practical. Both strategies thus have their advantages and drawbacks, especially when considering the possibility of using dedicated tools in an open-source finite element code such as OOFEM, and will be studied here.

Another issue that may arise when using damage models with strain softening is the occurrence of instabilities (e.g. snap-backs), which needs to be handled with a dedicated driving strategy. Experimentally, the occurrence of such instabilities would correspond to a vertical drop in the load-displacement curve, which cannot be reproduced using the considered strain softening models since they do not account for any dynamic effects. The difference between the dissipation associated with the expected curve with a vertical drop after the peak and that associated

with the one exhibiting a snap-back is thus linked to the kinetic energy, which is not modeled here. While taking it into account might look like an excellent way to address the snap-back issue, it would require using a dedicated, dynamic solver while the rest of the equations are in a quasi-static framework.

A certain number of authors have thus looked for a way to compute the full response curve [Riks, 1979, Ramm, 1981, Crisfield, 1991, de Borst, 1987, Geers, 1999b, Geers, 1999a, Simo et al., 1986], indirectly controlling the evolution of the load by imposing the increase of a given quantity, usually linked to failure. It was recently proposed [Gutiérrez, 2004, Verhoosel et al., 2009] to keep this idea of an indirect (arc-length) control and apply it to a global quantity by imposing increments of the total dissipated energy. It is worth noting that, while those approaches allow the computation of the "at equilibrium" response with the dissipated energy dictated by the material behaviour, they do not necessarily allow the computation of the macroscopic response, especially in the presence of snap-back.

One way to handle this issue would be to renounce the computation of the exact dissipation and use a fictive path algorithm [Michel et al., 2018] to handle the unstable part of the loading. Similar results could also be obtained by increasing the dissipated energy using a rate-dependent damage model [Miehe et al., 2010a]. It is worth noting that, in such cases, the additional dissipation would correspond to the kinematic energy that would have been introduced through dynamic computations.

The main issue linked to material failure, along with additional considerations, was highlighted in this introduction. The work presented in this thesis, which was partly prepared at the Czech Technical University in Prague under the supervision of Professor Milan Jirásek, will thus unfold according to the following outline.

Chapter 1 : The first chapter will deal with the classical ways to handle material failure before focusing on the continuum damage framework. The issues associated with this type of model, along with the classical ways to handle them, will then be studied after defining what will be considered here as the properties of a "good" damage model. It will end by presenting the eikonal and eikonal-based formulation, focusing on how to get the gradient-type model considered here.

Chapter 2 : The second chapter will focus on the non-intrusive implementation in the Abaqus software of gradient-type formulations, including the eikonal-based gradient. Using a dissipation-based driving strategy, this implementation will then be used to assess the properties of the considered formulations.

Chapter 3 : The third chapter will focus on the study of an isotropic damage model and an isotropic damage-plastic model to see how plasticity's introduction affects material behaviour. After conducting this study on a material point, it will deal with the influence of plasticity on both localisation and structural response for a bar submitted to tension.

Chapter 4 : The fourth chapter will deal with the variational formulation associated with the previous isotropic damage and damage-plastic models coupled with the eikonal formulation before focusing on their implementation in the OOFEM finite element code.

Chapter 1

Bibliographic study

Contents

This chapter will present an overview of the classical methods that can be used to handle material failure. In particular, it will present what will be considered here as the properties of a good damage model, and help justify the choice of a gradient-type nonlocal formulation with damage-dependent interactions for this study.

1.1 General framework and associated notations

The aim of this part is to present the general framework and notations that will be used throughout the thesis. To do so, it will thus begin with some mathematical notations, before introducing the continuum mechanics framework through a classical example.

1.1.1 General notations

Throughout this thesis, the following conventions will be used when describing scalar or tensorial variables and parameters

- a will stand for a scalar
- $\boldsymbol{A}$ will stand for a first or second order tensor
- $\mathbf{1}$ will stand for the second order identity tensor
- $\mathbb{C}$ will stand for a fourth order tensor
- $\mathbb{I}$ will stand for the fourth order identity tensor

The-so called Einstein index notations will also be used, namely

- u_i will stand for a term of the first order tensor $\boldsymbol{u}$
- σ_{ij} will stand for a term of the second order tensor $\boldsymbol{\sigma}$
- C_{ijkl} will stand for a term of the fourth order tensor $\mathbb{C}$

along with the associated summing convention, giving for indexes going from 1 to 3

$$a_{ii} = a_{11} + a_{22} + a_{23} \tag{1.1}$$

The following time-derivative convention will also be used here,

$$\dot{a} = \frac{\partial a}{\partial t}, \quad \ddot{a} = \frac{\partial^2 a}{\partial t^2}$$

along with the spatial one

$$a_{,x} = \frac{\partial a}{\partial x}, \quad a_{,xy} = \frac{\partial}{\partial y}\left(\frac{\partial a}{\partial x}\right) = \frac{\partial^2 a}{\partial y \partial x}$$

which gives in index notations

$$a_{i,j} = \frac{\partial a_i}{\partial x_j}, \quad a_{i,jk} = \frac{\partial}{\partial x_k}\left(\frac{\partial a}{\partial x_j}\right) = \frac{\partial^2 a}{\partial x_k \partial x_j}$$

where x_j is the j^{th} spatial coordinate.

In addition to these general conventions, the following notations will also be adopted for linear algebra

- $\mathrm{tr}(\boldsymbol{A})$ will denote the trace of the second order tensor $\boldsymbol{A}$, i.e. $\mathrm{tr}(\boldsymbol{A}) = A_{ii}$
- ${}^t\boldsymbol{A}$ will denote the transpose of the second order tensor $\boldsymbol{A}$, i.e. ${}^tA_{ij} = A_{ji}$
- $\boldsymbol{A} \otimes \boldsymbol{B}$ will stand for the tensorial product defined by

$$\mathbb{C} = \boldsymbol{A} \otimes \boldsymbol{B} \Leftrightarrow C_{ijkl} = A_{ij}B_{kl}$$

- $\boldsymbol{A}\underline{\otimes}\boldsymbol{B}$ will stand for the tensorial product defined by

$$\mathbb{C} = \boldsymbol{A}\underline{\otimes}\boldsymbol{B} \Leftrightarrow C_{ijkl} = \frac{1}{2}\left(A_{ik}B_{jl} + A_{il}B_{jk}\right)$$

The following notations will also be adopted for the parameters describing the properties of an undamaged material

- E will stand for a material's Young modulus
- ν will stand for its Poisson ratio
- λ and μ will stand for the Lamé's parameters
- ρ will stand for its density

Finally, the following notations will be used for the divergence and gradient operators

- $\nabla \cdot \boldsymbol{A}$ will denote the divergence of the tensor $\boldsymbol{A}$, $\mathrm{div}(\boldsymbol{A})$
- ∇B will denote the gradient of the scalar B, $\mathrm{grad}(B)$
- $\nabla \boldsymbol{A}$ will denote the gradient of the tensor $\boldsymbol{A}$, $\mathrm{grad}(\boldsymbol{A})$

1.1.2 Continuum mechanics framework

First, let us consider a deformable and originally homogeneous and isotropic media Ω, along with its boundary $\partial\Omega$. In the framework of continuum mechanics that will be used here, three kinds of loading can be applied to it (Figure 1.1)

- imposed displacement $\boldsymbol{u}_d$ on part of the boundary $\partial\Omega_u$
- applied surface force $\boldsymbol{T}_d$ on part of the boundary $\partial\Omega_F$
- applied volume force $\boldsymbol{f}_v$ throughout the entire body Ω

Let us then denote $\boldsymbol{u}(M)$ the displacement at a given point M of Ω, and $\boldsymbol{\sigma}(M)$ the stress state, represented by Cauchy's tensor, at this point. The loadings introduced would then induce the following boundary conditions on $\boldsymbol{u}$ and $\boldsymbol{\sigma}$

$$\boldsymbol{u}(M) = \boldsymbol{u}_d(M), \quad \forall M \in \partial\Omega_u \tag{1.2}$$

$$\boldsymbol{\sigma}(M) \cdot \boldsymbol{n}(M) = \boldsymbol{T}_d(M), \quad \forall M \in \partial\Omega_F \tag{1.3}$$

where $\boldsymbol{n}(M)$ stands for the normal to $\partial\Omega_F$ at point M.

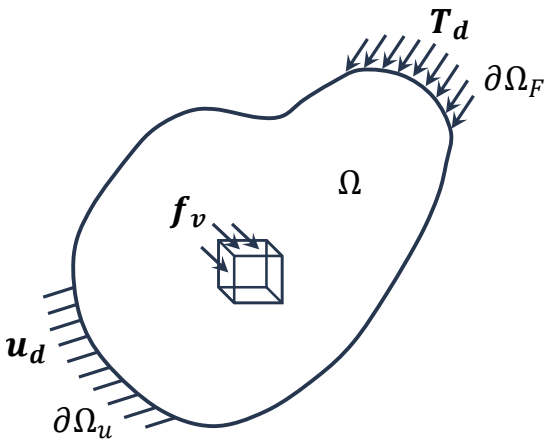

Figure 1.1: Volume forces and boundary conditions applied to Ω

In this framework, the equilibrium equation writes

$$\nabla \cdot \boldsymbol{\sigma} + \boldsymbol{f}_v = \rho \ddot{\boldsymbol{u}} \tag{1.4}$$

and becomes for a quasi-static modelling, i.e. neglecting the inertia terms,

$$\nabla \cdot \boldsymbol{\sigma} + \boldsymbol{f}_v = \boldsymbol{0} \tag{1.5}$$

At this point, to solve the mechanical problem, i.e. to find a displacement field $\boldsymbol{u}$ such that equations (1.5), (1.2) and (1.3) are verified, one needs to define the link between the stress field $\boldsymbol{\sigma}$ and the displacement field $\boldsymbol{u}$. Under the small strain assumption, $\boldsymbol{\sigma}$ is usually computed from the strain tensor $\boldsymbol{\varepsilon}$, defined as the symmetric part of the displacement's gradient.

It is worth noting that, for the problem to be well-posed, both force and displacement cannot be imposed simultaneously, i.e. $\partial\Omega_u \cap \partial\Omega_F = \emptyset$. One can also note that, when no condition is imposed in part of the boundary, it will be considered as a free boundary, i.e. $\boldsymbol{\sigma} \cdot \boldsymbol{n} = \boldsymbol{0}$, thus ensuring that $\partial\Omega_u \cup \partial\Omega_F = \partial\Omega$.

The problem on which this thesis focuses is, in this general framework, how can one predict the occurrence and the propagation of cracks within Ω.

1.2 Fracture mechanics

This part will first deal with the most classical way to address structural failure, namely the linear elastic fracture mechanics approach.

1.2.1 Experimental observations and notations

Before moving to the theoretical aspects of this problem, this part will focus on qualitative results to get some hindsight on what can be expected.

A well-known result of fracture mechanics, which can be observed with photoelasticity, is the fact that stresses tend to concentrate at the crack tip. Without

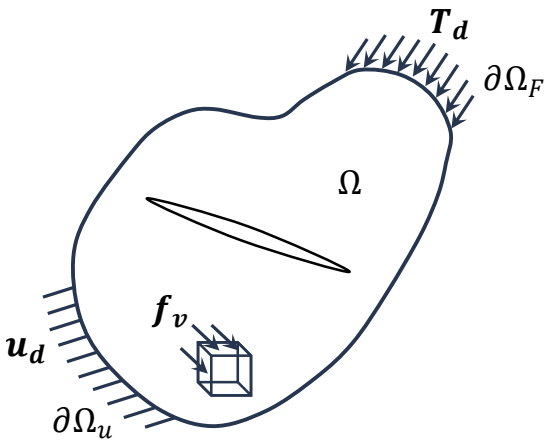

Figure 1.2: General case of a crack embedded in an elastic solid Ω

any knowledge regarding the associated criterion, one can still get an idea on the crack path since it can be expected to go through areas of higher tensile stress.

A simple $2D$ experiment, stretching a sheet of paper with embedded notches, both horizontal and tilted, can be conducted to assess the relevance of this natural assumption. A kinking will then be observed in the crack path following the tilted notch in order to realign with a horizontal propagation. One can thus observe that, beside the fact that a notched sheet is much easier to tear than an virgin one, a crack will tend to propagate under an opening mode.

On the other hand, when considering a $3D$ problem with an out-of-plane loading such as a tube with a horizontal crack submitted to torsion, the crack can be expected to propagate horizontally in a tearing mode instead of an opening one.

This part will present the most classical way to explain these observations, namely the linear elastic fracture mechanics.

1.2.2 Principle and general ideas

Considering the general case of a crack embedded in an elastic solid (Figure 1.2), the goal of the linear elastic fracture mechanics is to answer the three following questions

- under which condition
- in which direction
- along which distance

will the crack propagate.

One can note that any crack can be seen as a combination of three elementary cracking modes which can be defined by the relative displacements of the crack's lips with respect to the crack plane, or by the stress state, as

- mode I, or opening mode: tensile stress normal to the crack plane
- mode II, or sliding mode: in-plane shear stress

- mode III, or tearing mode: out-of-plane shear stress

It can be shown that, in a linear elastic media, stresses tend to diverge in $1/\sqrt{r}$ near the crack tip, where r is the distance to the tip, where the material will damage. This damaging area, located behind the so-called process-zone, corresponds to the area where the material response is no longer elastic, and where the crack will propagate.

In the case of brittle fracture, this zone remains rather small, and the material can be seen as mainly elastic, with a stress amplification near the crack tip. This local amplification can be modelled using the three stress intensity factors corresponding to each cracking modes.

1.2.3 Crack propagation criterion

While a crack can propagate continuously, at a rate proportional to the loading, e.g. in fatigue, we will here focus on the instantaneous propagation associated with brittle fracture. In that case, one needs to define a threshold beyond which the crack will propagate.

Such a criterion was first proposed by Griffith [Griffith, 1921], and is still widely used. It states that a given crack will propagate if and only if the energy $\mathcal{G}$ released by the crack propagation is greater than the fracturing energy G_c needed to create new surfaces. Simply put, on gets

$$\begin{cases} \mathcal{G} < G_c \Rightarrow \text{no crack propagation} \\ \mathcal{G} = G_c \Rightarrow \text{the crack propagates} \end{cases} \tag{1.6}$$

It is worth noting that this only provides a global energy-based criterion for crack propagation, with no indication on how it will propagate locally. To address this issue, Irwin later proposed [Irwin, 1957] a link between the energy release rate $\mathcal{G}$ and the Stress Intensity Factors in order to get a more local criterion. This later allowed him to propose a new propagation criterion for mode I fracture based on the stress intensity factors [Irwin, 1958], thus introducing a new material property: the fracture toughness K_c.

This new criterion stated that, for a given crack to propagate in mode I, the associated stress intensity factor K_I had to overcome the local material toughness, i.e.

$$\begin{cases} K_I < K_c \Rightarrow \text{no crack propagation} \\ K_I = K_c \Rightarrow \text{the crack propagates} \end{cases} \tag{1.7}$$

It is worth noting that, since this local criterion only considers the stress intensity factor associated with mode I, it cannot predict any kinking linked to mixed mode propagation.

In the end, though both criteria can be used to determine whether a crack will propagate or not, they are not sufficient to predict the direction of its propagation

1.2.4 Prediction of the crack path

Now that we have seen how to predict whether an existing crack will propagate or not, it is important to know how, and especially where, it will propagate. The question of crack branching being an important issue, three main criterion have been proposed to handle it, namely

- the maximum tangential stress [Erdogan and Sih, 1963]
- the maximum energy release rate [Erdogan and Sih, 1963]
- the principle of local symmetry [Gol'dstein and Salganik, 1974]

The first criterion, proposed by Erdogan and Sih [Erdogan and Sih, 1963], is based on the idea that the crack opening is mainly induced by the tangential stress $\sigma_{\theta\theta}$. Assuming that the crack is more likely to propagate in the direction that favors its opening, this criterion states that it will tend to realign with the direction that maximizes the tangential stress.

A second criterion, based on similar considerations but using Griffith criterion instead of tangential stress, was also proposed by Erdogan and Sih [Erdogan and Sih, 1963]. It states that the crack will most likely propagate in the direction where the energy release rate first reaches the fracture energy, and that it will thus tend to realign with the direction that maximizes $\mathcal{G}$.

The last criterion, proposed by Gol'dstein and Salganik [Gol'dstein and Salganik, 1974] is based on the principle of local symmetry, and states that a crack will tend to realign with the direction for which K_{II} will be equal to 0. Though the physical ground for this criterion is not as straightforward as for the others, its main advantage comes from the fact that it is the only one who predicts $\mathcal{C}^\infty$ crack paths.

All those criteria were studied and compared in [Amestoy and Leblond, 1992] and later in [Leblond, 2003]. They did not show quantitative differences, especially compared to the experimental uncertainties.

It is worth noting that energy-based criteria can also be used to predict crack propagation, including the cracking path, in architectured material [Glacet et al., 2018], namely by considering the energy stored in each beam of a given lattice.

Using the linear elastic fracture mechanics, one can thus predict whether an existing crack will propagate and, using an additional numerical treatment, whether the propagation crack will exhibit branching. However, it cannot be used to model a crack initiation, nor the associated progressive loss of stiffness due to the appearance and coalescence of micro defects.

To address this issue, a new variational theory of fracture mechanics was thus proposed by Francfort and Marigo in [Francfort and Marigo, 1998]. Following the work of [Ambrosio and Tortorelli, 1990, Ambrosio and Tortorelli, 1992] on the regularization of Mumford Shah image processing problem, an approximation of this formulation was then proposed in [Bourdin et al., 2000]. It was later shown

to converge toward fracture mechanics, and one can note that its formulation presents some similarities with that of a nonlocal damage model. Besides, due to both its physical background and their strong similarities, it can serve as a physical justification for the Phase-Field formulations presented part 1.4.3.

1.3 Local damage formulations and associated issues

This part introduces the local damage model used in this thesis, identifies the issues associated with such a model, and then specifies the properties that could be expected of what will be called here a "good" damage model.

Unlike the linear elastic fracture mechanics which only addresses the propagation of existing cracks, the continuum damage framework was developed to address the progressive loss of stiffness induced by the appearance and coalescence of micro-cracks and micro-defects. The first concept of a continuous damage variable was first proposed by Kachanov ([Kachanov, 1958]) for creep in metallic alloys, and later expanded by other authors [Rabotnov, 1969, Lemaitre, 1971, Chaboche, 1978, Marigo, 1981, Mazars, 1984].

This part will focus on a simple example, in order to get an intuitive definition of damage before moving to a more rigorous and theoretical approach.

Let us consider the simple case of a cube with embedded micro-cracks. It is quite straightforward that, when studying the response to a tensile load F, one would need to take into account the influence of the cracked surface on the stress.

As it is, noting S the total cross-section of the cube, and S_D the cracked area, the stress seen locally by the material would no longer be $\sigma = F/S$, but rather

$$\tilde{\sigma} = \frac{F}{S - S_D} = \frac{F}{S\left(1 - \frac{S_D}{S}\right)} \tag{1.8}$$

Noting D the relative importance of the cracked area with respect to the total section, the so-called effective stress seen by the material writes:

$$\tilde{\sigma} = \frac{\sigma}{1 - D} \tag{1.9}$$

Using the principle of strain equivalence

$$\begin{cases} \tilde{\sigma} = E\varepsilon^e \\ \sigma = \tilde{E}\varepsilon^e \end{cases} \tag{1.10}$$

where ε^e stands for the elastic strain, and the effective elastic stiffness $\tilde{E}$ can thus be defined as

$$\tilde{E} = (1 - D)E \tag{1.11}$$

This simple example allowed for an intuitive definition of damage D associated with the micro-cracks density, along with a modelling of the material's associated

loss of stiffness. The principle of effective stress [Lemaitre, 1971, Lemaitre and Chaboche, 1985] was also generalized to more complex cases such as anisotropic damage [Chaboche, 1978, Chaboche, 1979, Lemaitre and Desmorat, 2005].

1.3.1 Local isotropic damage model

3D formulation

The local damage model considered here is a modified version of Mazars [Mazars, 1984] model which represents a material with an isotropic elastic behaviour and isotropic damage. It is worth noting that it does not take plasticity nor thermal expansion into account. The associated stress-strain law

$$\boldsymbol{\sigma} = \tilde{\mathbb{C}} : \boldsymbol{\varepsilon} = (1 - D)\ \mathbb{C} : \boldsymbol{\varepsilon} \tag{1.12}$$

is based on Hooke's law extended to damage, and can be rewritten using Lamé's coefficients (λ, μ) as

$$\boldsymbol{\sigma} = \lambda(1 - D)\mathrm{tr}\,(\boldsymbol{\varepsilon})\,\mathbf{1} + 2\mu\,(1 - D)\,\boldsymbol{\varepsilon} \tag{1.13}$$

Here, $\mathbb{C}$ is the stiffness of the undamaged material, $\tilde{\mathbb{C}}$ the effective stiffness of the damaged material and D is the damage variable that evolves from 0 to 1.

The evolution of damage is assumed to be driven by Mazars' equivalent strain $\hat{\varepsilon}$, defined as

$$\hat{\varepsilon} = \sqrt{\langle \varepsilon_1 \rangle_+^2 + \langle \varepsilon_2 \rangle_+^2 + \langle \varepsilon_3 \rangle_+^2} \tag{1.14}$$

where ε_1, ε_2 and ε_3 denote the principal strains, i.e the eigenvalues of the strain tensor, and where $\langle \varepsilon_i \rangle_+ = \max(0, \varepsilon_i)$ are the so-called extensions.

Due to irreversibility, the current damage depends on the maximum previously reached value of equivalent strain,

$$\kappa(t) = \max_{\tau \leq t} \hat{\varepsilon}(\tau) \tag{1.15}$$

which ensures that a decrease in equivalent strain does not affect the damage value. Moreover, after a decrease in strain, damage will only begin to grow again when the equivalent strain exceeds its previous maximum value.

The damage evolution law is postulated in the form

$$D \quad = \quad g(\kappa) = \begin{cases} 0 & \text{if } \kappa < \varepsilon_0 \\ 1 - \dfrac{\varepsilon_0}{\kappa} \exp\left(-\dfrac{\kappa - \varepsilon_0}{\varepsilon_f - \varepsilon_0} \right) & \text{if } \kappa \geq \varepsilon_0 \end{cases} \tag{1.16}$$

where ε_0 is the damage threshold taken here equal to 0.03, and ε_f is a damage parameter taken here equal to 0.15.

The damage evolution law and the normalized material response associated with this model are presented in Figure 1.3.

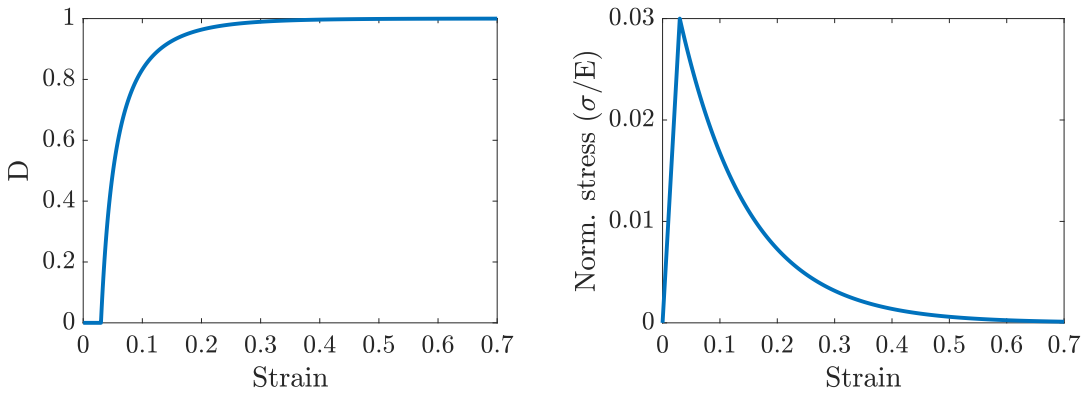

(a) Damage evolution law (b) Stress-strain curve

Figure 1.3: Material behaviour considered here.

1D formulation

To assess the properties of both the local and nonlocal damage models, a $1D$ version of the model presented in the previous part will be considered.

In a one-dimensional setting, the stress-strain law would write

$$\sigma = \tilde{E}\varepsilon = (1 - D)E\varepsilon \tag{1.17}$$

where E is the elastic modulus of the undamaged material, $\tilde{E}$ the effective elastic modulus of the damaged material, and D is still the damage variable that evolves from 0 to 1.

The evolution of damage is still assumed to be driven by Mazars' equivalent strain $\hat{\varepsilon}$, which writes in a $1D$ setting

$$\hat{\varepsilon} = \langle \varepsilon \rangle_+ \tag{1.18}$$

Due to irreversibility, the current damage still depends on the maximum previously reached value of equivalent strain,

$$\kappa(t) = \max_{\tau \leq t} \hat{\varepsilon}(\tau) \tag{1.19}$$

and the damage evolution law remains in the form

$$D = g(\kappa) = \begin{cases} 0 & \text{if } \kappa < \varepsilon_0 \\ 1 - \dfrac{\varepsilon_0}{\kappa} \exp\left(-\dfrac{\kappa - \varepsilon_0}{\varepsilon_f - \varepsilon_0}\right) & \text{if } \kappa \geq \varepsilon_0 \end{cases} \tag{1.20}$$

with $\varepsilon_0 = 0.03$, and $\varepsilon_f = 0.15$.

1.3.2 Classical reference problem and localization phenomenon

Classical reference problem

The reference problem considered here (Figure 1.4) is the classical case of a bar submitted to tension with the isotropic material behaviour described equations

(1.17) to (1.20). A defect (smaller section) has been introduced in the element located at the middle of the bar, in order to trigger bifurcation toward a non-homogeneous solution in the bar.

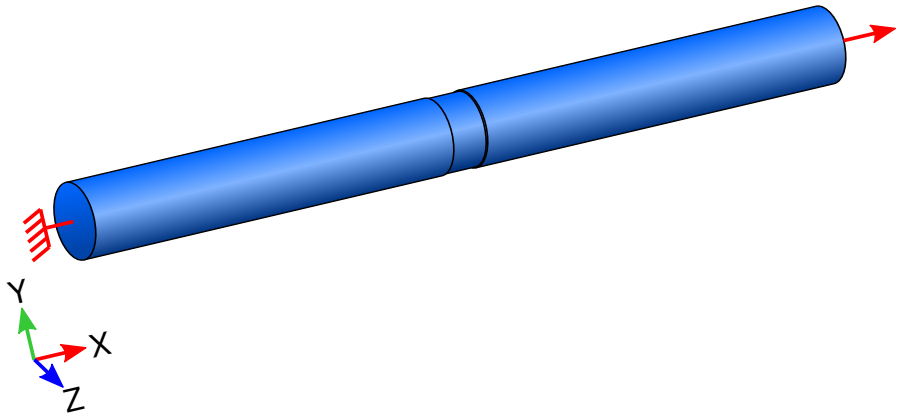

Figure 1.4: Reference one-dimensional tensile test considered here.

This simple reference problem will be used here to highlight the localization phenomenon and the associated issues through classical results. It will also be reused in Chapter 2 to assess the efficiency of the different nonlocal formulations.

Localization phenomenon

In the case presented above (Figure 1.4), one first observes a phase of elastic loading, until damage appears in the weaker part of the bar, inducing softening. From this point, the damaged part of the bar will keep loading and damaging while the rest of the bar is unloading, thus inducing localization of strain and damage.

Even though this phenomenon is physical, it has a major intrinsic drawback: the size of the localization area is not fixed, and the same holds for the energy needed to break the bar. In numerical simulations, damage will tend to localize in a single element, and the solution will thus exhibit a strong and spurious mesh dependency.

This can be observed in Figure 1.5, where the force-displacement curve and the damage profile are plotted for various element sizes. It is worth noting that, in the present 1D setting, only the number of elements used to discretize the geometry was changed, while one would also have to change their orientation for 2D and 3D computations.

As shown in [Hillerborg et al., 1976, Hillerborg, 1978, Pijaudier-Cabot and Bažant, 1987], sensitivity to spatial discretization can be observed through the influence of the mesh size on the response curve (Figure 1.5a). It is thus essential to improve the model to address this issue, for instance through the introduction of an internal length.

1.3.3 Expected properties of a damage model

It is possible, based on what precedes and on the literature, to determine the properties that we would expect from a damage model, defining what would be

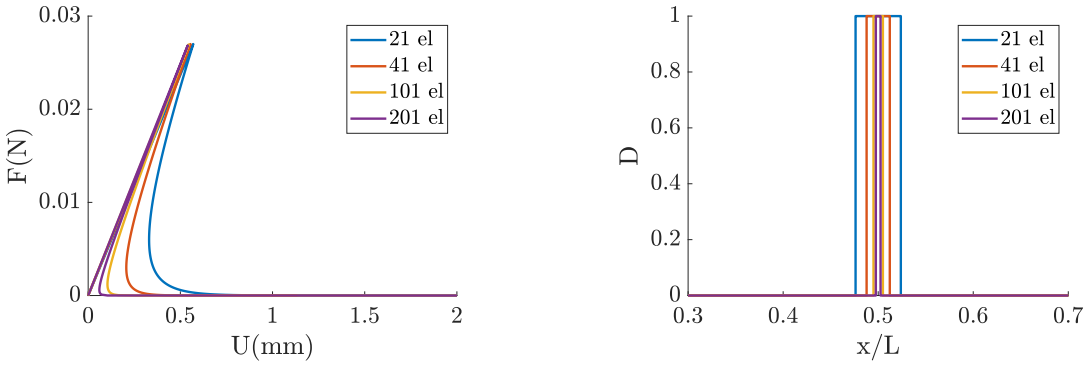

(a) Response curves

(b) Damage profiles

Figure 1.5: Damage localization and mesh dependency.

called thereafter a "good" damage model. It is worth noting that, since the material behaviour remains elastic up to the peak, only the post-peak part of the curve needs to be enhanced by the considered formulation. Other models with inelastic pre-peak behaviour, e.g. diffuse damage, might lead to different requirements. In the end, using a "good" damage model, one should have:

- a realistic behaviour, both before and after the peak [Jirásek, 1998]
  - before the peak: unchanged elastic response
  - after the peak: realistic shape with respect to experiments (stress drop)
- convergence and mesh-independence [Pijaudier-Cabot and Bažant, 1987]
  - convergence toward a solution with a non zero dissipated energy
  - damage spread over a non-zero area
  - low sensitivity to the finite element mesh for a small enough element size
- a highly damaged zone behaving as a crack [Desmorat and Gatuingt, 2007]
  - final zero stress
  - localization in a single element when $D = 1$
  - no interaction through a pseudo-crack (when $D = 1$)
  - existence of a solution with a displacement jump at $D = 1$
- the possibility to implement the model in a non intrusive way in an industrial finite element code [Azinpour et al., 2018, Wangermez et al., 2022]

The last criterion comes from the fact that, for the considered damage model to be of better use, one should be able to use it as easily as possible on any geometry. It is worth noting that, even though they are not discussed here, the issues associated with the boundary conditions remain important, especially in 2D and 3D settings. One can also note that the potential issues linked to damage

initiation [Eringen et al., 1977, Simone et al., 2004], which are tightly linked to the handling of boundaries [Bažant et al., 2010] and existing cracks [Giry et al., 2011], will not be discussed here.

It will now be possible to use these criteria to assess the relevance of the different damage models, especially the nonlocal formulations on which this thesis is focused.

1.4 Nonlocal damage models

This part will first introduce the general framework of nonlocal damage models before focusing on some nonlocal formulations with both fixed and evolving internal length, including a Phase Field formulation. It is worth noting that one could also have chosen to write everything in a thermodynamics framework as was done in [Ganghoffer and de Borst, 2000, Ganghoffer et al., 1999] for nonlocal damage and damage-plastic models.

To take into account the state of the neighbourhood of a material point, one has to replace a local variable by its nonlocal counterpart. In the presence of strain softening, the nonlocal variables are usually those associated with dissipative phenomena, namely damage growth in the framework of continuum damage mechanics. Thus, the possible nonlocal variables are damage and the damage driving variable; details of the nonlocal treatment of course depend on the specific damage model.

In our case, Following the work of [Pijaudier-Cabot and Bažant, 1987] and [Jirásek, 1998], the damage driving variable is the equivalent strain $\hat{\varepsilon}$, thus equations (1.12) and (1.14) still hold while equation (1.15) is replaced by

$$\bar{\varepsilon} = \mathcal{F}(\hat{\varepsilon}) \tag{1.21}$$

$$\kappa(t) = \max_{\tau \leq t} \bar{\varepsilon}(\tau) \tag{1.22}$$

where $\mathcal{F}$ is the nonlocal operator, which can take various forms such as a differential expression or a convolution.

The damage evolution law (1.16) is still used to evaluate damage, but from the maximum value of the nonlocal equivalent strain computed from equation (1.22).

1.4.1 Nonlocal formulations with fixed internal length

Integral-type formulation

As pointed out before, the main idea of the original nonlocal formulation [Pijaudier-Cabot and Bažant, 1987] was to fix the dissipated energy by spreading damage over a non zero and mesh-independent area. This was done by replacing the damage driving variable at a given point by its nonlocal counterpart $\mathcal{F}(\hat{\varepsilon})$, namely its weighted average over a fixed neighborhood centered at this point. Using this formulation, equation (1.21) is specified as

$$\bar{\varepsilon}(\boldsymbol{x}) = \frac{1}{V_0(\boldsymbol{x})} \int_\Omega \hat{\varepsilon}(\boldsymbol{\xi}) \alpha \left(\frac{\|\boldsymbol{x} - \boldsymbol{\xi}\|}{l_c} \right) \mathrm{d}\boldsymbol{\xi} \tag{1.23}$$

$$V_0(\boldsymbol{x}) = \int_\Omega \alpha \left(\frac{\|\boldsymbol{x} - \boldsymbol{\xi}\|}{l_c} \right) \mathrm{d}\boldsymbol{\xi} \tag{1.24}$$

where α is a suitable weight function, typically decreasing with increasing relative distance $\|\boldsymbol{x} - \boldsymbol{\xi}\|/l_c$ and equal to zero when the distance exceeds a certain limit.

It is worth noting that in this case l_c is not a numerical parameter, but rather a characteristic length of the material, supposed to be constant here. It will thus have to be experimentally determined so as to impose the right cracking energy and damage spreading [Pijaudier-Cabot et al., 2001, Le Bellégo et al., 2003].

Despite its qualities, this integral approach brings many numerical difficulties, namely the need to detect each point's neighbours and to evaluate the distance between them in order to compute the nonlocal field. Even though this is not nowadays prohibitive in the general case, such information might not be available in commercial software, especially in the case of a non intrusive implementation. For example, the commercial Abaqus software offers the possibility to compute the average of a given variable at a given point, but only over the connected elements, which would not be sufficient here.

Gradient-type formulations

Part of the drawbacks associated with the nonlocal integral approach could be solved using a related gradient-type approach. This approach was proposed in 1996 by Peerlings et al. ([Peerlings et al., 1996]), based on calculations done in 1987 by Aifantis ([Aifantis, 1987]).

The idea here is to get an equivalent expression of the nonlocal strain (1.23)-(1.24) by replacing the equivalent strain with its expansion in to a Taylor series. This gives, after neglecting the high order terms, the following explicit gradient-type formulation

$$\bar{\varepsilon} = \hat{\varepsilon} + c^2 \ \nabla^2 \hat{\varepsilon} \tag{1.25}$$

where c is an internal length linked to l_c and to the nonlocal weight function α.

However, this formulation is not well suited for numerical implementation since it requires the $\mathcal{C}^1$ continuity of the displacement. After additional adjustments of a rather heuristic nature, it gives the more stable implicit gradient-type formulation:

$$\bar{\varepsilon} - c^2 \nabla^2 \bar{\varepsilon} = \hat{\varepsilon} \tag{1.26}$$

which introduces the same order of approximation and the same internal length as equation (1.25), and is much less restrictive regarding displacement properties.

It is worth noting that a more rigorous argument, based on Green's function, was later provided in [Peerlings et al., 2001] to justify the link between the original integral-type formulation and the implicit gradient one. This argument is based on the fact that computing $\bar{\varepsilon}$ as the solution of differential equation (1.26) with appropriate boundary conditions is equivalent to computing it with the integral formulation (1.23)-(1.24), using the Green's function of the boundary value problem as weight function.

Moreover, it was shown numerically in [Peerlings et al., 1996] that this formulation exhibits regularization properties that are similar to those of the integral formulation. It also has a huge advantage for the purpose of numerical implementation since the associated nonlocal treatment only consists in solving an additional

differential equation. However, the additional degree of freedom tends to increase the global numerical cost, and raises the question of the boundary conditions that need to be applied on $\bar{\varepsilon}$ and $\nabla\bar{\varepsilon}$ in order to ensure the uniqueness of the solution. On this regard, the most common choice is to set $\nabla\bar{\varepsilon} \cdot \boldsymbol{n} = 0$ on the boundary of normal $\boldsymbol{n}$, thus imposing that $\bar{\varepsilon}$ should there be equal to $\hat{\varepsilon}$, which might seem questionable when a crack propagates near the boundary.

Choice of the nonlocal variable

It is worth noting that, although the previous nonlocal formulations were introduced through their application on Mazars equivalent strain, other nonlocal variables could also be considered including damage itself.

This matter was addressed for the nonlocal formulation (1.23)-(1.24) in [Jirásek, 1998], where the author considered different candidates in order to assess their suitability as nonlocal variables. The idea then was to run one-dimensional tensile testings, with different damage models and nonlocal variables, and to study the relevance of the obtained load-displacement curve.

While a common choice might be to use nonlocal strain due to the versatility of such an approach, it suffers from certain disadvantages. As it is, the use of a nonlocal strain tensor is compatible with any damage evolution law since most damage driving variables, such as Mazars equivalent strain and the damage energy release rate, are computed from it. This choice would provide good numerical results so long as one did not use the nonlocal strain to compute the stress, which would wrongly affect the material's elastic response. However, applying a nonlocal treatment to a second order tensor induces a high computational cost since it has to be applied on all of its components.

Similar considerations appeared when using a nonlocal inelastic strain since it provided a versatile formulation with good regularization properties, but induced a prohibitive computational cost.

The goal of this formulation being to address the spurious mesh dependency linked to damage localization, one might consider applying the nonlocal treatment directly to damage itself. This natural solution was thus tested in the one-dimensional setting considered here but, despite the softening, the load asymptotically tends to a finite non-zero value after the peak.

This, so-called stress locking, unrealistic phenomenon was also observed when using nonlocal inelastic stress rate, while the use of nonlocal inelastic stress and inelastic stress computed from nonlocal strain both gave unrealistic response curves with alternating ascending and descending stresses.

In the end, the use of a scalar damage driving variable, namely Mazars equivalent strain and damage energy release rate, provided good numerical results, without the prohibitive computational cost associated with nonlocal strain tensor.

It was thus decided in this thesis to stick to nonlocal scalar damage driving variables, and mainly to Mazars equivalent strain.

1.4.2 Nonlocal formulations with evolving internal length

The previous formulations successfully address the issue of spurious mesh dependency, and were shown to induce convergence toward meaningful solutions with a finite non-zero dissipated energy [Pijaudier-Cabot and Benallal, 1993]. However, despite those advantages, they still suffer from a certain number of deficiencies that need to be addressed.

Shortcomings of the standard nonlocal formulations

The first drawback inherent to integral-type formulations comes from the computation of the nonlocal average near boundary, especially when the averaging area exceeds the material's boundary. A rather straightforward solution [Pijaudier-Cabot and Bažant, 1987] is to re-scale the weight function in order to take the discontinuity into account. However, it was shown in [Borino et al., 2003, Krayani et al., 2009, Bažant et al., 2010] that it is not sufficient, especially when considering homogeneous field who tend to become in-homogeneous by nonlocal averaging near boundaries. Two solutions were proposed to address this issue, namely changing the nonlocal treatment near boundaries [Pijaudier-Cabot and Dufour, 2010, Giry et al., 2010, Giry et al., 2011] or directly introducing a nonlocal boundary layer [Bažant et al., 2010]. It is worth noting that, in the case of a gradient-type formulation, this is directly handled through the natural Neumann boundary condition which is rather simple and practical from a numerical point of view.

It was rightly pointed out in [Pijaudier-Cabot and Dufour, 2010, Giry et al., 2011] that the issues regarding the taking into account of boundaries in the computation of nonlocal treatment is especially true for the free surfaces associated with the presence of cracks. A first solution was also proposed in [Pijaudier-Cabot and Dufour, 2010] where the authors also suggested that one might need to use damage-dependent interactions to properly model cracks by becoming local in their vicinity.

Another drawback linked to the modelling of material failure, and which also concerns both gradient-type [Krayani et al., 2007] and integral-type nonlocal formulation [Jirásek et al., 2004] is the ability to represent the size effect on the fracturing energy. It was thus pointed out in [Jirásek et al., 2004] that, to take such effects into account, one would have to properly model the interactions both around and between the cracks, and that modeling existing notch as predamaged areas might help doing so.

The main issue linked to the computation of nonlocal treatments near a crack comes from the fact that, since each side should behave as a free boundary, no interaction should exist between two points located on opposite sides of it. One way to do this would be to use the visibility check method [Belytschko et al., 1996], and to replace the direct distance between two points by the shortest path that does not cross the crack. This method was successfully used with the element-free Galerkin method [Belytschko et al., 1994, Lu et al., 1994, Belytschko et al., 1995] which is beyond the scope of this thesis, but one might keep the basic idea to improve nonlocal formulations. As it is, such a modification of the interaction

distances would allow the proper modelling of a crack, at least in the nonlocal treatment, without changing the weight function or the nonlocal treatment.

Although the previous comments were made for pre-existing cracks, they remain relevant when dealing with highly damaged zones which are supposed to behave in the same way. This is made even more difficult by the fact that, in this case, no clear boundary exists, and the classical nonlocal treatments are thus applied in the same way as anywhere else. As a consequence, the nonlocal treatments transfer information from fully damaged zones (i.e. cracks) to partly damaged zones, resulting in a spurious expansion of the damage profile at the late stages of failure [Geers et al., 1998].

It is worth noting that, according to [Simone et al., 2004], the use of a nonlocal damage driving variable prevents the proper modelling of damage initiation, even with specific treatments dedicated to handling excising cracks in the nonloal treatment.

Nonlocal formulations with evolving internal length

Nonlocal damage models with evolving internal lengths were thus introduced by a certain number of authors to address those issues. The idea here is to introduce a dependency of the nonlocal treatment with respect to the local material's state in both integral-type and gradient-type formulations.

In the case of integral-type formulations based on the one proposed in [Pijaudier-Cabot and Bažant, 1987], the general form of the associated nonlocal equation still writes

$$\bar{\varepsilon}(\boldsymbol{x}) = \frac{1}{V_0(\boldsymbol{x})} \int_\Omega \hat{\varepsilon}(\boldsymbol{\xi}) \alpha \left(\frac{\|\boldsymbol{x} - \boldsymbol{\xi}\|}{l_c} \right) \mathrm{d}\boldsymbol{\xi} \tag{1.27}$$

$$V_0(\boldsymbol{x}) = \int_\Omega \alpha \left(\frac{\|\boldsymbol{x} - \boldsymbol{\xi}\|}{l_c} \right) \mathrm{d}\boldsymbol{\xi} \tag{1.28}$$

where l_c is is now a function that may depend on state variables such as stress [Giry et al., 2011], strain or damage [Nguyen, 2011]. In a similar fashion, the general form of a gradient-type formulation based of the one proposed in [Peerlings et al., 1996] writes

$$\bar{\varepsilon} - a \, \nabla \cdot (b \, \nabla \bar{\varepsilon}) = \hat{\varepsilon} \tag{1.29}$$

where a and b are functions that may depend on state variables such as stress [Vandoren and Simone, 2018], strain [Geers et al., 1998] or damage.

The need for such a formulation was first pointed out in [Geers et al., 1998] as a mean to avoid the spurious expansion of the damage profile in the late stages of damage. The authors thus proposed a strain-based gradient-type damage model where the nonlocal activity, i.e. the internal length, was determined from the local strain. The idea was that the nonlocal treatment is not needed when the material behaves in an elastic way, but needs to be activated on the occurrence of damage

to handle its localization and prevent spurious mesh dependency. The associated internal length would then increase from 0 in an unloaded media to the value c when Mazars equivalent strain would be greater or equal to the damage threshold. Other gradient-type formulations were later proposed based on similar considerations, using either an improved strain-dependency [Saroukhani et al., 2013] or a stress dependency [Vandoren and Simone, 2018] to drive the internal length's evolution.

Integral-type formulations, using the local stress [Giry et al., 2011] or damage [Nguyen, 2011] to activate the nonlocal treatment were also proposed based on similar considerations.

It is worth noting that, while they address the spurious expansion of damage profile and allow the proper taking into account of cracks and boundaries in the nonlocal treatment, the strain-based [Geers et al., 1998, Saroukhani et al., 2013] and damage-based [Nguyen, 2011] formulations do not suppress the interactions accross a highly damaged zone.

One can also note that the use of anisotropic internal length allows the stress-based formulations [Giry et al., 2011, Vandoren and Simone, 2018] to properly handle the vicinity of boundaries through stress redistribution, and might help cutting nonlocal interactions across a highly damaged zone.

To address this issue, a new nonlocal formulation using damage-dependent interactions motivated by internal time was proposed in [Desmorat and Gatuingt, 2007, Desmorat and Gatuingt, 2010] and will be detailed in Part 1.6. This thesis will thus focus on the implementation and study of the gradient-type formulation that was later derived from it in [Desmorat et al., 2015].

1.4.3 Phase-Field formulation

Another way to handle progressive material failure would be, following [Pons and Karma, 2010, Miehe et al., 2010b, Miehe et al., 2010a, Miehe et al., 2015] to use the framework of phase-field modelling.

The idea of such formulations is to use an auxiliary field variable d to describe the crack topology. In the particular case of an infinite bar with a sharp crack embedded at $x = 0$, this variable would write

$$d(x) = \begin{cases} 1 & \text{if } x = 0 \\ 0 & \text{elsewhere} \end{cases} \tag{1.30}$$

Due to the similarities between this crack field variable and damage, one might consider defining it as

$$d(x) = \exp\left(-\frac{|x|}{l_d}\right) \tag{1.31}$$

which introduces a more diffuse and realistic representation of the crack topology, and the area around it since

$$d(0) = 1 \text{ and } \lim_{|x|\to\infty|} d(x) = 0 \tag{1.32}$$

It is worth noting that this approach introduces a regularization similar to the one associated with nonlocal models since the size of the damaged zone is fixed by the internal length l_d. Moreover, such a variable would be solution to the problem

$$d(x) - {l_d}^2 d''(x) = 0, \forall x \in \mathbb{R} \tag{1.33}$$

which is the Euler equation of the variational formulation

$$d = \arg\left\{\inf_{d\in W}\left(\frac{1}{2}\int_{\mathbb{R}}\left(d^2 + {l_d}^2 d'^2\right)\mathrm{d}V\right)\right\} \tag{1.34}$$

where $W = \left\{d \mid d(0) = 1 \text{ and } \lim_{|x|\to\infty|} d(x) = 0\right\}$.

This condition can be generalized in multiple dimensions as

$$d = \arg\left\{\inf_{d\in W}\left(\int_{\mathbb{R}}\gamma\left(d, \nabla d\right)\mathrm{d}V\right)\right\} \tag{1.35}$$

where γ, the crack surface density function per unite volume of the solid, writes

$$\gamma\left(d, \nabla d\right) = \frac{1}{2l}d^2 + \frac{l}{2}|\nabla d|^2 \tag{1.36}$$

A possible choice of a dissipation function ϕ, taking into account the evolution of the crack surface [Miehe et al., 2010b], is then

$$\phi\left(d, \nabla d; \dot{d}, \nabla\dot{d}\right) = \left(\frac{G_c}{l_d}d\right)\dot{d} + \left(G_c l \nabla d\right)\nabla\dot{d} \tag{1.37}$$

where G_c is the fracturing energy introduced in Part 1.2.

A classical choice for the free energy density, taking into account the crack closure under compression, is then

$$\begin{aligned}\psi\left(\boldsymbol{\varepsilon}, d\right) = \left(1-d\right)^2\left[\frac{\lambda}{2}\langle\mathrm{tr}\left(\boldsymbol{\varepsilon}\right)\rangle_+^2 + \mu\ \mathrm{tr}\left(\langle\boldsymbol{\varepsilon}\rangle_+^2\right)\right] \\ + \frac{\lambda}{2}\langle\mathrm{tr}\left(\boldsymbol{\varepsilon}\right)\rangle_-^2 + \mu\ \mathrm{tr}\left(\langle\boldsymbol{\varepsilon}\rangle_-^2\right)\end{aligned} \tag{1.38}$$

It is worth noting that this choice of a convex function in d ensures that the tangent operator will be equal to 0 when $d = 1$.

The stress then writes

$$\begin{aligned}\boldsymbol{\sigma} = \frac{\partial\psi}{\partial\boldsymbol{\varepsilon}} = \left(1-d\right)^2\left[\lambda\langle\mathrm{tr}\left(\boldsymbol{\varepsilon}\right)\rangle_+\mathbf{1} + 2\mu\langle\boldsymbol{\varepsilon}\rangle_+\right] \\ + \left[\lambda\langle\mathrm{tr}\left(\boldsymbol{\varepsilon}\right)\rangle_-\mathbf{1} + 2\mu\langle\boldsymbol{\varepsilon}\rangle_-\right]\end{aligned} \tag{1.39}$$

and, due to energy balance, the crack phase-field variable is indirectly defined through

$$\frac{G_c}{l_d}\left[d - {l_d}^2\nabla^2 d\right] = 2\left(1-d\right)Y \tag{1.40}$$

where Y is the usual driving variable defined as

$$Y = \lambda \langle \mathrm{tr}\,(\boldsymbol{\varepsilon}) \rangle_+^2 + 2\mu\ \mathrm{tr}\left(\langle \boldsymbol{\varepsilon} \rangle_+^2 \right) \tag{1.41}$$

To ensure crack irreversibility, i.e. $\dot{d} \geq 0$, one needs to replace Y with its maximum value over time, Y_M. The phase-field equation (1.40) would then become

$$\frac{G_c}{l_d} \left[d - {l_d}^2 \nabla^2 d \right] = 2\,(1-d)\,Y_M \tag{1.42}$$

where, due to the right hand side of the equation, the shape of d is no longer governed only by (1.33), but also by the local material history.

Though they were not constructed in the same way, this formulation is known to be quite similar to the numerical implementation of the variational approach to fracture [Francfort and Marigo, 1998, Bourdin et al., 2000, Tanné et al., 2018] which is consistent with Griffith theory. An alternative way to obtain similar formulations would be, following the work done by [Mielke, 2003] and [Jayet, 2021], to use an approach based on pseudo-potential to ensure the irreversibility of damage.

It is worth noting that all those formulations are also similar to nonlocal damage models, the main difference being that in the phase-field approaches both the evolution law and the nonlocal treatment are usually combined in a single equation, namely (1.42) for the present model.

1.5 Bounded rate damage model

One of the features that could be expected from a damage model, whether local or nonlocal, is the ability to model the rate dependency of a material's behaviour.

We will here focus on the so-called bounded rate damage models [Allix and Deü, 1997, Allix et al., 2003, Guimard et al., 2009], and their nonlocal counterpart [Desmorat et al., 2010a], which were developed to take into account this dependency. Models with similar visco-damage features were also obtained within the thermodynamic framework [Dubé et al., 1996], but are beyond the scope of this work.

1.5.1 Local bounded rate damage models

The idea of such models is to rewrite the damage evolution law in order to ensure that the damage evolution rate does not exceed a given value.

Since they were initially developed for laminated composites, such formulations were first proposed for two damage models, namely a $1D$ damage model and a damage mesomodel taking the composite ply behaviour into account. The key point here is that an increase of the damage energy release rate does not lead to an instantaneous increase of damage.

Initial unidirectional damage model

Following the works of [Ladeveze and Lemaitre, 1984] and of [Marigo, 1981], the unidirectional damage model proposed in [Allix and Deü, 1997] was defined through the free energy density

$$\psi(\varepsilon, D) = \frac{1}{2}\left[(1-D)E\langle\varepsilon\rangle_+^2 + E\langle\varepsilon\rangle_-^2\right] \tag{1.43}$$

giving

$$\sigma = \frac{\partial\psi}{\partial\varepsilon} = (1-D)E\langle\varepsilon\rangle_+ + E\langle\varepsilon\rangle_- \tag{1.44}$$

$$Y = \frac{\partial\psi}{\partial D} = E\langle\varepsilon\rangle_+^2 \tag{1.45}$$

Then, while the unbounded damage model handles damage evolution in a rather classical way

$$\kappa(t) = \max_{\tau\leq t} Y(\tau) \tag{1.46}$$

$$g(\kappa) = \frac{\sqrt{\kappa} - \sqrt{Y_0}}{\sqrt{Y_c}} \tag{1.47}$$

$$D = \begin{cases} \langle g(\kappa)\rangle_+ & \text{if } D < 1 \\ 1 & \text{else} \end{cases} \tag{1.48}$$

where Y_0 is the damage threshold and Y_c a parameter governing the damage evolution, the bounded damage model only deals with $\dot{D}$ up to $D = 1$, writing

$$g(Y) = \frac{\sqrt{Y} - \sqrt{Y_0}}{\sqrt{Y_c}} \tag{1.49}$$

$$\begin{cases} \dot{D} = \dot{D}_\infty\left[1 - \exp\left(-k\langle g(Y) - D\rangle_+\right)\right] & \text{if } D < 1 \\ D = 1 & \text{else} \end{cases} \tag{1.50}$$

where $\dot{D}_\infty$ is the maximum damage rate, and k a parameter characterizing the delay effect on damage.

It is worth noting that, in this case, the irreversibility of damage is introduced in equation (1.50) through the Macauley brackets around $g(Y) - D$.

Application to the damage model considered here

Using similar considerations, this dynamics treatment could also be applied to the damage model considered here (1.13)-(1.16).

While equations (1.13) and (1.14) defining the stress and the equivalent strain would remain unchanged, those handling damage irreversibility (1.15) and evolution (1.16) would have to be replaced by

$$\begin{cases} \dot{D} = \dot{D}_\infty\left[1 - \exp\left(-k\langle g(\hat{\varepsilon}) - D\rangle_+\right)\right] & \text{if } D < 1 \\ D = 1 & \text{else} \end{cases} \tag{1.51}$$

where g would still be defined as

$$g(\hat{\varepsilon}) = \begin{cases} 0 & \text{if } \hat{\varepsilon} < \varepsilon_0 \\ 1 - \dfrac{\varepsilon_0}{\hat{\varepsilon}} \exp\left(-\dfrac{\hat{\varepsilon} - \varepsilon_0}{\varepsilon_f - \varepsilon_0}\right) & \text{if } \hat{\varepsilon} \geq \varepsilon_0 \end{cases} \tag{1.52}$$

The $1D$ version of this formulation, constructed by associating equations (1.51)-(1.52) to (1.17)-(1.18) instead of (1.13)-(1.14), was implemented in Abaqus during this PhD, and numerical simulations were conducted to assess the influence of the bounded-damage treatment on the considered model.

First, simulations using only 3 elements were conducted to study the influence of the bounding rate parameter $\dot{D}_\infty$ on the material behaviour in the absence of snap-back instabilities. As expected, one can see in Figure 1.6a, the bounded-rate treatment tends to slow damage evolution, thus increasing the energy dissipated through material failure.

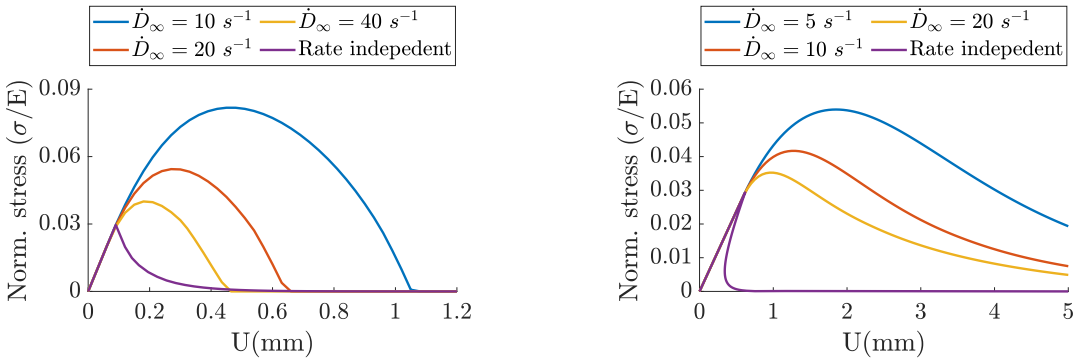

(a) With 3 elements

(b) With 21 elements

Figure 1.6: Influence of the bounded rate treatment on the isotropic damage model.

Computations were also conducted with a finer mesh (21 elements) to study its influence in presence of snap-back instabilities. As one can see in Figure 1.6b, the reduction of damage evolution rate tends to stabilize the response by increasing the dissipated energy. The idea of stabilizing the response curve by introducing a time-dependence in the materials behavior is worth noting, and will be used in Part 2.3.1.

It was shown in [Desmorat et al., 2010a] that, as expected, applying the bounded-rate treatment on a given damage model for concrete enabled the modelling of this material strain-rate effect on damage evolution. It also addressed the issue of spurious mesh dependency under dynamic loading, bot not in quasi-statics. This is consistent with the link between a bounded rate and an internal length in dynamics presented in [Allix et al., 2003] for a dynamic loading.

It was thus proposed to use a nonlocal bounded rate damage model in order to get a proper modeling under both quasi-static and dynamic loading. While this look quite promising, one should pay attention to the fact that, in the aforementioned articles such as [Allix and Deü, 1997] and [Allix et al., 2003], the value of

$g(Y)$ used in the bounding function could go way beyond 1, which here is not true for $g(\hat{\varepsilon})$.

1.5.2 Nonlocal bounded rate damage model

The principle of the proposed formulation is to replace the damage driving variable in the bounded-rate equation, (1.50) with the present model, by its nonlocal counterpart. By doing so, one would first ensure the spatial regularization of the damage-driving variable through the nonlocal treatment, before introducing the strain rate effect.

Applying those considerations to the bounded damage model presented in Part 1.5.1, and using the general gradient-type formulation (1.29), one would keep equations (1.13) and (1.14) while (1.51) and (1.52) would be replaced by

$$\bar{\varepsilon} - a\ \nabla \cdot (b\ \nabla \bar{\varepsilon}) = \hat{\varepsilon} \tag{1.53}$$

$$g(\bar{\varepsilon}) = \begin{cases} 0 & \text{if } \bar{\varepsilon} < \varepsilon_0 \\ 1 - \dfrac{\varepsilon_0}{\bar{\varepsilon}} \exp\left(-\dfrac{\bar{\varepsilon} - \varepsilon_0}{\varepsilon_f - \varepsilon_0}\right) & \text{if } \bar{\varepsilon} \geq \varepsilon_0 \end{cases} \tag{1.54}$$

$$\dot{D} = \dot{D}_\infty \left[1 - \exp\left(-k\langle g(\bar{\varepsilon}) - D\rangle_+\right)\right] \tag{1.55}$$

It is worth noting that the model proposed in [Desmorat et al., 2010a] was based on the classical gradient-type formulation (1.26), and thus still exhibited the drawbacks associated with nonlocal damage models with fixed internal length. A model based on a more suited gradient-type formulation, i.e. using the adequate functions a and b, could then be expected to address this issue while keeping both the spatial regularization and the rate dependency of damage evolution.

On can also note that, since the regularisations are applied in a row, the bounded rate treatment will only be effective if it is still needed after the nonlocal one has been applied. An alternative solution could also be to start with the bounded rate treatment, before applying the nonlocal one on the bounded variable.

In such a case, one should probably bound the evolution of the damage-driving variable, instead of damage itself. By doing so, one should still indirectly bound the evolution of damage, while avoiding the issues encountered when applying a nonlocal treatment to damage [Jirásek, 1998].

1.6 Eikonal and eikonal-based formulations

This part will focus on the eikonal and eikonal-based formulations which are at the center of this study. It will start from a brief reminder of the integral-types formulations [Desmorat and Gatuingt, 2007, Desmorat and Gatuingt, 2010, Desmorat et al., 2015], before introducing the new eikonal-based gradient-type formulation that will be implemented and studied in this thesis.

1.6.1 The original time-based integral formulation

A new nonlocal damage model was proposed in 2007 in [Desmorat and Gatuingt, 2007]. It is based on the original integral formulation proposed in [Pijaudier-Cabot and Bažant, 1987], but the distances are replaced by propagation time. The integral formulation with nonlocal equivalent strain is described by

$$\bar{\varepsilon}(\boldsymbol{x}) = \frac{1}{V_0(\boldsymbol{x})} \int_\Omega \hat{\varepsilon}(\boldsymbol{\xi})\, \alpha\left(\frac{\tau_{x\xi}}{\tau_c}\right) \mathrm{d}\boldsymbol{\xi} \tag{1.56}$$

$$V_0(\boldsymbol{x}) = \int_\Omega \alpha\left(\frac{\tau_{x\xi}}{\tau_c}\right) \mathrm{d}\boldsymbol{\xi} \tag{1.57}$$

where $\tau_{x\xi}$ represents the time needed for propagation of a (fictitious) wave between $\boldsymbol{x}$ and $\boldsymbol{\xi}$ in the considered material, possible affected by damage, while τ_c is the propagation time in the undamaged material over the characteristic length l_c.

The key idea of this approach is that, owing to the wave celerity dependency on the material stiffness, the nonlocal treatment will evolve with damage. In the $1D$ case with scalar damage D, this dependency enters through the expression of the effective wave celerity

$$\tilde{c} = \sqrt{\frac{\tilde{E}}{\rho}} = \sqrt{\frac{(1-D)E}{\rho}} = \sqrt{1-D}\; c_0 \tag{1.58}$$

where E and ρ are respectively the Young modulus and mass density of the material, and $c_0 = \sqrt{E/\rho}$ is the one-dimensional wave celerity without damage.

The $1D$ propagation time τ_{12} between two points x_1 and x_2 such that $x_1 < x_2$ is then given by

$$\tau_{12} = \int_{x_1}^{x_2} \frac{\mathrm{d}x}{\tilde{c}(x)} = \frac{1}{c_0} \int_{x_1}^{x_2} \frac{\mathrm{d}x}{\sqrt{1-D(x)}} \tag{1.59}$$

and tends to increase with damage, thus reducing the influence of a highly damaged zone on the averaging process.

One can also note that, should damage reach 1 at a given point, the wave speed would locally tend to 0, and the propagation time can be expected to blow up, cutting all interactions as one would expect near a crack. It was also shown through dynamics computations [Desmorat and Gatuingt, 2007] that, in a given body, replacing a crack by a fully damaged zone does not affect wave propagation. This means that, as far as the nonlocal treatment is concerned, a highly damaged zone can be expected to behave just as a crack, and one can thus hope to use the eikonal approach to properly handle the damage-fracture transition.

It was also shown in [Desmorat et al., 2015] that this approach gives very good results in terms of damage localization for a bar submitted to tension. As damage grows, the nonlocal treatment tends to be disentangled on each side of the highly damaged zone. This effect cuts all interactions through the crack, thus removing one of the main deficiencies of the classical approach.

In the particular case of 1D simulations, the propagation time can be replaced with an effective "dynamic" distance weighted by damage. The "dynamic" distance

$$\tilde{l}_{12} = c_0 \, \tau_{12} = \int_{x_1}^{x_2} \frac{\mathrm{d}x}{\sqrt{1 - D(x)}} \tag{1.60}$$

between two points x_1 and x_2 (still assuming that $x_1 < x_2$) can be interpreted as the distance covered, in an undamaged material, during the time lapse τ_{12} defined in (1.59). The associated one-dimensional nonlocal formulation is given by

$$\bar{\varepsilon}\,(x) = \frac{1}{V_0(x)} \int_\Omega \hat{\varepsilon}\,(\xi)\, \alpha \left(\frac{\tilde{l}_{x\xi}}{l_c} \right) \mathrm{d}\xi \tag{1.61}$$

$$V_0(x) = \int_\Omega \alpha \left(\frac{\tilde{l}_{x\xi}}{l_c} \right) \mathrm{d}\xi \tag{1.62}$$

However, despite all its qualities, this approach requires the computation of a propagation time at each point and at each time step, which induces a prohibitive computational cost for $2D$ and $3D$ computations.

1.6.2 Alternative integral formulation based on effective distances

It was shown in [Desmorat et al., 2015] that, working under the WKB approximation [Wentzel, 1926, Kramers, 1926, Brillouin, 1926, Bender and Orszag, 1978, Hall, 2013], the influence of damage on wave propagation can be taken into account by considering a space curved by damage (see Appendix A for more details).

This can be modeled using a Riemannian damage-dependent metric $\boldsymbol{g}$, which would define the space curvature, and thus fix the geodesic along which the distance between two points, used for the nonlocal treatment, will have to be computed.

In the case of isotropic damage, the damage-dependent metric tensor writes

$$\boldsymbol{g} = \frac{1}{1 - D} \mathbf{1} \tag{1.63}$$

while, in the case of anisotropic damage represented by a second-order damage tensor [Murakami and Ohno, 1978, Cordebois and F., 1982], it can be defined as

$$\boldsymbol{g} = (\mathbf{1} - \boldsymbol{D})^{-1} \tag{1.64}$$

where $\mathbf{1}$ is the second-order unit tensor.

It can be used to evaluate the effective distance $\tilde{l}$, locally given by its differential

$$\mathrm{d}\tilde{l} = \sqrt{\mathrm{d}\boldsymbol{x} \cdot \boldsymbol{g} \cdot \mathrm{d}\boldsymbol{x}} \tag{1.65}$$

which means that the effective distance between two points A and B will tend to increase in the presence of damage, the shortest path between those two points then corresponding to a curved, damage-dependent, line.

It is worth noting that, since damage is not homogeneous in the general case, neither is the space curvature. As a consequence, identifying the shortest path between two point is not straightforward since it requires the computation and comparison of many trajectories. An analogy could be done with the computation of the shortest path between two points on a sphere, e.g. computing the optimal flight between two cities, though the curvature is then constant.

One can also note that, due to the important space curvature, the shortest path between two points will be more likely to go around a highly damaged zone than across it. This is illustrated in Figure 1.7 where one can see that the shortest way to reach the other side of a "highly curved" area, namely a mountain, might be to go around it rather than over it. As a consequence, since these effective distances are meant to be used in the nonlocal treatment, one could expect all interactions to be cut across highly damaged zones, making them equivalent to cracks.

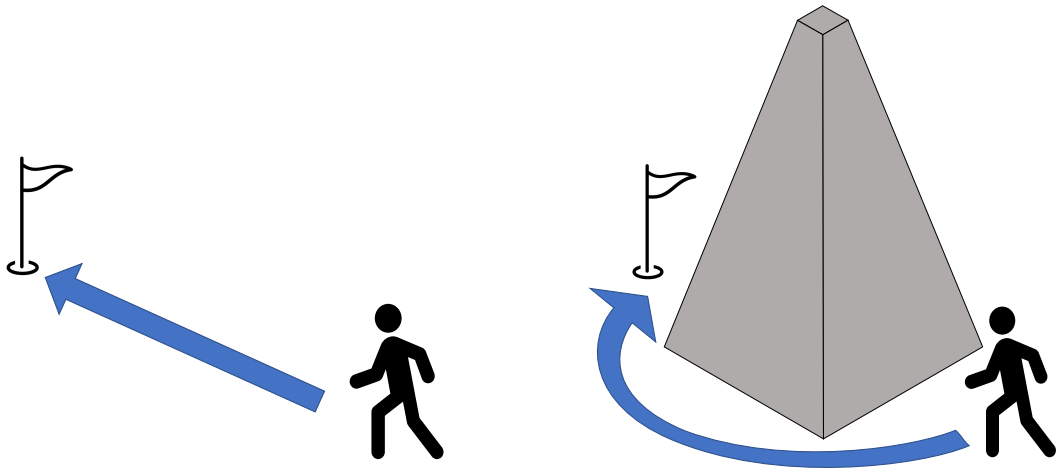

(a) Flat space. (b) "Highly curved" space.

Figure 1.7: Influence of space curvature on the shortest path between two points.

The resulting nonlocal formulation then writes

$$\bar{\varepsilon}(\boldsymbol{x}) = \frac{1}{V_0(\boldsymbol{x})} \int_\Omega \hat{\varepsilon}(\boldsymbol{\xi})\, \alpha\left(\frac{\tilde{l}_{x\xi}}{l_c}\right) \mathrm{d}\boldsymbol{\xi} \tag{1.66}$$

$$V_0(\boldsymbol{x}) = \int_\Omega \alpha\left(\frac{\tilde{l}_{x\xi}}{l_c}\right) \mathrm{d}\boldsymbol{\xi} \tag{1.67}$$

and can be understood as a generalization of (1.61)–(1.62) to multiple dimensions.

The main advantage of this formulation is that it does not require the systematic computation of propagation times, which reduces the numerical cost induced by the nonlocal treatment. However, it still requires the computation of effective distances along geodesics which, as shown in [Rastiello et al., 2018a, Rastiello et al., 2018b], can be done using a dedicated algorithm such as Dijkstra-like algorithms and Fast Marching Methods [Dijkstra, 1959, Tsitsiklis, 1995, Sethian,

1996, Sethian, 1999]. The latter was successfully used with this formulation associated with an isotropic damage model [Rastiello et al., 2018a, Rastiello et al., 2018b].

It is worth noting that, providing one can choose the adequate nonlocal variable, this formulation should be compatible with any damage model, including anisotropic ones. As it is, it was successfully applied in [Jirásek and Desmorat, 2019] to models that combine damage and plasticity, and displayed the expected properties in terms of damage localization. One should also note that, though they are not treated here, special care will have to be taken when dealing with models involving more than one damage variable such as the one used in [Allix and Deü, 1997] for composites.

However, even this formulation still induces a high computational cost since, at each time step, one has to compute all the effective distances for all pairs of interacting Gauss points in the entire curved space. It also suffers from the drawbacks associated with the implementation of integral-type nonlocal formulations, especially since the averaging process is damage-dependent. To address this issue, a gradient-type formulation was derived from this formulation in [Desmorat et al., 2015] and will be studied in the next section.

1.6.3 The associated gradient-type formulation

As already pointed out, one way to address the numerical issues associated with the formulation (1.66)–(1.67) would be to follow the approach presented in [Peerlings et al., 1996], in order to derive an equivalent gradient-type formulation. However, applying it directly to this formulation might not produce the expected results due to the effective lengths computed in the space curved by the damage-dependent metric $\boldsymbol{g}$ introduced before.

It was thus decided in [Desmorat et al., 2015] to write it directly in the curved space in order to deal with a single set of coordinates. As an example, focusing on a two-dimensional setting, one would have an initially flat space that would warp in the presence of damage, the local curvature increasing with the damage level.

The resulting formulation

$$\bar{\varepsilon}(\boldsymbol{x}) = \frac{1}{V_0(\boldsymbol{x})} \int_\Omega \hat{\varepsilon}\left(\tilde{\boldsymbol{\xi}}\right) \alpha\left(\frac{\tilde{l}_{x\xi}}{l_c}\right) \mathrm{d}\tilde{\boldsymbol{\xi}} \tag{1.68}$$

$$V_0(\boldsymbol{x}) = \int_\Omega \alpha\left(\frac{\tilde{l}_{x\xi}}{l_c}\right) \mathrm{d}\tilde{\boldsymbol{\xi}} \tag{1.69}$$

differs from (1.66)–(1.67) by the fact that the integration variable $\tilde{\boldsymbol{\xi}}$ resides in the curved space. The corresponding gradient-type formulation was shown to be described by the differential equation

$$\bar{\varepsilon} - c^2 \frac{1}{\sqrt{\det \boldsymbol{g}}} \nabla \cdot \left(\sqrt{\det \boldsymbol{g}}\, \boldsymbol{g}^{-1} \cdot \nabla \bar{\varepsilon}\right) = \hat{\varepsilon} \tag{1.70}$$

which represents a particular form of (1.29).

This formulation should be easier to implement, provided one can compute the determinant and inverse of the metric tensor $\boldsymbol{g}$. In the case of isotropic damage D, the metric tensor is given by $\boldsymbol{g} = (1-D)\mathbf{1}$ and equation (1.70) reads

$$\bar{\varepsilon} - c^2(1-D)^{3/2}\ \nabla\cdot\left((1-D)^{-1/2}\ \nabla\bar{\varepsilon}\right) = \hat{\varepsilon} \tag{1.71}$$

On the other hand, in the case of unidirectional damage D_1 taken as the only nonzero component of second order variable $\boldsymbol{D}$, the result is slightly different since the metric tensor is given by $\boldsymbol{g} = (\mathbf{1}-\boldsymbol{D})^{-1}$, and one thus gets

$$\bar{\varepsilon} - c^2(1-D_1)^{1/2}\ \nabla\cdot\left((1-D_1)^{1/2}\ \nabla\bar{\varepsilon}\right) = \hat{\varepsilon} \tag{1.72}$$

This is the equation defining $\bar{\varepsilon}$ which will be used for the 1D numerical simulation.

This gradient-type formulation should keep the properties of the integral eikonal formulations while avoiding the issues linked to both the averaging process and the effective distance computation.

This thesis will thus focus on its implementation, and on the assessment of its regularization properties.

Chapter 2

1D non intrusive implementation and analysis of nonlocal isotropic damage models

Contents

After reminding the formulations associated with both the classical and the eikonal-based nonlocal damage models, a phase-field-based gradient-type formulation based on the same isotropic damage model is introduced. The numerical implementation of these three models in the Abaqus software is then presented, along with a suited dissipation-based strategy. These implementations will then be used to assess the efficiency of the considered damage models in a one-dimensional setting.

2.1 Considered damage models

For the non-intrusive implementation to be possible, this chapter will only involve nonlocal gradient-type formulations which, for the sake of simplicity, will be used in a one-dimensional setting.

All the models considered here will be based on the isotropic damage model presented in equations (1.17) to (1.20), and some of the nonlocal and Phase-field formulations introduced in Chapter 1.

2.1.1 Nonlocal gradient-type damage models

1D nonlocal gradient-type damage model using Peerling's formulation

The first nonlocal damage model considered here is based on the classical nonlocal gradient-type formulation introduced in [Peerlings et al., 1996], and is defined in a one-dimensional setting by the following set of equations

$$\sigma = (1-D)E\varepsilon \tag{2.1}$$

$$\hat{\varepsilon} = \langle \varepsilon \rangle_+ \tag{2.2}$$

$$\bar{\varepsilon} - c^2 \frac{\partial^2 \bar{\varepsilon}}{\partial x^2} = \hat{\varepsilon} \tag{2.3}$$

$$\kappa(t) = \max_{\tau \leq t} \bar{\varepsilon}(\tau) \tag{2.4}$$

$$D = \begin{cases} 0 & \text{if } \kappa < \varepsilon_0 \\ 1 - \dfrac{\varepsilon_0}{\kappa} \exp\left(-\dfrac{\kappa - \varepsilon_0}{\varepsilon_f - \varepsilon_0}\right) & \text{if } \kappa \geq \varepsilon_0 \end{cases} \tag{2.5}$$

Though this formulation is quite classical, and its properties well-known, it will serve as a good comparison point to study the two other formulations.

1D nonlocal eikonal-based damage model

The second nonlocal damage model considered here derives from the eikonal-based gradient-type formulation introduced in Part 1.6.3. To remain consisent with the fact that this chapter focuses on what happens in a one-dimensional setting, it was decided here to work with the formulation corresponding to unidirectional damage, namely (1.72). As a consequence, the eikonal-based model considered here is defined, in a one-dimensional setting, by the following set of equations

$$\sigma = (1-D)E\varepsilon \tag{2.6}$$

$$\hat{\varepsilon} = \langle \varepsilon \rangle_+ \tag{2.7}$$

$$\bar{\varepsilon} - c^2 (1-D)^{1/2} \frac{\partial}{\partial x} \left((1-D)^{1/2} \frac{\partial \bar{\varepsilon}}{\partial x} \right) = \hat{\varepsilon} \tag{2.8}$$

$$\kappa(t) = \max_{\tau \leq t} \bar{\varepsilon}(\tau) \tag{2.9}$$

$$D = \begin{cases} 0 & \text{if } \kappa < \varepsilon_0 \\ 1 - \dfrac{\varepsilon_0}{\kappa} \exp\left(-\dfrac{\kappa - \varepsilon_0}{\varepsilon_f - \varepsilon_0} \right) & \text{if } \kappa \geq \varepsilon_0 \end{cases} \tag{2.10}$$

2.1.2 1D nonlocal phase-field-based damage model

In addition to the two nonlocal models presented in the previous part, one might want to study the properties of phase-field formulations such as the one presented in Part 1.4.3. However, as pointed out before, the main drawback of such a formulation is that both evolution and regularization of the phase-field variable, and thus damage, are contained within a single equation. To get a meaningful comparison with nonlocal formulations, one would first have to rewrite it as a nonlocal damage model, before replacing the damage evolution law with the one used for the other formulations while keeping the specific nonlocal treatment.

Considering the rate-independent formulation proposed in [Miehe et al., 2010a] and detailed in Part 1.4.3, one would have in a 1D setting

$$\sigma = (1-d)^2 E \langle \varepsilon \rangle_+ + E \langle \varepsilon \rangle_- \tag{2.11}$$

$$Y_M(t) = \max_{\tau \leq t} \frac{E}{2} \langle \varepsilon(\tau) \rangle_+^2 \tag{2.12}$$

$$d - l_d^2 \frac{\partial^2 d}{\partial x^2} = (1-d) \frac{2 l_d Y_M}{G_c} \tag{2.13}$$

Introducing the intermediate damage variable y, whose evolution law writes

$$y = \frac{2 l_d Y_M}{2 l_d Y_M + G_c} \tag{2.14}$$

in the phase-field formulation, and keeping equation (2.12), one gets

$$\sigma = (1-D) E \langle \varepsilon \rangle_+ + E \langle \varepsilon \rangle_- \tag{2.15}$$

$$d - l_d^2 (1-y) \frac{\partial^2 d}{\partial x^2} = y \tag{2.16}$$

$$D = 1 - (1-d)^2 \tag{2.17}$$

In this case, by analogy with the general nonlocal formulation, equation (2.16) will play the role of (1.21), while (1.20) should be replaced with both (2.14) and (2.17). It is worth noting that, here, the damage evolution law is split in two, and the nonlocal treatment is applied to the intermediate damage variable y. As a consequence, the non-decreasing condition is here applied to the local damage driving variable used to compute y, and not to the nonlocal variable d.

The damage evolution law associated with the corresponding local formulation, obtained by setting $\frac{\partial d}{\partial x} = 0$ and thus $d = y$, then writes

$$y = \frac{2l_d Y_M}{2l_d Y_M + G_c} \tag{2.18}$$

$$D = 1 - (1 - y)^2 \tag{2.19}$$

and should be replaced by

$$y = 1 - \sqrt{1 - g(\kappa)} \tag{2.20}$$

$$D = 1 - (1 - y)^2 \tag{2.21}$$

to get a meaningful comparison with other nonlocal damage models.

Using the nonlocal equation (2.16) associated with the Phase-Field formulation, along with this local damage evolution law, one can get the following gradient-type Phase-Field-based nonlocal damage model

$$\sigma = (1 - D)E\langle\varepsilon\rangle_+ - E\langle\varepsilon\rangle_- \tag{2.22}$$

$$\hat{\varepsilon} = \langle\varepsilon\rangle_+ \tag{2.23}$$

$$\kappa(t) = \max_{\tau \leq t} \hat{\varepsilon}(\tau) \tag{2.24}$$

$$y = \begin{cases} 0 & \text{if } \kappa < \varepsilon_0 \\ 1 - \sqrt{\frac{\varepsilon_0}{\kappa}} \exp\left(-\frac{\kappa - \varepsilon_0}{2\left(\varepsilon_f - \varepsilon_0\right)}\right) & \text{if } \kappa \geq \varepsilon_0 \end{cases} \tag{2.25}$$

$$d - l_d^2 \left(1 - y\right) \frac{\partial^2 d}{\partial x^2} = y \tag{2.26}$$

$$D = 1 - (1 - d)^2 \tag{2.27}$$

whose local counterpart is the same as that of the other nonlocal formulations.

It will thus be used in the rest of this chapter to assess the regularization properties associated with the Phase-Field formulation, and compared to the other nonlocal formulations.

A $3D$ version of this formulation could also be determined following the same steps, but starting directly from the formulation detailed in Part 1.4.3. In the end, keeping equations (1.39), (1.14), (1.15), (2.25) and (2.27), the associated gradient-type equation would then write

$$d - l_d^2 \left(1 - y\right) \nabla^2 d = y \tag{2.28}$$

It is worth noting that this study mainly focuses on the regularization properties of the considered approaches when applied to continuum damage models. The convergence towards fracture mechanics, which has been studied for the Phase-Field approach e.g. in [Bourdin et al., 2008], is beyond the scope of this thesis.

2.2 Non intrusive numerical implementation

This part will detail the non-intrusive implementation in the Abaqus software of the models introduced in the previous part, using a thermo-mechanical analogy, similarly to what was done in [Azinpour et al., 2018].

2.2.1 Implementation possibilities

Before discussing the non-intrusive implementation of the considered nonlocal damage models, one first needs to assess the different implementation possibilities. When using a specific material model in a commercial finite element software such as Abaqus, one can usually encounter three kinds of implementation (Figure 2.1) with different levels of intrusiveness.

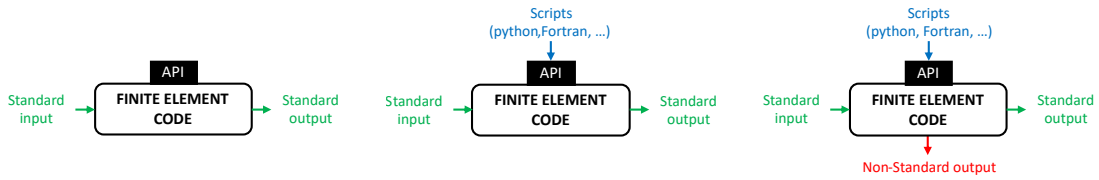

(a) Simple (b) Non intrusive (c) Fully intrusive

Figure 2.1: Implementation possibilities in a finite element code.

The first and most basic implementation (Figure 2.1a) corresponds to a fully graphical use of the software, without any scripts. In this case, the geometry, mesh and boundary conditions are defined through the Graphical User Interface, which is already used to choose the considered material and handle the post-treatment. This only works with materials that are already embedded in the software, including parametric models, and whose behaviour will be computed using only standard inputs and outputs.

More complex implementations (Figure 2.1b), using additional scripts, can also be envisioned, either to handle the computations or to deal with material models that are not already implemented in the finite element code Abaqus. Pythons scripts can thus be used to automate everything that can be done through the graphical user interface, such as defining problems, running simulations and post-treating results. Other scripts, such as the UMAT subroutine, can also be used to define the material behaviour associated with models that are not already implemented in the finite element software. While this subroutine is mainly meant to solve mechanical problems, updating state variables based on both their previous values and the strain increment, it can also be associated with other subroutines to handle more complex behaviours. As an example, solving thermo-mechanical problems can be done by coupling it to either UMATHT or HETVAL subroutines. The UMAT subroutine would then handle the mechanical variables, while the other subroutine handles the thermal ones.

In the case of a local damage model, the only equation that needs to be solved is the equilibrium equation

$$\nabla \cdot \boldsymbol{\sigma} = \mathbf{0} \tag{2.29}$$

whose variational formulation can be rewriten as

$$\Phi_{\mathcal{U}}(\mathcal{U}) = \mathcal{F}_{ext} \tag{2.30}$$

where Φ_u and $\mathcal{F}_{ext}$ are the internal and external forces associated with the displacement degree of freedom $\mathcal{U}$. After linearization, this problem would then write :

$$\mathbb{K}_{\mathcal{U}\mathcal{U}} \cdot \{\mathcal{U}\} = \{\mathcal{F}_{ext}\} \tag{2.31}$$

where $\mathbb{K}_{\mathcal{U}\mathcal{U}}$ is the tangent stiffness defined as

$$\mathbb{K}_{\mathcal{U}\mathcal{U}} = \frac{\partial \Phi_{\mathcal{U}}}{\partial \mathcal{U}} \tag{2.32}$$

One could also consider using the secant stiffness which is usually easier to compute, but induces a slower convergence. It is worth noting that, since the user-material script is used through a dedicated API, this implementation requires only standard inputs and outputs such as stress, strain, and other state variables and can thus be seen as non-intrusive.

In the more complex case of nonlocal damage models, one can differentiate the implementation of the integral-type and gradient-type formulations. While integral-type formulations do not require to solve any additional equation, the computation of the nonlocal variable $\bar{\varepsilon}$ at a given point $\boldsymbol{x}$ requires access to its neighbourhood, namely the value of the local field $\hat{\varepsilon}$ at each other point $\boldsymbol{\xi}$, and their relative distance to $\boldsymbol{x}$, $l_{x\xi}$. Since these information are usually not accessible, one would need an intrusive implementation (Figure 2.1c) to get access to these non-standard outputs.

On the other hand, gradient-type formulations do require to solve an additional equation which can be written under the general form

$$\bar{\varepsilon} - a\ \nabla \cdot (b\ \nabla \bar{\varepsilon}) = \hat{\varepsilon} \tag{2.33}$$

where a and b are scalar fonctions that might depend on both local and nonlocal variables, and $\hat{\varepsilon}$ and $\bar{\varepsilon}$ would be replaced by s and d for the Phase-Field-based model. The full coupled nonlinear problem thus writes

$$\begin{cases} \nabla \cdot \boldsymbol{\sigma} = \mathbf{0} \\ \bar{\varepsilon} - a\ \nabla \cdot (b\ \nabla \bar{\varepsilon}) = \hat{\varepsilon} \end{cases} \tag{2.34}$$

and its variational formulation can be rewritten as

$$\begin{cases} \Phi_{\mathcal{U}}(\mathcal{U}, \mathcal{E}) = \mathcal{F}_{ext} \\ \Phi_{\mathcal{E}}(\mathcal{U}, \mathcal{E}) = 0 \end{cases} \tag{2.35}$$

where $\Phi_{\mathcal{E}}$ are the internal forces associated with the nonlocal degree of freedom $\mathcal{E}$.

In this case, due to the additional equation and degree of freedom, one would not be able to use directly the embedded mechanical solver, nor the associated elements, to solve a problem using this model. This issue was addressed in [Molnár and Gravouil, 2017] for the Phase-Field model proposed in [Miehe et al., 2010a] using user-defined elements (UEL) and material (UMAT) to handle both the additional equation and the associated degree of freedom. This implementation, using non-standard outputs, enabled the staggered resolution (Figure 2.2a) of the coupled problem with a dedicated set of finite elements.

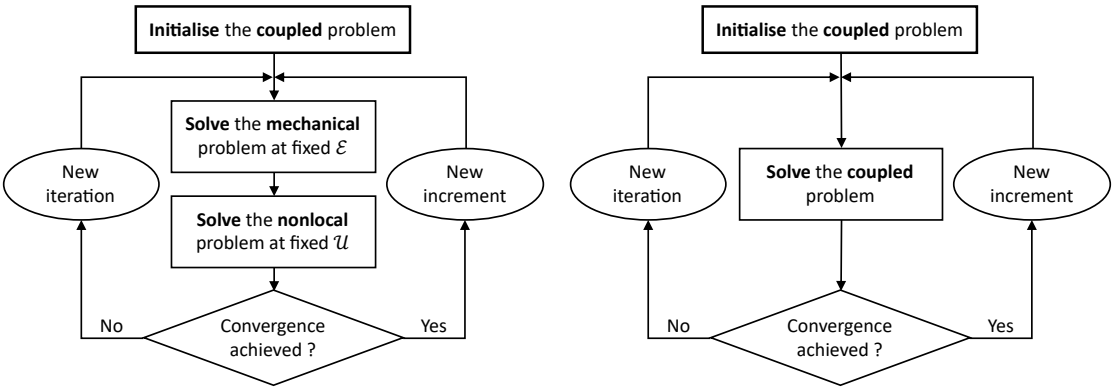

(a) Staggered resolution (b) Monolithic resolution

Figure 2.2: Resolution schemes for the coupled problem.

When using such a resolution scheme, uncoupling the problem and handling only one equation at a time, one would first fix the nonlocal degree of freedom $\mathcal{E}$ and solve the linearized equilibrium equation

$$\mathbb{K}_{\mathcal{U}\mathcal{U}} \cdot \{\mathcal{U}\} = \{\mathcal{F}_{ext}\} \tag{2.36}$$

before fixing the displacement degree of freedom $\mathcal{U}$ and solving the linearized nonlocal equation

$$\mathbb{K}_{\mathcal{E}\mathcal{E}} \cdot \{\mathcal{E}\} = \{0\} \tag{2.37}$$

where $\mathbb{K}_{\mathcal{U}\mathcal{U}}$ and $\mathbb{K}_{\mathcal{E}\mathcal{E}}$ are the stiffness related respectively to the displacement and nonlocal degrees of freedom

$$\begin{cases} \mathbb{K}_{\mathcal{U}\mathcal{U}} = \dfrac{\partial \Phi_{\mathcal{U}}}{\partial \mathcal{U}} \\ \mathbb{K}_{\mathcal{E}\mathcal{E}} = \dfrac{\partial \Phi_{\mathcal{E}}}{\partial \mathcal{E}} \end{cases} \tag{2.38}$$

On the other hand, in order to handle both equations simultaneously, one could also consider a coupled monolithic resolution (Figure 2.2b), solving directly the linearized coupled problem

$$\begin{bmatrix} \mathbb{K}_{\mathcal{U}\mathcal{U}} & \mathbb{K}_{\mathcal{U}\mathcal{E}} \\ \mathbb{K}_{\mathcal{E}\mathcal{U}} & \mathbb{K}_{\mathcal{E}\mathcal{E}} \end{bmatrix} \cdot \begin{bmatrix} \mathcal{U} \\ \mathcal{E} \end{bmatrix} = \begin{Bmatrix} \mathcal{F}_{ext} \\ 0 \end{Bmatrix} \tag{2.39}$$

where the diagonal terms of the stiffness matrix $\mathbb{K}_{\mathcal{U}\mathcal{U}}$ and $\mathbb{K}_{\mathcal{E}\mathcal{E}}$ are still defined as in (2.38), and the coupling terms $\mathbb{K}_{\mathcal{U}\mathcal{E}}$ and $\mathbb{K}_{\mathcal{E}\mathcal{U}}$ are defined as

$$\begin{cases} \mathbb{K}_{\mathcal{U}\mathcal{E}} = \dfrac{\partial \Phi_{\mathcal{U}}}{\partial \mathcal{E}} \\ \mathbb{K}_{\mathcal{E}\mathcal{U}} = \dfrac{\partial \Phi_{\mathcal{E}}}{\partial \mathcal{U}} \end{cases} \tag{2.40}$$

An intermediate and less efficient scheme that could also be envisioned is the monolithic resolution of the system (2.35) treated as an uncoupled problem. To do so, starting from (2.39), one would have to set $\mathbb{K}_{\mathcal{U}\mathcal{E}}$ and $\mathbb{K}_{\mathcal{E}\mathcal{U}}$ to zero, giving the linearized problem

$$\begin{bmatrix} \mathbb{K}_{\mathcal{U}\mathcal{U}} & 0 \\ 0 & \mathbb{K}_{\mathcal{E}\mathcal{E}} \end{bmatrix} \cdot \begin{bmatrix} \mathcal{U} \\ \mathcal{E} \end{bmatrix} = \begin{Bmatrix} \mathcal{F}_{ext} \\ 0 \end{Bmatrix} \tag{2.41}$$

which is easier to implement due to the absence of coupling terms.

While the staggered resolution might be easier to implement, solving the coupled problem should enable the monolithic approach to have a better convergence rate, especially when using the tangent stiffness. However, the monolithic resolution cannot be implemented by simply creating a new set of user-defined elements since one would also need to use a completely different solver.

2.2.2 Thermo-mechanical analogy

As seen in the previous part, the implementation of gradient-type nonlocal damage models usually requires the use of dedicated elements and solver with an additional degree of freedom, which can be done through an intrusive implementation. However, the goal of this chapter is to conduct a non-intrusive implementation of the models introduced previously. To do so, one would have to use existing solver and elements that already have an additional degree of freedom, e.g. temperature, instead of creating new ones.

One can rewrite the general gradient-type equation (2.33) as

$$-\nabla \cdot (b\ \nabla \bar{\varepsilon}) = \frac{\hat{\varepsilon} - \bar{\varepsilon}}{a} \tag{2.42}$$

and, based on its similarities with the transient heat equation

$$\rho c_p \frac{\partial T}{\partial t} - \nabla \cdot (\kappa\ \nabla T) = r(T) \tag{2.43}$$

where ρ is the density, c_p the specific heat, κ the conductivity, T the temperature, ∇T its gradient, and r a heat source, one could consider using thermo-mechanical solver and elements to handle both the equilibrium and the nonlocal equations.

As pointed out before, thermo-mechanical models can be handled in Abaqus using the UMAT subroutine associated either to the HETVAL or UMATHT subroutines. By using one of these subroutines, one could also avoid writing and

implementing the model's variational formulation, simply replacing the terms of the thermal equation by those of the nonlocal one. The main difference between the two subroutines comes from the fact that, while the resolution scheme associated with HETVAL is a staggered one (Figure 2.3), the UMATHT subroutine enables the monolithic resolution of a fully coupled problem (2.4).

When using HETVAL, each equation of the problem

$$\begin{cases} \rho c_p \dfrac{\partial T}{\partial t} - \nabla \cdot (\kappa \, \nabla T) = r(T) \\ \nabla \cdot \boldsymbol{\sigma} = \mathbf{0} \end{cases} \tag{2.44}$$

is handled separately, and one has to define ρ, c_p and κ as fixed material parameters while r, $\boldsymbol{\sigma}$, and their derivatives are defined through the scripts using each subroutine standard inputs, namely

- the initial values of stress, strain, temperature and the other state variables, along with the increments of strain and temperature for UMAT
- the increment, initial value and gradient of temperature for HETVAL

Regarding the solving algorithm (Figure 2.3), one can note that, at each integration point, the code first calls the UMAT subroutine to define the terms related to the equilibrium equation

$$\boldsymbol{\sigma}, \ \frac{\partial \boldsymbol{\sigma}}{\partial \boldsymbol{\varepsilon}} \tag{2.45}$$

before calling the HETVAL subroutine to define the terms related to the thermal equation

$$r, \ \frac{\partial r}{\partial T} \tag{2.46}$$

The thermal and mechanical stiffness are then assembled, the residuals computed and, depending on whether convergence is achieved, the code either moves on to the next increment or try a new iteration for the current one.

This procedure can be used with any thermo-mechanical element and allows for the uncoupled resolution of the thermo-mechanical problem. This was done by Azinpour et al. ([Azinpour et al., 2018]) for both the classical gradient [Peerlings et al., 1996] and the stationary Phase Field [Miehe et al., 2010a] formulations. However, it only allows the use of constant thermal parameters, which is not sufficient when using a state dependent function b as in the eikonal-based formulation.

The alternative implementation, using UMATHT instead of HETVAL, allows for a more extensive implementation, solving simultaneously both equations of the problem

$$\begin{cases} \rho \dfrac{\partial e}{\partial t} - \nabla \cdot \boldsymbol{q} = r(T) \\ \nabla \cdot \boldsymbol{\sigma} = \mathbf{0} \end{cases} \tag{2.47}$$

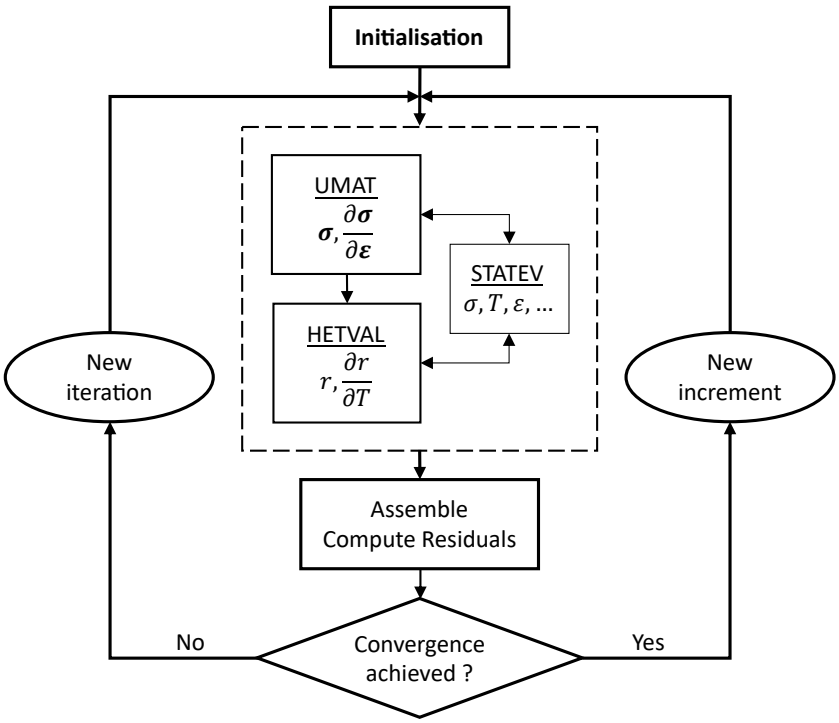

Figure 2.3: Resolution using HETVAL and UMAT subroutines.

where the internal thermal energy e is still defined as

$$e = c_p \, T \tag{2.48}$$

and the heat flux $\boldsymbol{q}$ is still defined as

$$\boldsymbol{q} = -\kappa \, \nabla T \tag{2.49}$$

Moreover, while ρ is still defined as a fixed material parameter, each term ($\boldsymbol{u}$, r, $\boldsymbol{q}$ and $\boldsymbol{\sigma}$), along with its derivatives, is defined through the scripts using each subroutine standard inputs, namely

- the initial values of stress, strain, temperature and the other state variables, along with the increments of strain and temperature for UMAT
- the state variables and the increment, initial value and gradient of temperature for UMATHT

Regarding the solving algorithm (Figure 2.4), one can note that, to handle the monolithic resolution, both subroutines are called simultaneously at each integration point. Unlike the previous implementation, the terms related to the heat source

$$r, \ \frac{\partial r}{\partial \boldsymbol{\varepsilon}}, \ \frac{\partial r}{\partial T} \tag{2.50}$$

are computed through the UMAT subroutine, along with the terms related to stresses

$$\boldsymbol{\sigma}, \ \frac{\partial \boldsymbol{\sigma}}{\partial \boldsymbol{\varepsilon}}, \ \frac{\partial \boldsymbol{\sigma}}{\partial T} \tag{2.51}$$

while those linked to the internal energy and the heat flux

$$\boldsymbol{q},\ \frac{\partial \boldsymbol{q}}{\partial T},\ \frac{\partial \boldsymbol{q}}{\partial (\nabla T)},\ e,\ \frac{\partial e}{\partial T},\ \frac{\partial e}{\partial (\nabla T)} \tag{2.52}$$

are computed through the thermal subroutine. It is worth noting that, when computing the derivatives in the UMATHT subroutine, T and ∇T are taken as independent variables.

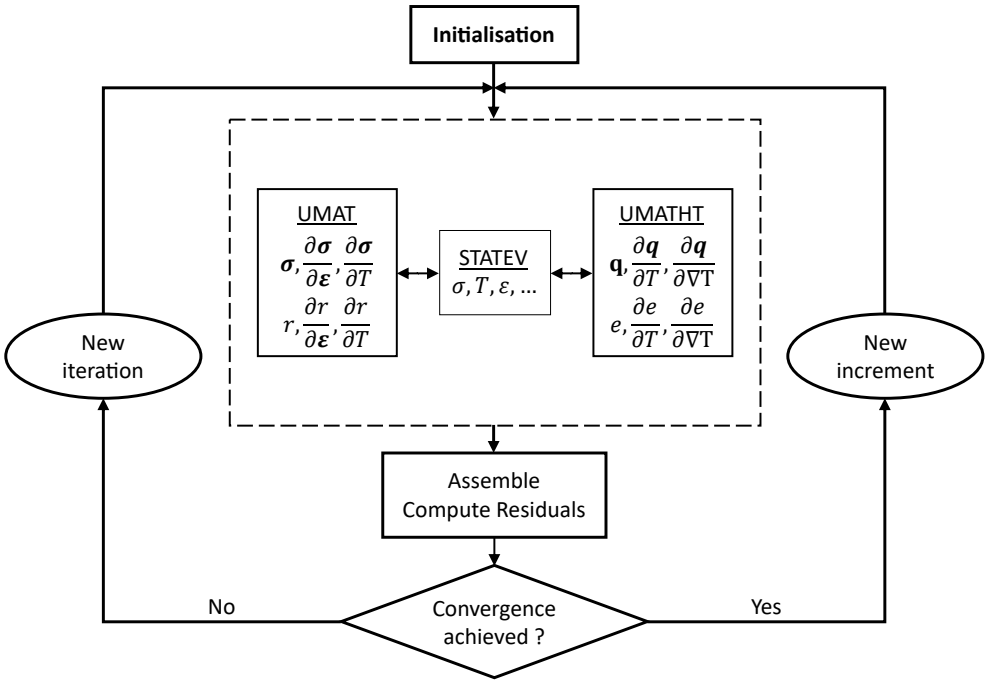

Figure 2.4: Resolution using UMATHT and UMAT subroutines.

This procedure can also be used with any thermo-mechanical element, and it allows for the monolithic resolution of the coupled thermo-mechanical problem, using state dependent thermal parameters and tangent stiffness.

It was thus decided here to use the UMAT and UMATHT subroutines to handle the coupled problem (2.34), in order to take advantage of both the non-intrusive implementation and the monolithic resolution. The implementation of the different gradient-type damage models considered here will be detailed in the next part.

It is worth noting that the use of standard thermo-mechanical elements imposes both the interpolation and the integration associated with temperature in Abaqus, which was here assumed to be sufficient. On the other hand, the use of a dedicated implementation such as the one conducted by Molnar and Gravouil [Molnár and Gravouil, 2017] allowed them to use a quadratic interpolation of the additional degree of freedom. As far as the integration is concerned, it could be interesting to study whether the integration used with both implementation is sufficient to properly handle the right hand side of the gradient-type equation.

Depending on the outcome of this study, one might then consider taking advantage of a dedicated implementation in order to improve the integration.

2.2.3 Application to the considered gradient-type formulations

This part will focus on the thermo-mechanical analogies related to the non-intrusive implementation of each gradient-type formulation considered here, using the UMAT and UMATHT subroutines.

On a general matter, based on the analogy related to the general gradient-type formulation

$$\begin{aligned} & \rho\frac{\partial e}{\partial t} - \nabla\cdot\boldsymbol{q} = r(T) \\ \Leftrightarrow\ & -\nabla\cdot(b\ \nabla\bar{\varepsilon}) = \frac{\hat{\varepsilon}-\bar{\varepsilon}}{a} \end{aligned} \tag{2.53}$$

one can note that all terms related to the internal energy e should be put to 0.

This point will be discussed in more details in Part 2.3, but until then one can consider from now on that

$$e = 0,\ \frac{\partial e}{\partial T} = 0,\ \frac{\partial e}{\partial\left(\nabla T\right)} = 0 \tag{2.54}$$

Classical gradient-type formulation

The first formulations considered here are the classical gradient-type formulation (1.26), introduced in [Peerlings et al., 1996] and for which the thermo-mechanical analogy writes

$$\begin{aligned} & \rho\frac{\partial e}{\partial t} - \nabla\cdot\boldsymbol{q} = r(T) \\ \Leftrightarrow\ & -\nabla\cdot\left(c^2\nabla\bar{\varepsilon}\right) = \hat{\varepsilon}-\bar{\varepsilon} \end{aligned} \tag{2.55}$$

giving term by term

$$\begin{aligned} \boldsymbol{q} &\Leftrightarrow c^2\nabla\bar{\varepsilon} \\ T &\Leftrightarrow \bar{\varepsilon} \\ r &\Leftrightarrow \hat{\varepsilon}-\bar{\varepsilon} \end{aligned} \tag{2.56}$$

in addition to the conditions introduced in equation (2.54).

This means that, in this case, the heat source r should be replaced by the term $\hat{\varepsilon}-\bar{\varepsilon}$, the conductivity κ by the square value of the internal length c, and the temperature T by the nonlocal strain $\bar{\varepsilon}$.

The derivatives of $\boldsymbol{\sigma}$ and r with respect to $\boldsymbol{\varepsilon}$ and T, that have to be implemented in the UMAT subroutine, then write for $1D$ simulations

$$\begin{aligned} &\frac{\partial\boldsymbol{\sigma}}{\partial\boldsymbol{\varepsilon}} = (1-D)E, && \frac{\partial\boldsymbol{\sigma}}{\partial T} = \begin{cases} -g^{'}(\kappa)\ E\varepsilon & \text{if } \bar{\varepsilon}\geq\kappa \\ 0 & \text{if } \bar{\varepsilon}<\kappa \end{cases} \\ &\frac{\partial r}{\partial\boldsymbol{\varepsilon}} = \begin{cases} 1 & \text{if } \varepsilon\geq 0 \\ 0 & \text{if } \varepsilon<0 \end{cases}, && \frac{\partial r}{\partial T} = -1 \end{aligned} \tag{2.57}$$

And, considering the analogy for the heat flux (2.56), its derivatives, that should be implemented in the UMATHT subroutine, simply write

$$\frac{\partial\boldsymbol{q}}{\partial T} = \boldsymbol{0},\quad \frac{\partial\boldsymbol{q}}{\partial\nabla T} = c^2 \tag{2.58}$$

Phase-Field-based formulation

Following the same steps with the Phase-Field-based formulation (2.28), one gets the thermo-mechanical analogy

$$\begin{aligned} \rho\frac{\partial e}{\partial t} - \nabla\cdot\boldsymbol{q} &= r(T) \\ \Leftrightarrow\ -\nabla\cdot\left({l_d}^2\nabla d\right) &= \frac{y-d}{1-y} \end{aligned} \tag{2.59}$$

and thus, term by term

$$\begin{aligned} \boldsymbol{q} &\Leftrightarrow {l_d}^2\nabla d \\ T &\Leftrightarrow d \\ r &\Leftrightarrow \frac{y-d}{1-y} \end{aligned} \tag{2.60}$$

in addition to the conditions introduced in equation (2.54).

This means that, in this case, the heat source r should be replaced by the term $y-d/1-y$, the conductivity κ by the square value of the internal length l_d, and the temperature T by the Phase-Field variable d.

The derivatives of $\boldsymbol{\sigma}$ and r with respect to $\boldsymbol{\varepsilon}$ and T, that have to be implemented in the UMAT subroutine, then write for $1D$ simulations

$$\begin{aligned} &\frac{\partial\boldsymbol{\sigma}}{\partial\boldsymbol{\varepsilon}} = (1-D)E, && \frac{\partial\boldsymbol{\sigma}}{\partial T} = 2\sqrt{1-D}\ E\varepsilon \\ &\frac{\partial r}{\partial\boldsymbol{\varepsilon}} = \begin{cases} y^{'}(\kappa)\ \dfrac{\langle\varepsilon\rangle_+}{\varepsilon}\ \dfrac{1-d}{(1-y)^2} & \text{if } \hat{\varepsilon}\geq\kappa>0. \\ 0. & \text{otherwise} \end{cases}, && \frac{\partial r}{\partial T} = \frac{-1}{1-y} \end{aligned} \tag{2.61}$$

And, considering the analogy for the heat flux (2.56), its derivatives, that should be implemented in the UMATHT subroutine, simply write

$$\frac{\partial\boldsymbol{q}}{\partial T} = \mathbf{0.}, \quad \frac{\partial\boldsymbol{q}}{\partial\nabla T} = {l_d}^2 \tag{2.62}$$

One can note that, when y gets close to 1., singularities may appear when computing r, $\partial r/\partial T$ and $\partial r/\partial\boldsymbol{\varepsilon}$. This issue was here addressed by bounding the value of y used to compute those terms to avoid division by 0.

It is worth noting that this only affects the nonlocal treatment and the tangent operator approximation, and not damage itself which can take higher values that will be used to compute the stress $\boldsymbol{\sigma}$.

Eikonal-based gradient-type formulation

This approach can also be applied to any of the eikonal-based gradient-type formulations presented in Part 1.6.3. Focusing on the one studied in this chapter, i.e involving unidirectional damage (1.72), the thermo-mechanical analogy writes

$$\begin{aligned} \rho\frac{\partial e}{\partial t} - \nabla\cdot\boldsymbol{q} &= r(T) \\ \Leftrightarrow\ -\nabla\cdot\left(c^2\sqrt{1-D}\ \nabla\bar{\varepsilon}\right) &= \frac{\hat{\varepsilon}-\bar{\varepsilon}}{\sqrt{1-D}} \end{aligned} \tag{2.63}$$

and thus, term by term

$$\begin{aligned} \boldsymbol{q} &\Leftrightarrow c^2\sqrt{1-D}\ \nabla\bar{\varepsilon} \\ T &\Leftrightarrow \bar{\varepsilon} \\ r &\Leftrightarrow \frac{\hat{\varepsilon}-\bar{\varepsilon}}{\sqrt{1-D}} \end{aligned} \tag{2.64}$$

in addition to the conditions introduced in equation (2.54).

This means that, in this case, the heat source r should be replaced by the term $(\hat{\varepsilon}-\bar{\varepsilon})/\sqrt{1-D}$, the conductivity κ by the square value of the effective internal length $c(1-D)^{1/4}$, and the temperature T by the nonlocal strain $\bar{\varepsilon}$.

The derivatives of $\boldsymbol{\sigma}$ and r with respect to $\boldsymbol{\varepsilon}$ and T, that have to be implemented in the UMAT subroutine, then write for $1D$ simulations

$$\begin{aligned} \frac{\partial\boldsymbol{\sigma}}{\partial\boldsymbol{\varepsilon}} &= (1-D)E \\ \frac{\partial\boldsymbol{\sigma}}{\partial T} &= \begin{cases} -\,g^{'}(\kappa)\ E\varepsilon & \text{if } \bar{\varepsilon}\geq\kappa \\ 0. & \text{if } \bar{\varepsilon}<\kappa \end{cases} \\ \frac{\partial r}{\partial\boldsymbol{\varepsilon}} &= \begin{cases} \dfrac{1.}{\sqrt{1-D}} & \text{if } \varepsilon\geq 0. \\ 0. & \text{if } \varepsilon<0. \end{cases} \\ \frac{\partial r}{\partial T} &= \frac{-1}{\sqrt{1-D}} + \begin{cases} -\dfrac{g^{'}(\kappa)\ (\hat{\varepsilon}-\bar{\varepsilon})}{2\ (1-D)^{3/2}} & \text{if } \bar{\varepsilon}\geq\kappa \\ 0 & \text{if } \bar{\varepsilon}<\kappa \end{cases} \end{aligned} \tag{2.65}$$

And, considering the analogy for the heat flux (2.56), its derivatives, that should be implemented in the UMATHT subroutine, simply write

$$\frac{\partial\boldsymbol{q}}{\partial T} = \begin{cases} -\dfrac{c^2\ g^{'}(\kappa)}{2\ \sqrt{1-D}}\ \nabla\bar{\varepsilon} & \text{if } \bar{\varepsilon}\geq\kappa \\ 0 & \text{if } \bar{\varepsilon}<\kappa \end{cases}, \quad \frac{\partial\boldsymbol{q}}{\partial\nabla T} = c^2\ \sqrt{1-D} \tag{2.66}$$

Again, specific care will need to be taken when D gets close to 1 in order to avoid singularities when computing the nonlocal treatment and the tangent operator approximation.

2.3 Driving strategies and associated issues

This part will deal with the driving strategy used here to assess the properties of the considered formulations through the computations of 1D numerical examples. It will first focus on the more classical driving strategy before considering its associated issues and proposing a way to address them.

2.3.1 Displacement-based driving and stabilization using numerical viscosity

Displacement-based driving, principle and associated issues

The most simple way to handle a monotonic loading with a softening behaviour (Figure 2.5a) is to impose the displacement at the end of the bar, since the driving variable thus have a monotonic evolution. One could also consider using it for alternate loading with elastic unloading (Figure 2.5b) since a given increment of displacement, whether positive or negative, will correspond to a unique point on the response curve.

It is worth noting that, in this case, one could not use a force based driving strategy since, even for a loading following the material's response (Figure 1.3b), the force would not have a monotonic evolution. Moreover, after the peak, a given force increment does not correspond to a unique point on the response curve since a decrease in the force could be induced either by unloading or softening.

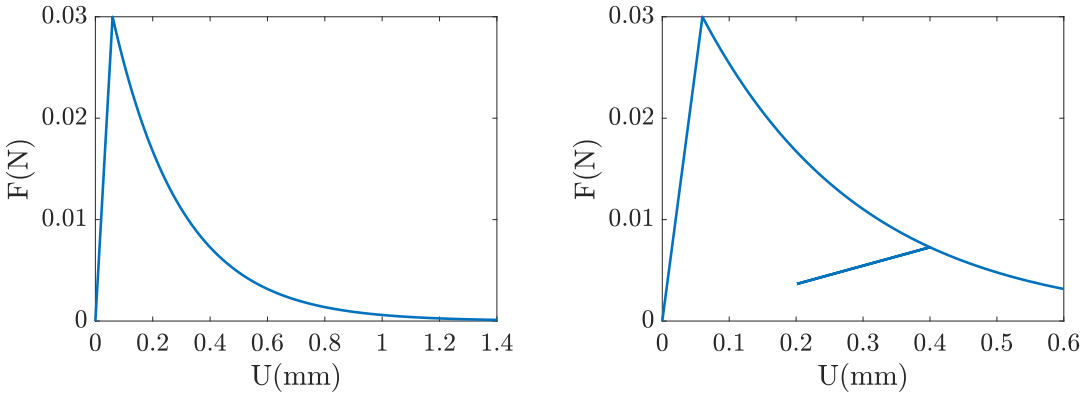

(a) Monotonic loading

(b) Alternate loading

Figure 2.5: Response curves for monotonic and alternate loading.

Numerical simulations were conducted in order to assess the relevance of the strain-based driving strategy, and it seems to be working well with the classical gradient-type formulation. However, when using small internal length, or when computing responses using the local formulation, it does not appear to be sufficient.

Snap-back instabilities

The issue encountered in the previous part for small internal lengths is linked to the occurrence of snap-back instabilities when damage localizes in small area. In this case, after the stress reaches its maximum value, the unloading of the elastic part exceeds the loading of the localization zone, and both stress and displacement at the bar's end decrease. This phenomenon comes from the fact that, depending on the load, geometry and model considered, the elastic energy stored during the first part of the loading exceeds the energy that can be dissipated after the peak. It is thus a structural effect inherent to stress softening and localization, and not specific to the considered nonlocal damage model. Though such instabilities can

also occur in $2D$ and $3D$ settings, they cannot be avoided in $1D$ settings due to the absence of load sharing, and one thus have to find a way to handle it.

As it is, in the particular case of a bar submitted to tension, it is possible to demonstrate that snap-back instabilities will occur when the size of the localization area l is smaller than a critical size. Considering a homogeneous bar of length L made of a material whose behaviour corresponds to the local damage model described in Part 1.3.1, the condition for such instabilities thus writes (cf. Appendix B)

$$l < \frac{\varepsilon_0}{\varepsilon_f} L \tag{2.67}$$

One can thus conclude that, the occurrence of a snap-back is linked to the damage rate through the term $\varepsilon_0/\varepsilon_f$, and to the relative importance of the localization area through l/L. In the scope of this chapter, using $\varepsilon_0 = 0.03$ and $\varepsilon_f = 0.15$, one can expect this structure effect when damage localizes in less than 20% of the bar. Numerical simulations were conducted in order to assess the relevance of this result and, as one can see in Figure 2.6, the slope of the response curve tends to get steeper when the localization area shrinks, and snap-back instabilities finally occur when $l < 0.2L$ which is consistent with the analytical result (2.67).

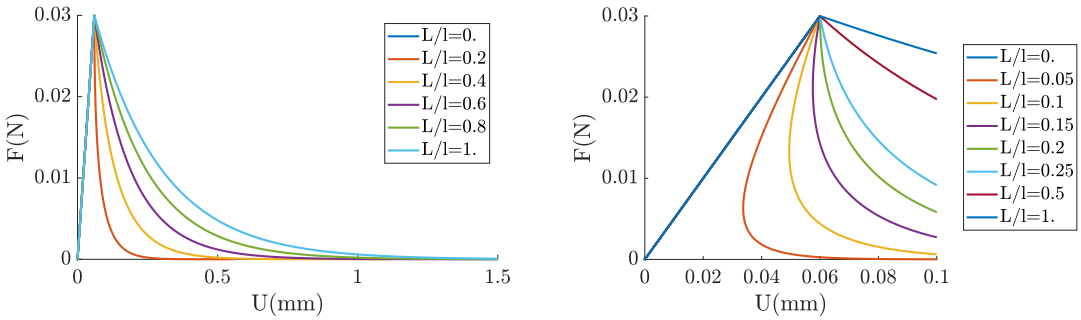

Figure 2.6: Force-displacement curves of the local model for different localization sizes.

The occurrence of these instabilities explains the loss of convergence for small internal length, i.e. small localization area, for displacement driven computations. In such cases, the displacement at the end of the bar does not have a monotonic evolution, hence it cannot be used to drive the whole computation. One way to address this issue would be to find another, more suited, driving strategy compatible with the considered instabilities.

Though it was not available here, another option could also be to take into account the dissipation linked to the kinetic energy, thus ensuring a continuous increase of the displacement and stabilizing the response curve.

Stabilization of the response

As pointed out before, one way to address the snap-back issue would be to stabilize the response curve by taking into account the kinetic energy. However,

even though this would enable one to remain consistent with the energy balance, it would require the modelling of dynamic effects, which is not possible with this Abaqus formulation and is beyond the scope of this work. Based on this idea, another classical way to obtain similar stabilization properties would be to add a dissipative phenomenon in the material model, which can be done either by changing the local material behaviour or the nonlocal treatment.

Regarding the change in the local material behaviour, it could be done by using a bounded rate damage model ([Allix and Deü, 1997], [Allix et al., 2003], [Desmorat et al., 2010a]), or a damage plastic model ([Jirásek and Desmorat, 2019]). It was however decided here to keep the local damage model, and to increase the dissipated energy by changing the nonlocal treatment.

This classical modification was done, pursuing the thermo-mechanical analogy, by adding the term corresponding to the time derivative of the internal energy $\partial e/\partial t$ in the general gradient-type formulation (2.42) equation, writing

$$\rho \frac{\partial \upsilon}{\partial t} - \nabla \cdot (b \, \nabla \bar{\varepsilon}) = \frac{\hat{\varepsilon} - \bar{\varepsilon}}{a} \tag{2.68}$$

where υ represents the additional energy defined, using a numerical parameter ζ, as

$$\upsilon = \zeta \bar{\varepsilon} \tag{2.69}$$

It is worth noting that, using the resulting formulation, one could express $\dot{\bar{\varepsilon}}$ as a function of $\bar{\varepsilon}$ and $\bar{\varepsilon} - \hat{\varepsilon}$, which is similar to bounded-rate and nonlocal bounded-rate damage models. This modification of the nonlocal treatment would induce a numerical viscosity, delaying damage evolution in order to stabilize the curve and prevent the occurrence of snap-back instabilities.

The thermo-mechanical analogy of the stabilized classical gradient-type formulation would then write

$$\begin{aligned} & \rho \frac{\partial e}{\partial t} - \nabla \cdot \boldsymbol{q} = r(T) \\ \Leftrightarrow \quad & \rho \frac{\partial \upsilon}{\partial t} - \nabla \cdot \left(c^2 \nabla \bar{\varepsilon} \right) = \hat{\varepsilon} - \bar{\varepsilon} \end{aligned} \tag{2.70}$$

giving term by term

$$\begin{aligned} e &\Leftrightarrow \upsilon \\ \boldsymbol{q} &\Leftrightarrow c^2 \nabla \bar{\varepsilon} \\ T &\Leftrightarrow \bar{\varepsilon} \\ r &\Leftrightarrow \hat{\varepsilon} - \bar{\varepsilon} \end{aligned} \tag{2.71}$$

which, apart from the term related to the additional energy, is the same as the one presented Part 2.2.3.

One could thus expect the other terms, r, $\boldsymbol{\sigma}$ and $\boldsymbol{q}$, and their derivatives, $\partial r/\partial \boldsymbol{\varepsilon}$, $\partial r/\partial T$, $\partial \boldsymbol{\sigma}/\partial \boldsymbol{\varepsilon}$, $\partial \boldsymbol{\sigma}/\partial T$, $\partial \boldsymbol{q}/\partial T$ and $\partial \boldsymbol{q}/\partial (\nabla T)$ to remain unchanged, while the conditions established in equation (2.54) would become

$$e \;=\; \rho \zeta T \tag{2.72}$$

$$\frac{\partial e}{\partial T} = \rho\zeta \tag{2.73}$$

$$\frac{\partial e}{\partial (\nabla T)} = 0 \tag{2.74}$$

Using this stabilized formulation with an additional energy, one should be able to use a displacement-based strategy to drive simulations that would exhibit a snap-back with the classical formulation.

Numerical examples

This new formulation was used, along with displacement based driving strategy, to run the same simulations as the ones computed in Part 2.3.1, including those who did not converge due to the snap-back instabilities.

As one can see in Figure 2.7, no instabilities appear when damage is localized in more than 20% of the bar, i.e for $\kappa = 2, 1, 0.5$.

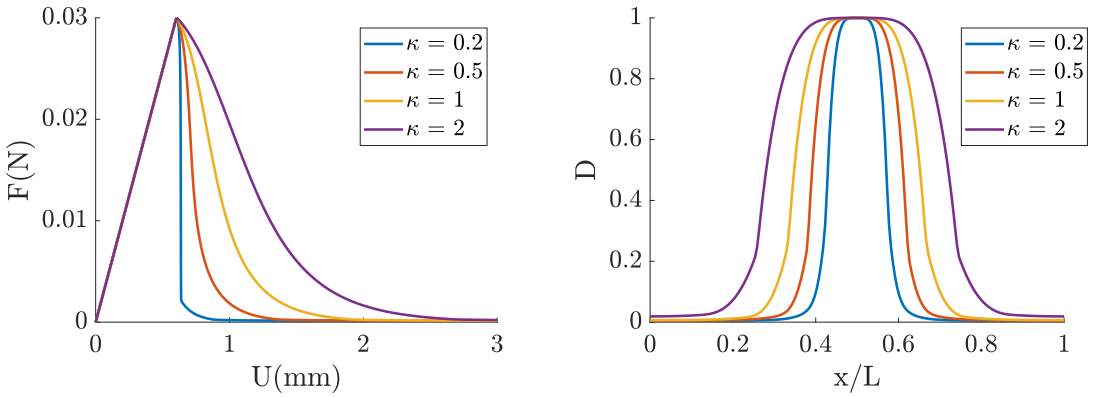

(a) Force-displacement curves

(b) Damage profiles

Figure 2.7: Response curves of the nonlocal model with numerical viscosity and displacement driven computations for different internal length.

However, even though it was possible to compute the response curve for $\kappa = 0.2$, one can note that it exhibits a quasi-vertical slope after the peak. This corresponds to a snap-back instability which is consistent with the fact that, in this case, damage localizes in less than 20% of the bar (Figure 2.7b). It thus appears that this formulation enables the stabilization of a response curve exhibiting a snap-back instability, which can be computed using a displacement based driving strategy. Moreover, one can note (Figure 2.8) that the stabilizing modification allows the existence of converged increments along the quasi-vertical part of the curve.

It is worth noting that this does not allow one to compute the dissipated energy associated with the original model, since part of the area under the curve represents the numerical stabilizing energy e. While this is quite straightforward for initially unstable response curves, one should note that it is also true for the stable ones since the additional dissipation will still be introduced through the viscous term. Another driving strategy, allowing the computation of snap-back instabilities, is thus needed in order to properly handle these computations.

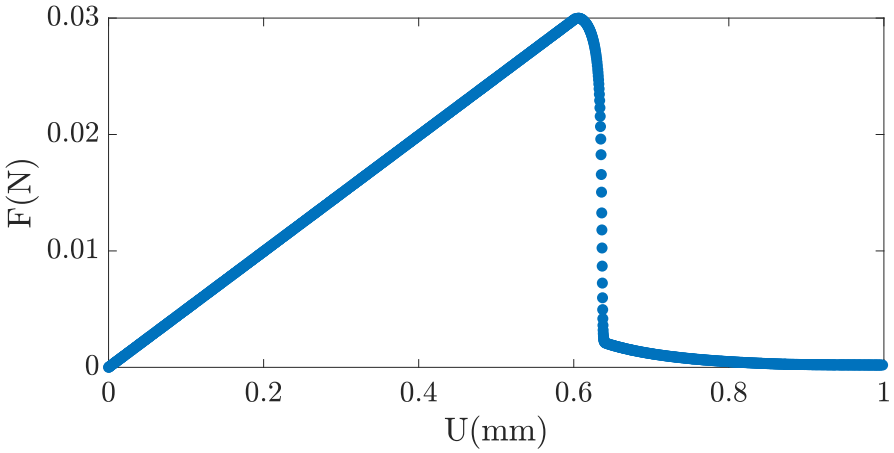

Figure 2.8: Force-displacement curve of the nonlocal model with numerical viscosity and displacement driven computations for $\kappa = 0.2$.

2.3.2 Dissipation-driven computations

Principle

As pointed out in Part 2.3.1, the occurrence of snap-back instabilities raises the issues of the computations' driving since a direct method controlling either force or displacement at the end of the bar cannot be used. Another option would be to use an indirect driving strategy, such as the arc length method [Riks, 1979, Crisfield, 1991], controlling both force and displacement at the end of the bar by imposing the increase of a given quantity.

A natural choice could then be to fix the evolution of a local and monotonic variable such as damage or strain in the localization zone. However, this would require the geometrical identification of this area, either before or during the computation, and the driving itself wont be done in a non intrusive fashion. Instead, one can fix the evolution of a global variable, computed directly from the force and displacement at the end of the bar, thus addressing the issue of the driving intrusiveness.

It was thus decided, following [Gutiérrez, 2004, Verhoosel et al., 2009], to use a dissipation-based global driving method to handle the post-peak part of the problem. In this case, one imposes the increment of dissipated energy at each step, and the force and displacement at the end of the bar are computed accordingly. As one can see in Figure 2.9, the energy dissipated between two time steps can be observed on the response curve as the area of the triangle defined by the corresponding portion of the response curve and the two elastic unloadings at those time steps.

First, one needs to consider the simple case of strain softening without snap-back instabilities. A portion of such a response curve between two points (U_1, F_1) and point (U_2, F_2) with $U_2 \geq U_1$ and $F_2 \leq F_1$ is displayed in Figure 2.10. As one can see, the increment of dissipated energy ΔA, which is equal to the area of the triangle defined by the blue, green and red lines, can be defined as the sum of the

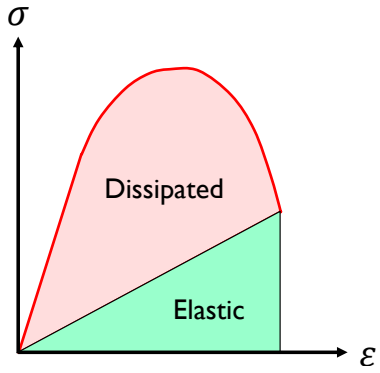

(a) Energy partition

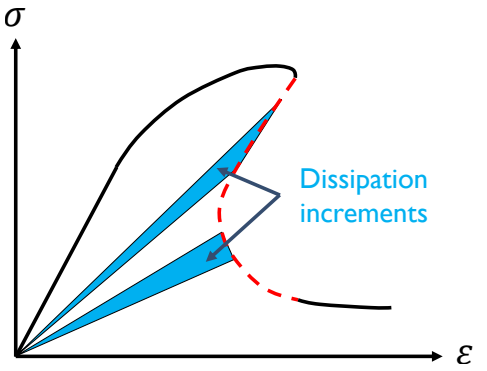

(b) Dissipation between two time steps

Figure 2.9: Partition between elastic and dissipated energy, and increments of dissipation, in the absence of plasticity.

areas of the blue, green and red triangles, giving

$$\Delta A = \frac{1}{2}\left[F_1\left(U_2 - U_1\right) - U_1\left(F_2 - F_1\right)\right] \tag{2.75}$$

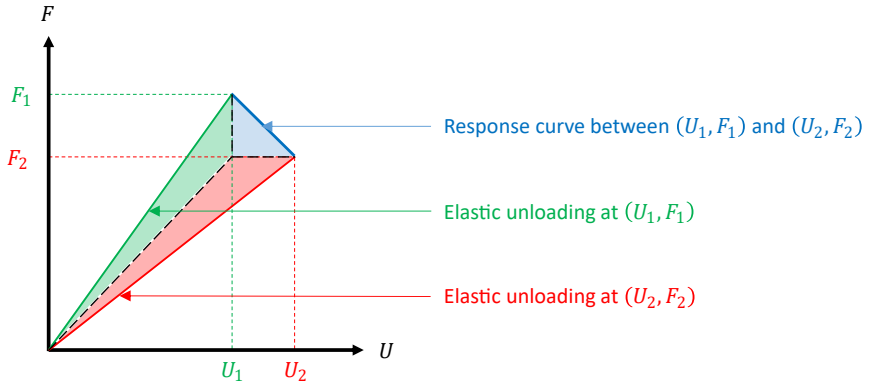

Figure 2.10: Computation of the increment of dissipated energy with strain softening.

On the other hand, the occurrence of a snapback would bring the response curve displayed in Figure 2.11, where one $U_2 \geq U_1$ and $F_2 \leq F_1$. In that case, the increment of dissipated energy ΔA would still be equal to the area of the triangle defined by the blue, green and red lines, which would be equal to the area of the green triangle, minus those of the blue and red ones, giving just as before

$$\Delta A = \frac{1}{2}\left[F_1\left(U_2 - U_1\right) - U_1\left(F_2 - F_1\right)\right] \tag{2.76}$$

In the end one can conclude that, to impose an increment of dissipated energy ΔA, one needs to have

$$\Delta A = \frac{1}{2}\left(F\Delta U - U\Delta F\right) \tag{2.77}$$

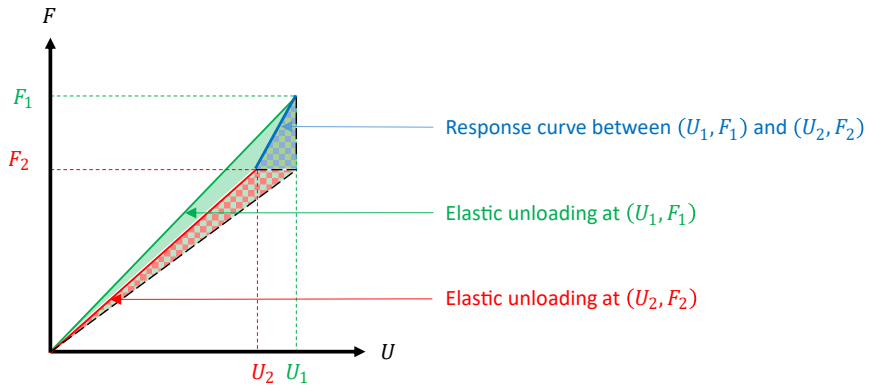

Figure 2.11: Computation of the increment of dissipated energy with snapback.

where F and U are the initial values of the force and displacement at the end of the bar, and ΔF and ΔU are their increments.

However, unlike the displacement-based strategy, this one cannot be directly used through a classical boundary condition, and requires a dedicated implementation that will be detailed in the next part. It is also worth noting that this driving strategy does not work with additional dissipation mechanisms, e.g. plasticity, since the elastic unloadings have to go through the origin of the response curve.

Numerical implementation and driving algorithm

As pointed out before, using the dissipation-based driving strategy requires a dedicated implementation, since the increment of force ΔF at the end of the bar needs to become an unknown just as the increments of displacement ΔU and nonlocal strain $\Delta\bar{\varepsilon}$. This was done by using a connecting user-defined element (UEL) located at the end of the bar (Figure 2.12), linking an unused rotational degree of freedom to the force at the end of the bar.

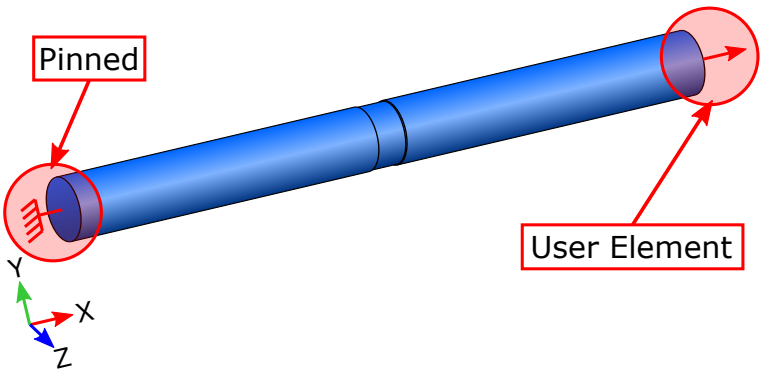

Figure 2.12: Considered geometry with boundary condition and UEL

Using the residuals associated with the element's behaviour, it was then possible to add the driving equation (2.77) to the coupled linearized problem (2.39), imposing the increment of energy dissipated in the bar. Noting A_0 the loading

parameter associated with this strategy, the driving equation writes

$$F\Delta U - U\Delta F = 2\ A_0\ dt \tag{2.78}$$

and the problem associated with the last element becomes

$$\begin{bmatrix} \mathbb{K}_{\mathcal{U}\mathcal{U}} & \mathbb{K}_{\mathcal{U}\mathcal{E}} & -1. \\ \mathbb{K}_{\mathcal{E}\mathcal{U}} & \mathbb{K}_{\mathcal{E}\mathcal{E}} & 0. \\ F & 0. & -U \end{bmatrix} \cdot \begin{bmatrix} \Delta U \\ \Delta\bar{\varepsilon} \\ \Delta F \end{bmatrix} = \begin{Bmatrix} 0. \\ 0 \\ A_0\ dt \end{Bmatrix} \tag{2.79}$$

Regarding the solving algorithm (Figure 2.13), one can note that the UEL subroutine associated with the connecting element is called at each time step, before moving to the other elements, and contributes to the global residual that is used to check convergence.

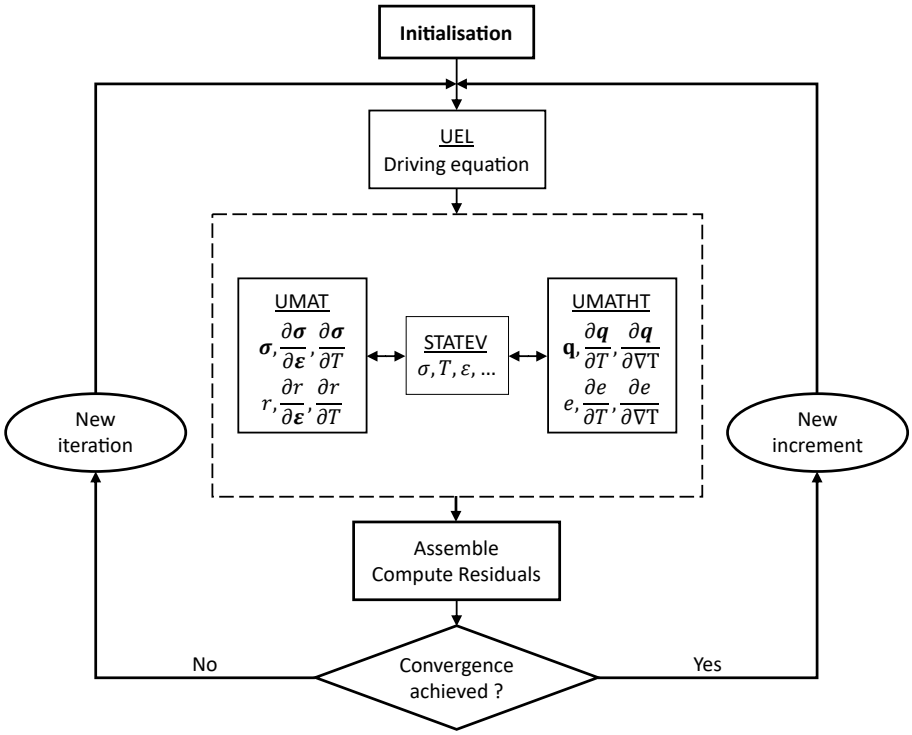

Figure 2.13: Resolution using UMATHT and UMAT subroutines along with a UEL at the bar's end.

This strategy appears to be well suited to compute the post-peak part of the curve, even with snap-back instabilities, but it cannot be used to drive the elastic loading since no energy is dissipated in this part. One thus needs to find a driving algorithm that handles both part of the curve without knowing in advance when the peak will be reached, and whether snap-back instabilities will occur or not.

Based on the advantages and drawbacks inherent to the displacement-based and dissipation based strategies, it was decided here to use both with a suitable commuting condition. The idea was to use the displacement based strategy for the non-dissipatve part of the loading, namely the elastic part before the peak, and to move to the dissipation based strategy after the peak for the softening part. Doing

so should ensure that the post-peak part of the curve can be computed, along with the elastic part, whether snap-back instabilities occur or not.

In that case, the displacement-based strategy needs to be implemented using the same tools, imposing the increment in displacement through the UEL's residuals. Noting U_0 the loading parameter associated with this strategy, the driving equation thus writes

$$\Delta U = U_0 \; dt \tag{2.80}$$

and the problem associated with the last element becomes

$$\begin{bmatrix} \mathbb{K}_{\mathcal{U}\mathcal{U}} & \mathbb{K}_{\mathcal{U}\mathcal{E}} & -1. \\ \mathbb{K}_{\mathcal{E}\mathcal{U}} & \mathbb{K}_{\mathcal{E}\mathcal{E}} & 0. \\ 1. & 0. & 0. \end{bmatrix} \cdot \begin{bmatrix} \Delta U \\ \Delta \bar{\varepsilon} \\ \Delta F \end{bmatrix} = \begin{Bmatrix} 0. \\ 0 \\ U_0 \; dt \end{Bmatrix} \tag{2.81}$$

The main issue was then to detect the peak in order to change the driving strategy precisely at the beginning of the softening. It was thus decided to use an energy based criterion, checking whether the new increment is likely to dissipate some energy and choosing the driving method accordingly. This choice was handled on the UEL level, by checking whether the dissipation ΔA_{try} associated with the new increment, defined as

$$\Delta A_{try} = \frac{1}{2} \left(F \Delta U - U \Delta F \right) \tag{2.82}$$

was equal to 0. The dissipation-based strategy (2.79) would then be used when ΔA_{try} is greater than 0, namely during most of the post-peak part of the curve, while the displacement-based strategy (2.81) would be used during the elastic loading and the last part of the curve when F gets close to 0.

This driving algorithm enables the computation of all three parts of the curve without knowing a priori when the peak will be reached, and whether snap-back instabilities will occur or not. It was used to handle the numerical simulations that will be presented in the next part and used to assess the properties of the different nonlocal models that will be studied here.

2.4 Numerical results and properties of the nonlocal approaches

This part presents the numerical results obtained with the driving algorithm introduced in Part 2.3.2 in order to assess the properties of the nonlocal damage models considered here. This assessment was done based on the expected properties of what we call here a "good" damage model (cf.Part 1.3.3), and especially the one regarding the crack behaviour

- final zero stress
- convergence and mesh independence

- no interaction through a pseudo-crack (when $D = 1$)
- existence of a solution with a displacement jump at $D = 1$
- localization in a single element when $D = 1$

The numerical problem studied here is the one described in Figure 2.12, a 1D bar under tension made of an homogeneous isotropic material, with a weakened element at the middle.

2.4.1 Realism of the associated behaviour

The first criterion considered here is the "realism" of the response curve, which will be studied by comparing the results obtained with each nonlocal formulation to those obtained with the local one.

The response curves and damage profiles obtained with both the local and classical (Peerlings') nonlocal formulation are plotted in Figure 2.14. First, one can note that the elastic part of the loading is identical for both models, and that the curve exhibits the expected stress drop after the peak. Moreover, the damage profile is much wider with the nonlocal damage model, which seems more realistic in the sense that damage is not only localized in a single element. However, the fact that damage reaches 1 in such a wide area is not consistent with the expected properties since it is not likely to reproduce a crack behaviour due to the width of the pseudo-crack.

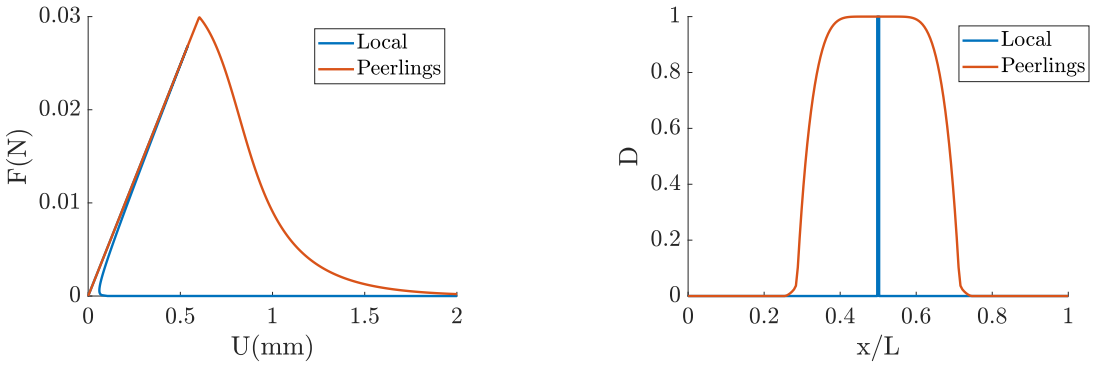

(a) On the force-displacement curves

(b) On the damage profiles

Figure 2.14: Influence of the Peerling's formulation on the local behaviour.

Moving on to the Phase-Field based formulation, the response curves and damage profiles obtained with both this formulation and the local one are plotted in Figure 2.15. First, one can note that, as for the previous formulation, the elastic part of the loading is identical for both models, and that the curve exhibits the expected stress drop after the peak. Moreover, damage is still spread over a non-zero zone, which is consistent with the physical spreading of damage, but here it only reaches 1 in a single element and is thus more likely to reproduce a crack behaviour.

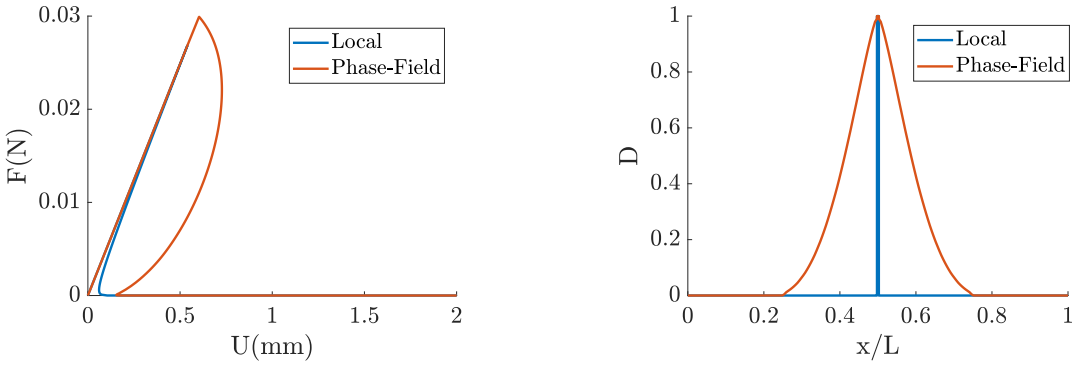

(a) On the force-displacement curves (b) On the damage profiles

Figure 2.15: Influence of the Phase-Field based formulation on the local behaviour.

Finally, regarding the eikonal-based formulation, the response curves and damage profiles obtained with both this formulation and the local one are plotted in Figure 2.16. First, one can note that, as for the previous formulation, the elastic part of the loading is identical for both models, and that the curve exhibits the expected stress drop after the peak. Moreover, as for the Phase-Field based formulation, damage is spread over a non-zero zone and reaches 1 in a single element which is fully consistent with the requirements of what we call a "good" damage model.

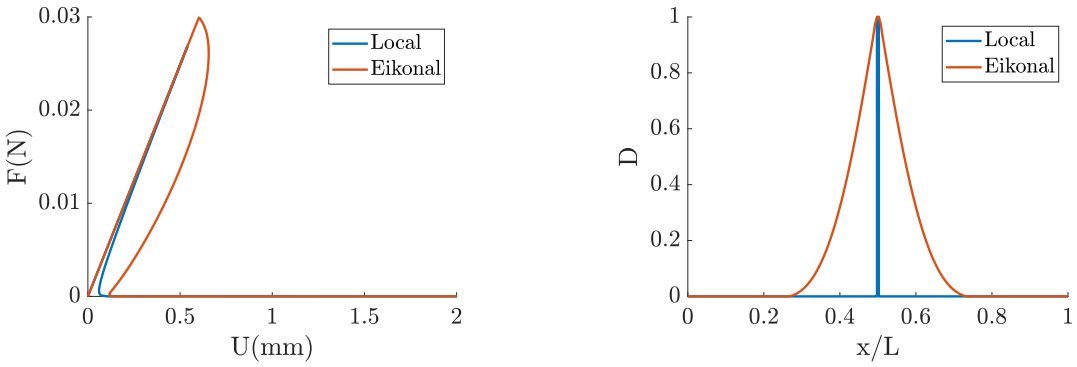

(a) On the response curves (b) On the damage profiles

Figure 2.16: Influence of the eikonal-based formulation on the local behaviour.

In the end, one can note that all three damage models meet this first requirement, associated with the response curve, even though only the eikonal-based and the Phase-Field based models seem likely to accurately reproduce a crack behaviour.

It is worth noting that the response curves obtained with both the eikonal-based and Phase-Field-based formulations are much more brittle than the one obtained with the classical one.

2.4.2 Convergence and mesh independence

Now that it has been checked that the considered formulations produce realistic results, one has to ensure that they converge toward a realistic solution, and become mesh-independent for a small enough element size.

The response curves and damage profiles obtained with the classical nonlocal formulation were plotted in Figure 2.17 for different levels of discretization (21, 41, 101 and 201 elements) of the considered geometry. First, one can note that both the response curve (Figure 2.17a) and the damage profile (Figure 2.17b) appear to become mesh independent for a small enough element size. Moreover, the results converge toward a realistic solution with a non-zero dissipated energy since the area under the response curve does not tend to 0, and the size of the damaged zone is constant and does not shrink to 0.

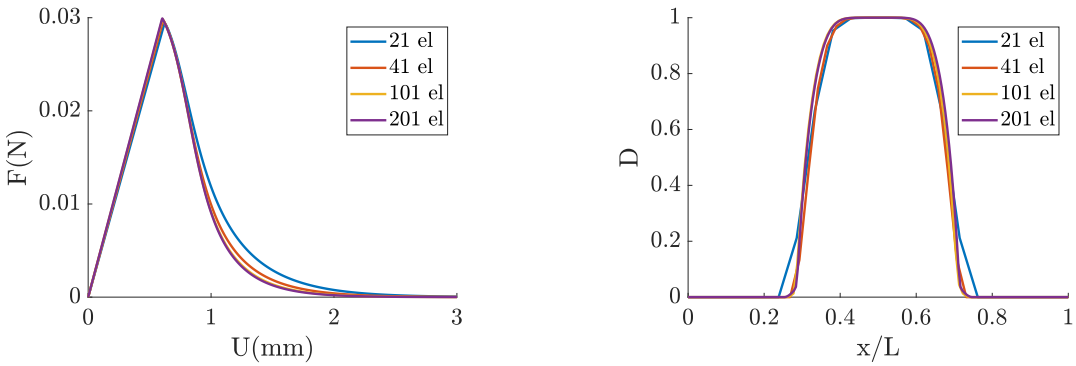

(a) On the force-displacement curves

(b) On the damage profiles

Figure 2.17: Mesh convergence of the classical nonlocal formulation.

Moving on to the Phase-Field based formulation, the response curves and damage profiles obtained with this formulation for different levels of discretization (21, 41, 101 and 201 elements) of the considered geometry were plotted in Figure 2.18. First, it can be seen that one still has convergence toward a realistic solution with a non-zero dissipated energy. However, although the damage profile becomes mesh-independent for a small element size (Figure 2.18b), it is not strictly the case for the response curve (Figure 2.18a). This small discrepancy is linked to the fact that, when reaching high damage levels, the size of the localization shrinks to 0, and thus becomes slightly mesh dependent. Despite this, one can note that for rather fine discretizations, namely for 101 and 201 elements, the difference between the response curves becomes negligible since it only concerns a very small part of the curve. As it is, the area under the curve has a very low sensitivity with respect to the element size, which results in a 1.9% variation in the dissipated energy.

Finally, regarding the eikonal-based nonlocal formulation, the response curves and damage profiles obtained with this formulation for the same levels of discretization of the considered geometry were plotted in Figure 2.19. First, it can be seen that one still has convergence toward a realistic solution with a non-zero dissipated energy. However, just as for the Phase-Field based formulation and despite the mesh independence of the damage profile (Figure 2.18b), the response curve does

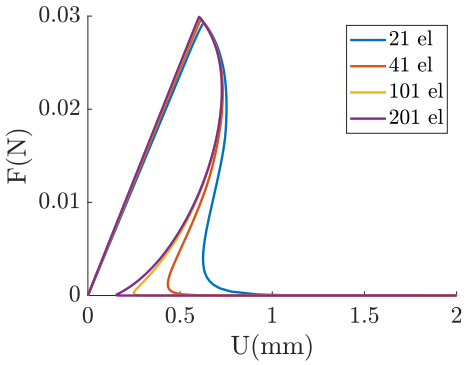

(a) On the force-displacement curves

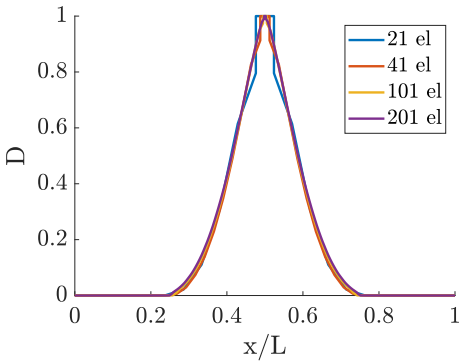

(b) On the damage profiles

Figure 2.18: Mesh convergence of the Phase-Field based nonlocal formulation.

not become strictly mesh independent (Figure 2.18a) due to the shrinkage of the damage profile at high levels of damage. Nonetheless, one can note that for rather fine discretization the difference between the response curves is once again negligible since it only concerns a very small part of the curve. The area under the curve still has a low mesh sensitivity, which results in a 4.4% variation in the dissipation.

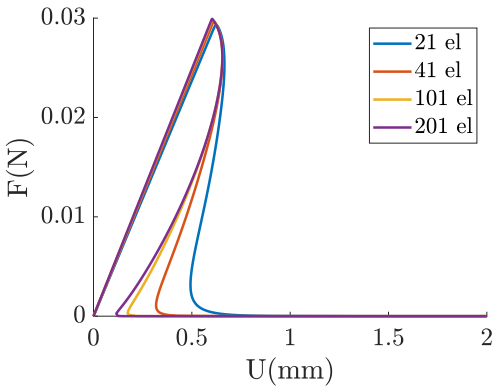

(a) On the force-displacement curves

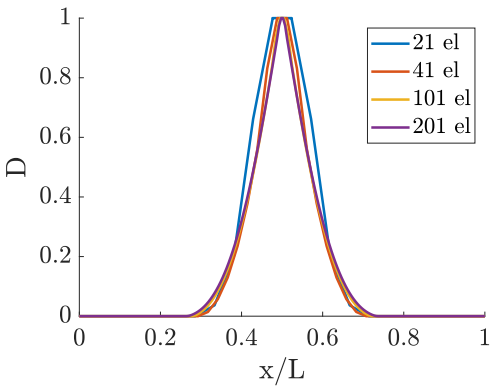

(b) On the damage profiles

Figure 2.19: Mesh convergence of the eikonal-based nonlocal formulation.

In the end, one can note that the results obtained with all three damage models tend to converge toward realistic solutions with a non zero dissipated energy. Moreover, the solution obtained with the classical nonlocal formulation becomes mesh-independent for small enough element size and, to some extend, so do the solutions obtained with the Phase Field based and eikonal-based formulations.

2.4.3 Pseudo-crack behaviour

The last criterion considered here is the fact that a highly damaged zone should behave as a crack, which means that no interaction should exist through a pseudo-crack ($D \approx 1$), and a solution with a displacement jump should exist at $D = 1$.

To meet the first requirement, the damage active zone, i.e the zone where damage increases, should shrink after the peak and tend to vanish when D gets close to 1, inducing a sharp damage profile. The size of this area, also referred to as the active length, will thus have to be studied in order to ensure that it tends to 0.

As one can see, this is not truly the case for the classical nonlocal formulation (Figure 2.20a) since, even though it slightly shrinks after a small increase in the early stages of damage, the active length does not tend to 0, and even increases when damage reaches 1 (Figure 2.20b).

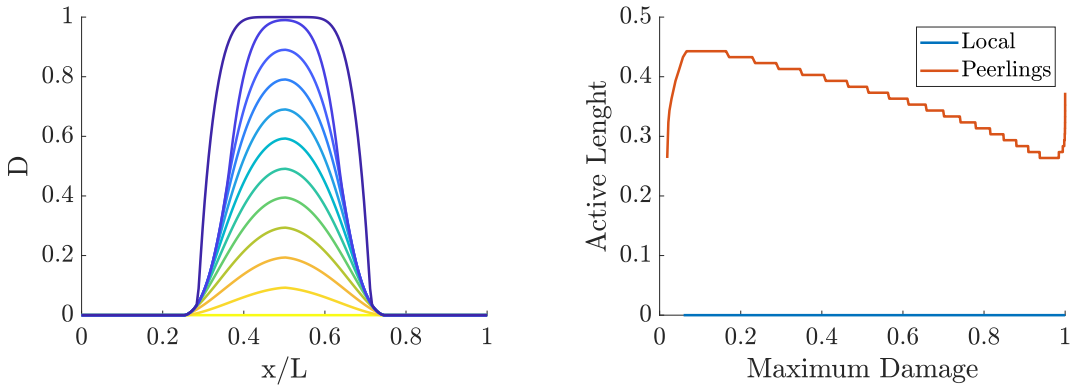

(a) Damage profile (b) Active zone

Figure 2.20: Evolution of the damage profile and active zone with the classical formulation.

On the other hand, the damage profile obtained with the Phase-Field based model (Figure 2.21a) does appear to shrink when damage increases, which is consistent with the decrease of the active length who tends to 0 when D gets close to 1 (Figure 2.21b). The initial peak observed on the evolution of the active length

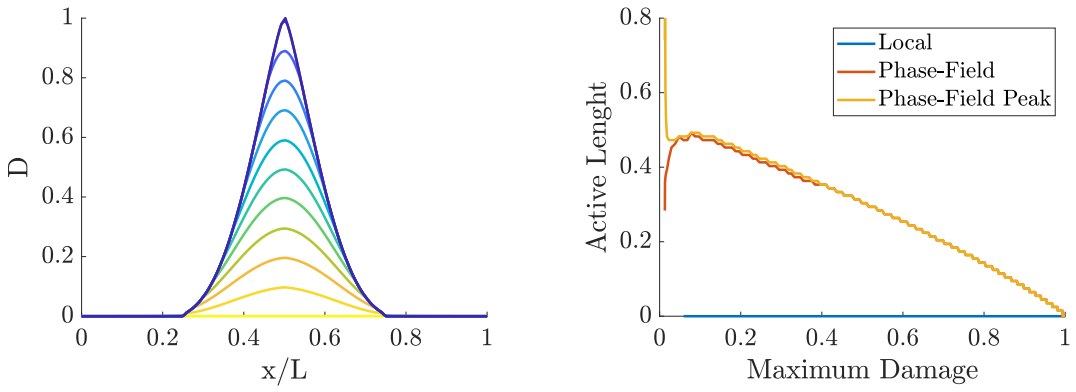

(a) Damage profile (b) Active zone

Figure 2.21: Evolution of the damage profile and active zone with the Phase-Field based formulation.

(orange curve) is linked to the fact that, due to the absence of damage thresh-

old with this formulation, one can observe very low levels of damage everywhere. Those very low levels of damage were not taken into account which explains the absence of the initial peak, and the occurrence of the initial increase also observed with the classical formulation.

Apart from the initial peak, the same thing can be said of the eikonal-based formulation, whose damage profile also shrinks when damage increases (Figure 2.22b), and whose damage active length also tends to 0 when D gets close to 1 after a small increase in the very early stages of damage (Figure 2.22a).

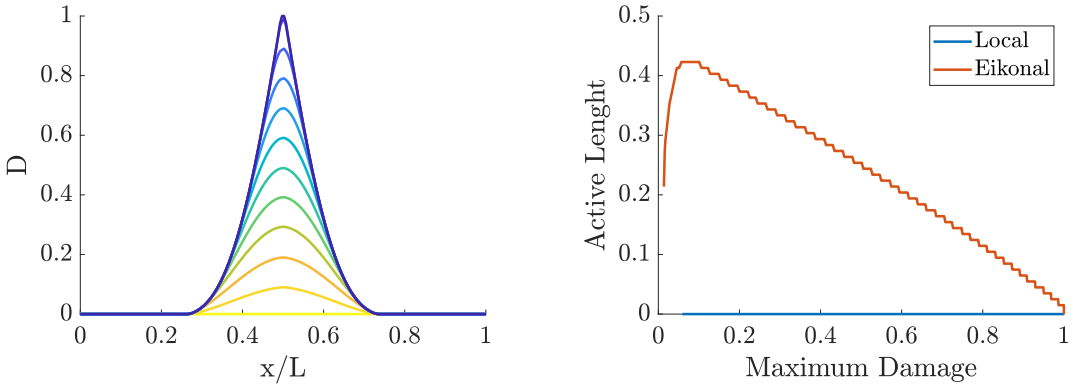

(a) Damage profile (b) Active zone

Figure 2.22: Evolution of the damage profile and active zone with the eikonal-based formulation.

Regarding the existence of a solution with a displacement jump, the displacement appears to be condensed near the middle of the bar, i.e where damage gets close to 1, at the end of the loading (Figure 2.23a), which is consistent with a crack behaviour. However, as one can see in Figure 2.23b, the classical nonlocal

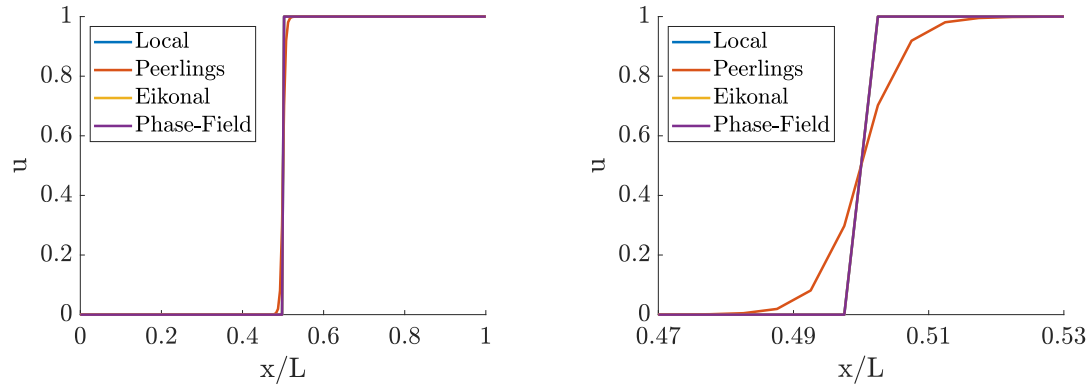

(a) In the entire bar (b) Near the middle

Figure 2.23: Displacement jump observed with all damage models.

model does not exhibit a true displacement jump which is consistent with the fact that the pseudo-crack is wider than a single element. On the other hand,

both the Phase-Field based and the eikonal-based formulations exhibit the same displacement discontinuity on a single element as the local formulation.

2.5 Conclusion of chapter 2

After having presented the formulations associated with the considered nonlocal damage models, their non-intrusive implementation was proposed using a thermo-mechanical analogy and a monolithic resolution with the tangent stiffness.

Two solutions were then proposed to handle the instabilities associated with the brittle responses: a stabilizing modification of the nonlocal treatments or the use of a dedicated dissipation based driving strategy. While the former might be easier to implement, only the second allows the precise computation of the complete response, which was needed to study the three nonlocal damage models properly.

Numerical simulations were then conducted using the non-intrusive implementation and the dissipation-based driving strategy to assess the relevance of the three considered formulations.

As expected, even though the classical nonlocal formulation addresses the issues linked to the spurious mesh dependency while keeping a "realistic" behaviour, it does not make a highly damaged zone equivalent to a crack. Thus it cannot be used to successfully bridge the gap between continuum damage mechanics and fracture mechanics.

As far as the Phase-Field-based and eikonal-based gradient-type formulations are concerned, they still address the issues linked to the spurious mesh dependency while keeping a "realistic" behaviour. The only possible drawbacks would be that the associated responses might be too brittle to reproduce a realistic material behaviour accurately. Moreover, both approaches appear to make a highly damaged zone equivalent to a crack and thus match all the requirements of what is called a "good" damage model here.

It thus confirms that both the eikonal-based and the Phase-Field-based formulations could be successfully used to fill the gap between continuum damage and fracture mechanics. Moreover, since its nonlocal treatment can be directly applied to any scalar damage driving variable, the eikonal-based formulation might be more versatile in terms of material behaviour. One could thus expect that this nonlocal model could be associated with other material behaviours, e.g. damage-plastic models, to get better modelling of materials such as concrete.

Chapter 3

Localization analysis of nonlocal isotropic damage and damage-plastic models

Contents

As seen in Chapter 2, coupling a pure isotropic damage model to the eikonal-based gradient-type formulation addresses the spurious mesh dependency associated with local formulations. Moreover, it also addresses one of the main issues associated with nonlocal formulations with fixed internal lengths since a highly damaged zone does behave as a crack.

However, one can note that, for a given set of material parameters, the load displacement curves obtained with the eikonal-based formulation are much more brittle than the ones obtained with the classical one. Besides, as pointed out before, the proper modelling of concrete failure requires taking into account the dissipation linked to crack friction and imperfect crack closure, which induces permanent strains [Terrien, 1980, Mazars et al., 1989, Mazars et al., 1990].

A classical way to address this issue would be to introduce plasticity in the considered damage model, namely by using the so-called damage-plastic framework [Simo and Ju, 1987a, Simo and Ju, 1987b, Ju, 1989, Govindjee et al., 1995, Feenstra and Borst, 1996, Meschke et al., 1998, Burlion et al., 2000, Nechnech et al., 2002, Gatuingt and Pijaudier-Cabot, 2003, Lemaitre and Desmorat, 2005, Jason et al., 2006, Grassl and Jirásek, 2006, Grassl and Jirásek, 2005, Desmorat et al., 2007b, Matallah and Borderie, 2009, Lemaitre et al., 2009]. A recent study by Jirasek and Desmorat [Jirásek and Desmorat, 2019] has shown the advantages of using such models coupled with nonlocal formulations with damage dependent interactions.

In order to see whether the introduction of plasticity can address the issues linked to the eikonal-based formulations, this chapter will focus on the study of two isotropic damage models, namely a pure damage one and damage-plastic one.

These models will first be studied on a single material point to compare the associated behaviors, before focusing on the formulations obtained by coupling them to the classical and eikonal-based nonlocal treatments. The bifurcation points, corresponding to the initial localization associated with each formulation, were then studied and later used to focus on how plasticity affects the material behavior in presence of both fixed and shrinking localization.

It is worth noting that, in order to get some insight on the influence of each component of the considered formulations, it was decided here to use simplified versions of the classical and eikonal-based nonlocal treatments.

3.1 Considered material behaviours

This part will present the local material behaviours considered in this chapter, namely a pure isotropic damage model and an isotropic damage-plastic model, along with a study of the influence of plasticity on stress evolution. It will then present the nonlocal formulations associated with these models that will be used throughout this chapter. It is worth noting that, since this chapter will only deal with one-dimensional cases, the models presented in this part will be written in a one-dimensional setting.

3.1.1 Local damage models

This part will first remind the pure isotropic damage model used previously, before introducing the damage-plastic model to which it will be compared here.

Isotropic damage model

The first local damage model considered here is the one presented in Chapter 1 which represents a pure isotropic model with isotropic damage. It is worth noting that, in this case, damage is driven by Mazars' equivalent strain, and no plasticity is considered. The model thus writes in a one-dimensional setting

$$\sigma = \tilde{E}\varepsilon = (1-D)E\boldsymbol{\varepsilon} \tag{3.1}$$

$$\hat{\varepsilon} = \langle \varepsilon \rangle \tag{3.2}$$

$$\kappa(t) = \max_{\tau \leq t} \hat{\varepsilon}(\tau) \tag{3.3}$$

$$D = g(\kappa) = \begin{cases} 0 & \text{if } \kappa < \varepsilon_0 \\ 1 - \dfrac{\varepsilon_0}{\kappa} \exp\left(-\dfrac{\kappa - \varepsilon_0}{\varepsilon_f - \varepsilon_0}\right) & \text{if } \kappa \geq \varepsilon_0 \end{cases} \tag{3.4}$$

Isotropic damage-plastic model

As pointed out before, the introduction of plasticity is mainly motivated by the need to introduce permanent strain for the modelling of concrete, though it should also help to increase the ductility of the eikonal-based damage model. Based on those considerations, and in order to get a meaningful comparison with the pure damage model, one could consider using a damage-plastic model with the same stress-strain law, the additional ductility being introduced through the permanent plastic strain. It was thus decided to use a plasticity-driven damage model with a Rankine criterion for plasticity.

Noting ε^p the uniaxial plastic strain, the stress-strain relation based on Hooke's law extended to plasticity and damage writes in a one-dimensional setting

$$\sigma = \tilde{E}\left(\varepsilon - \varepsilon^p\right) = (1-D)E\left(\varepsilon - \varepsilon^p\right) \tag{3.5}$$

In this case, damage evolution is assumed to be driven by the cumulative plastic strain p, defined through

$$\dot{p} = |\dot{\boldsymbol{\varepsilon}}^p| \tag{3.6}$$

The damage-driving variable κ then writes

$$\kappa(t) = \int_0^t \dot{p}(\tau)\mathrm{d}\tau = p(t) \tag{3.7}$$

which allows the taking into account of the plastic history, and ensures that damage does not decrease since $\dot{\kappa} \geq 0$.

One can note that, due to the differences in the driving phenomenon, the irreversibility condition is quite different from the one associated with the pure damage model. As it is, irreversibiliy is here imposed by integrating the norm of a function's derivative instead of taking the maximum value of the function's norm.

From this point, one still needs to address the issue of the plastic strain evolution. It was decided, due to the presence of damage, to use a criterion f based on the effective stress $\tilde{\sigma}$ introduced in [Lemaitre and Chaboche, 1985] and defined as

$$\tilde{\sigma} = \frac{\sigma}{1-D} = E\left(\varepsilon - \varepsilon^p\right) \tag{3.8}$$

The Rankine plasticity criterion used in this chapter thus writes in a one-dimensional setting

$$f\left(\tilde{\sigma}, p\right) = \tilde{\sigma} - \sigma_y(p) \tag{3.9}$$

$$f\ \dot{p} = 0, \quad f \leq 0, \quad \dot{p} \geq 0 \tag{3.10}$$

where σ_y is the yield stress that may depend on p in presence of hardening.

In the case of linear isotropic hardening R considered here, the yield stress writes

$$\sigma_y = \sigma_0 + R(p) = \sigma_0 + H\ p \tag{3.11}$$

where σ_0 is the yield stress of the virgin material, and H is the hardening coefficient.

In the end, to get a meaningfull comparison, one should use a damage evolution law that yields the same softening curve as the one associated with the pure damage model. Damage is thus assumed to be defined as

$$D = g(\kappa) = 1 - \frac{\sigma_0}{\sigma_0 + H\kappa} \exp\left(-\frac{(1 + H/E)\kappa}{\varepsilon_f - \varepsilon_0}\right) \tag{3.12}$$

where ε_f and ε_0 are still parameters governing damage evolution.

It is worth noting that no threshold is introduced in the damage evolution law, such a condition will be introduced through the plasticity criterion, and that the stress triaxiality effect is not taken into account.

Now that the considered local damage models have been introduced, one needs to compare the associated behaviours in simple settings such as a material point.

3.1.2 Comparison on a material point under tension

Using the model introduced in Part 3.1.1 in a uniaxial setting, one could expect that, in the absence of localization, the stress-strain law would be the same as the one associated with the pure damage plastic model, and that damage would have a slower evolution with respect to the total strain due to the introduction of plastic strain. One can thus expect that the influence of plasticity can be observed, either when localization occurs after the onset of plasticity, or when the localization area tends to shrink when damage grows.

This part will thus focus on the behaviour associated with both models when considering a single material point under monotonic uniaxial tension.

Influence of plasticity

First, one needs to check that the stress-strain laws associated with both models are identical. To do so, let's first consider the case of a material whose behaviour corresponds to the pure damage model with the set of material parameters described in Table 3.1 where $\varepsilon_f = 5\varepsilon_0$.

E	ν	ε_0	ε_f
30000 MPa	0.3	$1.e-4$	$5.e-4$

Table 3.1: Material parameters used with the pure damage model

In this case, keeping the stress-strain law (3.1), the equivalent strain will be equal to the constantly increasing total strain, giving the damage driving variable

$$\kappa(t) = \max_{\tau \leq t} \hat{\varepsilon}(\tau) = \varepsilon(t) \tag{3.13}$$

The damage evolution law then writes

$$D = \begin{cases} 0 & \text{if } \varepsilon < \varepsilon_0 \\ 1 - \dfrac{\varepsilon_0}{\varepsilon} \exp\left(-\dfrac{\varepsilon - \varepsilon_0}{\varepsilon_f - \varepsilon_0}\right) & \text{if } \varepsilon \geq \varepsilon_0 \end{cases} \tag{3.14}$$

which gives for the stress-strain law

$$\sigma = \begin{cases} E\varepsilon & \text{if } \varepsilon < \varepsilon_0 \\ E\varepsilon_0 \ \exp\left(-\dfrac{\varepsilon - \varepsilon_0}{\varepsilon_f - \varepsilon_0}\right) & \text{if } \varepsilon \geq \varepsilon_0 \end{cases} \tag{3.15}$$

On the other hand, in the case of a material whose behaviour is described by the damage-plastic model, one would need to use a set of parameters consistent with the one described in Table 3.1. It is worth noting that, though the peak stress σ_0 might look like an additional parameter, it is actually defined as $\sigma_0 = E\varepsilon_0$, the only additional parameter thus being the hardening parameter H.

Using $H = E/30$ as a default value for H, and in order to get meaningful comparison with the pure damage model, one can consider using the set of parameters described in Table 3.2 for the damage-plastic one.

E	ν	ε_0	ε_f	σ_0	H
30000 MPa	0.3	$1.e-4$	$5.e-4$	3 Mpa	1000 MPa

Table 3.2: Material parameters used with the damage-plastic model

Keeping the stress-strain law (3.5), the time derivative of the cumulative plastic strain will be equal to that of the plastic strain, giving for the damage-driving variable κ

$$\kappa(t) \quad = \quad \int_0^t \dot{p}(\tau) \mathrm{d}\tau = \varepsilon_p(t) \tag{3.16}$$

The plasticity criterion then gives

$$E(\varepsilon - \varepsilon_p) = \sigma_y = \sigma_0 + H\varepsilon_p \tag{3.17}$$

which, when ε is greater than ε_0, gives for the plastic strain

$$\varepsilon_p = E\left(\frac{\varepsilon - \varepsilon_0}{E + H}\right) \tag{3.18}$$

The damage evolution law then writes

$$D = \begin{cases} 0 & \text{if } \varepsilon < \varepsilon_0 \\ 1 - \dfrac{(E+H)\varepsilon_0}{E\varepsilon_0 + H\varepsilon} \exp\left(-\dfrac{\varepsilon - \varepsilon_0}{\varepsilon_f - \varepsilon_0}\right) & \text{if } \varepsilon \geq \varepsilon_0 \end{cases} \tag{3.19}$$

and, in the end, one has the stress-strain law

$$\sigma = \begin{cases} E\varepsilon & \text{if } \varepsilon < \varepsilon_0 \\ E\varepsilon_0 \ \exp\left(-\dfrac{\varepsilon - \varepsilon_0}{\varepsilon_f - \varepsilon_0}\right) & \text{if } \varepsilon \geq \varepsilon_0 \end{cases} \tag{3.20}$$

which is the same as the one obtained with the pure damage model.

Moreover, noting D_D and D_{DP} the damage levels associated respectively to the damage and damage plastic models, and defined in equations (3.14) and (3.19), one would also have for $\varepsilon \geq \varepsilon_0$

$$D_D - D_{DP} = \frac{E\varepsilon_0(\varepsilon - \varepsilon_0)}{\varepsilon(E\varepsilon_0 + H\varepsilon)} \exp\left(-\frac{\varepsilon - \varepsilon_0}{\varepsilon_f - \varepsilon_0}\right) \tag{3.21}$$

which is obviously greater than zero, meaning that $D_{DP} < D_D$.

The evolution of stress and damage with respect to strain is plotted in Figure 3.1 for both the damage and damage-plastic models, using the parameters described in Tables 3.1 and 3.2. One can see in Figure 3.1a that, as expected, the introduction of plasticity does not influence the stress-strain law, and thus the total energy dissipated up to complete failure. Moreover, Figure 3.1b shows that, as expected, it tends to slow damage evolution since, for a given strain, the damage level associated with the damage plastic model will be lower than the one associated with the pure damage model. This is also consistent with the fact that, to keep the same dissipated energy, the dissipation induced by plasticity needs to be compensated by a decrease in the one linked to damage.

Since $(E, \nu, \varepsilon_0, \varepsilon_f)$ are common to both models, and since σ_0 can be defined from (E, ε_0), the only additional parameter introduced by the damage-plastic model, and whose influence thus needs to be studied here, is the hardening parameter H.

Influence of hardening

After studying how the introduction of plasticity affects the material behaviour, one needs to study the influence of hardening which is controlled through H.

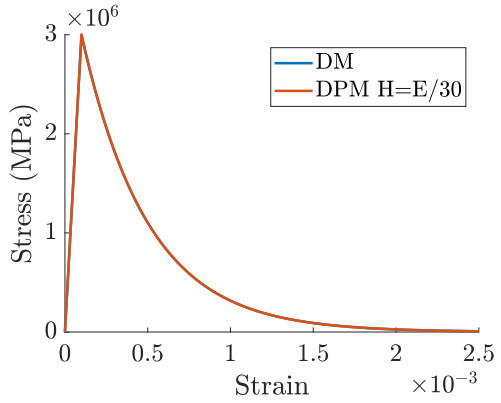

(a) Stress-strain curves.

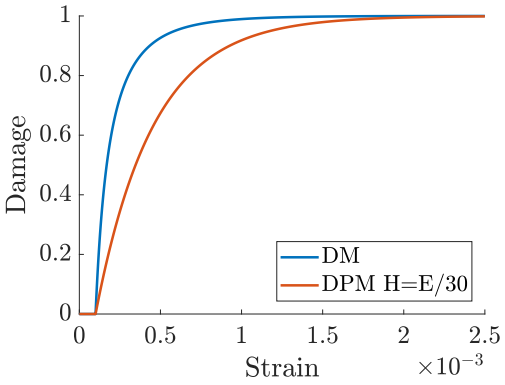

(b) Damage evolution.

Figure 3.1: Stress-strain curves and damage evolution associated with both models.

The first and straightforward effect of this parameter is to influence the evolution of plasticity since, according to equation (3.18), any increase in H could be expected to induce an increase in the plastic strain rate. Since plasticity has been shown to have no influence on the stress-strain curve, one can assume that changing its evolution rate will have no influence either.

The evolution of both stress and plastic strain with respect to the total strain have been plotted in Figure 3.2 for different values of H in order to check the influence of this parameter. As expected, one can thus see in Figure 3.2a that it does not have any influence on the stress-strain curve, while Figure 3.2b shows that, for a given strain level ε, any increase in H would induce a decrease in ε_p.

As far as damage is concerned, one could expect that, based on equation (4.16), an increase in the hardening parameter would tend to increase the evolution rate of damage with respect to the plastic strain. Moreover, due to its negative influence on the plastic strain rate, the hardening parameter can also be expected to have a positive effect on damage evolution with respect to the total strain since, in order to keep a constant dissipated energy, a decrease in plasticity should be compensated by an increase in damage. This assumption can be easily checked since, for a given strain $\varepsilon > \varepsilon_0$ and set of parameters (E, ε_0, ε_f), when considering the damages D_1 and D_2 corresponding respectively to the hardening parameters $H_1 = H$ and $H_2 = H + \delta H$ ($\delta H > 0$), one would get based on equation (3.19)

$$D_2 - D_1 = \frac{\delta H E(\varepsilon - \varepsilon_0)\varepsilon_0}{(E\varepsilon_0 + H\varepsilon)(E\varepsilon_0 + H\varepsilon + \delta H\varepsilon)} \exp\left(-\frac{\varepsilon - \varepsilon_0}{\varepsilon_f - \varepsilon_0}\right) \tag{3.22}$$

which is greater than zero.

In order to check those assumptions, the evolution of damage with respect to both the total strain and the plastic strain has been plotted in Figure 3.3 for different values of H. One can thus see in Figure 3.3b that, for a given strain ε, an increase in the hardening parameter would induce an increase in damage, while Figure 3.3a shows that it has a similar influence on damage for a given plastic strain.

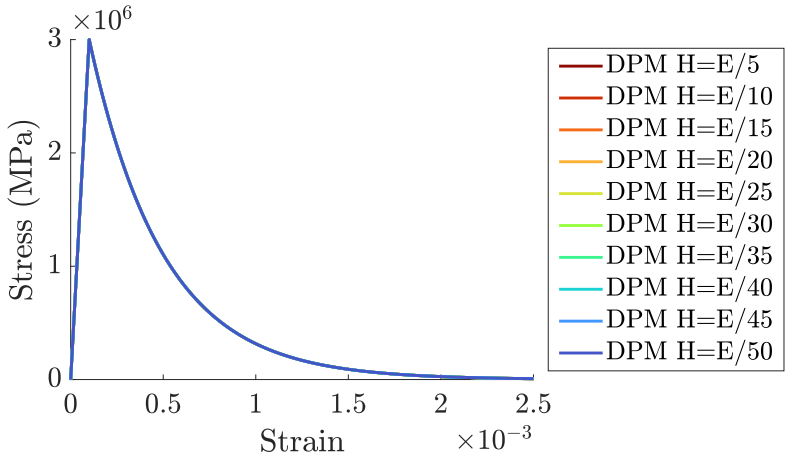

(a) Stress-strain curves.

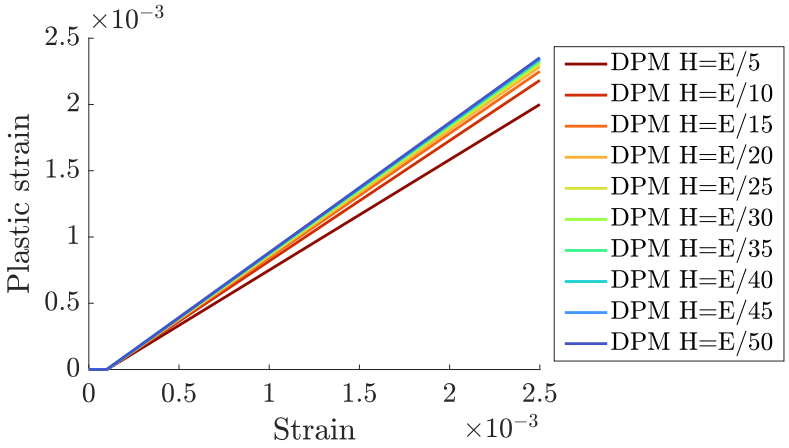

(b) Plastic strain evolution.

Figure 3.2: Influence of hardening on stress and plastic strain evolution.

This part has shown that, as expected, the introduction of plasticity does not affect the evolution of stress with respect to strain, but it does tend to slow down damage evolution. Moreover, though it does not affect the stress-strain law, the hardening parameter can be used to control both plasticity and damage evolutions.

Now that one has seen the influence of plasticity on a material point, its influence in presence of localization, either in a fixed or shrinking area, needs to be studied.

3.1.3 Considered nonlocal formulations

This part will present the formulations associated with both the isotropic damage and damage-plastic models coupled with a general nonlocal operator $\mathcal{F}$ used to handle localization, before introducing the nonlocal treatments considered here. As before, this part will only deal with one dimensional equations.

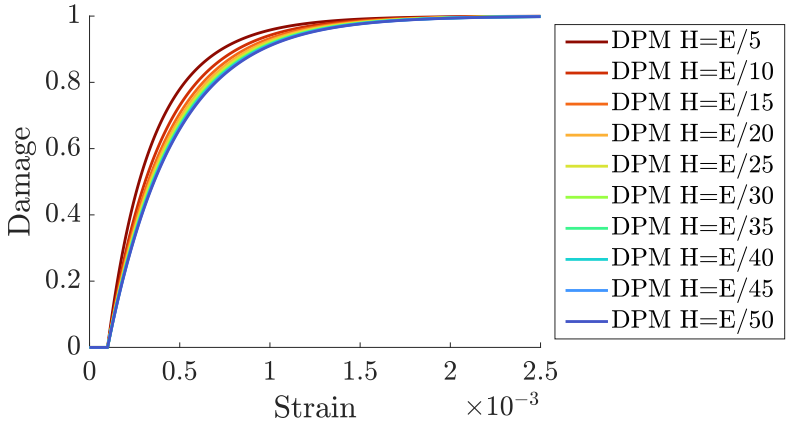

(a) Evolution with respect to the total strain.

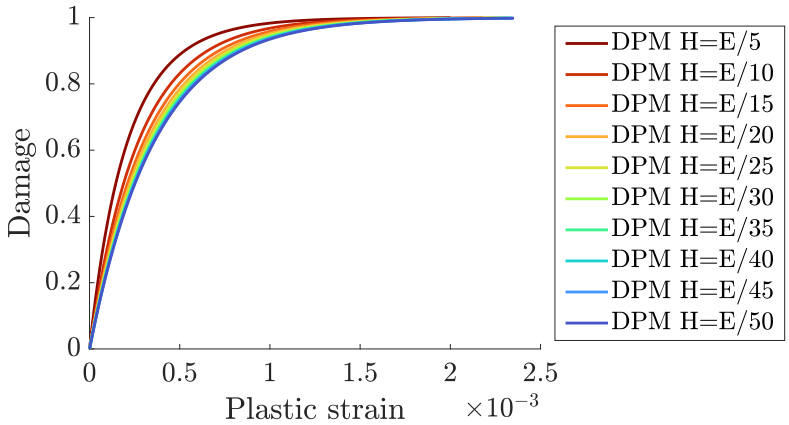

(b) Evolution with respect to plasticity.

Figure 3.3: Influence of hardening on damage evolution.

Nonlocal isotropic damage model

As pointed out, Chapter 1, the formulation associated with a nonlocal isotropic damage model keeps both the stress-strain law (3.1) and damage evolution law (3.4) of the local damage model. However, the damage driving variable κ is then defined as the maximum value of the nonlocal strain $\bar{\varepsilon}$ computed from Mazars equivalent strain (4.2) as

$$\bar{\varepsilon} = \mathcal{F}\left(\hat{\varepsilon}\right) \tag{3.23}$$

where $\mathcal{F}$ is the nonlocal operator, which can take various forms such as a differential expression or a convolution.

Nonlocal isotropic damage-plastic model

In a similar fashion, in the case of a nonlocal isotropic damage-plastic model, the formulation would keep both the stress-strain law (3.5) and damage evolution law (3.12), along with equations (3.6) to (3.11) linked to plasticity evolution.

However, following the work done for nonlocal plasticity [Vermeer and Brinkgreve, 1994, Strömberg and Ristinmaa, 1996] and later extended to nonlocal plasticity

combined with damage [Grassl and Jirásek, 2005], one uses the so-called over-nonlocal damage driving variable κ defined as

$$\kappa = m\ \bar{p} + (1-m)p \tag{3.24}$$

where m is a numerical parameter, and $\bar{p}$ is the nonlocal cumulative plastic strain computed from p through

$$\bar{p} = \mathcal{F}(p) = 0 \tag{3.25}$$

where $\mathcal{F}$ is still the nonlocal operator. It is worth noting that the particular cases $m = 0$ and $m = 1$ respectively correspond to the use of the local and nonlocal damage-driving variables. The so-called over-nonlocal formulations correspond to the cases where $m > 1$.

Considered gradient-type formulations

This section will present the equations associated with the considered nonlocal treatments, that will be used to replace equation (3.23) for the pure damage model and (3.25) for the damage plastic one.

The nonlocal formulations presented in this section will involve a local variable $\mathcal{V}$, and its nonlocal counterpart $\bar{\mathcal{V}}$, which will need to be replaced either by $\hat{\varepsilon}$ and $\bar{\varepsilon}$ for the pure damage model, or by p and $\bar{p}$ for the damage-plastic model.

The first gradient-type formulation considered here is the classical one, which writes in a one-dimensional setting

$$\bar{\mathcal{V}} - c^2\ \bar{\mathcal{V}}'' = \mathcal{V} \tag{3.26}$$

where $\bar{\mathcal{V}}''$ stands for the second order spatial derivative of $\bar{\mathcal{V}}$.

Similarly, the second gradient-type formulation is the general one, which writes

$$\bar{\mathcal{V}} - a\ \left(b\ \bar{\mathcal{V}}'\right)' = \mathcal{V} \tag{3.27}$$

where $\bar{\mathcal{V}}'$ and $\left(b\ \bar{\mathcal{V}}'\right)'$ stand for the spatial derivatives of $\bar{\mathcal{V}}$ and $\left(b\ \bar{\mathcal{V}}'\right)$, and a and b are functions that may depend on state variables such as stress, strain or damage.

It is worth noting that equation (3.27) can stand for any gradient-type formulations, including the eikonal-based ones, provided one choose the functions a and b accordingly. As an example, to use the eikonal-based formulation (2.8) interpreted as the one-dimensional version of the anisotropic damage model, which writes

$$\bar{\varepsilon} - c^2\ (1-D)^{1/2}\ \left((1-D)^{1/2}\ \bar{\varepsilon}'\right)' = \hat{\varepsilon} \tag{3.28}$$

one would need to set

$$a = c^2(1-D)^{1/2}, \quad b = (1-D)^{1/2} \tag{3.29}$$

The formulations introduced in this section will be studied in the rest of this chapter in order to study how the introduction of plasticity affects the regularization properties of gradient-type nonlocal treatments.

3.2 Study of the bifurcation point, and prediction of the initial localization in 1D

Since the considered formulations are expected to address the spurious mesh dependency of strain localization by fixing the size of the area where it develops, one could start with their localization analysis. Following the work done in [Jirásek, 2018], this part will study the bifurcation point in order to check that the size of the initial localization is indeed imposed, and to determine its value.

These analyses will be conducted in a one-dimensional setting, considering the simple case of a homogeneous bar submitted to tension, which allows the study of this property through relatively simple nonlinear equations. In this case, the onset of localization will be seen as the bifurcation from a homogeneous and potentially damaged state, further evolution of the active zone will not be considered here.

3.2.1 Gradient damage model

The first formulation considered here is the one obtained with the pure damage model and the classical gradient-type nonlocal treatment.

To do so, one must first consider an initially homogeneous material, and then study the nonlocal equation on the onset of localization. At this point, damage will localize in a zone $\mathcal{Z}_d$ of size L_d, whilst it will stop growing in the rest of the bar $\mathcal{Z}_e$.

In the case of a bar submitted to tension, Mazars' equivalent strain $\hat{\varepsilon}$ is still equal to the total strain ε, the stress is still defined through (3.1), and the gradient equation (3.26), used to compute the nonlocal strain $\bar{\varepsilon}$, writes

$$\bar{\varepsilon} - c^2\ \bar{\varepsilon}'' = \varepsilon \tag{3.30}$$

where $\bar{\varepsilon}''$ stands for the second space derivative of $\bar{\varepsilon}$.

In the damaging zone $\mathcal{Z}_d$ one thus has $D = g(\bar{\varepsilon})$, and the Hooke's law (3.1) can be derived as

$$\dot{\sigma} = E_s\dot{\varepsilon} + (E_t - E_s)\dot{\bar{\varepsilon}} \tag{3.31}$$

where g_κ is the derivative of function g, and E_s and E_t are respectively the secant and tangent moduli defined as

$$E_s = (1 - g(\bar{\varepsilon}))E \tag{3.32}$$

$$E_t = (1 - g(\bar{\varepsilon}) - \varepsilon g_\kappa(\bar{\varepsilon}))E \tag{3.33}$$

on the other hand, in the non-damaging zone $\mathcal{Z}_e$, D is constant and the Hooke's law (3.1) can be derived as

$$\dot{\sigma} = E_s\dot{\varepsilon} \tag{3.34}$$

As far as the nonlocal equation (3.30) is concerned, considering that, on the onset of damage, the solution is initially homogeneous ($\bar{\varepsilon}'' = 0$), one has in $\mathcal{Z}_d$

$$\dot{\bar{\varepsilon}}E_t - c^2\ \dot{\bar{\varepsilon}}''E_s = \dot{\sigma} \tag{3.35}$$

and in $\mathcal{Z}_e$

$$\dot{\bar{\varepsilon}} E_s - c^2 \, \dot{\bar{\varepsilon}}'' E_s = \dot{\sigma} \tag{3.36}$$

Focusing on $\dot{\bar{\varepsilon}}_d$, one can note that it should be maximum at $x = 0$ and that, based on (3.35), one needs to have

$$c^2 \frac{E_s}{E_t} < 0 \tag{3.37}$$

to get a harmonic (not exponential) solution in $\mathcal{Z}_d$, while the solutions in both parts of $\mathcal{Z}_e$ should be decreasing exponential functions. Hence, localization can only occur when the tangent modulus becomes negative, i.e. during the softening part and, considering a localization area centered at $x = 0$, one has $x \in \mathcal{Z}_d \;\Leftrightarrow\; |x| < L_d/2$ and $x \in \mathcal{Z}_e \;\Leftrightarrow\; |x| \geq L_d/2$.

Since $\dot{\bar{\varepsilon}}_d$ needs to be continuous throughout the bar, and especially in $x = \pm L_d/2$ where it is equal to 0, one would get for $\dot{\bar{\varepsilon}}$

$$\dot{\bar{\varepsilon}}(x) = \begin{cases} \dfrac{\dot{\sigma}}{E_s}\left(1 - \exp\left(\dfrac{L_d + 2x}{2c}\right)\right), & \text{for } x < -\dfrac{L_d}{2} \\ \dfrac{\dot{\sigma}}{E_t}\left(1 - \dfrac{\cos(\lambda x)}{\cos(\lambda L_d/2)}\right), & \text{for } |x| \leq \dfrac{L_d}{2} \\ \dfrac{\dot{\sigma}}{E_s}\left(1 - \exp\left(\dfrac{L_d - 2x}{2c}\right)\right), & \text{for } x > \dfrac{L_d}{2} \end{cases} \tag{3.38}$$

and for its gradient

$$\dot{\bar{\varepsilon}}_d{}'(x) = \begin{cases} \dfrac{\dot{\sigma}}{cE_s} \exp\left(\dfrac{L_d - 2x}{2c}\right), & \text{for } x < -\dfrac{L_d}{2} \\ \dfrac{\lambda\dot{\sigma}}{E_t} \dfrac{\sin(\lambda x)}{\cos\left(\lambda \frac{L_d}{2}\right)}, & \text{for } |x| \leq \dfrac{L_d}{2} \\ \dfrac{-\dot{\sigma}}{cE_s} \exp\left(\dfrac{L_d + 2x}{2c}\right), & \text{for } x > \dfrac{L_d}{2} \end{cases} \tag{3.39}$$

where the parameter λ is defined as

$$\lambda = \frac{1}{c}\sqrt{-\frac{E_t}{E_s}} \tag{3.40}$$

Finally, taking the continuity of $\dot{\bar{\varepsilon}}'$ at $x = \pm L_d/2$ into account, one gets

$$\tan(\lambda L_d/2) = \frac{E_t}{E_s}\frac{1}{\lambda c} \tag{3.41}$$

which gives

$$L_d = 2c\sqrt{-\frac{E_s}{E_t}}\left(n_1\pi - \arctan\left(\sqrt{-\frac{E_t}{E_s}}\right)\right) \tag{3.42}$$

where n_1 is an integer.

Since the distance L_d has to be positive, one needs to have $n_1 \geq 1$, and since the more localized solution can be expected to be the more stable one, n_1 will thus be taken equal to 1 giving

$$L_d = 2c\sqrt{-\frac{E_s}{E_t}}\left(\pi - \arctan\left(\sqrt{-\frac{E_t}{E_s}}\right)\right) \tag{3.43}$$

On the onset of damage, one has $\varepsilon = \bar{\varepsilon} = \varepsilon_0$ and, based on equations (3.32) and (3.33), the ratio E_t/E_s writes

$$\frac{E_t}{E_s} = \frac{1 - g(\varepsilon_0) - \varepsilon_0 g_\kappa(\varepsilon_0)}{1 - g(\varepsilon_0)} = 1 - \varepsilon_0 g_\kappa(\varepsilon_0) = \frac{\varepsilon_0}{(\varepsilon_f - \varepsilon_0)} \tag{3.44}$$

In the end, using the material parameters detailed in Table 3.1, one gets

$$L_d = 4c(\pi - \arctan(1/2)) \tag{3.45}$$

$$\Rightarrow \quad L_d \approx 10.71c \tag{3.46}$$

Damage can then be expected to spread over a zone $\mathcal{Z}_d \approx [-5.35c; 5.35c]$, which will be compared to what can be expected with the damage-plastic model.

Let us now focus on the formulation associated with the general gradient-type nonlocal treatment. In that case, all equations would remain unchanged except the gradient one (3.30) which would be generalized to

$$\bar{\varepsilon} - a\ (b\ \bar{\varepsilon}')' = \hat{\varepsilon} \tag{3.47}$$

where a and b are functions of damage. As an example, in the particular case of the eikonal-based formulation (3.28), the rate form of equation (3.47) would write

$$\dot{\bar{\varepsilon}} - a_D\dot{D}(b\bar{\varepsilon}')' - a\Big(b_D\dot{D}\bar{\varepsilon}' + b\dot{\bar{\varepsilon}}'\Big)' = \dot{\varepsilon} \tag{3.48}$$

where a_D and b_D stand for the derivatives of functions a and b, defined in equation (3.29), with respect to damage. On the onset of localization, the nonlocal strain $\bar{\varepsilon}$ is uniform, and its spatial derivative thus vanishes giving

$$\dot{\bar{\varepsilon}} - a\Big(b\dot{\bar{\varepsilon}}'\Big)' = \dot{\varepsilon} \tag{3.49}$$

Moreover, if localization is still assumed to occur on the onset of damage, one also has $a = c^2$ and $b = 1$, and the rate equation (3.49) is then the same as the one associated with the classical gradient-type formulation. Therefore, all the analytical results describing the initial localization obtained with the classical gradient still hold true for the one obtained with the eikonal-based gradient, even though its active zone is expected to shrink afterwards.

3.2.2 Gradient damage-plastic model

After studying the initial localization of the gradient damage model, one must now focus on the damage-plastic one.

To do so, one will again consider a homogeneous material, before studying the nonlocal equation on the onset of localization. At this point, both plasticity and damage will localize in a zone $\mathcal{Z}_p$ of size L_p, and stop growing in the rest of the bar noted here $\mathcal{Z}_e$.

It is worth noting that in the specific case of a bar under tension considered here, the cumulative plastic strain p is simply equal to the plastic strain ε_p, and the gradient equation, used to compute its nonlocal counterpart $\bar{\varepsilon}_p$, thus write

$$\bar{\varepsilon}_p - c^2\ \bar{\varepsilon}_p'' = \varepsilon_p \tag{3.50}$$

As described in Part 3.1, damage is here driven by a combination of local and nonlocal plastic strain whose rate gives

$$\dot{\kappa} = m\dot{\bar{\varepsilon}}_p + (1-m)\dot{\varepsilon}_p \tag{3.51}$$

For convenience, the damage evolution law (3.12) will be written in the form

$$D = g(\kappa) = 1 - \frac{\sigma_0}{\sigma_0 + H\kappa}\exp\left(-\gamma\kappa\right) \tag{3.52}$$

where γ is an additional parameter defined as

$$\gamma = \frac{1 + H/E}{\varepsilon_f - \varepsilon_0} \tag{3.53}$$

which gives for the damage rate

$$g_\kappa(\kappa) = \frac{\sigma_0}{\sigma_0 + H\kappa}\left(\gamma + \frac{H}{\sigma_0 + H\kappa}\right)\exp\left(-\gamma\kappa\right) \tag{3.54}$$

and for its value on the onset of damage

$$g_\kappa^0 = g_\kappa(0) = \gamma + \frac{H}{\sigma_0} \tag{3.55}$$

The model considered here suggests that plastic yielding and damage growth will start simultaneously when the elastic limit σ_0 is attained.

Stress in the localization area would then be given by

$$\sigma = (1 - g(\kappa))(\sigma_0 + H\varepsilon_p) \tag{3.56}$$

and its differentiation with respect to time writes

$$\dot{\sigma} = (1 - g(\kappa))H\dot{\varepsilon}_p - g_\kappa(\kappa)(\sigma_0 + H\varepsilon_p)\dot{\kappa} \tag{3.57}$$

On the onset of plasticity, which also corresponds to the onset of damage, one has $\kappa = \varepsilon_p = 0$ and $g(\kappa) = 0$, which brings

$$\dot{\sigma} = \left(H - g_\kappa^0\sigma_0(1-m)\right)\dot{\varepsilon}_p - mg_\kappa^0\sigma_0\dot{\bar{\varepsilon}}_p \tag{3.58}$$

and, since the rate of the local plastic strain is given by

$$\dot{\varepsilon}_p = \dot{\bar{\varepsilon}}_p - c^2 \dot{\bar{\varepsilon}}''_p \tag{3.59}$$

equation (3.58) becomes

$$\left(H - g^0_\kappa \sigma_0\right) \dot{\bar{\varepsilon}}_p - c^2 \left(H - g^0_\kappa \sigma_0 (1-m)\right) \dot{\bar{\varepsilon}}''_p = \dot{\sigma} \tag{3.60}$$

It is worth noting that, due to equilibrium, the stress rate is uniform along the bar, and (3.60) is thus a second-order differential equation with constant coefficients and constant right-hand side.

A harmonic (not exponential) solution exists if and only if $H - g^0_\kappa \sigma_0$ and $H - (1-m) g^0_\kappa \sigma_0$ are of opposite signs. Since m, g^0_κ and σ_0 are positive, one has

$$H - g^0_\kappa \sigma_0 < H - (1-m) g^0_\kappa \sigma_0 \tag{3.61}$$

and the conditions for the existence of a harmonic solution then writes

$$\begin{cases} H - g^0_\kappa \sigma_0 < 0 \\ H - (1-m) g^0_\kappa \sigma_0 > 0 \end{cases} \tag{3.62}$$

For $m \geq 1$ and $H > 0$ (or $m > 1$ and $H \geq 0$), the second condition is always satisfied, and the first one gives

$$g^0_\kappa > \frac{H}{\sigma_0} \tag{3.63}$$

Considering a process zone centered on $x = 0$, $\dot{\varepsilon}_p$ should be maximum at this point and equal to 0 at $x = \pm L_d/2$, which gives

$$\dot{\bar{\varepsilon}}_p(x) = -\frac{\dot{\sigma}}{g^0_\kappa \sigma_0 - H} + A_1 \cos \frac{\lambda x}{c} \tag{3.64}$$

where

$$\lambda = \sqrt{\frac{g^0_\kappa \sigma_0 - H}{(m-1) g^0_\kappa \sigma_0 + H}} \tag{3.65}$$

and, using (3.59), one gets the condition

$$A_1 (1 + \lambda^2) \cos \frac{\lambda L_p}{2c} = \frac{\dot{\sigma}}{g^0_\kappa \sigma_0 - H} \tag{3.66}$$

To get an estimation of the localization length, one now needs to focus on the unloading zone $\mathcal{Z}_e$ where the plastic strain rate satisfies the differential equation

$$\dot{\bar{\varepsilon}}_p(x) - c^2 \dot{\bar{\varepsilon}}''_p(x) = 0 \tag{3.67}$$

which, in order to keep the solution bounded when x tends to ∞, $\dot{\bar{\varepsilon}}_p$, gives

$$\dot{\bar{\varepsilon}}_p(x) = A_2 \exp(-x/c) \tag{3.68}$$

for which one has

$$\dot{\bar{\varepsilon}}_p(x) + c\dot{\bar{\varepsilon}}'_p(x) = 0 \tag{3.69}$$

Imposing this condition at $x = L_p/2$ using the expression of $\dot{\bar{\varepsilon}}_p$ in $\mathcal{Z}_p$, one gets

$$-\frac{\dot{\sigma}}{g_\kappa^0\sigma_0 - H} + A_1 \cos\frac{\lambda L_p}{2c} - A_1\lambda \sin\frac{\lambda L_p}{2c} = 0 \tag{3.70}$$

which, when coupled with (3.66), gives

$$\tan\left(\frac{\lambda L_p}{2c}\right) = -\lambda \tag{3.71}$$

In the end, using the parameters detailed in Table 3.2 and setting $m = 1$ to use the nonlocal damage driving variable, the size of the initial localization area writes

$$L_p = \frac{2c}{\lambda}\left[\pi - \arctan\left(\sqrt{\frac{g_\kappa^0\sigma_0 - H}{(m-1)g_\kappa^0\sigma_0 + H}}\right)\right] \tag{3.72}$$

$$\Rightarrow \quad L_p \approx 1.38c \tag{3.73}$$

Both damage and plastic strain can then be expected to spread over a zone $\mathcal{Z}_p \approx [-1.38c; 1.38c]$ which, for a given internal length c, is smaller than the one associated with the pure damage model.

As for the pure damage model, one now needs to focus on the general gradient-type formulation. All equations would then remain identical, except for the gradient-one (3.50) which would be generalized to

$$\bar{p} - a\ (b\ \bar{p}')' = p \tag{3.74}$$

where a and b are still functions of damage.

Focusing on the eikonal-based formulation (3.28) associated with the damage plastic model, one can then follow the same steps as the pure damage model. Assuming that localization still occurs on the onset of both damage and plasticity, it can be shown that the rate equation deriving from it will be identical to the one associated with the classical gradient-type formulation.

As before, the analytical results regarding the initial localization obtained with the classical gradient and the damage-plastic model still hold true with this formulation, even though the active zone will shrink afterwards.

It has been shown in this part that both the classical and general gradient-type formulations coupled with damage and damage-plastic models impose the size of the localization area. This implies that they should address the ill-posedness of local models with strain softening.

3.3 Localization in a fixed area

After studying the influence of plasticity on both stresses and damage evolution, and on the localisation induced by the considered gradient-type formulations, one now needs to focus on its influence in presence of localization. As it is, to get some insight on whether it could be used to address the excessive brittleness observed in Chapter 2 with the eikonal-based formulation, one needs to see how the introduction of plasticity affects the associated response in a one-dimensional setting.

One way to do so without introducing any bias linked to numerical approximation would be to put aside the gradient-type equation and to compute the responses obtained by fixing the size of the localization area, along with its possible evolution. Besides, before moving on to a shrinking localization area that would represent the eikonal-based formulation, one should focus on the influence of plasticity when dealing with a fixed localization area like the one imposed by Peerling's formulation.

To do so, this part will deal with the case of a homogeneous bar of length L and section S, made up of a material whose behaviour corresponds either to the pure damage model or the damage-plastic one, and submitted to tension. In his fictitious case, localization will be assumed to occur in a fixed area of length l, which will play the role of L_d or L_p depending on the considered damage model. One will first compare the results thus obtained with both models when the size of the associated localization areas are identical, before studying the influence of variations in plasticity evolution through modifications of the hardening parameter.

3.3.1 Principle

To compute the global response of the bar submitted to tension, even on the occurrence of snap-back instabilities, it was decided here to use a local strain-based driving strategy. As it is, to get a loading that would not depend on either the material model, the set of parameters, or the size of the localization area, the idea was to impose a homogeneous strain throughout the localization area, with a linear time evolution. It is worth noting that, here, the size of the localization area will be considered as a given material parameter that, according to the results presented in Part 3.2, might depend on the hardening parameter.

Let's consider a centered localization area, i.e. corresponding to the portion of the bar between $x_- = (L-l)/2$ and $x_+ = (L+l)/2$, and let us control the loading process by prescribing the evolution of the total strain ε in the localization area as

$$\varepsilon = \xi_0 \, t \tag{3.75}$$

where t stands for the time, and ξ_0 is a loading parameter.

Since localization has been shown to occur only after the damage threshold $\varepsilon = \varepsilon_0$ is reached, one would have an elastic behaviour throughout all the bar as long as $t \leq \varepsilon_0/\xi_0$. Then, for both damage models, the strain throughout the all

bar would be given by (3.75), and the stress would thus write

$$\sigma = E\varepsilon = E\xi_0\, t \tag{3.76}$$

while the plastic strain and damage will remain equal to 0.

The computation of both the force and displacement at the end of the bar is then straightforward since $U = \varepsilon L$ and $F = S\sigma$.

When t reaches ε_0/ξ_0, the strain will equal the damage threshold and localization will occur for both damage models. Then, damage and plasticity will keep evolving in the localization area, while they will remain equal to zero in the rest of the bar. Let us denote respectively (ε^d, ε_p^d, σ^d, D^d) the strain, plastic strain, stress and damage in the localization area, and (ε^e, ε_p^e, σ^e, D^e) those in the rest of the bar.

When dealing with the pure damage model, the strain in the localization area ε^d would then be equal to the driving strain defined equation (3.75), and the stress σ^d will then be defined as

$$\sigma^d = E(1 - D^d)\varepsilon^d \tag{3.77}$$

where D^d is computed from ε^d using the damage evolution law (3.4).

Regarding the rest of the bar, the stress σ^e will be equal to σ^d due to equilibrium, and since damage D^e will remain equal to 0, the strain will be given by

$$\varepsilon^e = \frac{\sigma^e}{E(1 - D^e)} = (1 - D^d)\varepsilon^d \tag{3.78}$$

In the end, the force at the end of the bar will still be defined as $F = S\sigma^d$, while the displacement will take into account the contribution of both the localization and the unloading parts of the bar, writing

$$U = l\varepsilon^d + (L - l)\varepsilon^e \tag{3.79}$$

As far as the damage-plastic model is concerned, the total strain in the localization area will still be equal to the driving strain (3.75), and the stress σ^d will write

$$\sigma^d = E(1 - D^d)\left(\varepsilon^d - \varepsilon_p^d\right) \tag{3.80}$$

where damage D^d in the localization area is computed, using the damage evolution law (3.12), from the corresponding plastic strain ε_p^d defined as

$$\varepsilon_p^d = \frac{E(\varepsilon^d - \varepsilon_0)}{E + H} \tag{3.81}$$

As for the pure damage model, the stress in the rest of the bar σ^e will be equal to σ^d, and since both ε_p^e and D^e will be equal to 0 , the total strain will write

$$\varepsilon^e = \frac{\sigma^e}{E(1 - D^e)} = (1 - D^d)\left(\varepsilon^d - \varepsilon_p^d\right) \tag{3.82}$$

The force at the end of the bar can then be directly computed from σ^d while the displacement will have to take into account both the localization and unloading areas, as described equation (3.79).

The local and global responses associated with the damage and damage-plastic models with a fixed localization and different sets of parameters will be used in the next sections to study the influence of both plasticity and hardening.

3.3.2 Influence of plasticity

It has been shown in Part 3.1.2 that, when considering the monotonic tensile loading of a material point, both the damage and damage-plastic models would give similar results. It is thus straightforward that, when considering a fixed localization area, its contribution to the global force-displacement curve will be identical with both damage models. Moreover, since localization occurs on the offset of plasticity and damage, the unloading parts will remain elastic throughout the entire process, the stress level being imposed by the localization parts.

In the end, when considering a bar under tension with a fixed localization area, one can expect to get identical response curves with both damage models as long as the localization areas are identical. As in the case of a material point, one can expect the introduction of plasticity to slow damage evolution in the localization area in order to keep the dissipated energy constant. Besides, based on (3.79), and since $\varepsilon^e \leq \varepsilon^d$, an increase in the localization length can be expected to induce in the ductility, since a given force will be associated with a larger displacement.

In order to study the influence of plasticity, this part will use the material parameters described in Table 3.3 for both damage models, along with those described in Table 3.4 which deal with the geometry and localization.

E	ν	ε_0	ε_f	σ_0	H
30000 MPa	0.3	$1.e-4$	$5.e-4$	3 MPa	1000 MPa

Table 3.3: Parameters used for the study with a fixed localization area.

L	S	l_0	c_0
1000 mm	100 mm^2	250 mm	181 mm

Table 3.4: Geometrical and localization default parameters.

The force-displacement curves thus obtained are plotted in Figure 3.4 for sizes of the localization area l equal to l_0, $2l_0$ and $3l_0$, along with the associated damage profiles. One can thus ensure that, as expected, the size of the localization area l does control the ductility of the response, and both models always give identical responses for a given value of l.

The evolution of the damage profiles with respect to the total strain were also plotted in Figures 3.5a and 3.5b respectively for the damage and damage-plastic models with $l = l_0$. One can thus see that, though the damage profiles end up identical, the one obtained with the damage-plastic model clearly has a slower evolution.

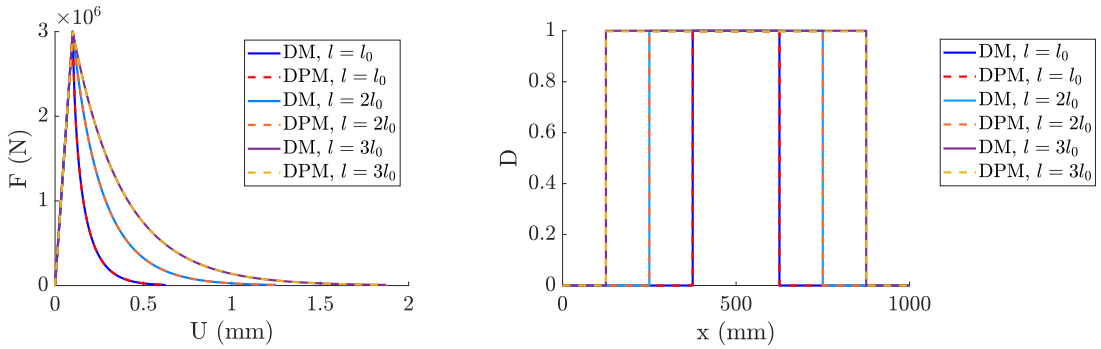

(a) On the force-displacement curve. (b) On the damage profile.

Figure 3.4: Influence of plasticity for different sizes of the fixed localization area.

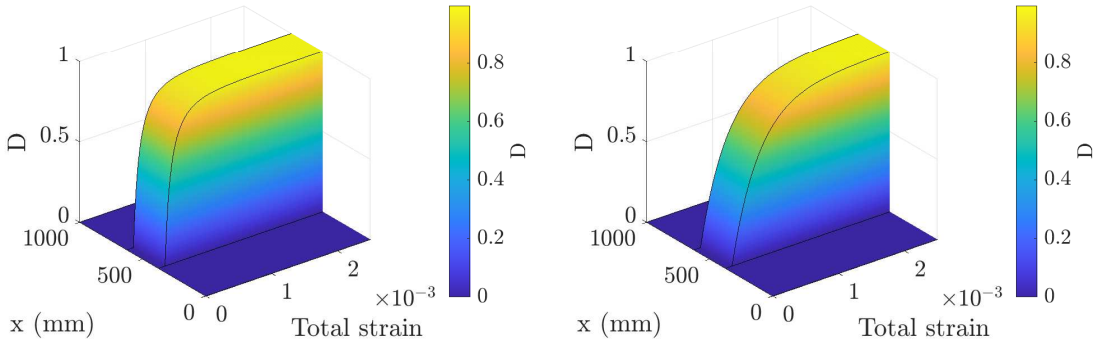

(a) For the pure damage model. (b) For the damage-plastic model.

Figure 3.5: Influence of plasticity on the evolution of the damage profiles with respect to the total strain.

It is worth noting that, here, one does not compare the responses obtained with the same internal length c, since it would lead to completely different sizes of the localization areas, and thus completely different responses.

After studying how the introduction of plasticity affects the global response, one needs to focus on the influence of the hardening parameter.

3.3.3 Influence of hardening

This part will focus on the influence of hardening, and especially variations of the hardening parameter, on both the global response and damage evolution.

Hardening-independent localization

Starting with the global response, one can expect that, since it was not affected by the introduction of plasticity, it should not be affected by variations in the hardening parameter either. This idea is further confirmed by the fact that, as was shown in Part 3.1.2, the hardening parameter has no influence on the stress-strain curve on a single material point, which can be straightforwardly extended to the case of a bar's portion submitted to homogeneous tension. It is worth noting that this only holds true as long as the size of the localization area l is considered independent from the hardening parameter H, different considerations might arise when taking into account the dependency of l with respect to H detailed in Part 3.2.2.

However one has seen that, when considering a single material point under tension, an increase in the hardening parameter would induce a decrease in the plastic evolution rate, and thus an increase in damage evolution. As for the influence on the force-displacement curve, this consideration can be directly extended to the case of a homogeneous bar under continuous tension, and thus to the current case of a bar with a fixed localization area.

The force displacement curves obtained for different values of the hardening parameter H were plotted in Figure 3.6 for different sizes of the localization area, along with the associated damage profiles.

On can thus see that, as expected, the hardening parameter has no influence on the response curve, while an increase in the size of the localization area still tends to increase the global ductility of the response.

The evolution of both the plastic strain and damage profiles have also been plotted respectively in Figures 3.7 and 3.8, which allowed to ensure that the hardening parameter has the expected influence on the evolution of both plasticity and damage with respect to the total strain.

As pointed out before, the previous consideration do not take into account the dependence of the localization area with respect to the hardening parameter which was described in Part 3.2.2. It is quite straightforward that taking this dependency into account would lead to hardening-dependent damage profiles and force displacement curves.

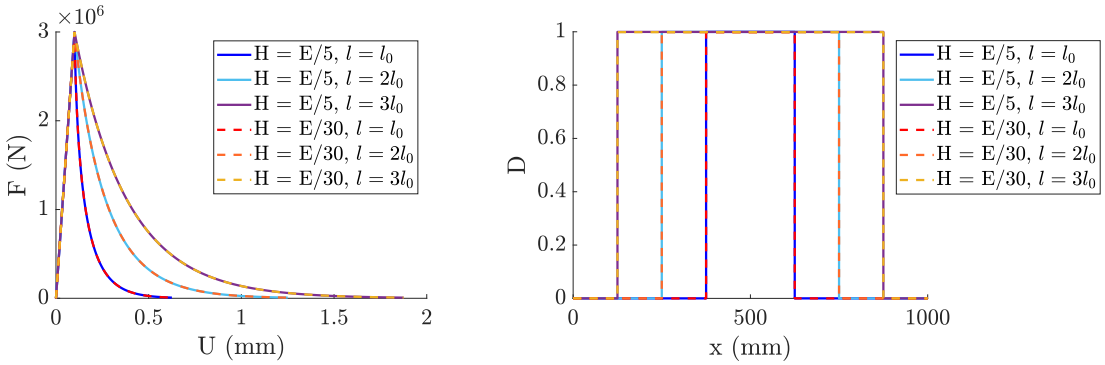

(a) On the force-displacement curve. (b) On the damage profile.

Figure 3.6: Influence of hardening on the response curve for different sizes of the fixed localization area.

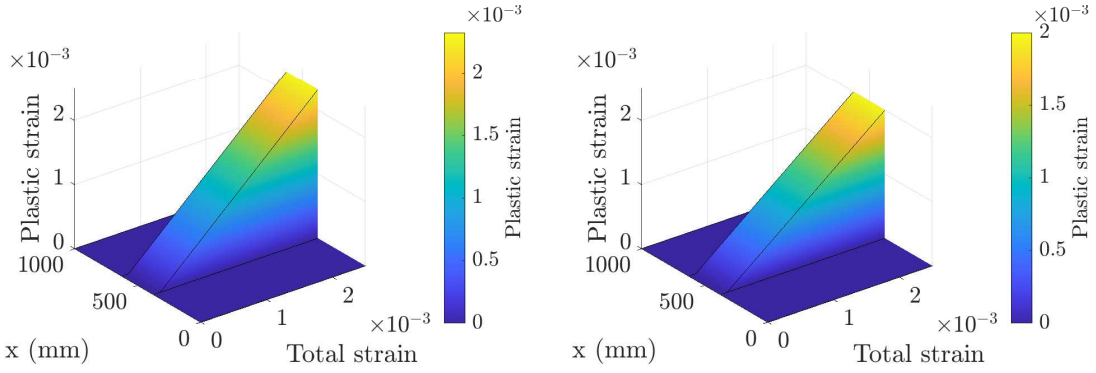

(a) Profile for $H = E/30$. (b) Profile for $H = E/5$.

Figure 3.7: Influence of hardening on the evolution of the plasticity profiles with a fixed localization length.

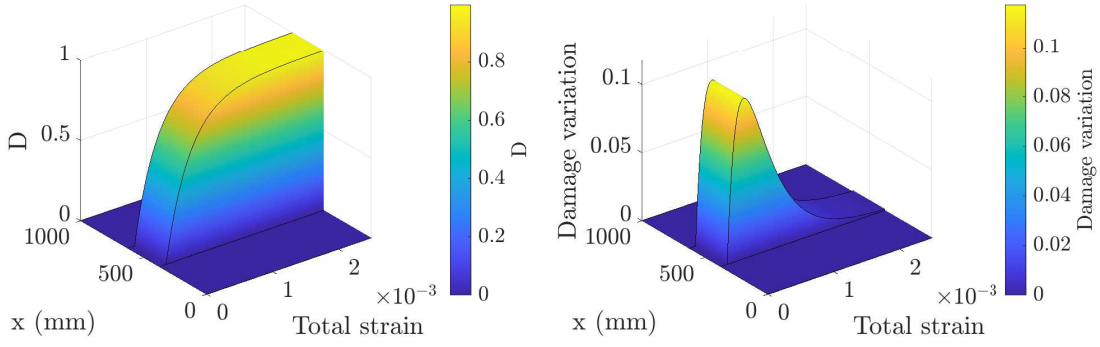

(a) Profile for $H = E/30$. (b) Profile variation between $H = E/5$ and $H = E/30$.

Figure 3.8: Influence of hardening on the evolution of the damage profiles with a fixed localization length.

Hardening-dependent localization

In order to properly assess the influence of hardening on both the local and global responses, one should no longer see l as a fixed parameter, but rather use the expression given in equation (3.72), especially when computing the total displacement (3.79). The evolution of the localization length associated with the damage-plastic model with respect to the hardening parameter has been plotted in Figure 3.9 for $c = 181\text{mm}$, which gives $l \approx 250\text{mm}$ for $H = E/30$. One can thus see that an increase in the hardening parameter H would induce an increase in the localization area l which should induce an increase in the global ductility of the force-displacement curve.

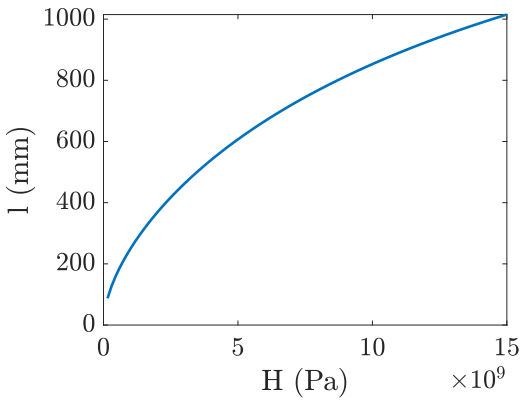

Figure 3.9: Evolution of the localization length with respect to the hardening parameter.

The damage profiles and force-displacement curves obtained for different values of H and using hardening dependent localization are plotted in Figure 3.10, which allows one to see that hardening does have the expected influence on both the force-displacement curves and the localization length.

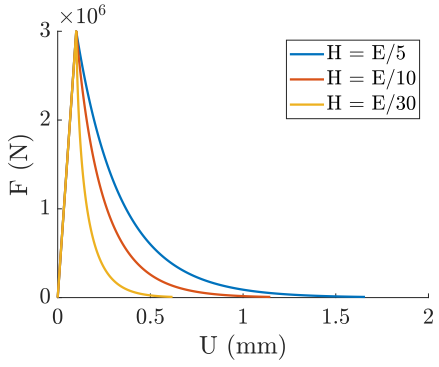

(a) On the force-displacement curve.

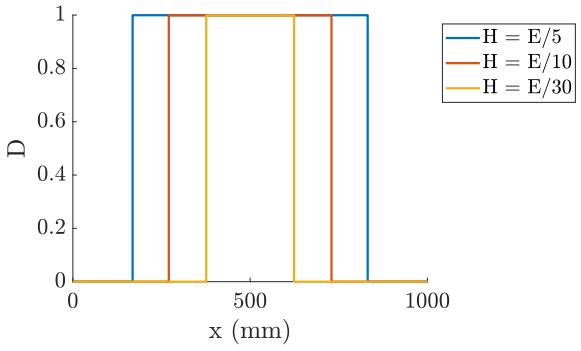

(b) On the damage profile.

Figure 3.10: Influence of hardening on the response curve for a fixed hardening-dependent localization.

Moreover, looking at the evolution of the plastic strain profiles plotted in Figure 3.11, one can see that an increase in the hardening parameter also tends to increase

the width of the localization area, and to lower the plasticity evolution rate. The evolution of the maximum plastic strain plotted in Figure 3.11d helps to confirm the differences in the plastic strain evolution.

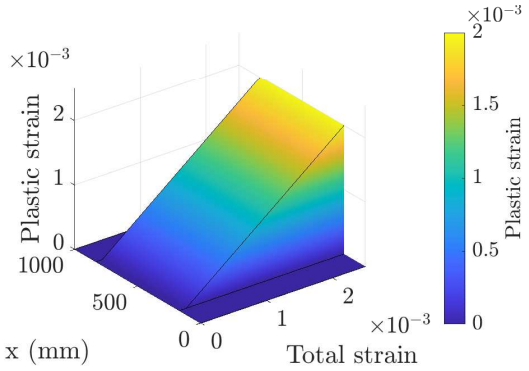

(a) Profile for $H = E/5$.

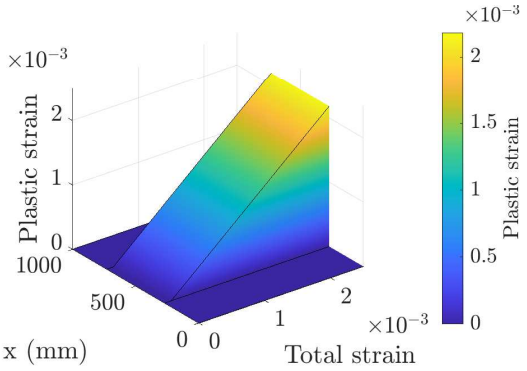

(b) Profile for $H = E/10$.

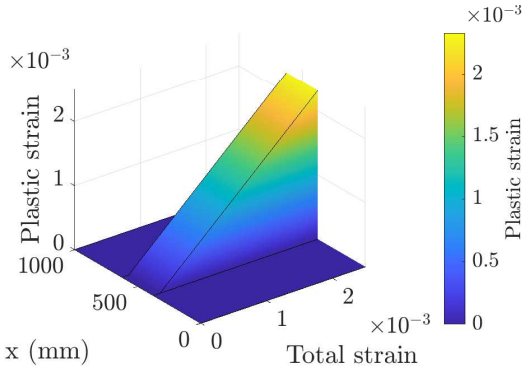

(c) Profile for $H = E/30$.

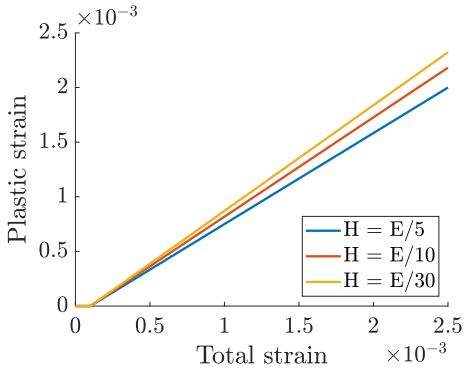

(d) Evolution of the maximum plastic strain.

Figure 3.11: Influence of hardening on the evolution of the plastic strain profiles with a fixed hardening-dependent localization.

Finally, the evolution of the damage profiles plotted in Figure 3.12 allows one to confirm the influence of the hardening parameter on the width of the localization area, and to check that an increase in its value does tend to increase the damage evolution rate. As before, the evolution of the maximum damage plotted in Figure 3.12d helps to confirm the differences in damage evolution.

This part has shown that, when considering a bar under tension with a fixed given localization area, the introduction of plasticity does not affect the global response but tends to slow damage evolution, and the hardening parameter can be used to adjust the damage evolution rate but has no influence on the response curve either.

However, when taking into account its influence on the localization area, one can see that the hardening parameter does have some influence on the global response, as well as on plasticity and damage evolution.

Based on the results presented here, one can expect both the introduction of plasticity and variations of the hardening parameter to have some influence on the force-displacement curve when considering a shrinking localization area, even

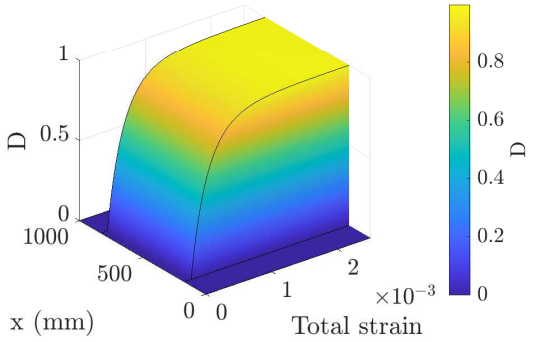

(a) Profile for $H = E/5$.

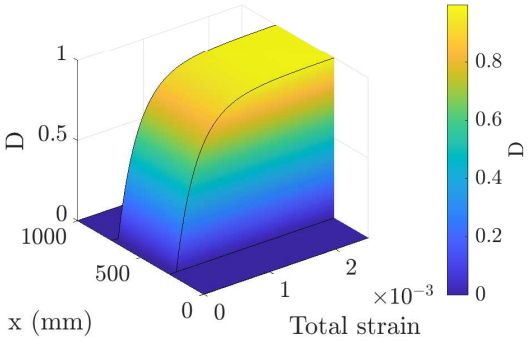

(b) Profile for $H = E/10$.

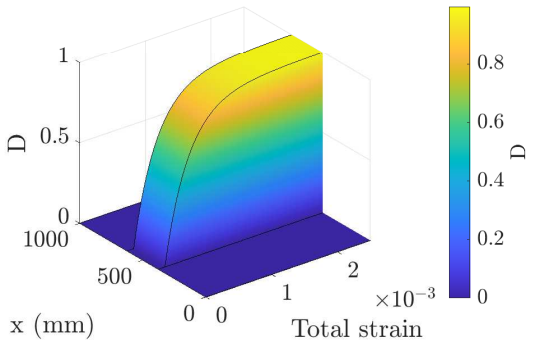

(c) Profile for $H = E/30$.

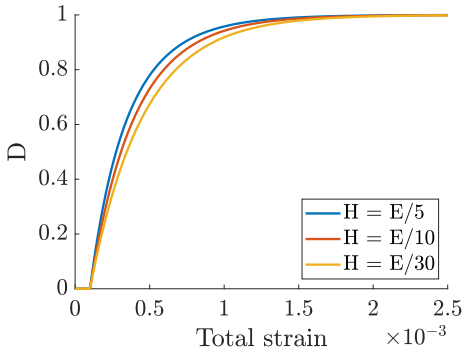

(d) Evolution of the maximum damage.

Figure 3.12: Influence of hardening on the evolution of the damage profiles with a fixed hardening-dependent localization.

for a hardening-independent initial localization. This is linked to the fact that, unlike the case of fixed localization, some of the unloading parts will have non-zero plastic strain, which will increase the ductility of the response and might address the brittleness issue observed with eikonal-based formulations.

3.4 Localization in a Shrinking area

The aim of this part is to study how the introduction of plasticity will affect the response obtained in a one-dimensional setting when considering an isotropic damage model with a shrinking localization area. This should give some insight on whether such a modification could be used to address the brittleness issue linked to the formulation obtained by coupling the eikonal-based gradient-type formulation with a pure isotropic damage model.

To do so, this part will stick to the case of the homogeneous bar of length L and section S studied when assessing the properties of the formulation with a fixed localization. Here one will first compare the results obtained, for both damage models, when localization occurs in a fixed area to those obtained with a shrinking one of the same initial size. One will then study the influence of hardening on the local and global responses, for both hardening independent and dependent initial localizations.

3.4.1 Principle

As before, the global response was here computed using a local strain-based loading, imposing a linear time evolution of ε in the localization area (3.75).

It is worth noting that, here, one will consider a shrinking localization area whose initial size l will be considered as a given parameter that might still depend on the hardening parameter. The localization will still be assumed to be centered, corresponding at each time to the portion of the bar located between $x_- = (L - l_{eff})/2$ and $x_+ = (L + l_{eff})/2$, where l_{eff} denotes the current size of the shrinking area.

It is worth noting that the main idea here is not to predict the exact response associated with the eikonal-based formulation, but rather to understand how the introduction of plasticity affects the response obtained with a shrinking localization area. As it is, the introduction of permanent strain is expected to reduce the brittleness induced by the progressive unloading associated with the shrinking localization area.

Following the work presented in Part 1.6 on the damage-dependence of the effective distances in a space curved by damage, one will here consider a shrinking of the localization area similar to the one associated with the eikonal formulation. Moreover, to get a meaningful comparison with the case of a fixed localization area, one needs here to ensure that the initial size of the localization area will be equal to l, and tends to 0 when D gets close to 1. The effective localization length is thus assumed to have the following fictitious damage-dependence

$$l_{eff} = l\sqrt{1 - D} \tag{3.83}$$

which should allow one to get some insight on the influence of plasticity when using an eikonal-based formulation.

As before, localization only occurs after the damage threshold is reached, which means that, until t reaches ε_0/ξ_0, one can still expect a homogeneous elastic response identical to the one described in Part 3.3.1. On the onset of localization, one can expect damage and plasticity to keep growing in the localization area, while they should stop evolving in the rest of the bar.

The main difference with the approach involving a fixed localization area comes from the fact that, based on equation (3.83), it is here likely to continuously shrink once the damage threshold has been reached. This part will now detail how this can be expected to affect both the local and global responses in the case considered here, and for both damage models.

Pure damage model

When dealing with the pure damage model, one can expect that, when ε reaches ε_0, both strain and damage will keep evolving in the initial localization area located between x_-^0 and x_+^0 defined as $x_\pm^0 = (L \pm l)/2$, while the rest of the bar will remain elastic. Since the expressions of all the variables at this point are the same as the

ones obtained with the fixed localization, and detailed in Part 3.3.1, one now needs to study what happens beyond it.

When the total strain grows beyond the damage threshold, the area where strain and damage will keep growing will continuously shrink, which means that at each time step a new portion of the bar will start unloading. It is worth noting that, unlike what happened for the initial localization, damage has a non-zero value in the new unloading part, which affects its unloading.

Let us here denote respectively $(\varepsilon^{d,i},\ \varepsilon_p^{d,i},\ \sigma^{d,i},\ D^{d,i})$ the strain, plastic strain, stress and damage in the localization area at a given time t_i, and $(\varepsilon^{e,i},\ \varepsilon_p^{e,i},\ \sigma^{e,i},\ D^{e,i})$ those in the rest of the bar. Let us also denote l_{eff}^i the effective length at this time, defined according to (3.83) as $l_{eff}^i = l\sqrt{1-D^{d,i}}$, and (x_-^i, x_+^i) the coordinates delimiting the localization area defined as $x_\pm^i = (L \pm l_{eff}^i)/2$.

At a given time $t_n > 0$, the strain $\varepsilon^{d,n}$ in the new localization area, i.e between x_-^n and x_+^n, will be equal to the driving strain (3.75), and the stress $\sigma^{d,n}$ will write

$$\sigma^{d,n} = E\left(1 - D^{d,n}\right)\varepsilon^{d,n} \tag{3.84}$$

where $D^{d,n}$ is computed from $\varepsilon^{d,n}$ using the damage evolution law (3.4).

For any j such that $0 \leq j < n$, the stress $\sigma^{e,n}$ between x_-^j and x_-^{j+1}, as well as between x_+^{j+1} and x_+^j, will be equal to $\sigma^{d,n}$, while the damage $D^{e,n}$ will be equal to its maximum value when it was localized between x_-^j and x_+^j, i.e. $D^{d,j}$. The strain in this area will then be defined as

$$\varepsilon^{e,n} = \frac{\sigma^{d,n}}{E(1-D^{e,n})} = \left(\frac{1-D^{d,n}}{1-D^{d,j}}\right)\varepsilon^{d,n} \tag{3.85}$$

In the end, the force at the end of the bar will still be computed as $F = S\sigma^{d,n}$, while the displacement will have to take into account every successive localization area, writing

$$U = \varepsilon^{d,n}\left[l_{eff}^n + \sum_{j=0}^{n-1}\left(\frac{1-D^{d,n}}{1-D^{d,j}}\right)\left(l_{eff}^j - l_{eff}^{j+1}\right) + \left(1-D^{d,n}\right)(L-l)\right] \tag{3.86}$$

where U is computed by summing the contributions of all the successive localization areas to that of the rest of the bar who remained elastic.

Damage-plastic model

As far as the damage-plastic model is concerned, one can still expect that, when ε reaches ε_0, damage, plasticity and strain will localize between the points x_-^0 and x_+^0, and stop evolving in the rest of the bar.

As for the pure damage model, the expressions of all the variables are the same as the ones described in Part 3.3.1 for the fixed localization. Now, one thus needs to study what happens when the strain grows beyond the damage threshold, and the area where damage, plasticity and strain starts shrinking.

As for the pure damage model, for any given time $t_n > 0$ the strain $\varepsilon^{d,n}$ in the localization area is equal to the driving strain defined in equation (3.75), and the stress then writes

$$\sigma^{d,n} = E\left(1 - D^{d,n}\right)\left(\varepsilon^{d,n} - \varepsilon_p^{d,n}\right) \tag{3.87}$$

where $\varepsilon_p^{d,n}$ denotes the plastic strain in the localization area at this time defined as

$$\varepsilon_p{}^{d,n} = \frac{E(\varepsilon^{d,n} - \varepsilon_0)}{E + H} \tag{3.88}$$

which is used to compute damage $D^{d,n}$ according to the evolution law (3.12).

Moreover, for any j such that $0 \leq j < n$, the stress $\sigma^{e,n}$ between x_-^j and x_-^{j+1}, as well as between x_+^{j+1} and x_+^j, will be equal to $\sigma^{d,n}$, while the damage $D^{e,n}$ and plastic strain $\varepsilon_p^{e,n}$ will be respectively equal to $D^{d,j}$ and $\varepsilon_p^{d,j}$. The strain in this area will then be defined as

$$\varepsilon^{e,n} = \frac{\sigma^{d,n}}{E(1 - D^{e,n})} + \varepsilon_p^{e,n} = \left(\frac{1 - D^{d,n}}{1 - D^{d,j}}\right)\left(\varepsilon^{d,n} - \varepsilon_p^{d,n}\right) + \varepsilon_p^{d,j} \tag{3.89}$$

As before, the force at the end of the bar will be computed as $F = S\sigma^{d,n}$, and the displacement, taking into account every successive localization area, will write

$$\begin{aligned} U =& l_{eff}^n\ \varepsilon^{d,n} + \sum_{j=0}^{n-1}\left(l_{eff}^j - l_{eff}^{j+1}\right)\left[\left(\frac{1 - D^{d,n}}{1 - D^{d,j}}\right)\left(\varepsilon^{d,n} - \varepsilon_p^{d,n}\right) + \varepsilon_p^{d,j}\right] \\ &+ \left(1 - D^{d,n}\right)(L - l)\varepsilon^{d,n} \end{aligned} \tag{3.90}$$

It is worth noting that, here, the strain in the unloading area and the total displacement are increased by the presence of plasticity which should, as expected, reduce the brittleness of the global response.

The local and global responses obtained with both damage models and considering a shrinking localization will be used in the next sections to study the influence of plasticity, and more specifically hardening.

3.4.2 Influence of plasticity

It has been shown in Chapter 2 that imposing a shrinking localization area, e.g through an eikonal-based formulation, addresses the issue linked to the ill-posedness of the problem, and allows one to make a highly damaged zone equivalent to a crack. However, the use of a pure damage model induces a rather brittle response with no permanent strain, which makes it ill-suited to properly represent the behaviour of materials such as concrete.

The previous studies tend to indicate that, though the introduction of plasticity does not affect the global material response when considering a fixed localization, it can be expected to increase its ductility when considering a shrinking one. This part will thus focus on the comparison of the results obtained with the pure damage and damage-plastic models associated with both fixed and shrinking localizations, in order to see whether the introduction of plasticity addresses the issues associated with shrinking localization.

The response curves and damage profiles thus obtained were plotted in Figure 3.13 in order to study how they may be influenced by both plasticity and shrinking localization. One can thus see in Figure 3.13a that, as expected, the introduction of plasticity tends to reduce the brittleness of the response obtained with the shrinking localization, though it remains more brittle than the one obtained with the fixed localization, which is unaffected by plasticity. It is worth noting that, with the considered set of parameters, the increase in ductility induced by plasticity prevents the occurrence of snap-back instabilities with the damage-plastic model, while they do occur with the pure damage model.

One can also note in Figure 3.13 that, as for the fixed localization, the plasticity does not seem to affect the damage profile for a shrinking localization, which seems to have the expected zero width when D gets close to 1.

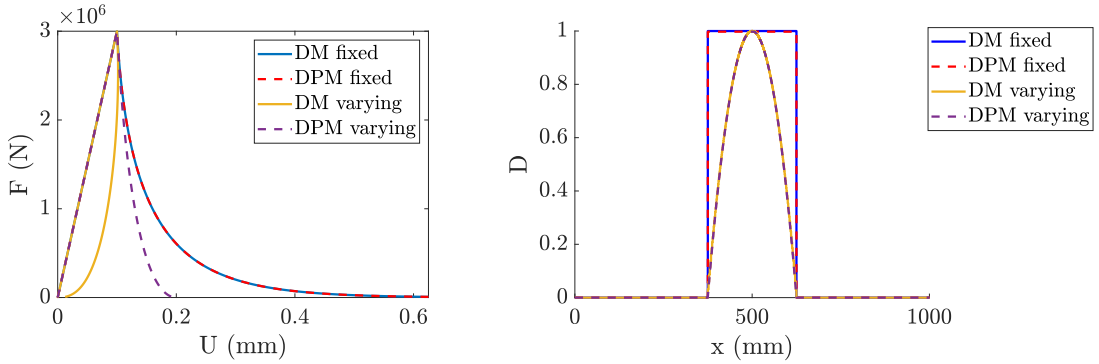

(a) On the force-displacement curve.

(b) On the damage profile.

Figure 3.13: Influence of plasticity with fixed and shrinking localization.

After studying the influence of plasticity and shrinking localization on the final damage profile, the evolution of the damage profiles with respect to the total strain were also plotted in Figure 3.14 in order to see how they are affected by the introduction of plasticity and shrinking localization.

One can thus see that, while the shrinking localization tends to sharpen the damage profile, the introduction of plasticity tends to slow damage evolution, which is consistent with what was observed for the fixed localization.

The influence of plasticity on the damage evolution rate can be confirmed in Figure 3.15a where the evolution of damage with respect to strain has been plotted for all the considered formulations, which also allows one to see that a shrinking localization does not affect the evolution of damage with respect to strain.

Moreover, the evolution of the damage active lengths plotted in Figure 3.15b allows one to check that, while a fixed localization induces a constant active length, the one obtained with the shrinking localization has the same initial size, but tends to 0 when D tends to 1. The fact that this property is not affected by plasticity is consistent with the expression of the effective localization length (3.83), and confirms that the introduction of plasticity might be a good way to address the issues associated with shrinking localization while keeping its properties.

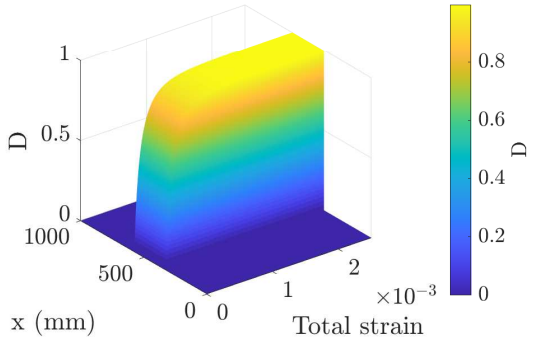

(a) Pure damage model and fixed localization.

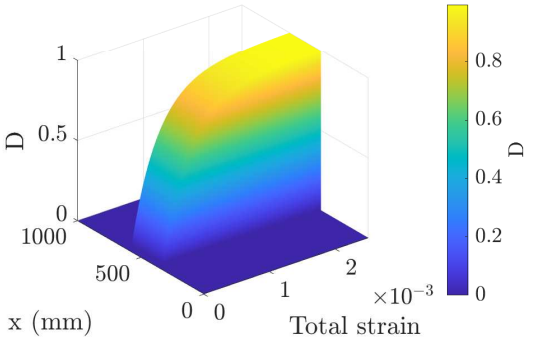

(b) Damage-plastic model and fixed localization.

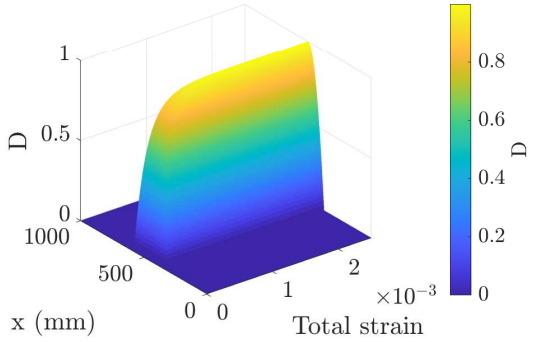

(c) Pure damage model and shrinking localization.

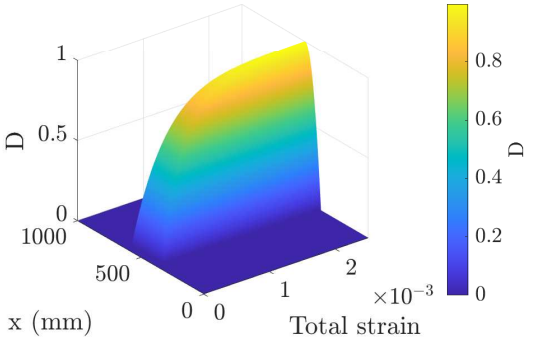

(d) Damage-plastic model and shrinking localization.

Figure 3.14: Influence of hardening on the evolution of the damage profiles with fixed and shrinking localization. to the total strain.

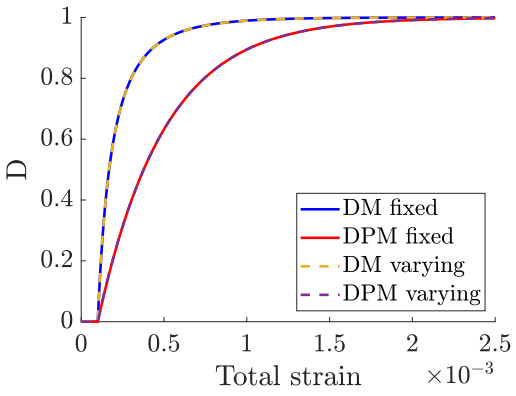

(a) On damage evolution.

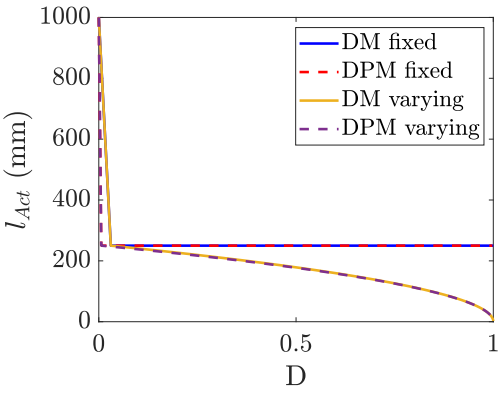

(b) On the damage active length.

Figure 3.15: Influence of plasticity with fixed and shrinking localization.

As before, this part compared the responses obtained with the same initial localization length l, and not the same internal length c which would lead to completely different sizes of the localization areas, and thus completely different responses.

After studying how the introduction of plasticity affects both the global and local responses obtained with a shrinking localization, especially in comparison with what can be observed with a fixed localization, one will now study the influence of the hardening parameter.

3.4.3 Influence of hardening

It has been shown in Part 3.4.2 that the introduction of plasticity with a shrinking localization tends to increase the ductility of the response and to slow damage evolution, without changing the final damage profile.

This part will now focus on how variations in the hardening parameter, and thus in hardening, will affect both the local and global responses when considering a bar under monotonic tension and a shrinking localization.

Hardening-independent localization

First, one will consider the case of a hardening-independent localization in order to focus on the variations linked to the changes in plastic evolution induced by a modification of the hardening parameter.

Based on the results obtained in Part 3.3.3 with the fixed localization, one can expect an increase in the hardening parameter to slow the evolution of plasticity with respect to strain, while increasing the damage evolution rate.

It has also been shown in Part 3.4.2 that, for a given size of the initial localization, the introduction of plasticity with a shrinking localization would tend to increase the ductility of the global response. Since an increase in the hardening parameter has been shown to slow plastic evolution with respect to strain, one can thus expect it to reduce the ductility of the force-displacement curve.

To assess the relevance of these assumptions, one will thus stick to the study of the bar under tension studied previously for two values of the hardening parameter, $H = E/30$ and $H = E/5$, and of the localization length, $l = l_0$ and $l = 2l_0$.

The force-displacement curves thus obtained were plotted in Figure 3.16, along with the associated final damage profiles. One can thus see that, as expected, variations in the localization length l have an influence on the width of the damage profile, and thus on the ductility of the global response. It is also possible to check that, though variations of the hardening parameter do not affect the damage profile, they do have the expected influence on the force-displacement curve.

As far as the evolution of damage with respect to strain is concerned, Figure 3.17a allows one to ensure that, while it is not affected by the localization length, the hardening parameter has a positive evolution on its rate. On the other hand, one can see in Figure 3.17b that the evolution of the damage active length, whose initial value is imposed by the localization length, is not affected by the hardening parameter.

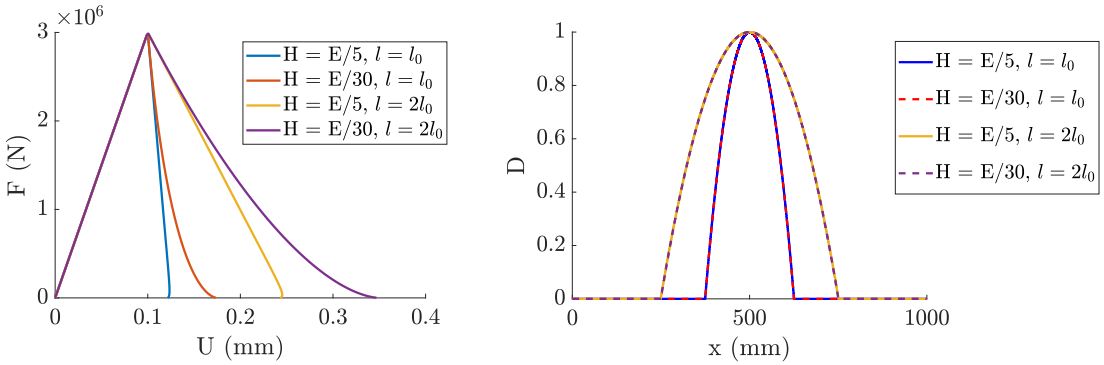

(a) Force-displacement curves.

(b) Damage profiles.

Figure 3.16: Influence of hardening on the force-displacement curves and damage profile for different sizes of the initial localization area.

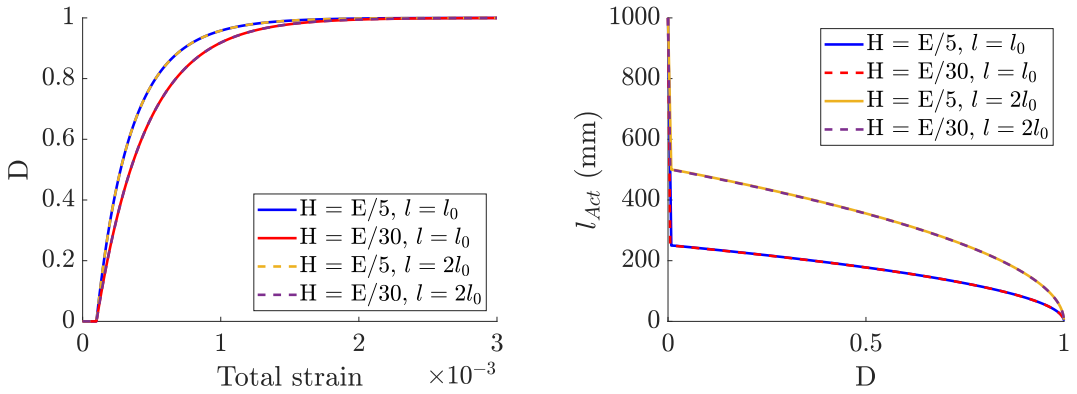

(a) Damage evolution.

(b) Damage active length evolution.

Figure 3.17: Influence of hardening on the evolution of damage and damage-active length for different sizes of the initial localization area.

Regarding the plastic strain evolution, one can see in Figure 3.18b that, as for damage evolution, it is not affected by the localization length, while the hardening parameter has a negative influence on its rate. On the other hand, one can note that both the hardening parameter and the localization length have an influence on the plasticity active length, defined as the size of the area where plasticity keeps evolving. While the dependence of the initial value with respect to the localization length is identical to what was observed for the damage active length, the influence of the hardening parameter on its evolution rate is due to the fact that, unlike damage, the evolution of plasticity is hardening-dependent. It is worth noting that, here, the active length tends to 0 when the plastic strain tends to infinity, which is consistent with what can be observed in Figure 3.17b, since an infinite plastic strain would correspond to damage being equal to 1.

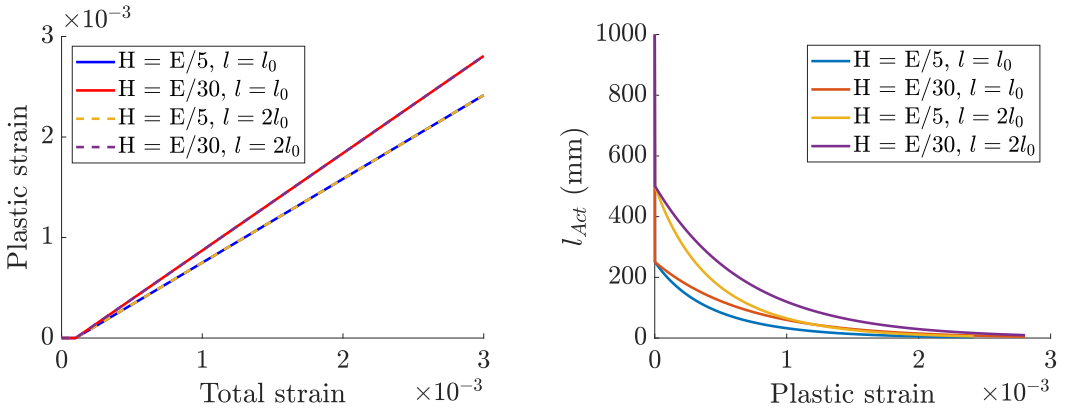

(a) Plastic strain evolution.

(b) Plasticity active length evolution.

Figure 3.18: Influence of hardening on the evolution of plasticity and plasticity-active length for different sizes of the initial localization area.

Here one has seen that the hardening parameter and localization length could be used to control the width of the damage profile, along with the evolution of both plasticity and damage, which gives indirect control over the ductility of the global response curve. It is worth noting that the results presented in this part do not take into account the dependence of the localization area with respect to hardening, which now needs to be studied.

Hardening-dependent localization

As for the fixed localization, in order to properly take into account the influence of hardening on both the local and global responses, l should no longer be taken as fixed, but rather as being dependent on both the hardening parameter H and the internal length c.

Based on the results presented in Part 3.3.3 for a fixed hardening-dependent localization, one might expect an increase in the hardening parameter to induce an increase in the size of the initial localization, thus inducing an increase in the global ductility. However, based on the results presented in the previous section for a shrinking hardening-independent localization, one could also expect an increase

in the hardening parameter to reduce the ductility of the response, due to both the induced decrease in plasticity ad increase in damage.

This part will thus focus on finding out which one of those phenomenon could be expected to be predominant, and how it will affect the response curve and both damage and plasticity evolutions.

In an attempt to answer those questions, the damage profiles and displacement curves obtained for two values of the hardening parameter, $H = E/30$ and $H = E/10$, and of the internal length $c = c_0$ and $c = 2c_0$ were plotted in Figure 3.19. First, one can ensure here that the internal length has the expected effects, i.e. an increase in its value induces an increase in the final damage profile, and thus an increase in the ductility. In a similar fashion, it seems that, for the considered set of parameters, the widening of the localization area associated with an increase in the hardening parameter does induce an increase in the global ductility, despite its supposed effect on damage and plasticity evolution. It is worth noting that, here, one can get very similar responses with completely different set of parameters, namely ($H = E/10$,$c = c_0$) and ($H = E/30$,$c = 2c_0$).

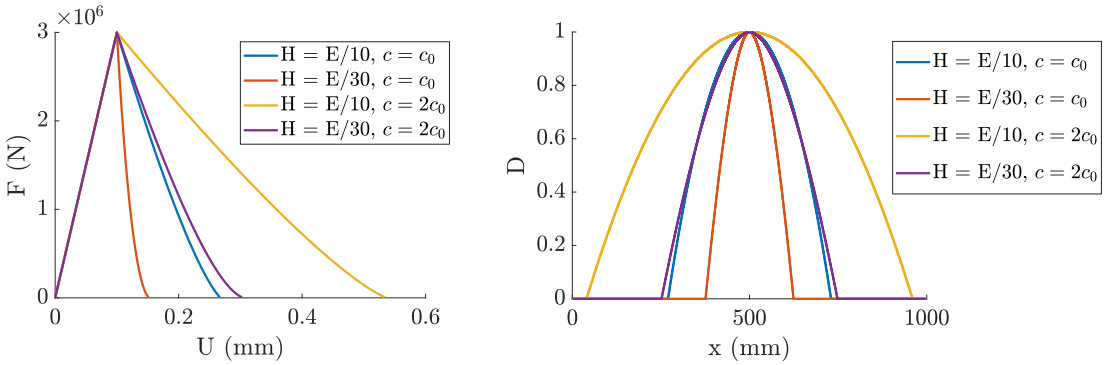

(a) Force-displacement curves.

(b) Damage profiles.

Figure 3.19: Influence of hardening on the force-displacement curves and damage profile for different sizes of the initial hardening-dependent localization area.

In order to ascertain the influence of hardening throughout the loading, and not only on the size of the localization, the evolution of the damage profiles obtained for the four sets of parameters considered here were plotted in Figure 3.20.

One can thus ensure that the damage profile tends to shrink when damage grows, which is confirmed in Figure 3.21 where one can see that, though the initial size of the active length is fixed by H and c, it systematically tends to 0 when D gets close to 1. One can also see that, for a given internal length, a decrease in the hardening parameter would tend to slow down damage evolution, which is confirmed in Figure 3.21a where one can also check that the internal length has no influence on it.

As far as the influence on plasticity is concerned, one can see in Figure 3.22 that the plastic strain evolution tends to slow when the hardening parameter increases which, along with the fact that it is not affected by the internal length, can be checked in Figure 3.23a.

One can also observe in Figure 3.22 that both the hardening parameter and

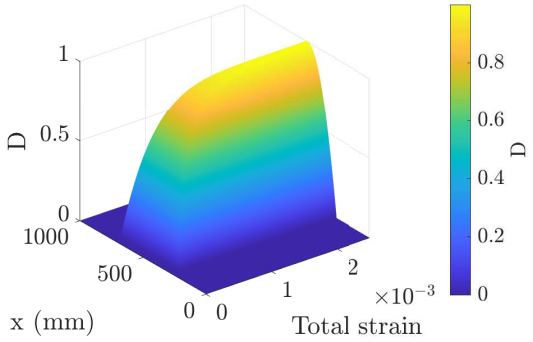

(a) Profile for $H = E/10$ and $c = c_0$.

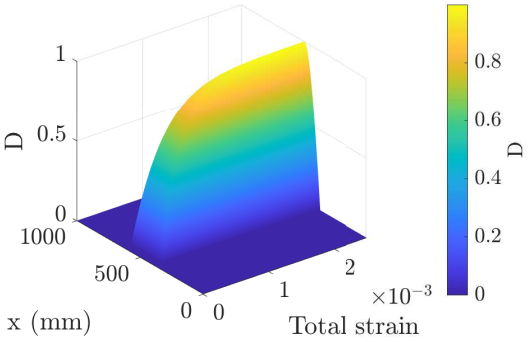

(b) Profile for $H = E/30$ and $c = c0$.

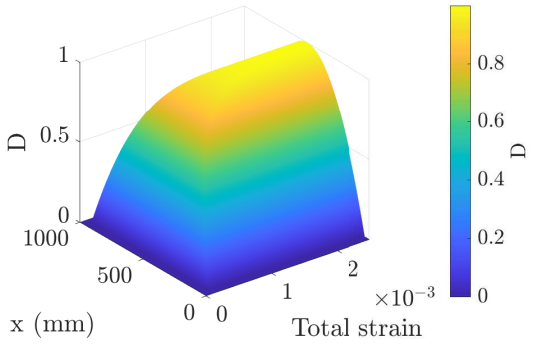

(c) Profile for $H = E/10$ and $c = 2c_0$.

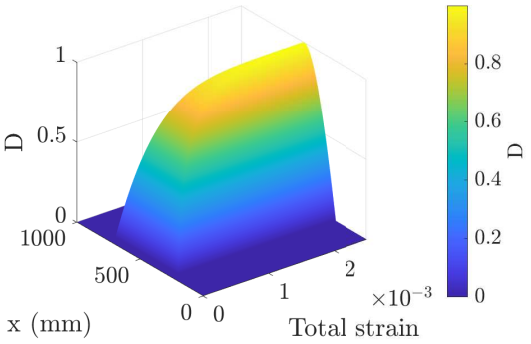

(d) Profile for $H = E/30$ and $c = 2c_0$.

Figure 3.20: Influence of hardening on the evolution of the damage profile for different sizes of the initial hardening-dependent localization area.

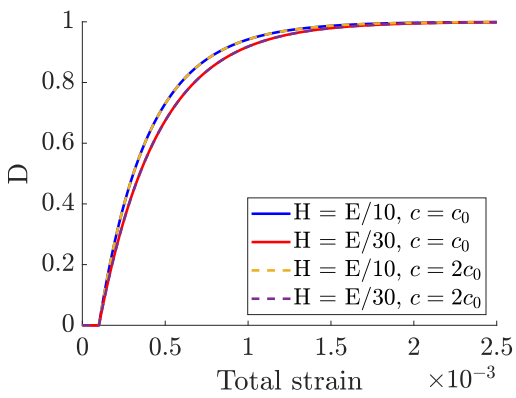

(a) Damage evolution.

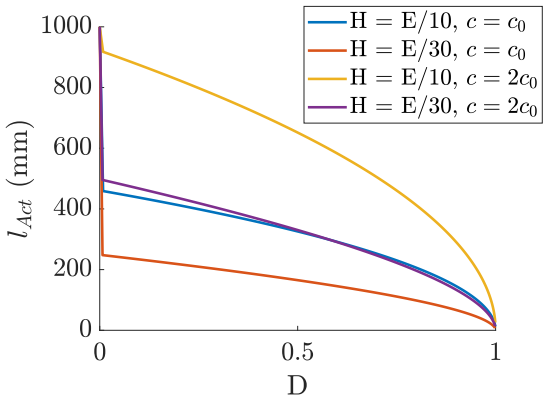

(b) Damage active length evolution.

Figure 3.21: Influence of hardening on the evolution of damage and damage-active length for different sizes of the hardening-dependent initial localization area.

the internal length have the expected influence on the width of the plastic strain profile, which tends to shrink when plasticity grows. This can also be checked in Figure 3.23b where one can easily visualize the initial value of the plasticity active length for all the considered sets of parameters, along with the fact that it tends to zero for high values of plastic strain, i.e when damage gets close to 1.

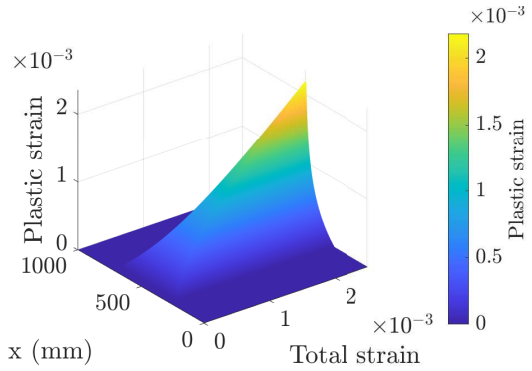

(a) Profile for $H = E/10$ and $c = c_0$.

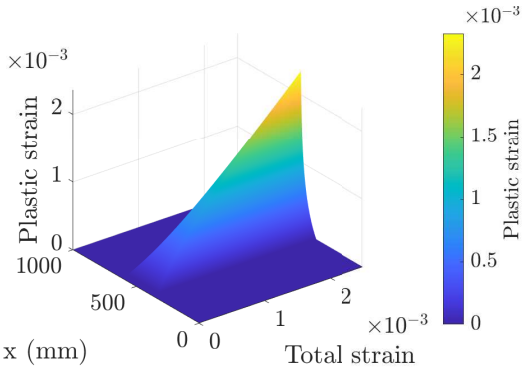

(b) Profile for $H = E/30$ and $c = c0$.

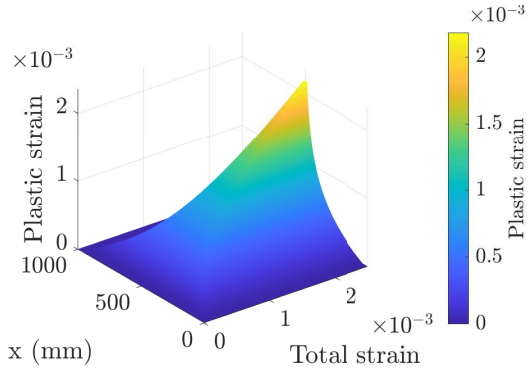

(c) Profile for $H = E/10$ and $c = 2c_0$.

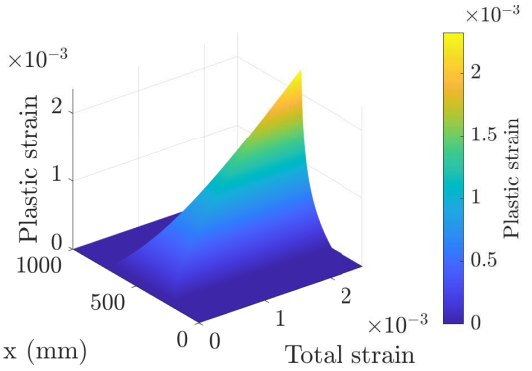

(d) Profile for $H = E/30$ and $c = 2c_0$.

Figure 3.22: Influence of hardening on the evolution of the plastic strain profile for different sizes of the initial hardening-dependent localization area.

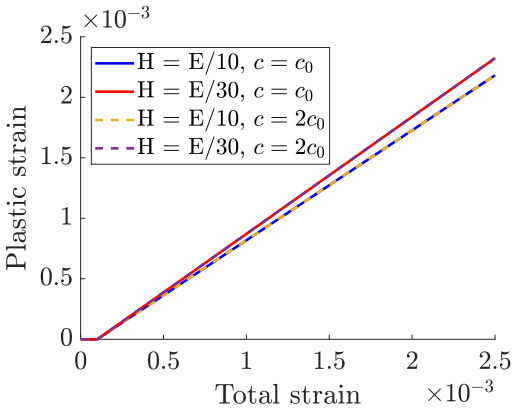

(a) Plastic strain evolution.

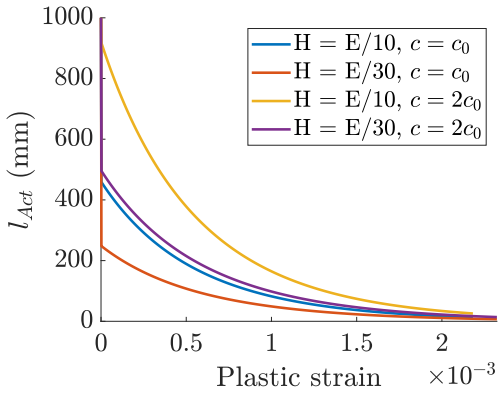

(b) Plasticity active length evolution.

Figure 3.23: Influence of hardening on the evolution of plasticity and plasticity-active length for different sizes of the initial hardening-dependent localization area.

This part has shown that, when considering a bar under tension with a shrinking localization, the introduction of plasticity tends to increase the ductility of the global response which, along with the width of the localization area, can be controlled through the hardening parameter and the internal length.

This result is quite promising since one could thus expect to reduce the excessive fragility observed when coupling an eikonal-based formulation to a pure damage model by introducing plasticity, which might also help model materials who exhibit permanent strain.

3.5 Conclusion of chapter 3

After presenting the new damage-plastic model studied in this chapter, its response on a single material point was compared to the one associated with the pure damage model studied in Chapter 2. One could thus ensure that, though it is expected to address the excessive brittleness associated with the pure damage model, the introduction of plasticity does not affect the local material behaviour under monotonic tension. Moreover, though changing the hardening parameter influenced the evolution of both damage and plasticity, it did not appear to affect the global response curve.

The formulations obtained by coupling the damage and damage-plastic models to Peerlings' and the eikonal-based gradient-type formulations were then introduced. A localisation analysis was then conducted to ensure that all the considered formulations imposed the size of the localisation area, thus addressing the issue linked to the ill-posedness of problems involving local models with strain softening. It is worth noting that this study focused on the formulations associated with Peerlings' approach since they are identical to the ones based on the eikonal approach on the onset of localisation. Aside from demonstrating the formulations' regularisation properties, one can also note that this study confirmed that the localisation area's size depends not only on the internal length but also on the damage model and the associated parameters.

One then studied how the introduction of plasticity and variations in the hardening parameter would affect the local and global responses associated with both fixed and shrinking localisations. First, one could see that when associated with a non-shrinking localisation area, the introduction of plasticity does not affect the global response as long as the initial localisation areas are identical. It was also possible to demonstrate that using a damage-plastic model associated with a shrinking localisation increases the ductility of the response, which can be controlled through both the internal length and the hardening parameter.

Thus, one could expect that, in addition to introducing the permanent strain required to model concrete, coupling the eikonal-based approach to a damage-plastic model instead of a pure damage one should help address the brittleness observed in Chapter 2. One now needs to implement the formulations obtained by coupling both the pure damage model and the damage-plastic one to the eikonal-based approach to confirm the insights regarding these formulations.

Chapter 4

Structures computations with the nonlocal isotropic damage and damage-plastic models

Contents

It was shown in Chapter 2 that applying an eikonal-based nonlocal treatment to an isotropic damage model allowed one to get what was described in Part 1.3.3 as a good damage model. As it is, the resulting formulation did not suffer neither from the drawbacks linked to local damage models with strain softening, nor from those associated with nonlocal models with fixed lengths.

However, it appears that the shrinking localisation zone associated with the nonlocal treatment induced an excessive brittleness of the macroscopic response obtained in a one-dimensional setting. This issue, along with the lack of permanent strain, was investigated in Chapter 3 where one compared a pure damage model and a damage-plastic model associated with fixed and shrinking localisations. It was thus shown that replacing the previous pure damage model with the damage-plastic model introduced in Chapter 3 should be a good way to address both issues simultaneously.

Following this, one now needs to implement the nonlocal damage models obtained by coupling both the pure damage model and the damage-plastic one to the eikonal-based gradient-type formulation in a finite element code. It was decided here to work with the finite element code OOFEM, developed at the Czech Technical University, that already includes different damage models and gradient-type formulations. Thanks to OOFEM being open source and to a stay of six months in Prague during this thesis, this has allow the author to take advantage of all the dedicated tools developed for those models, while also being able to create new ones.

This chapter will thus begin by introducing the nonlocal damage and damage-plastic models considered here, along with the associated variational formulations which will be used to handle their implementation. Numerical $2D$ simulations will then be conducted to ensure that those damage models exhibit the properties that could be expected based on the work presented in Chapters 2 and 3.

4.1 Considered damage models and variational formulations

This part will present the local damage and damage-plastic models considered here, along with the formulations obtained by coupling them with the general gradient-type equation (1.29). The associated variational formulations used to implement them in OOFEM will also be presented thereafter, and the details on how they were obtained can be found in Appendix C.

4.1.1 Pure isotropic damage model

The first damage model considered here is the generalisation to $3D$ of the pure damage model studied in Chapter 3.

Local formulation

As far as the local model is concerned, damage can still be expected to be driven by Mazars' equivalent strain. The model then writes

$$\begin{aligned}
\boldsymbol{\sigma} &= \tilde{\mathbb{C}} : \boldsymbol{\varepsilon} = (1-D)\ \mathbb{C} : \boldsymbol{\varepsilon} && (4.1)\\
\hat{\varepsilon} &= \sqrt{\langle \varepsilon_1 \rangle_+^2 + \langle \varepsilon_2 \rangle_+^2 + \langle \varepsilon_3 \rangle_+^2} && (4.2)\\
\kappa(t) &= \max_{\tau \leq t} \hat{\varepsilon}(\tau) && (4.3)\\
D &= g(\kappa) = \begin{cases} 0 & \text{if } \kappa < \varepsilon_0 \\ 1 - \dfrac{\varepsilon_0}{\kappa} \exp\left(-\dfrac{\kappa - \varepsilon_0}{\varepsilon_f - \varepsilon_0} \right) & \text{if } \kappa \geq \varepsilon_0 \end{cases} && (4.4)
\end{aligned}$$

Nonlocal gradient-type formulation

As before, this formulation keeps both the stress-strain law (4.1) and the damage evolution law (4.4) of the local damage model. The damage driving variable κ is still defined as the maximum value over the loading history of the nonlocal strain $\bar{\varepsilon}$.

Focusing on the general gradient-type equation (1.29), $\bar{\varepsilon}$ should be computed from Mazars equivalent strain (4.2) as

$$\bar{\varepsilon} - a\ \nabla \cdot (b\ \nabla\ \bar{\varepsilon}) = \hat{\varepsilon} \tag{4.5}$$

where a and b are functions that may depend on state variables, according to the considered model.

It is worth noting that equation (4.2) can still stand for any gradient-type formulation, provided one chooses a and b accordingly. As before, the eikonal-based formulation (1.72) can be recovered by setting $a = c^2(1-D)^{1/2}$ and $b = (1-D)^{1/2}$, while the classical Peerlings' one (1.26) can be obtained by setting $a = 1$ and $b = c^2$.

Associated variational formulation

Moving on to the variational formulation, one would get for the equilibrium equation $\nabla \cdot \boldsymbol{\sigma} = \mathbf{0}$ the classical weak form

$$\int_\Omega \nabla \boldsymbol{u}^* : \tilde{\mathbb{C}} : \nabla \boldsymbol{u}\ \mathrm{d}V = \int_{\partial\Omega} \boldsymbol{u}^* \cdot \boldsymbol{T}\ \mathrm{d}S \tag{4.6}$$

where $\boldsymbol{u}^*$ stands for a virtual displacement field. It is worth noting that this remains true as long as one keeps the classical boundary condition $\boldsymbol{\sigma} \cdot \mathbf{n} = \boldsymbol{T}$ on $\partial\Omega$ of normal $\boldsymbol{n}$.

On the other hand, to avoid numerical difficulties when determining the weak form associated with the general gradient-type equation, one would need to follow the work of [Saroukhani et al., 2013] and to divide equation (4.5) by a. By doing so, one would get

$$\frac{\bar{\varepsilon}}{a} - \nabla \cdot (b\ \ (\nabla\ \bar{\varepsilon})) = \frac{\hat{\varepsilon}}{a} \tag{4.7}$$

which, using the homogeneous Neumann boundary condition $(\nabla\ \bar{\varepsilon}) \cdot \boldsymbol{n} = 0$ on $\partial\Omega$ of normal $\boldsymbol{n}$, yields

$$\int_\Omega \left(\frac{\bar{\varepsilon}\ \bar{\varepsilon}^*}{a} + b\ (\nabla\ \bar{\varepsilon}) \cdot (\nabla\ \bar{\varepsilon}^*) \right) \mathrm{d}V = \int_\Omega \frac{\hat{\varepsilon}}{a}\ \bar{\varepsilon}^*\ \mathrm{d}V\ ,\quad \forall\ \bar{\varepsilon}^* \tag{4.8}$$

where $\bar{\varepsilon}^*$ is a virtual nonlocal strain field.

It is worth knowing that this remains true as long as a is not equal to 0 and that the weak form associated with both classical and eikonal-based gradient-type formulations can be recovered by choosing a and b accordingly.

4.1.2 Isotropic damage-plastic model

One now needs to focus on the damage-plastic model that will be studied here, and whose behavior will be compared to the one associated with the pure damage model. Following the work presented in Chapter 3, it was decided to study the generalization to $3D$ of the previous damage-plastic model.

Local formulation

Keeping the idea of a plasticity-driven damage model with a Rankine plasticity criterion, and noting $\boldsymbol{\varepsilon}^p$ the plastic strain tensor, the stress-strain relation based on Hooke's law extended to plasticity and damage writes

$$\boldsymbol{\sigma}\ = \tilde{\mathbb{C}} : (\boldsymbol{\varepsilon} - \boldsymbol{\varepsilon}^p) = (1 - D)\ \mathbb{C} : (\boldsymbol{\varepsilon} - \boldsymbol{\varepsilon}^p) \tag{4.9}$$

Damage evolution is then assumed to be driven by the cumulative plastic strain p, defined from the plastic strain tensor $\boldsymbol{\varepsilon}^p$ as

$$\dot{p} = \sqrt{\frac{2}{3}\ \dot{\boldsymbol{\varepsilon}}^p : \dot{\boldsymbol{\varepsilon}}^p} \tag{4.10}$$

which gives back (3.6) in the one-dimensional setting.

As for the one-dimensional formulation, the irreversibility of damage is imposed through the definition of the damage-driving variable κ, which writes

$$\kappa(t) = p(t) = \int_0^t \dot{p}(\tau)\mathrm{d}\tau \tag{4.11}$$

allowing the taking into account of the plastic history.

Keeping the idea of a criterion f based on the effective stress $\tilde{\boldsymbol{\sigma}}$ defined in [Lemaitre and Chaboche, 1985] as

$$\tilde{\boldsymbol{\sigma}} = \frac{\boldsymbol{\sigma}}{1 - D} = \mathbb{C} : (\boldsymbol{\varepsilon} - \boldsymbol{\varepsilon}^p) \tag{4.12}$$

one would get

$$f\left(\tilde{\boldsymbol{\sigma}}, p\right) = \max\left(\tilde{\sigma}_I, \tilde{\sigma}_{II}, \tilde{\sigma}_{III}\right) - \sigma_y(p) \tag{4.13}$$

$$f\ \dot{p} = 0, \quad f \leq 0, \quad \dot{p} \geq 0 \tag{4.14}$$

Here, σ_y still stands for the yield stress that may depend on p in presence of hardening, while $\tilde{\sigma}_I$, $\tilde{\sigma}_{II}$ and $\tilde{\sigma}_{III}$ denote the effective stress eigenvalues.

Noting σ_0 the yield stress of the virgin material, and keeping a linear isotropic hardening R defined by the hardening modulus H, the yield stress writes

$$\sigma_y(p) = \sigma_0 + R(p) = \sigma_0 + H\ p \tag{4.15}$$

It is worth noting that the Rankine criterion (4.13), along with the definition of the yield stress (4.15), introduces a threshold in the evolution of plasticity. As a consequence, and as only monotonic loadings are considered, one does not need to introduce an additional threshold in the damage evolution, which still writes

$$D = g(\kappa) = 1 - \frac{\sigma_0}{\sigma_0 + H\kappa} \exp\left(-\frac{(1 + H/E)\kappa}{\varepsilon_f - \varepsilon_0}\right) \tag{4.16}$$

where ε_f and ε_0 are the material parameters governing damage evolution.

Nonlocal gradient-type formulation

As before, the nonlocal formulation keeps both the stress-strain law (4.9) and the damage evolution law (4.16), along with the definition of the cumulative plastic strain (4.10) and equations (4.12) to (4.15) governing the evolution of plasticity.

Besides, following the work done in [Vermeer and Brinkgreve, 1994, Strömberg and Ristinmaa, 1996] and [Grassl and Jirásek, 2005], it was decided here to consider an over-nonlocal damage-driving variable κ defined as

$$\kappa = m\ \bar{p} + (1 - m)p \tag{4.17}$$

Here m is still a numerical parameter, the particular cases $m = 1$ and $m > 1$ corresponding respectively to the use of the nonlocal damage-driving variable and of the so-called over-nonlocal formulations. Besides, the nonlocal cumulative plastic strain $\bar{p}$ is defined through the general gradient-type equation

$$\bar{p} - a\ \nabla \cdot (b\ \nabla\ \bar{p}) = p \tag{4.18}$$

with p the local variable, and where the functions a and b may still depend on some state variables.

Again, provided a and b are chosen accordingly, equation (4.2) can stand for any gradient-type formulation. As an example, setting $a = c^2(1 - D)^{1/2}$ and $b = (1 - D)^{1/2}$ would give the eikonal-based formulation (1.72), while the classical (Peerlings) one (1.26) could be obtained by setting $a = 1$ and $b = c^2$.

Associated variational formulation

Similarly to the pure damage model, the weak form associated with the equilibrium equation writes here

$$\int_\Omega \nabla \boldsymbol{u}^* : \tilde{\mathbb{C}} : (\nabla \boldsymbol{u} - \boldsymbol{\varepsilon}^p) \ \mathrm{d}V = \int_{\partial\Omega} \boldsymbol{u}^* \cdot \boldsymbol{T} \ \mathrm{d}S \tag{4.19}$$

where $\boldsymbol{u}^*$ still stands for a virtual displacement field and $\boldsymbol{T}$ is still defined through $\boldsymbol{\sigma} \cdot \boldsymbol{n} = \boldsymbol{T}$ on $\partial\Omega$ of normal $\boldsymbol{n}$.

As far as the nonlocal equation (4.18) is concerned, one would get, following the same steps as for the pure damage model and keeping a homogeneous Neumann boundary condition $(\nabla\ \bar{p}) \cdot \boldsymbol{n} = 0$ on $\partial\Omega$ of normal $\boldsymbol{n}$,

$$\int_\Omega \left(\frac{\bar{p}\ \bar{p}^*}{a} + b\ (\nabla\ \bar{p}) \cdot (\nabla\ \bar{p}^*) \right) \mathrm{d}V = \int_\Omega \frac{p}{a}\ \bar{p}^*\ \mathrm{d}V\ , \quad \forall\ \bar{p}^* \tag{4.20}$$

where $\bar{p}^*$ is virtual nonlocal plastic strain field and a still cannot be equal to 0.

4.2 Numerical implementation in OOFEM

This part will first present the general framework used to implement gradient-type damage models in OOFEM, especially the terms that need to be specified. It will then focus on the particular cases of the isotropic damage and damage-plastic models considered here, especially when using the general gradient-type formulation, which constitutes the main innovative contribution to OOFEM here. It is worth noting that the discretisation and linearisation of the considered models' weak forms, used to handle the numerical implementation, are detailed in Appendix C.

4.2.1 General framework and notations used for the implementation of gradient-type damage models

This part will present the framework used to implement a gradient-type damage model in the OOFEM finite element code, along with the notations used to detail the terms of the linearized formulations used for the implementation.

General notations

This part will present the notations used to introduce the linearized forms of the equations associated with the considered formulations. The following notations will be used for the main degrees of freedom, associated with displacement:

- $[\boldsymbol{N}_\mathcal{U}]$ will denote the matrix containing the shape functions for $\boldsymbol{u}$
- $[\boldsymbol{B}_\mathcal{U}]$ will denote the matrix containing the derivatives of the shape functions
- $\{\mathcal{U}\}$ will denote the vector containing the solution displacement's nodal value

and for the degrees of freedom associated with the nonlocal variable:

- $[\boldsymbol{N}_{\mathcal{E}}]$ will denote the matrix containing the shape functions
- $[\boldsymbol{B}_{\mathcal{E}}]$ will denote the matrix containing the derivatives of the shape functions
- $\{\mathcal{E}\}$ will denote the vector containing the solution nonlocal equivalent or cumulative plastic strain's nodal values

The terms linked to both the displacement and nonlocal degrees of freedom can then be expressed from $\{\mathcal{U}\}$, $[\boldsymbol{N}_{\mathcal{U}}]$ and $[\boldsymbol{B}_{\mathcal{U}}]$ as described in Table 4.1. In a similar fashion, the expression of the terms linked to the solution nonlocal equivalent strain and nonlocal cumulative plastic strain can be expressed from $[\boldsymbol{N}_{\mathcal{E}}]$, $[\boldsymbol{B}_{\mathcal{E}}]$ and $\{\mathcal{E}\}$ as detailed in Table 4.1.

$\boldsymbol{u}$	$\nabla \cdot \boldsymbol{u}$	$\bar{\varepsilon}$	$\nabla\ \bar{\varepsilon}$	$\bar{p}$	$\nabla\ \bar{p}$
$[\boldsymbol{N}_{\mathcal{U}}]\{\mathcal{U}\}$	$[\boldsymbol{B}_{\mathcal{U}}]\{\mathcal{U}\}$	$[\boldsymbol{N}_{\mathcal{E}}]\{\mathcal{E}\}$	$[\boldsymbol{B}_{\mathcal{E}}]\{\mathcal{E}\}$	$[\boldsymbol{N}_{\mathcal{E}}]\{\mathcal{E}\}$	$[\boldsymbol{B}_{\mathcal{E}}]\{\mathcal{E}\}$

Table 4.1: Terms linked to the displacement and nonlocal degrees of freedom.

As far as the linearized forms are concerned, the ones associated with the equilibrium equations of both formulations will be written as

$$\int_{\Omega} \Phi_{\mathcal{U}}\ \mathrm{d}V = \int_{\partial\Omega} [\boldsymbol{N}_{\mathcal{U}}]^t \cdot \boldsymbol{T}\ \mathrm{d}S \tag{4.21}$$

where $\Phi_{\mathcal{U}}$ and $\boldsymbol{T}$ respectively stand for the associated internal and external forces.

In a similar fashion, the linearized forms associated with the nonlocal equations of both formulations will be written as

$$\int_{\Omega} \Phi_{\mathcal{E}}\ \mathrm{d}V = 0 \tag{4.22}$$

where $\Phi_{\mathcal{E}}$ stands for the associated internal forces.

The notations presented in this section will now be used to detail the linearized forms of the considered formulations, along with their numerical implementation.

General framework

This section will now present the terms that need to be defined to implement both local and gradient-type material models in the finite element code OOFEM. It is worth noting that the application to the formulations considered here will be presented in the next sections.

Let's first focus on the implementation in the finite element code OOFEM of a material model where only the equilibrium has to be solved. In this case, one would only have to specify the internal force $\Phi_{\mathcal{U}}$ defined in equation (4.21), along with its derivative $\partial\Phi_{\mathcal{U}}/\partial\mathcal{U}$ with respect to the displacement degrees of freedom.

As far as nonlocal gradient-type formulations are concerned, one should still define the terms associated with the equilibrium, but also those linked to the nonlocal equation. As it is, one should specify the internal force $\Phi_{\mathcal{E}}$ defined in equation (4.22) and, as before, one would also have to define its derivative $\partial\Phi_{\mathcal{E}}/\partial\mathcal{E}$ with respect to the nonlocal degrees of freedom.

Besides, to use the tangent operator and to solve this as a coupled problem, one would also have to define the cross-derivatives, namely $\partial\Phi_{\mathcal{U}}/\partial\mathcal{E}$ and $\partial\Phi_{\mathcal{E}}/\partial\mathcal{U}$.

It is worth noting that, while all those terms are implemented in the file describing the material's behaviour, one should still ensure that the necessary components can still be transmitted from the element level. As it is, since the computation of every term requires information from the element level (e.g. $\mathcal{U}$, $[\boldsymbol{N}_{\mathcal{U}}]$, $[\boldsymbol{B}_{\mathcal{U}}]$, $\mathcal{E}$, $[\boldsymbol{N}_{\mathcal{E}}]$, $[\boldsymbol{B}_{\mathcal{E}}]$), a material class usually contains each component of each term in a specific format. To be compatible with such a model, a given element class would then have to contain the definition of those components, in order to provide the information needed on the material level.

As a consequence, when implementing a material model, one should ensure that it is associated with elements that are compatible with the components required for the computation of the internal forces and their derivatives. While this is usually straightforward for models which only involve the equilibrium and the displacement degrees of freedom, special care needs to be taken for more complex models.

As an example, when considering a nonlocal gradient-type formulation, the use of the dedicated elements which are designed to take into account the additional degrees of freedom might not be enough. As it is, while they are compatible with the models already implemented in OOFEM, special care will have to be taken when dealing with the general gradient-type formulations which will most likely involve additional components.

The next sections will present the terms that can be kept for the implementation of the general gradient-type formulations with both pure damage and damage-plastic models, and those that will have to be either modified or introduced.

4.2.2 Application to the isotropic damage model

Let's start with the implementation of the formulations based on the pure isotropic damage model. It has been shown in Appendix C.3.2 that the internal force associated with the equilibrium writes for both gradient-type formulations

$$\Phi_{\mathcal{U}} = [\boldsymbol{B}_{\mathcal{U}}]^t : (1-D)\mathbb{C} : \nabla\boldsymbol{u} \tag{4.23}$$

which gives for its derivatives

$$\frac{\partial\Phi_{\mathcal{U}}}{\partial\mathcal{U}} = [\boldsymbol{B}_{\mathcal{U}}]^t : (1-D)\mathbb{C} : [\boldsymbol{B}_{\mathcal{U}}] \tag{4.24}$$

$$\frac{\partial\Phi_{\mathcal{U}}}{\partial\mathcal{E}} = [\boldsymbol{B}_{\mathcal{U}}]^t \left(-D'(\kappa)\ \kappa'(\bar{\varepsilon})\ \mathbb{C} : \nabla\boldsymbol{u}\right) [\boldsymbol{N}_{\mathcal{E}}] \tag{4.25}$$

where D' and κ' respectively stand for the derivative of D with respect to κ and that of κ with respect to $\bar{\varepsilon}$.

Since the formulation associated with the classical gradient-type equation was already implemented in OOFEM, these terms were already defined on the material level and compatible with the gradient-type elements.

One now needs to focus on the implementation of the general gradient-type equation whose linearization is also detailed in Appendix C.3.2. The associated internal force was thus shown to be equal to

$$\Phi_{\mathcal{E}} = [\boldsymbol{N}_{\mathcal{E}}]^t \, \frac{1}{a} \, (\bar{\varepsilon} - \hat{\varepsilon}) + b \, [\boldsymbol{B}_{\mathcal{E}}]^t \nabla \bar{\varepsilon} \tag{4.26}$$

which gives for its derivatives with respect to the displacement degrees of freedom

$$\frac{\partial \Phi_{\mathcal{E}}}{\partial \mathcal{U}} \quad = \quad [\boldsymbol{N}_{\mathcal{E}}]^t \left(-\frac{1}{a} \, \frac{\partial \hat{\varepsilon}}{\partial \boldsymbol{\varepsilon}} \right) [\boldsymbol{B}_{\mathcal{U}}] \tag{4.27}$$

and to the nonlocal one

$$\begin{aligned} \frac{\partial \Phi_{\mathcal{E}}}{\partial \mathcal{E}} = [\boldsymbol{N}_{\mathcal{E}}]^t \left(\frac{1}{a} + \frac{1}{a^2} \, a'(D) \; D'(\kappa) \; \kappa'(\bar{\varepsilon}) \; (\hat{\varepsilon} - \bar{\varepsilon}) \right) [\boldsymbol{N}_{\mathcal{E}}] \\ + [\boldsymbol{B}_{\mathcal{E}}]^t \; b \; [\boldsymbol{B}_{\mathcal{E}}] + [\boldsymbol{B}_{\mathcal{E}}]^t \nabla \bar{\varepsilon} \Big(b'(D) \; D'(\kappa) \; \kappa'(\bar{\varepsilon}) \Big) [\boldsymbol{N}_{\mathcal{E}}] \end{aligned} \tag{4.28}$$

It is worth noting that here a' and b' respectively stand for the derivatives of a and b with respect to D.

Moving on to the classical gradient-type formulation, which will be used as a basis for the implementation of the general one, its terms were shown in Appendix C.3.2 to be defined as

$$\Phi_{\mathcal{E}} = [\boldsymbol{N}_{\mathcal{E}}]^t \; (\bar{\varepsilon} - \hat{\varepsilon}) + [\boldsymbol{B}_{\mathcal{E}}]^t \; c^2 \; \nabla \bar{\varepsilon} \tag{4.29}$$

$$\frac{\partial \Phi_{\mathcal{E}}}{\partial \mathcal{U}} = [\boldsymbol{N}_{\mathcal{E}}]^t \left(-\frac{\partial \hat{\varepsilon}}{\partial \boldsymbol{\varepsilon}} \right) [\boldsymbol{B}_{\mathcal{U}}] \tag{4.30}$$

$$\frac{\partial \Phi_{\mathcal{E}}}{\partial \mathcal{E}} = [\boldsymbol{N}_{\mathcal{E}}]^t \; [\boldsymbol{N}_{\mathcal{E}}] + [\boldsymbol{B}_{\mathcal{E}}]^t \; c^2 \; [\boldsymbol{B}_{\mathcal{E}}] \tag{4.31}$$

One should now compare the terms presented in equations (4.26) to (4.28) to those introduced in equations (4.29) to (4.31) in order to see the modifications required for this implementation.

Starting with the internal force, namely equations (4.26) and (4.29), one will only have to replace $\bar{\varepsilon} - \hat{\varepsilon}$ by $(\bar{\varepsilon} - \hat{\varepsilon})/a$ and c^2 by b, but no additional term will have to be introduced. Moving on to its derivative with respect to the displacement degrees of freedom, one can see that its implementation will not require an additional term either since $-\partial \hat{\varepsilon}/\partial \boldsymbol{\varepsilon}$ will simply have to be replaced by $-(1/a)(\partial \hat{\varepsilon}/\partial \boldsymbol{\varepsilon})$.

On the other hand, as far as the derivative of the internal force with respect to the nonlocal degrees of freedom is concerned, namely (4.27) and (4.30), one will still have to modify the existing terms, but a new one will also have to be

introduced. Starting with the first component of $\partial\Phi_{\mathcal{E}}/\partial\mathcal{E}$, one will simply have to replace 1 by $(1/a) + (1/a^2)\ a'(D)\ D'(\kappa)\ \kappa'(\bar{\varepsilon})\ (\hat{\varepsilon} - \bar{\varepsilon})$, and c^2 by b for the second one.

Regarding the third term, namely equations (4.28) and (4.31), its implementation will require the introduction of a new term, writing $[\boldsymbol{B}_{\mathcal{E}}]^t\ \boldsymbol{f_1}\ [\boldsymbol{N}_{\mathcal{E}}]$, on both the material and the element level. The function $\boldsymbol{f_1}$ should then be set equal to $\nabla\bar{\varepsilon}\Big(b'(D)\ D'(\kappa)\ \kappa'(\bar{\varepsilon})\Big)$ for the formulation associated with the general gradient, while it will be equal to $\mathbf{0}$ for the preexisting ones since b' would then be equal to 0

4.2.3 Application to the isotropic damage-plastic model

As for the pure damage model, it has been shown in Appendix C.3.3 that the internal force associated with the equilibrium writes for both the classical and general gradient-type formulations coupled with the damage-plastic model

$$\Phi_{\mathcal{U}} = [\boldsymbol{B}_{\mathcal{U}}]^t : (1-D)\mathbb{C} : (\boldsymbol{\varepsilon} - \boldsymbol{\varepsilon}^p) \tag{4.32}$$

Its derivative with respect to the displacement degrees of freedom then writes

$$\begin{aligned}\frac{\partial\Phi_{\mathcal{U}}}{\partial\mathcal{U}} =& [\boldsymbol{B}_{\mathcal{U}}]^t\ (1-D)\ \mathbb{C}\ [\boldsymbol{B}_{\mathcal{U}}] \\ &- [\boldsymbol{B}_{\mathcal{U}}]^t\ D'(\kappa)\ (1-m)\ p'(\boldsymbol{\varepsilon})\ \mathbb{C} : (\boldsymbol{\varepsilon} - \boldsymbol{\varepsilon}^p)\ [\boldsymbol{B}_{\mathcal{U}}]\end{aligned} \tag{4.33}$$

where p' stands for the derivative of the return-mapping algorithm, while the derivative of $\Phi_{\mathcal{U}}$ with respect to the nonlocal degrees of freedom writes

$$\frac{\partial\Phi_{\mathcal{U}}}{\partial\mathcal{E}} = [\boldsymbol{B}_{\mathcal{U}}]^t\,(-D'(\kappa)\ m\ \mathbb{C} : (\boldsymbol{\varepsilon} - \boldsymbol{\varepsilon}^p))\,[\boldsymbol{N}_{\mathcal{E}}] \tag{4.34}$$

Since the formulation associated with the classical gradient-type equation was already implemented in OOFEM, these terms were already defined on the material level and compatible with the dedicated elements.

Following the same steps as for the pure damage model, one should compare the terms associated with the general gradient-type formulation to those associated with the classical one. Starting with the general gradient-type formulation, the internal force has been shown in Appendix C.3.3 to be defined as

$$\Phi_{\mathcal{E}} = [\boldsymbol{N}_{\mathcal{E}}]^t\ \frac{1}{a}\ (\bar{p} - p) + b\ [\boldsymbol{B}_{\mathcal{E}}]^t\ \nabla\bar{p} \tag{4.35}$$

while its derivative with respect to the displacement degrees of freedom writes

$$\begin{aligned}\frac{\partial\Phi_{\mathcal{E}}}{\partial\mathcal{U}} =& [\boldsymbol{N}_{\mathcal{E}}]^t \left(-\frac{p'(\boldsymbol{\varepsilon})}{a} + \frac{p-\bar{p}}{a^2}\ a'(D)\ D'(\kappa)\ (1-m)\ p'(\boldsymbol{\varepsilon})\right)[\boldsymbol{B}_{\mathcal{U}}] \\ &+ [\boldsymbol{B}_{\mathcal{E}}]^t \nabla\bar{p}\Big(b'(D)\ D'(\kappa)\ (1-m)\Big) p'^t(\boldsymbol{\varepsilon}) [\boldsymbol{B}_{\mathcal{U}}]\end{aligned} \tag{4.36}$$

and its derivative with respect to the nonlocal degrees of freedom

$$\begin{aligned}\frac{\partial \Phi_{\mathcal{E}}}{\partial \mathcal{E}} &= [\boldsymbol{N}_{\mathcal{E}}]^t \left(\frac{1}{a} + \frac{1}{a^2}\, a'(D)\, D'(\kappa)\, m\,(p-\bar{p})\right)[\boldsymbol{N}_{\mathcal{E}}] \\ &+[\boldsymbol{B}_{\mathcal{E}}]^t\, (\nabla \bar{p}\, b'(D)\, D'(\kappa)\, m)\,[\boldsymbol{N}_{\mathcal{E}}] + b\,[\boldsymbol{B}_{\mathcal{E}}]^t\,[\boldsymbol{B}_{\mathcal{E}}]\end{aligned} \tag{4.37}$$

On the other hand, the terms associated with the classical gradient-type formulation write

$$\Phi_{\mathcal{E}} = [\boldsymbol{N}_{\mathcal{E}}]^t\, (\bar{p} - p) + [\boldsymbol{B}_{\mathcal{E}}]^t\, c^2\, \nabla \bar{p} \tag{4.38}$$

$$\frac{\partial \Phi_{\mathcal{E}}}{\partial \mathcal{U}} = [\boldsymbol{N}_{\mathcal{E}}]^t\, (-p'(\boldsymbol{\varepsilon}))\,[\boldsymbol{B}_{\mathcal{U}}] \tag{4.39}$$

$$\frac{\partial \Phi_{\mathcal{E}}}{\partial \mathcal{E}} = [\boldsymbol{N}_{\mathcal{E}}]^t\,[\boldsymbol{N}_{\mathcal{E}}] + [\boldsymbol{B}_{\mathcal{E}}]^t\, c^2\,[\boldsymbol{B}_{\mathcal{E}}] \tag{4.40}$$

To determine the modifications required for the implementation of the damage-plastic formulation, one now needs to compare the terms gathered in equations (4.35) to (4.37) to those introduced in equations (4.38) to (4.40).

By doing so, one can first see that, as for the pure damage model, the internal force will not require any additional term, since one will simply have to replace $\bar{p} - p$ by $(\bar{p} - p)/a$ and c^2 by b.

However, since the damage driving variable is here a combination of both the local and nonlocal cumulative plastic strain, one will here have to introduce a new component in $\partial \Phi_{\mathcal{E}} / \partial \mathcal{U}$ to account for the dependency of b with respect to p. To do so, one will first have to introduce a term writing $[\boldsymbol{B}_{\mathcal{E}}]^t\ \boldsymbol{f_2}\ [\boldsymbol{B}_{\mathcal{U}}]$ on both the material and element levels, where $\boldsymbol{f_2}$ should be set equal to 0 by default. Then, in addition to replacing $-p'(\boldsymbol{\varepsilon})$ with $(-p'(\boldsymbol{\varepsilon})/a) + (p - \bar{p}/a^2)\, a'(D)\, D'(\kappa)\, (1-m)\, p'(\boldsymbol{\varepsilon})$, one should set $\boldsymbol{f_2}$ to $\nabla \bar{p}\Big(b'(D)\, D'(\kappa)\, (1-m)\Big) p'^t(\boldsymbol{\varepsilon})$.

As before, the definition of $\partial \Phi_{\mathcal{E}} / \partial \mathcal{E}$ will require both the modification of the existing terms, and the introduction of a new one in the form $[\boldsymbol{B}_{\mathcal{E}}]^t\ \boldsymbol{f_1}\ [\boldsymbol{N}_{\mathcal{E}}]$. Provided such a term has already been implemented in the general gradient material and element classes, one will no longer have to define it since the current material will inherit it, along with the other components. In this case, one will simply have to set f_1 to $\nabla \bar{p}\, b'(D)\, D'(\kappa)\, m$, while replacing 1 with $\dfrac{1}{a} + \dfrac{1}{a^2}\, a'(D)\, D'(\kappa)\, m\,(p - \bar{p})$ and c^2 with b.

This part has presented the different steps for the numerical implementation in the computer code OOFEM of the formulations obtained by coupling the general gradient-type equation to the considered damage and damage-plastic models.

After properly setting the functions a and b, one should now use these implementations to run numerical simulations with the eikonal-based nonlocal damage models in order to study their properties.

4.3 Numerical results and properties of the damage and damage-plastic models

It was decided here, to assess the properties of the considered gradient-type damage and damage-plastic models in a more complex (standard) setting than the unidimensional one studied in Chapters 2 and 3, namely a three-point-bending testing.

After a general presentation of the numerical experiment conducted here, this part will thus start by studying the mesh sensitivity of the response obtained with the pure damage model. It will then focus on the influence of the internal length on both the brittleness of the response curve and the damage profile, before moving on to the computations with the damage-plastic model.

4.3.1 Numerical testing

The problem studied here is that of a notched beam submitted to a three-point-bending as described in Figure 4.1. As can be seen in Figure 4.1, the beam here lies on the extremities of its lower part (L and F), while the load (red arrow) is applied on top of it at the center (C), located right above the notch tip (I).

It is worth noting that only the displacements along the vertical axis are blocked on the support points, the horizontal ones being blocked along the line ($[IC]$) that links the notch tip and the loading point. The use of such boundary conditions is expected to prevent the occurrence of rigid body motions and to ensure the symmetry of the problem.

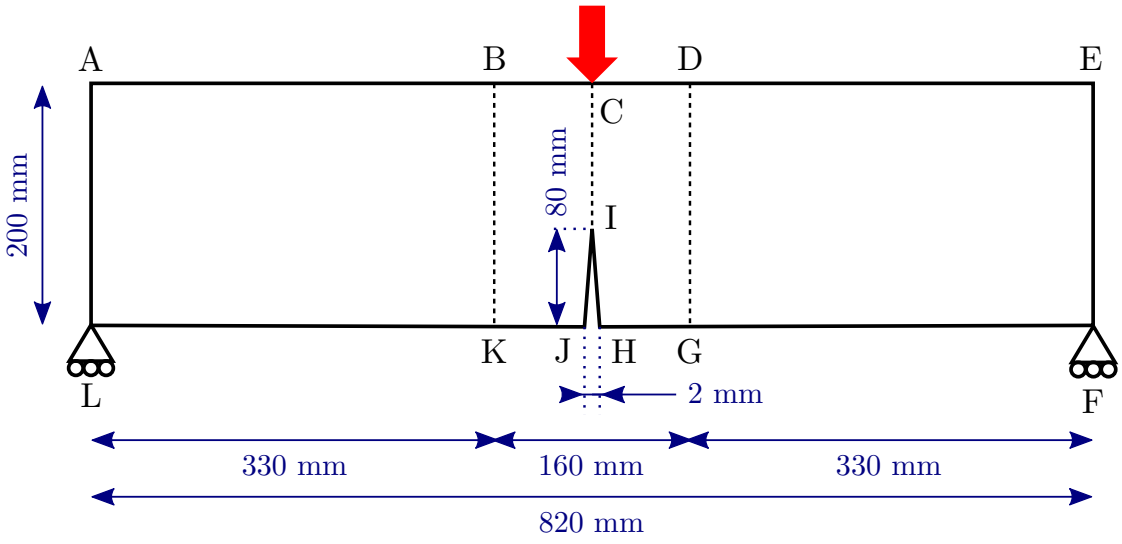

Figure 4.1: Three-point-bending test considered here.

As far as the spatial discretisation of the beam is concerned, four areas with different levels of mesh refinement were considered to have a rather fine mesh near the notch while limiting the numerical cost. As it is, while the areas constituting the main part of the beam, delimited by $ABKL$ and $DEFG$, have a rather coarse

mesh, the element size is smaller in those surrounding the notch, delimited by $BCIJK$ and $CDGHI$.

The first mesh considered here, displayed in Figure 4.2, involves a global element size of $l_s = 10$ mm far from the notch, i.e. along $[AB]$, $[KL]$, $[LA]$, $[DE]$, $[EF]$ and $[FG]$, and a local size of $l_s = 4$ mm close to it, i.e. in the areas surrounding the notch.

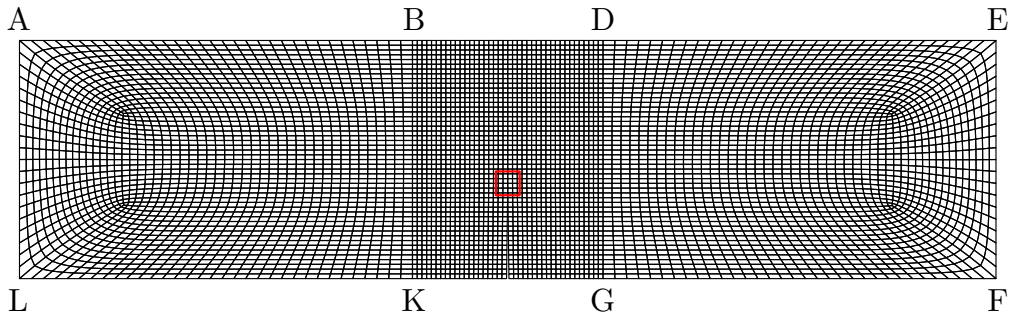

Figure 4.2: Mesh used for a local element size of 4 mm.

In order to study the mesh sensitivity of the results obtained with the considered models, it was decided here to keep the global element size and to change only the local size near the notch, which will here be taken equal to $l_s = 4$ mm, 2 mm and 1 mm. Samples of the meshes thus obtained in around the notch, in the area of 20 mm $\times$ 20 mm delimited by the red line in Figure 4.2, are respectively displayed in Figures 4.3a, 4.3b and 4.3c.

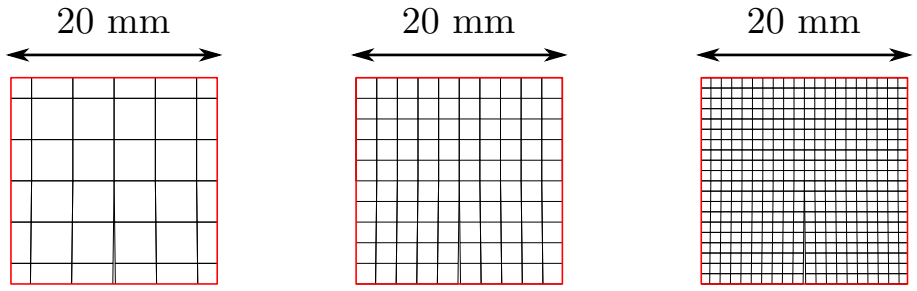

(a) Local size $l_s = 4$ mm. (b) Local size $l_s = 2$ mm. (c) Local size $l_s = 1$ mm.

Figure 4.3: Samples of the mesh around the notch for different local mesh sizes l_s.

The setting and meshes presented in this part will now be used to assess the properties of the formulations studied in this chapter, including the mesh sensitivity of the results, through displacement-driven computations

4.3.2 Mesh-independence of the pure damage model

First of all, one needs to study the properties of the formulation associated with the pure damage model when coupled to the eikonal-based approach as described in section 4.1.1, and especially the mesh independence of the results. To do so, numerical simulations were conducted using the setting detailed in Figure 4.1 and

the three local element sizes presented in Figure 4.3, along with the material parameters gathered in Table 4.2.

E	ν	ε_0	ε_f	c
30 000 MPa	0.2	$1.e-4$	$1.74e-4$	64 mm

Table 4.2: Parameters used for the study with a fixed localisation area.

As for the one-dimensional study conducted in Chapter 2, this part will first focus on the macroscopic response curves before moving on to the evolution and localisation of damage. It is worth noting that, due to the more complex setting considered here, one will not only focus on a single damage profile, but also on the distribution of both damage D and the damage-driving variable, namely Mazars' equivalent strain $\hat{\varepsilon}$ throughout the beam.

As one can see in Figure 4.4, the force-displacement curves obtained with the three levels of spatial discretisation are nearly identical until a certain (post-peak) point, which tends to indicate that the results are mesh-independent. As it is, the abrupt end of the curve is due to the occurrence of snap-back instabilities which cannot be handled with the displacement-based driving strategy used here. One can thus conclude that, in the absence of snap-back instabilities, the response curve, and thus the dissipated energy, are mesh-independent until local values of damage D reach 0.9.

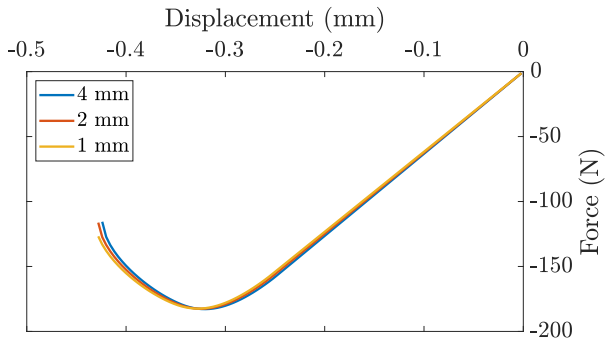

Figure 4.4: Force-displacement curves obtained for the three levels of refinements.

Though studying the macroscopic response curves gives some insight on the mesh sensitivity of the results, one now needs to focus on what happens at the structural level.

First, one can note that the final damage distribution throughout the beam, displayed in Figure 4.5 for the three levels of discretisation, appears to be mesh independent. Moreover, the area in which damage concentrates seems to shrinks when damage increases, which is consistent with the expected shrinking localisation associated with the eikonal-based formulation.

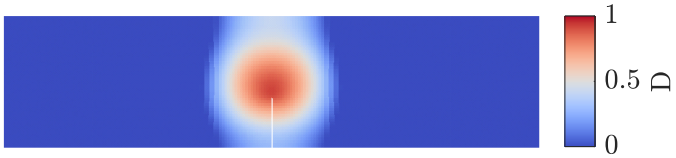

(a) Local size 4 mm.

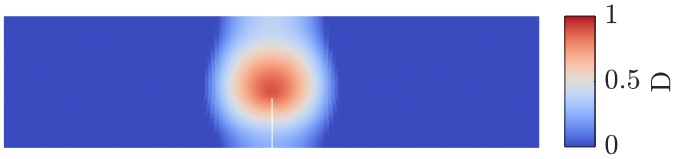

(b) Local size 2 mm.

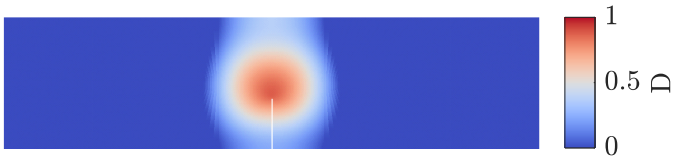

(c) Local size 1 mm.

Figure 4.5: Final damage maps obtained with the three levels of refinement.

Similar observations can also be made in Figure 4.6 where the final values of the local equivalent strain $\hat{\varepsilon}$ have been displayed throughout the beam. As it is, one can note that the $\hat{\varepsilon}$ maps are nearly identical, with small differences for the higher values near the center of the localisation area, and that it seems to concentrate in areas that get smaller for high levels of strain. This confirms the previous observations regarding both the mesh independence of the results and the shrinking localisation, the latter being much clearer here since $\hat{\varepsilon}$ tends to infinity while D is bounded to 1.

To confirm these global observations, this work will now focus on the profiles of both damage and its driving variable, along with their evolution. It is worth noting that these profiles will be taken along a horizontal line located just above the notch tip in order to be in the process zone while avoiding the geometrical singularity.

Starting with damage, one can see in Figure 4.7a that its final profile is nearly identical for the three levels of mesh refinement, the main difference coming from the accuracy of its discretisation. A small variation in the maximum damage can also be observed, but it tends to disappear when the element size decreases, and can thus be neglected.

Moreover, as far as the evolution of the damage profile is concerned, one can see in Figures 4.7b, 4.7c and 4.7d that it does not depend on the element size, which confirms the mesh independence of the damage distribution.

Its is also worth noting that, unlike the one-dimensional case, one does not get an initially wide damage profile that shrinks when damage increases. As it is, due to the different loading conditions, the damage profile is always sharp and its base expands until its maximum value reaches 1. Despite these differences, one still gets a sharp damage profile at the end of the process with a very thin highly damaged

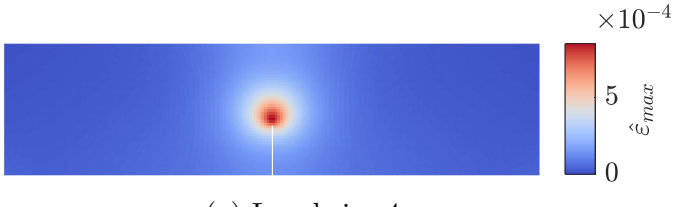

(a) Local size 4 mm.

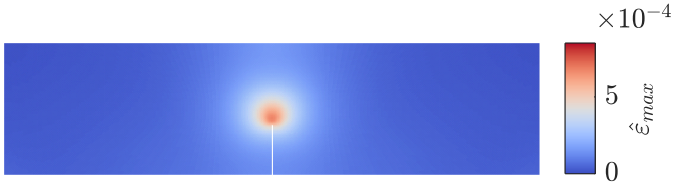

(b) Local size 2 mm.

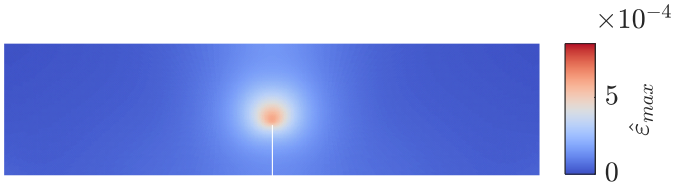

(c) Local size 1 mm.

Figure 4.6: Final equivalent strain maps obtained with the three levels of refinement.

area, which is consistent with the expected shrinking localisation area.

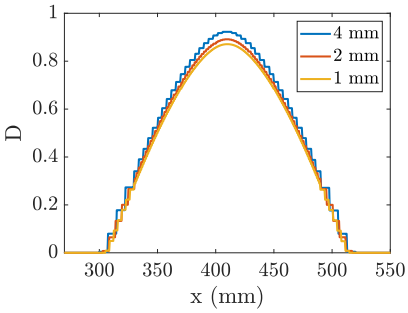

(a) Final profiles.

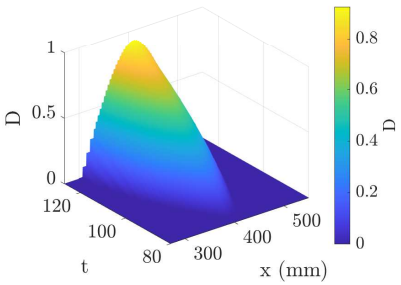

(b) Local size 4 mm.

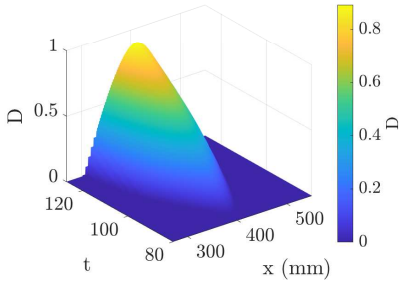

(c) Local size 2 mm.

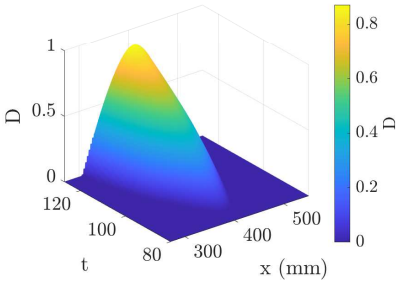

(d) Local size 1 mm.

Figure 4.7: Influence of the local mesh size on the evolution of the damage profile, along a horizontal line for different loading times t.

Moving on to the equivalent strain, one can see in Figure 4.8a that the final profiles are quite similar, though there are some differences for the high strain levels. This is consistent with the observations made on the damage profile, especially since the variation seems to disappear when the element size decreases. It is worth noting that, due to the damage evolution law, these variations are much more visible when considering the equivalent strain instead of damage.

One can also note in Figures 4.8b, 4.8c and 4.8d that, apart from the final values, the evolution of the equivalent strain profile seems to be mainly mesh independent. Moreover, as expected, the width of the equivalent strain profile tends to zero when $\hat{\varepsilon}$ increases, which, along with the sharpness of the final profile, confirms the shrinking of the localisation area.

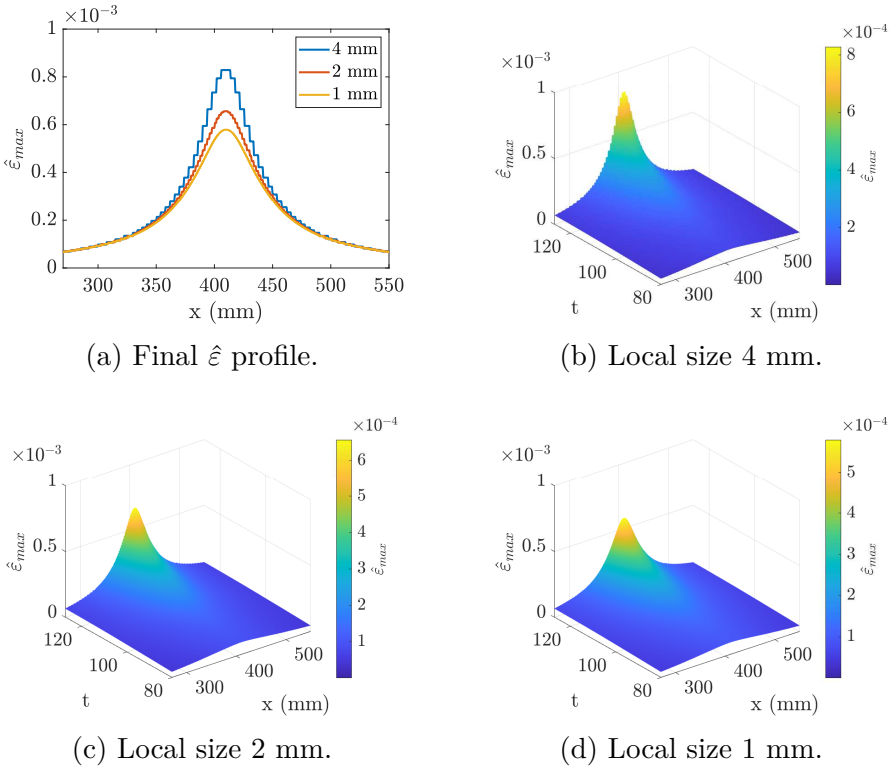

(a) Final $\hat{\varepsilon}$ profile.

(b) Local size 4 mm.

(c) Local size 2 mm.

(d) Local size 1 mm.

Figure 4.8: Influence of the local mesh size on the the evolution of the equivalent strain profile, along a horizontal line for different loading times t.

In the end, one can conclude that the results obtained with this formulation are mesh independent (at least in the absence of snap-back instabilities), which confirms the regularisation properties of the eikonal-based formulation. Moreover, the localisation area has been shown to shrink when damage increases, confirming the possibility to make a crack equivalent to a highly damaged zone. It is however worth noting that, due to the chosen displacement-based driving strategy, the occurrence of snap-back instabilities induced by the brittleness of the response prevented a study up to $D = 1$.

However, it must also be noted that, though the global response was rather brittle, damage was spread over a wide area, of size directly related to the internal

length parameter c.

4.3.3 Influence of the internal length

Now that the regularisation properties of the eikonal-based formulation associated with the pure damage model have been confirmed, one needs to study the influence of the internal length on the material behaviour. This was done by conducting numerical simulations with different internal lengths, keeping the three-point bending setting (Figure 4.1) and the finest mesh (Figure 4.3c) used for the mesh sensitivity study. Aside from c which was taken equal to 4 mm, 16 mm and 64 mm, it was also decided to keep the material parameters used in the previous part (Table 4.2).

As for the mesh sensitivity, this part will first deal with the macroscopic response curves, before moving on to the damage and equivalent strain distribution, and then to the evolution of their profiles along a line located above the notch tip.

Starting with the force-displacement curve, one can see in Figure 4.9 that the internal length has a direct influence on the maximal force, which seems to increase with it. Besides, one can note that increasing the internal length tends to increase the dissipated energy and thus the stability of the response. This numerical effect is consistent with the fact that the internal length supposedly controls the width of the localisation area where dissipation occurs [Pijaudier-Cabot et al., 2001, Le Bellégo et al., 2003].

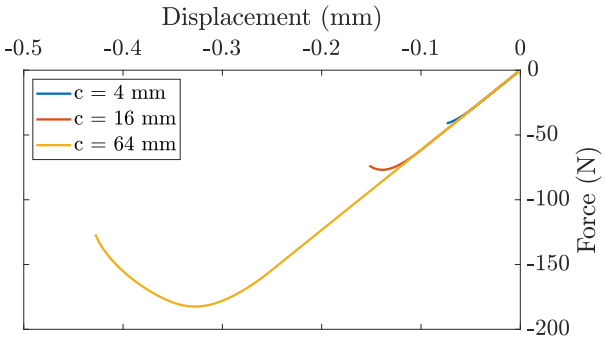

Figure 4.9: Force-displacement curves obtained for the three internal lengths.

Focusing on damage distribution, one can see in Figure 4.10 that the size of the damaged area is controlled by the internal length and that lowering its value allows for a more realistic damage spreading in the beam. However, as seen in Figure 4.9, the use of small internal lengths induces a very brittle behaviour which prevents stable crack propagation. One can also note that the high damage levels tend to localize at the centre of the damaged area, which indicates that the localisation area may still shrink with damage.

This can also be observed in Figure 4.11, where one can see that the high strain values tend to localize at the centre of the damaged area as well, which is

(a) $c = 4$ mm.

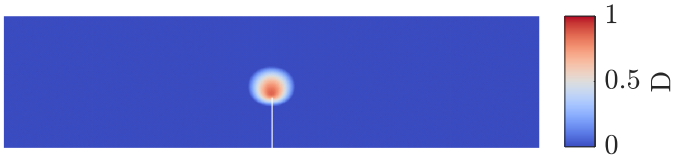

(b) $c = 16$ mm.

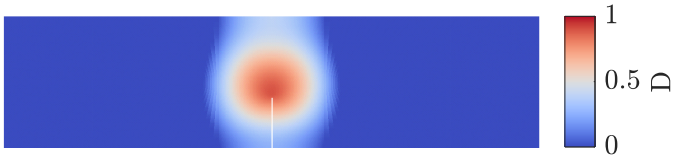

(c) $c = 64$ mm.

Figure 4.10: Final damage maps obtained with the three internal lengths.

consistent with a shrinking localisation area. Besides, as expected, the internal length also controls the equivalent strain distribution, which confirms its influence on the size of the localisation area.

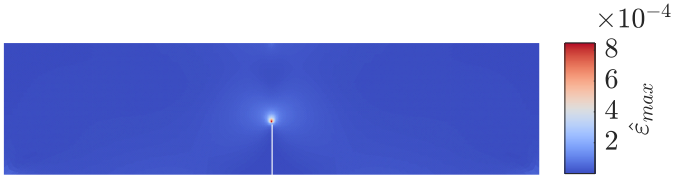

(a) $c = 4$ mm.

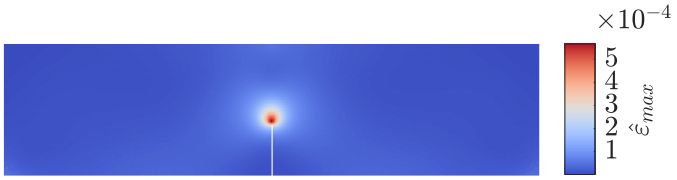

(b) $c = 16$ mm.

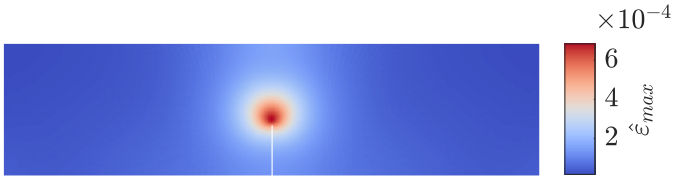

(c) $c = 64$ mm.

Figure 4.11: Final equivalent strain maps obtained with the three internal lengths.

To confirm these global observations, one now needs to focus on the evolution of damage and equivalent strain profiles taken just above the notch tip.

Starting with damage, one can see in Figure 4.12 that, as expected, the width of its profile is influenced by both the internal length and the current damage level throughout its evolution. As it is, while the final width of the damage profile is imposed by the internal length where D is close to 0, it shrinks to a single point when D gets close to 1.

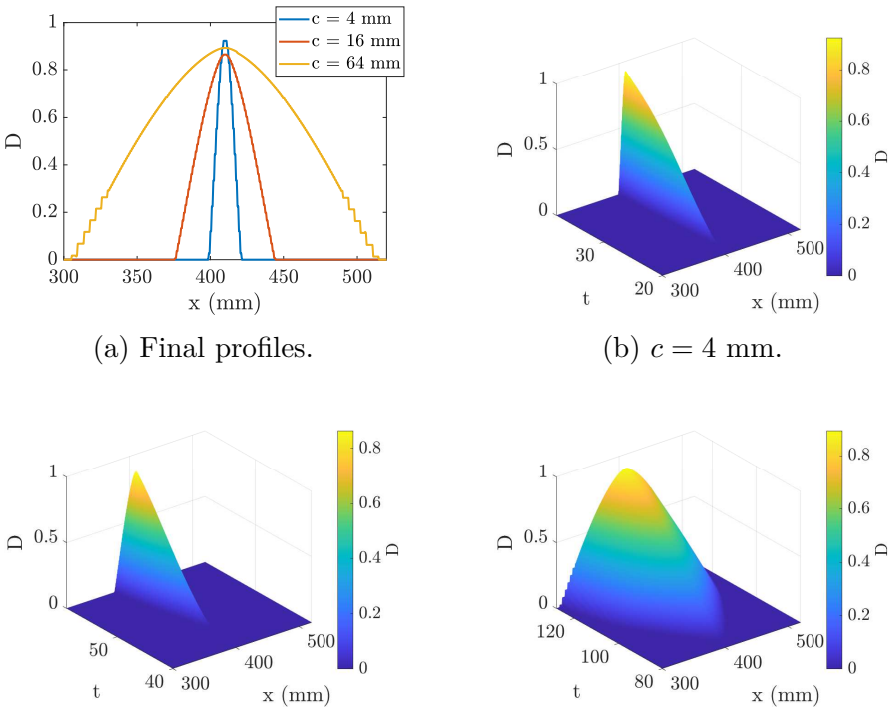

(a) Final profiles.

(b) $c = 4$ mm.

(c) $c = 16$ mm.

(d) $c = 64$ mm.

Figure 4.12: Influence of the internal length on the evolution of the damage profile, along a horizontal line for different loading times t.

As before, this is even more noticeable when considering the evolution of the equivalent strain profiles displayed in Figure 4.13 since they are even sharper due to the damage evolution law. Moreover, while these profiles are not bounded, it is observed that their final width is still controlled by both the internal length and the current equivalent strain level.

In the end, one can conclude that for the eikonal-based formulation, as expected, the internal length can be used to control the width of the localisation area and thus adjust the size of the damage zone. However, reducing the width of the damaged area to a more realistic value also reduces the dissipated energy and maximum force, thus increasing the brittleness of the global behaviour. It likewise tends to reduce the stability of the global response, which again prevented the study of stable crack propagation.

Despite the brittleness of the responses, the shrinking of the localisation area has also been shown to be independent from the internal length, confirming the possibility to make a highly damaged zone equivalent to a crack. To confirm the properties associated with the eikonal-based approach, one should now try

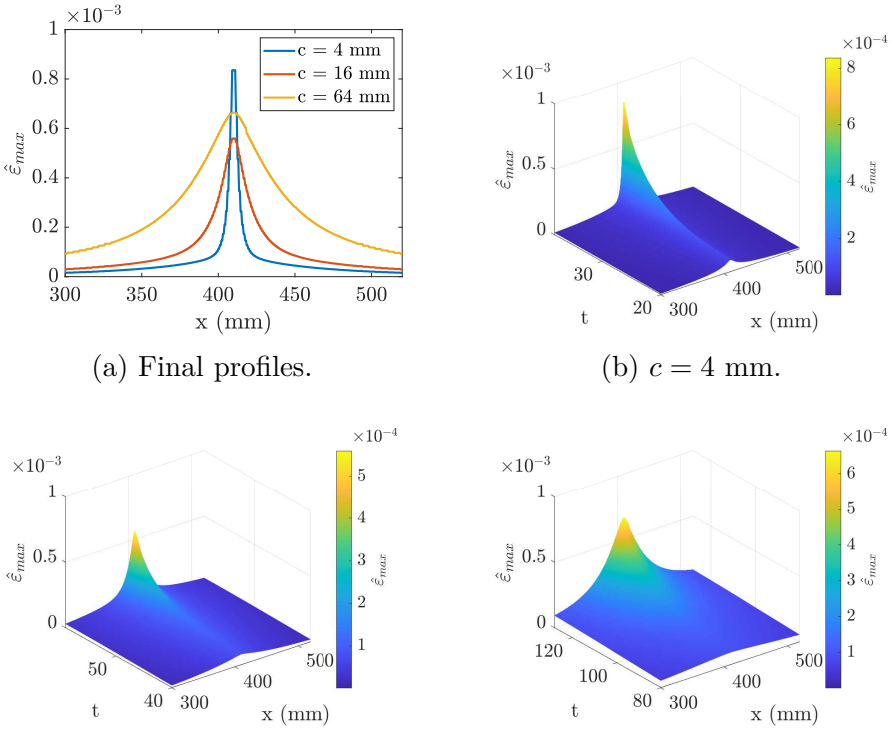

(a) Final profiles.

(b) $c = 4$ mm.

(c) $c = 16$ mm.

(d) $c = 64$ mm.

Figure 4.13: Influence of the internal length on the evolution of the equivalent strain profile, along a horizontal line for different loading times t.

to reduce the brittleness of the material behaviour through the introduction of plasticity.

As discussed before, a damage-plastic model is expected to be more suited to model concrete, mainly thanks to the introduction of permanent strain.

4.3.4 Mesh-independence of the damage-plastic model

After studying the properties of the eikonal-based approach associated with the pure damage model, one needs to move on to its association with the damage-plastic one presented in section 4.1.2. This part will thus focus on the mesh sensitivity of the eikonal-based damage-plastic formulation when used to handle the three-point bending problem described in Figure 4.1. As for the pure damage model, numerical simulations will thus be conducted using the spatial discretisations presented in Figure 4.2, and the parameters gathered in Table 4.3. It is worth noting that the parameters are consistent with those used for the pure damage model, except the hardening H, which is taken equal to 0 (perfect plasticity).

E	ν	ε_0	ε_f	σ_0	H	c	m
30 000 MPa	0.2	$1.e-4$	$1.74e-4$	3 MPa	0 MPa	64 mm	1.5

Table 4.3: Parameters used with the isotropic damage-plastic model.

To assess the properties of the considered model, this study will first focus on

the response curves before moving on to the damage and cumulative plastic strain distributions. It will then deal with the damage and cumulative plastic strain profiles along horizontal and vertical lines above the notch tip.

First, one can see in Figure 4.14 that the macroscopic response curves associated with the three local element sizes are nearly identical until a point where the computation of two of them stop. The differences around this point and the fact that two curves end there suggest instability at this loading level, which is consistent with the fact that only the simulation conducted with the biggest element size ($l_s = 4$ mm) can go beyond it. This tends to indicate that, as for the pure damage models, the results obtained with this formulation are mesh-independent at least up to this point.

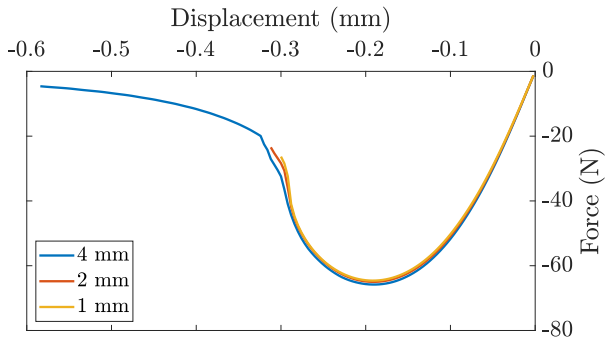

Figure 4.14: Force-displacement curves obtained for the three levels of mesh refinements.

The results mesh-independency can be confirmed by considering the damage distributions displayed in Figure 4.15 for a displacement level $U = 0.3$ mm, which do not appear to depend on the local element size. One can also note that the elements on the top of the beam (where the load is applied) start to damage, which could explain the instability observed on the macroscopic response curves. Besides, as for the pure damage model, one can note that the high levels of damage are concentrated at the centre of the localisation area, even after a vertical propagation, which confirms the shrinking of the localisation area.

This shrinking is even more evident when focusing on the distribution of the cumulative plastic strain displayed in Figure 4.16 since, as for the equivalent strain, its values tend to infinity while damage cannot exceed 1. One can also note that the distribution is nearly mesh-independent, the only variations being located at the notch tip where a strain concentration induces very high levels of plastic strain, especially for the most refined mesh.

To confirm these global observations, one now needs to focus on the damage and cumulative plastic strain profiles along vertical and horizontal lines. Starting with the damage profile along a horizontal line located above the notch tip, one can see in Figure 4.17a that, for a given loading, it does not depend on the element size. As

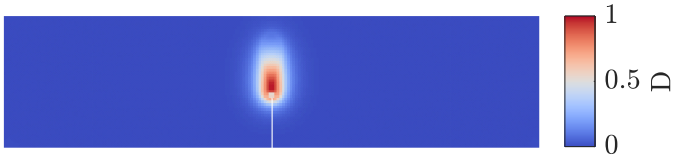

(a) Local size 4 mm.

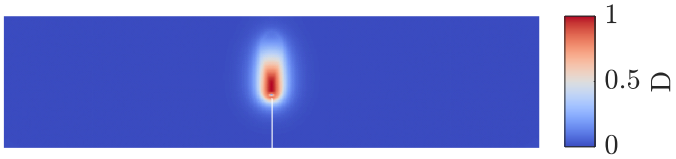

(b) Local size 2 mm.

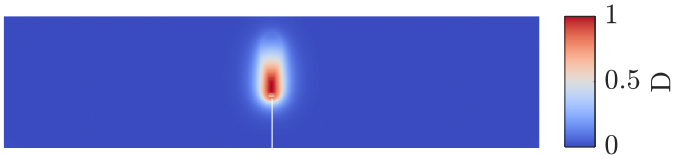

(c) Local size 1 mm.

Figure 4.15: Maps of damage obtained for the same applied displacement $U = 3$ mm.

(a) Local size 4 mm.

(b) Local size 2 mm.

(c) Local size 1 mm.

Figure 4.16: Maps of cumulative plastic strain obtained for the same applied displacement $U = 3$ mm.

it is, the only differences between the damage profiles come from the accuracy of the spatial discretisation, which is also true for their evolutions displayed in Figures 4.17b, 4.17c and 4.17d. In addition to being mesh-independent, the damage profiles also appear to have the expected damage-dependent width, which tends to zero when damage gets close to 1.

Similar observations can also be made on the cumulative plastic strain profiles displayed in Figure 4.18, whose width tends to zero for high levels of plasticity, i.e. damage. One can also note that, for a given loading, the profiles are nearly

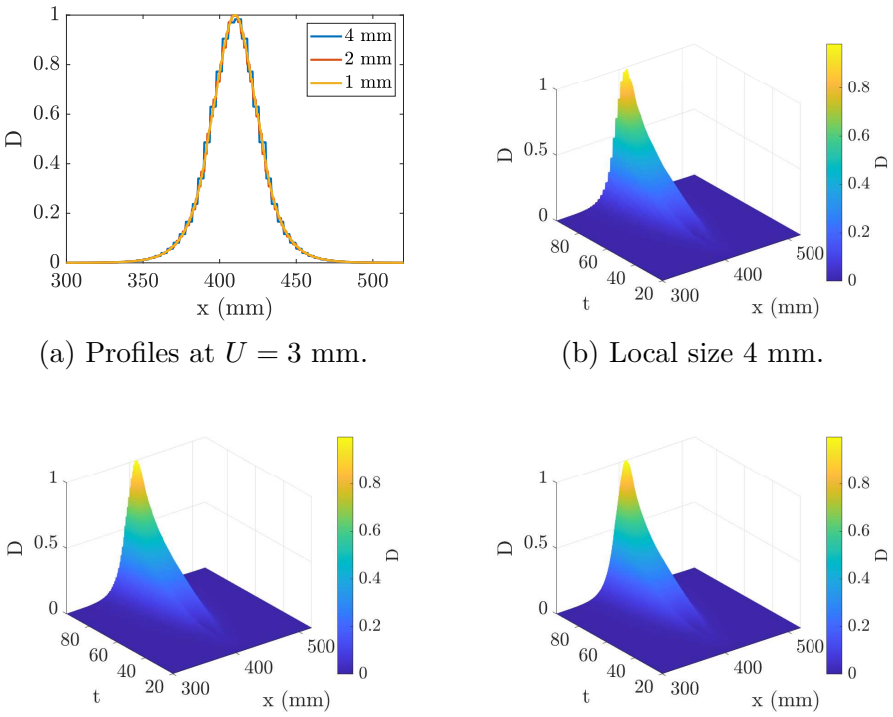

(a) Profiles at $U = 3$ mm.

(b) Local size 4 mm.

(c) Local size 2 mm.

(d) Local size 1 mm.

Figure 4.17: Influence of the local mesh size on the evolution of the damage profile, along a horizontal line for different loading times t.

identical, except for the maximum value located at the centre of the localisation area. It is worth noting that this discrepancy, enhanced by the shape of the damage evolution law, is most likely linked to a stress concentration after the notch tip and does not affect the global response.

After ensuring the localisation's mesh independency through the width of the damage profile, one should focus on the pseudo-crack propagation. To do so, one first looks at the damage and cumulative plastic strain profiles along a vertical line going from the notch tip to the loading point ($[IC]$).

Starting with the damage profile displayed in Figure 4.19a, one can note that damage propagation does not depend on the element size, aside from the accuracy of the discretisation.

Regarding the cumulative plastic strain whose profile is displayed in Figure 4.19b, one can note that the strain concentrations observed at the centre of the localisation area in Figure 4.18 are still present, though they seem to disappear away from the notch tip. A second peak can also be observed for the finest mesh in the area where damage is still nearly equal to 1.

In the end, one can conclude that the results obtained with this nonlocal eikonal-based formulation are mesh-independent and that the localisation area shrinks when damage increases, making a highly damaged zone equivalent to a crack. A strain concentration was also observed at the centre of the equivalent strain profile

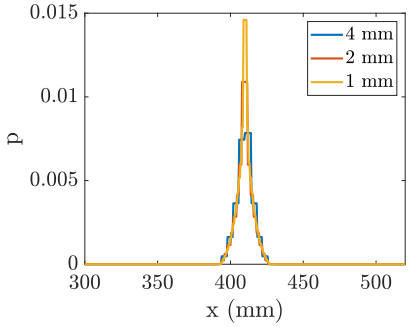

(a) Profiles at $U = 3$ mm.

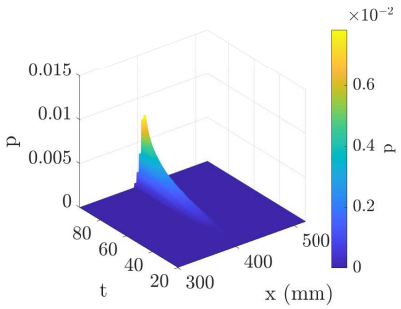

(b) Local size 4 mm.

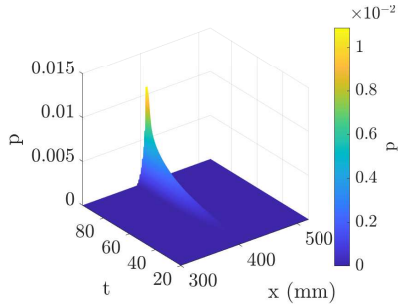

(c) Local size 2 mm.

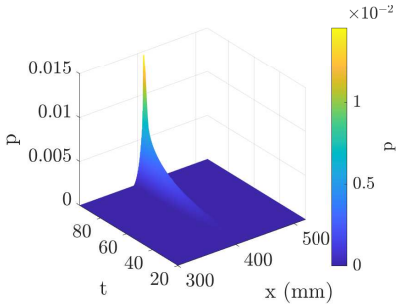

(d) Local size 1 mm.

Figure 4.18: Influence of the local mesh size on the evolution of the cumulative plastic strain profile, along a horizontal line for different loading times t.

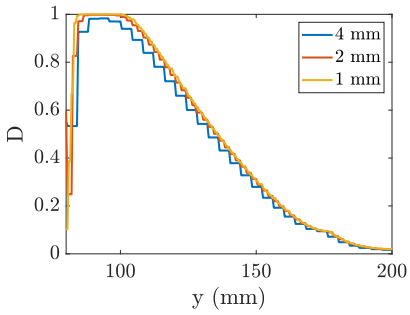

(a) Influence on D.

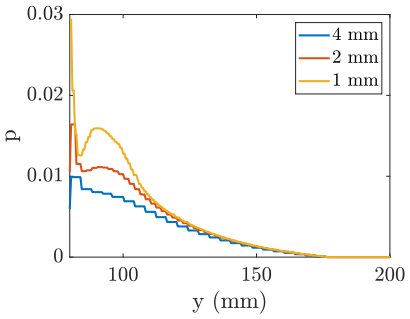

(b) Influence on p.

Figure 4.19: Influence of the local mesh size on the pseudo-crack propagation.

near the notch tip, but it does not seem to affect the global response.

It is worth noting that the occurrence of macroscopic instabilities prevented the complete study of crack propagation with the three levels of mesh refinement. This study should now be conducted with the largest element size, which helps to stabilise the model's response.

4.3.5 Handling material failure with the damage-plastic model

Now that the eikonal-based approach has been shown to produce mesh-independent results with a shrinking localization area, one needs to see whether it can make a highly damaged zone equivalent to a crack to model a crack propagation. This part will thus focus on the results obtained with the coarse mesh beyond the instability point where the two other responses stopped.

Starting with the damage distribution displayed in Figure 4.20a, one can see that the pseudo-crack (i.e. highly damaged zone) has propagated until it reached the loading point at the top of the beam. Moreover, as expected, the width of the damaged area did not expand after D reached 1, that the pseudo-crack is thus a two-element band. It is worth noting that the reason why damage does not localizes in a single element band is that the problem considered here is completely symmetric with a sharp initial notch whose tip is located between two elements. There is then no reason for localization to occur on one side of the notch instead of the other, which entails a two element wide final localization area.

Similar observations can also be made in Figure 4.20b, where the localization of plasticity in a two-element band is even more evident.

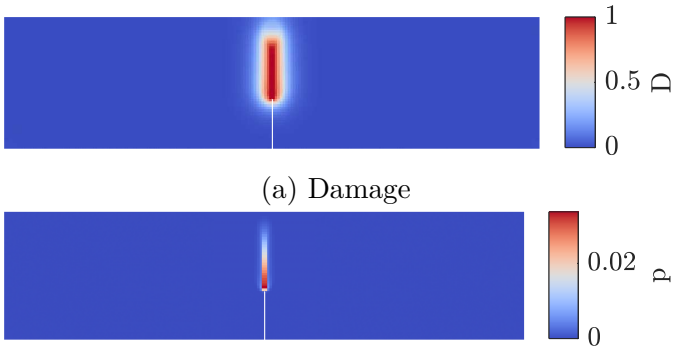

(a) Damage

(b) Cumulative plastic strain

Figure 4.20: Final maps of damage and cumulative plastic strain.

Focusing on the damage profile studied before, one can see in Figure 4.21a and 4.21b that it no longer evolves after D reaches one and the pseudo-crack tip moves beyond the considered point. Regarding the cumulative plastic strain profile displayed in Figure 4.21c and 4.21d, one can see that its width does not increase either while plasticity keeps increasing in the final localization area, which is consistent with a crack behaviour.

Moving on to the vertical profiles, taken along $[IC]$ and displayed in Figure 4.22, one can see that D is equal to 1 throughout most of the beam's height and that damage has reached the loading point at $y = 200$ mm. On the other hand, plasticity reaches its maximum value at the base of the pseudo-crack, i.e. the notch tip, and decreases toward its tip, which is consistent with a crack opening.

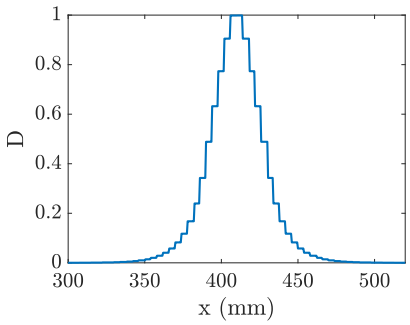

(a) Final damage profile.

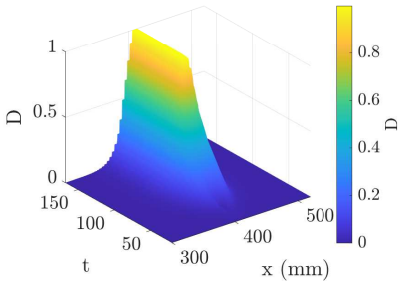

(b) Damage profile evolution.

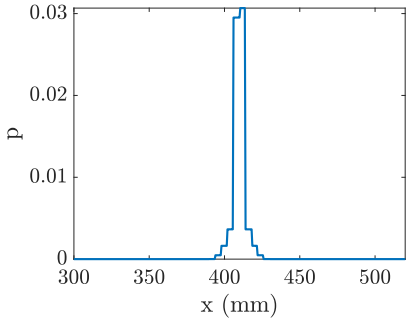

(c) Final plasticity profile.

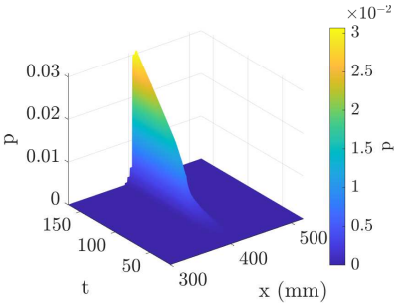

(d) Plasticity profile evolution.

Figure 4.21: Evolution of the damage and cumulative plastic strain profile, along a horizontal line for different loading times t.

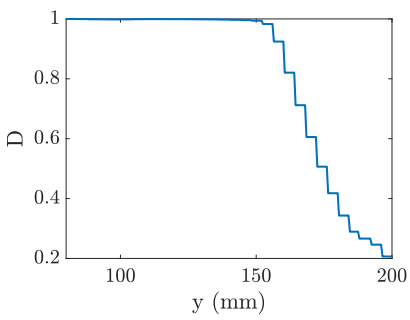

(a) D.

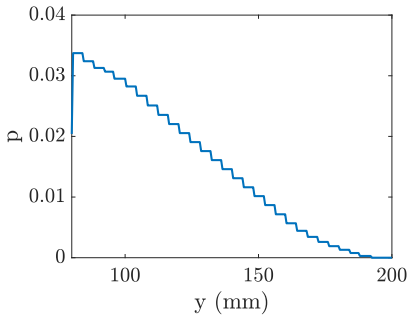

(b) p.

Figure 4.22: Final damage and cumulative plastic strain profile, along a vertical line..

In the end, one can conclude that the eikonal-based damage-plastic formulation does indeed make a crack equivalent to a highly damaged zone and can thus be used to model complete structural failure with crack propagation.

4.4 Conclusion of chapter 4

This chapter has introduced the weak forms associated with the nonlocal formulations obtained by coupling the damage and damage-plastic models studied in

Chapter 3 to both the classical and general gradients.

These formulations were then implemented in the object-oriented finite element solver OOFEM developed at the Czech Technical University's faculty of civil engineering, starting from the classical gradient-type damage and damage-plastic models already implemented. It is worth noting that the general procedure presented here could be followed to implement any material model in the finite element code. However, this should not be necessary for another gradient-type formulation since this implementation is rather versatile.

These implementations were finally used to study the properties of the eikonal-based approach associated with damage and damage plastic models to handle a three-point bending problem. Both formulations were shown to produce mesh-independent results, though the material behaviour associated with the pure damage model was very brittle, even for large localisation areas. It was also shown that, for both models, the localisation area would shrink to a single point when damage increases, making a highly damaged zone equivalent to a crack.

Due to the brittleness of the response associated with the pure damage model, it was not possible to study a pseudo-crack propagation across the beam. However, it was shown that the response's brittleness could be controlled by adjusting the width of the localisation area through the internal length parameter c.

In the end, it was shown that the damage-plastic formulation could be used to properly model material failure and pseudo-crack propagation by cutting all interactions across a highly damaged zone and thus preventing its extension.

Conclusion

The general framework commonly used to model material failure was first presented and used to introduce the two historical ways to handle it, namely the Linear Elastic Fracture Mechanics and the continuum damage mechanics. Focusing on the continuous approach, a local isotropic damage model with strain softening was introduced to model material failure with the associated progressive loss of stiffness. The flaws inherent to such a model were then pointed out to propose a definition of what will be called here a "good" damage model.

Following this, the classical ways to improve a local damage model, namely nonlocal damage, phase-field model and bounded rate damage, were presented, along with the associated drawbacks. A new eikonal-based nonlocal formulation, which should address these issues, was then presented along with the equivalent gradient-type formulation studied throughout this thesis.

The formulation obtained by coupling the local damage model to the gradient-type eikonal-based approach was introduced to determine whether it has the properties that can be expected from a good damage model. The formulations obtained by coupling it to Peerlings' approach and a Phase-Field-based one were also introduced to compare their properties to those of the eikonal-based formulation in a one-dimensional setting.

Since this numerical study was conducted with the Abaqus software, it was decided to implement the considered models in a non-intrusive fashion to take advantage of its nonlinear solver's efficiency. This implementation was handled through a thermo-mechanical analogy, taking advantage of the similarities between the heat equation and the nonlocal gradient-type ones.

It is worth noting that a dissipation-based strategy had to be introduced in order to compute the entire response curve when snap-back instabilities occurred. Though it required a monolithic resolution of the fully coupled nonlinear problem, this was permitted thanks to the embedded thermo-mechanical solver.

As expected, all formulations addressed the main issue inherent to local damage models, namely the spurious mesh dependency. However, the classical gradient-type formulation did not match the expected properties of a "good" damage model since it did not make a highly damaged zone equivalent to a crack. On the other hand, both the eikonal-based and phase-field based formulations were shown to match all the expected properties, including cutting all interactions across a highly damaged zone to reproduce a crack behaviour.

It thus appeared that both formulations could be used to bridge the gap between continuum damage and fracture mechanics. However, in addition to the lack

of permanent strain, the associated response curves were too brittle to reproduce the behaviour of a material such as concrete.

A damage-plastic model was then introduced to address the brittleness associated with the pure damage model and introduce the permanent strain required to accurately model geomaterials such as concrete. The material behaviours associated with both damage models were then compared on a single material point, demonstrating that the introduction of plasticity does not influence the global response though it does affect damage evolution.

The formulations obtained by coupling both damage models to Peerlings' and the eikonal-based approaches were introduced and used in a one-dimensional case to study the initial localisation associated with their first bifurcation. Their regularisation properties were hence confirmed, along with the dependence of the localisation area's size on both the internal length and the damage evolution law.

Taking those results into account, a theoretical study was conducted to see how plasticity would affect the brittleness of the responses obtained with both the classical and eikonal-based gradient-type formulations. It was thus possible to see that, while introducing plasticity does not influence the brittleness of the response obtained with a fixed localisation area, it does increase the ductility of the behaviour associated with a shrinking one.

Following this preliminary study, one had to see whether it could be generalised to more complex settings, which required additional numerical simulations. Due to the integrated features dedicated to gradient-type models, it was decided to work with the finite element code OOFEM developed at the Czech Technical University, where the author spent six months during the PhD under the supervision of professor Milan JIRÁSEK. The weak forms associated with the formulations obtained by coupling the damage and damage-plastic models to a general gradient-type approach were thus introduced and used for the numerical implementations.

Since the classical gradient-type formulations were already implemented in OOFEM, and thanks to its object-oriented design, implementing the general ones only required modifications of the existing material class. It is worth noting that the implementation of the general gradient is quite versatile since it can stand for any formulation with either a fixed or an evolving internal length, including the phase-field based and eikonal-based ones.

The properties of the damage and damage-plastic formulations were then studied in a three-point bending setting and were shown to produce mesh-independent results. Moreover, both models were shown to make a highly damaged zone equivalent to a crack, the localisation area shrinking to a single point when damage increases. However, the behaviour associated with the pure damage model was very brittle, even for large localisation areas, and the occurrence of snap-back instabilities prevented the study of the highly damaged zone's propagation. Though the brittleness of the response was shown to be adjustable through the internal length parameter c, one would need a more advanced driving strategy to study the properties of the pure damage formulation. Following what was done in Abaqus

with the dissipation-based driving strategy, one could consider using arc-length driving, imposing either a global dissipation or the notch opening.

It was finally shown that the eikonal-based gradient-type damage-plastic formulation could handle structural failure, though taking into account crack orientation would require the introduction of anisotropic damage. Some preliminary work has been conducted on this subject and can be used as a basis for further study with a unified anisotropic damage model.

Appendix A

Space curved by damage: arguments based on the WKB approximation

Contents

This appendix gives details regarding the study of damage's influence on wave propagation. To do so, working under the WKB approximation, a wave propagation study will first be conducted in the general case of a linear material, before moving to the particular case of an isotropic undamaged material. These results will then be compared to those obtained with isotropic damage to assess its influence.

A.1 Wave propagation in a linear material

One should first note that he considered material does not have to be homogeneous, thus all material parameters depend on the point $\boldsymbol{x}$ at which they are considered. The wave celerity $c_0(\boldsymbol{x})$ can then be defined at a given point $\boldsymbol{x}$ as

$$c_0(\boldsymbol{x}) = \frac{\omega}{k_0(\boldsymbol{x})} \tag{A.1}$$

where ω is the wave pulsation and $k_0(\boldsymbol{x}) = \|\boldsymbol{k}_0(\boldsymbol{x}\|$ the norm of its wave vector.

For convenience $k_0(\boldsymbol{x})$ and $c_0(\boldsymbol{x})$ will be noted k_0 and c_0 in the following developments, though they still implicitly depend on the point $\boldsymbol{x}$.

The displacement field induced by the wave propagation is here postulated as

$$\boldsymbol{u}(\boldsymbol{x}, t) = \boldsymbol{u}_0(\boldsymbol{x}) \ \exp\left[i\left(k_0 S(\boldsymbol{x}) - \omega t\right)\right] \tag{A.2}$$

where $\boldsymbol{x}$ denotes the spatial coordinate, t the time coordinate, $\boldsymbol{u}_0(\boldsymbol{x})$ the position-dependent wave amplitude, and $S(\boldsymbol{x})$ the so-called eikonal function that can be interpreted as a level set function.

Assuming that the virtual displacement field $\boldsymbol{u}^*$ has the same form as $\boldsymbol{u}$, and that only the slow variation term is modified, it can be defined as

$$\boldsymbol{u}^*(\boldsymbol{x}, t) = \boldsymbol{u}_0^*(\boldsymbol{x}) \ \exp\left[i\left(k_0 S(\boldsymbol{x}) - \omega t\right)\right] \tag{A.3}$$

From now on, the following variables $\boldsymbol{u}(\boldsymbol{x}, t)$, $\boldsymbol{u}^*(\boldsymbol{x}, t)$, $\boldsymbol{u}_0(\boldsymbol{x})$, $\boldsymbol{u}_0^*(\boldsymbol{x})$ and $S(\boldsymbol{x})$ will be respectively noted $\boldsymbol{u}$, $\boldsymbol{u}^*$, $\boldsymbol{u}_0$, $\boldsymbol{u}_0^*$ and S in order to use lighter notations.

The stiffness matrix $\mathbb{C}(\boldsymbol{x})$ and the density $\rho(\boldsymbol{x})$ at point $\boldsymbol{x}$, will also be noted $\mathbb{C}$ and ρ. The principle of virtual power then writes

$$\int_\Omega \rho \ \boldsymbol{u}^* \cdot \ddot{\boldsymbol{u}} \ \mathrm{d}V = \int_\Omega \nabla \boldsymbol{u} : \mathbb{C} : \nabla \boldsymbol{u}^* \ \mathrm{d}V \ , \quad \forall \boldsymbol{u}^* \tag{A.4}$$

It is important to keep in mind that,though the space variable $\boldsymbol{x}$ does not explicitly appear in the equations, every variable and parameter is space-dependent.

The strain energy density can be rewritten as

$$\begin{aligned}
&\nabla \boldsymbol{u} : \mathbb{C} : \nabla \boldsymbol{u}^* \\
=&\nabla \left(\boldsymbol{u}_0 \; e^{i(k_0 S - \omega t)} \right) \mathbb{C} : \nabla \left(\boldsymbol{u}_0^* \; e^{i(k_0 S - \omega t)} \right) \\
=&\left(\nabla \boldsymbol{u}_0 + i k_0 \; \boldsymbol{u}_0 \otimes \nabla S \right) e^{i(k_0 S - \omega t)} : \mathbb{C} : \left(\nabla \boldsymbol{u}_0^* + i k_0 \; \boldsymbol{u}_0^* \otimes \nabla S \right) e^{i(k_0 S - \omega t)}
\end{aligned}$$

giving

$$\begin{aligned}
&\nabla \boldsymbol{u} : \mathbb{C} : \nabla \boldsymbol{u}^* \\
&\qquad = \left(\nabla \boldsymbol{u}_0 + i k_0 \; \boldsymbol{u}_0 \otimes \nabla S \right) : \mathbb{C} : \left(\nabla \boldsymbol{u}_0^* + i k_0 \; \boldsymbol{u}_0^* \otimes \nabla S \right) e^{2i(k_0 S - \omega t)}
\end{aligned} \tag{A.5}$$

while the inertial term writes

$$\begin{aligned}
&\rho \; \boldsymbol{u}^* \cdot \ddot{\boldsymbol{u}} \\
=&\rho \; \left(\boldsymbol{u}_0^* \; e^{i(k_0 S - \omega t)} \right) \cdot \frac{\partial^2}{\partial t^2} \left(\boldsymbol{u}_0 \; e^{i(k_0 S - \omega t)} \right) \\
=&\rho \; \left(\boldsymbol{u}_0^* \; e^{i(k_0 S - \omega t)} \right) \cdot \left((-\omega^2) \; \boldsymbol{u}_0 \; e^{i(k_0 S - \omega t)} \right)
\end{aligned}$$

giving

$$\rho \; \boldsymbol{u}^* \cdot \boldsymbol{u} = -\rho \omega^2 \; \boldsymbol{u}_0 \cdot \boldsymbol{u}_0^* \; e^{2i(k_0 S - \omega t)} \tag{A.6}$$

The principle of virtual power (A.4) then becomes

$$\begin{aligned}
&\int_\Omega \left(\nabla \boldsymbol{u}_0 + i k_0 \; \boldsymbol{u}_0 \otimes \nabla S \right) : \mathbb{C} : \left(\nabla \boldsymbol{u}_0^* + i k_0 \; \boldsymbol{u}_0^* \otimes \nabla S \right) e^{2i(k_0 S - \omega t)} \; \mathrm{d}V \\
&\qquad\qquad = - \int_\Omega \rho \omega^2 \; \boldsymbol{u}_0 \cdot \boldsymbol{u}_0^* \; e^{2i(k_0 S - \omega t)} \; \mathrm{d}V \; , \quad \forall \boldsymbol{u}^* \\
\Leftrightarrow &\int_\Omega \left(\nabla \boldsymbol{u}_0 + i k_0 \; \boldsymbol{u}_0 \otimes \nabla S \right) : \mathbb{C} : \left(\nabla \boldsymbol{u}_0^* + i k_0 \; \boldsymbol{u}_0^* \otimes \nabla S \right) \; \mathrm{d}V = - \int_\Omega \rho \omega^2 \; \boldsymbol{u}_0 \cdot \boldsymbol{u}_0^* \; \mathrm{d}V \; , \quad \forall \boldsymbol{u}^*
\end{aligned}$$

giving in the general case

$$\left(c_0 \; \nabla \boldsymbol{u}_0 + i \omega \; \boldsymbol{u}_0 \otimes \nabla S \right) : \mathbb{C} : \left(c_0 \; \nabla \boldsymbol{u}_0^* + i \omega \; \boldsymbol{u}_0^* \otimes \nabla S \right) = -\rho {c_0}^2 \omega^2 \; \boldsymbol{u}_0 \cdot \boldsymbol{u}_0^* \tag{A.7}$$

At high frequencies, i.e. keeping only the terms proportional to ω^2, one gets

$$\left(\boldsymbol{u}_0 \otimes \nabla S \right) : \mathbb{C} : \left(\boldsymbol{u}_0^* \otimes \nabla S \right) = \rho {c_0}^2 \; \boldsymbol{u}_0 \cdot \boldsymbol{u}_0^* \tag{A.8}$$

and, using Einstein's notation

$$u_{0i} \; \nabla S_j \; \tilde{C}_{ijkl} \; \nabla S_k \; u_{0l}^* = \rho {c_0}^2 \; \delta_{il} \; u_{0i} \; u_{0l}^*$$

In the end, one gets

$$u_{0i} \left(\nabla S_j \; \tilde{C}_{ijkl} \; \nabla S_k \; - \; \rho {c_0}^2 \; \delta_{il} \right) u_{0l}^* = 0 \tag{A.9}$$

which implies that a non trivial solution exists if and only if one has

$$\det \left[\nabla S_j \; \tilde{C}_{ijkl} \; \nabla S_k \; - \; \rho {c_0}^2 \; \delta_{il} \right] = 0 \tag{A.10}$$

Since the aim of this part is to see the influence of damage on wave propagation, one needs to find out how it affects the gradient ∇S of the eikonal function. To do so, one would need more hypothesis on the material properties in order to determine the expression of the stiffness matrix $\mathbb{C}$ both with and without damage.

A.2 Wave propagation in a linear undamaged isotropic material

Under the hypothesis of an undamaged isotropic material, the stiffness matrix $\mathbb{C}$ can be defined using Lame coefficient λ and μ as:

$$\mathbb{C} = \lambda \mathbf{1} \otimes \mathbf{1} + 2\mu \mathbf{1} \underline{\otimes} \mathbf{1} \tag{A.11}$$

which, in index notation writes:

$$C_{ijkl} = \lambda\ \delta_{ij}\delta_{kl} + \mu\left(\delta_{ik}\delta_{jl} + \delta_{il}\delta_{jk}\right) \tag{A.12}$$

It is worth noting that, since our material is not homogeneous, the parameters λ et μ depend on the space coordinate $\boldsymbol{x}$, and thus so does the stiffness matrix $\mathbb{C}$.

In this case, starting from the existence condition (A.10) and replacing $\mathbb{C}$ by its expression, one gets

$$\begin{aligned}
&\det\left[\nabla S_j\ \left(\lambda\ \delta_{ij}\delta_{kl} + \mu\left(\delta_{ik}\delta_{jl} + \delta_{ik}\delta_{jl}\right)\right)\ \nabla S_k\ -\ \rho {c_0}^2\ \delta_{il}\right] = 0 \\
\Leftrightarrow &\det\left[\lambda \nabla S_i \nabla S_l\ + \mu \nabla S_l \nabla S_i\ + \mu \nabla S_k \nabla S_k\ \delta_{il}\ -\ \rho {c_0}^2\ \delta_{il}\right] = 0 \\
\Leftrightarrow &\det\left[\left(\lambda + \mu\right)\left(\nabla S_i \nabla S_l\right)\ -\ \left(\rho {c_0}^2 - \mu \|\nabla S\|^2\right)\delta_{il}\right] = 0 \\
\Leftrightarrow &\det\left[\left(\lambda + \mu\right)\left(\nabla S \otimes \nabla S\right)\ -\ \left(\rho {c_0}^2 - \mu \|\nabla S\|^2\right)\mathbb{I}\right] = 0
\end{aligned}$$

Since $\nabla S \otimes \nabla S$ is generated with one single base vector, it has 0 and $\|\nabla S\|^2$ eigenvalues, the first being a double one. Therefore, the previous condition is satisfied if either (A.13) or (A.14) is satisfied.

$$\left(\lambda + \mu\right)\|\nabla S\|^2\ -\ \left(\rho {c_0}^2 - \mu \|\nabla S\|^2\right) = 0 \tag{A.13}$$

$$\rho {c_0}^2 - \mu \|\nabla S\|^2 = 0 \tag{A.14}$$

The first condition (A.13), which corresponds to a pressure wave ($\nabla \times \boldsymbol{u}$), can be rewritten as

$$(\lambda + 2\mu)\|\nabla S\|^2 = \rho {c_0}^2 \tag{A.15}$$

giving

$$\|\nabla S\| = c_0 \sqrt{\frac{\rho}{\lambda + 2\mu}} \tag{A.16}$$

The second condition (A.13), which corresponds to a shear wave ($\nabla \cdot \boldsymbol{u}$), can be rewritten as

$$\mu \|\nabla S\|^2 = \rho {c_0}^2 \tag{A.17}$$

giving

$$\|\nabla S\| = c_0 \sqrt{\frac{\rho}{\mu}} \tag{A.18}$$

Considering that the wave speed in the undamaged medium can be defined as $c_0 = \sqrt{(\lambda + 2\mu)/\rho}$ for a pressure wave, and $c_0 = \sqrt{\mu/\rho}$ for a shear wave, both conditions can be unified through the following eikonal equation

$$\|\nabla S(\boldsymbol{x})\| = 1 \tag{A.19}$$

It is worth noting that this is consistent with the absence of damage, and that, though S and ∇S may still depend on $\boldsymbol{x}$, this remains true $\forall \boldsymbol{x}$.

A similar study will now be conducted with a damaged material in order to see how (A.19) will be affected by the presence of damage.

A.3 Wave propagation in a linear isotropic material with isotropic damage

Keeping the previous isotropic material model, this part will take into account the presence of isotropic damage, modeled here as a scalar field $D(\boldsymbol{x})$ (noted D) varying from 0 to 1. To do so, one has to work with the effective stiffness matrix $\mathbb{C}$ which can be defined as

$$\tilde{\mathbb{C}} = \tilde{\lambda}\, \mathbf{1} \otimes \mathbf{1} + 2\tilde{\mu}\, \mathbf{1} \underline{\otimes} \mathbf{1} \tag{A.20}$$

$$C_{ijkl} = \tilde{\lambda}\, \delta_{ij}\delta_{kl} + \mu\, (\delta_{ik}\delta_{jl} + \delta_{il}\delta_{jk}) \tag{A.21}$$

where $\tilde{\lambda}$ and $\tilde{\mu}$ are the effective Lame coefficients defined as

$$\tilde{\lambda} = \lambda\, (1 - D), \quad \tilde{\mu} = \mu\, (1 - D) \tag{A.22}$$

which might depend on $\boldsymbol{x}$, since D, λ and μ do.

In this case, following the same steps as for the undamaged material, the existence condition (A.10) writes

$$\det \left[\nabla S_j\, \tilde{C}_{ijkl}\, \nabla S_k - \rho {c_0}^2\, \delta_{il}\right] = 0 \tag{A.23}$$

$$\Leftrightarrow \det \left[\left(\tilde{\lambda} + \tilde{\mu}\right) (\nabla S \otimes \nabla S) - \left(\rho {c_0}^2 - \tilde{\mu}\|\nabla S\|^2\right) \mathbb{I}\right] = 0 \tag{A.24}$$

which gives the following conditions associated to the 2 eigenvalues of $\nabla S \otimes \nabla S$:

$$\left(\tilde{\lambda} + \tilde{\mu}\right) \|\nabla S\|^2 - \left(\rho {c_0}^2 - \tilde{\mu}\|\nabla S\|^2\right) = 0 \tag{A.25}$$

$$\rho {c_0}^2 - \tilde{\mu}\|\nabla S\|^2 = 0 \tag{A.26}$$

Keeping the previous definition of the associated wave speeds, and proceeding as for the undamaged material, the conditions (A.25) and (A.26), corresponding respectively to a pressure and a shear wave, can be unified through as

$$\|\nabla S\| = \frac{1}{\sqrt{1-D}} \tag{A.27}$$

One can note that this eikonal equation differs from the one associated to the undamaged material (A.19), which is recovered in the particular case $D = 0$.

Based on this, one can conclude that the distance seen by a wave propagating in a damaged material, characterized by S, is scaled by a factor $1/\sqrt{1-D}$. As a consequence, propagating across a distance $\mathrm{d}l$ in a damaged medium is equivalent to propagating across $\mathrm{d}\tilde{l} = \mathrm{d}l/\sqrt{1-D}$ in an undamaged one.

This scaling of the effective distances, equivalent to the increase of optical distance when light moves through different media, can be seen as a space curvature induced by damage. The effective distance between two points can then be seen as the shortest path between them in a spaced curve by a damage-dependent metric.

It is worth noting that, in this framework, the space curvature would have the same properties as damage: it would depend on $\boldsymbol{x}$ while remaining isotropic.

Appendix B

Conditions for the occurrence of snap-back instabilities

Contents

Let us try to determine the condition for the occurrence of snap-back instabilities when submitting a bar to tensile loading. To do so, one could consider the case of a homogeneous bar of length L and section S, made of a material whose behaviour corresponds to the local damage model described in Part 1.3.1 and writes

$$\sigma = E\,\varepsilon \tag{B.1}$$

$$\kappa(t) = \max_{\tau \leq t} \langle \varepsilon(\tau) \rangle \tag{B.2}$$

$$D = \begin{cases} 0 & \text{if } \kappa < \varepsilon_0 \\ 1 - \dfrac{\varepsilon_0}{\kappa} \exp\left(-\dfrac{\kappa - \varepsilon_0}{\varepsilon_f - \varepsilon_0} \right) & \text{if } \kappa \geq \varepsilon_0 \end{cases} \tag{B.3}$$

During the first, elastic, part of the tensile loading, one can consider imposing a homogeneous strain with a linear evolution with respect to time

$$\varepsilon(t) = \xi_0\, t, \quad \forall t \in \left[0.; \frac{\varepsilon_0}{\xi_0} \right] \tag{B.4}$$

where ξ_0 is a given loading parameter, giving the homogeneous stress

$$\sigma(t) = E\,\varepsilon = E\,\xi_0\, t, \quad \forall t \in \left[0.; \frac{\varepsilon_0}{\xi_0} \right] \tag{B.5}$$

During all this phase, the force and displacement and the end of the bar thus write

$$\begin{cases} F(t) = S\,\sigma(t) = E\,S\,\xi_0\, t \\ U(t) = L\,\varepsilon(t) = L\,\xi_0\, t \end{cases}, \quad \forall t \in \left[0.; \frac{\varepsilon_0}{\xi_0} \right] \tag{B.6}$$

giving the time derivatives

$$\begin{cases} \dfrac{\partial U}{\partial t} = L\,\xi_0 \geq 0. \\ \dfrac{\partial F}{\partial t} = E\,S\,\xi_0 \geq 0. \end{cases} \tag{B.7}$$

which, along with the constant ratio $F/U = ES/L$, is consistent with a linear elastic loading.

When t reaches ε_0/ξ_0, the strain will equal the damage threshold ε_0 everywhere in the bar, and the force at the end of the bar will be at its pic value $\sigma_0 = ES\varepsilon_0$. Any increase in the loading will then bring damage and strain localization in a zone whose length is not fixed by the model.

Considering that, from this point, damage localizes in the part of the bar of length l located at the middle of the bar, one would thus have

$$\begin{cases} \dot{\varepsilon} \geq 0., & \forall x \in \left[\dfrac{L-l}{2}; \dfrac{L+l}{2} \right] \\ \dot{\varepsilon} \leq 0., & \forall x \in \left[0.; \dfrac{L-l}{2} \right] \cup \left[\dfrac{L+l}{2}; L \right] \end{cases}, \quad \forall t > \frac{\varepsilon_0}{\xi_0} \tag{B.8}$$

From this point, a strain-based loading can still be used, giving in the localization area

$$\begin{aligned}
\varepsilon(t) &= \xi_0\ t && \text{(B.9)}\\
\kappa(t) &= \max_{\tau\leq t}\langle\varepsilon(\tau)\rangle = \xi_0\ t \geq \varepsilon_0 && \text{(B.10)}\\
D(t) &= g(\kappa) = 1 - \frac{\varepsilon_0}{\xi_0\ t}\exp\left(-\frac{\xi_0\ t - \varepsilon_0}{\varepsilon_f - \varepsilon_0}\right) && \text{(B.11)}\\
\sigma(t) &= (1-D)E\varepsilon = E\varepsilon_0\exp\left(\frac{\varepsilon_0 - \xi_0\ t}{\varepsilon_f - \varepsilon_0}\right) && \text{(B.12)}
\end{aligned}$$

and thus, in the rest of the bar which remains elastic

$$\begin{aligned}
\sigma(t) &= E\varepsilon_0\exp\left(\frac{\varepsilon_0 - \xi_0\ t}{\varepsilon_f - \varepsilon_0}\right) && \text{(B.13)}\\
\varepsilon(t) &= \frac{\sigma}{E} = \varepsilon_0\exp\left(\frac{\varepsilon_0 - \xi_0\ t}{\varepsilon_f - \varepsilon_0}\right) < \varepsilon_0 && \text{(B.14)}\\
\kappa(t) &= \max_{\tau\leq t}\langle\varepsilon(\tau)\rangle = \varepsilon_0 && \text{(B.15)}\\
D(t) &= 0. && \text{(B.16)}
\end{aligned}$$

The force and displacement at the end of the bar will then be given by

$$\begin{cases} U(t) = \displaystyle\int_0^L \varepsilon(x,t)\mathrm{d}x = l\ \xi_0\ t + (L-l)\ \varepsilon_0\exp\left(\frac{\varepsilon_0 - \xi_0\ t}{\varepsilon_f - \varepsilon_0}\right) \\ F(t) = S\ \sigma(t) = E\ S\ \varepsilon_0\exp\left(\frac{\varepsilon_0 - \xi_0\ t}{\varepsilon_f - \varepsilon_0}\right) \end{cases}, \quad \forall t \geq \frac{\varepsilon_0}{\xi_0} \quad \text{(B.17)}$$

giving the time derivatives

$$\begin{cases} \dfrac{\partial F}{\partial t} = -\dfrac{\xi_0\ E\ S\ \varepsilon_0}{\varepsilon_f - \varepsilon_0}\exp\left(\dfrac{\varepsilon_0 - \xi_0\ t}{\varepsilon_f - \varepsilon_0}\right) \leq 0. \\ \dfrac{\partial U}{\partial t} = \xi_0\ l - \dfrac{\xi_0\ (L-l)\ \varepsilon_0}{\varepsilon_f - \varepsilon_0}\exp\left(\dfrac{\varepsilon_0 - \xi_0\ t}{\varepsilon_f - \varepsilon_0}\right) \end{cases}, \quad \forall t \geq \frac{\varepsilon_0}{\xi_0} \quad \text{(B.18)}$$

One can note that, while the time derivative of the force is always negative, which is consistent with strain softening, the sign of the displacement's time derivative depends on both time and material parameters.

The stable case of a response curve without snap-back corresponds to a positive time derivative of displacement, while the occurrence of a snap-back can be characterized by the existence of a solution $t \geq \varepsilon_0/\xi_0$ to the equation

$$\frac{\partial U(t)}{\partial t} < 0. \quad \text{(B.19)}$$

which is equivalent to

$$\xi_0\ l - \frac{\xi_0\ (L-l)\ \varepsilon_0}{\varepsilon_f - \varepsilon_0}\exp\left(\frac{\varepsilon_0 - \xi_0\ t}{\varepsilon_f - \varepsilon_0}\right) < 0. \quad \text{(B.20)}$$

$$\Leftrightarrow \quad \frac{l\,(\varepsilon_f - \varepsilon_0)}{(L-l)\;\varepsilon_0} < \exp\left(\frac{\varepsilon_0 - \xi_0\;t}{\varepsilon_f - \varepsilon_0}\right) \tag{B.21}$$

$$\Leftrightarrow \quad \ln\left(\frac{l\,(\varepsilon_f - \varepsilon_0)}{\varepsilon_0(L-l)}\right) < \frac{\varepsilon_0 - \xi_0\;t}{\varepsilon_f - \varepsilon_0} \tag{B.22}$$

$$\Leftrightarrow \quad t < \frac{\varepsilon_0}{\xi_0}\left[1. - \frac{\varepsilon_f - \varepsilon_0}{\varepsilon_0}\ln\left(\frac{l\,(\varepsilon_f - \varepsilon_0)}{\varepsilon_0(L-l)}\right)\right] \tag{B.23}$$

For this equation to have a solution $t \geq \varepsilon_0/\xi_0$, one needs to have

$$-\frac{\varepsilon_f - \varepsilon_0}{\varepsilon_0}\ln\left(\frac{l\,(\varepsilon_f - \varepsilon_0)}{\varepsilon_0(L-l)}\right) > 0. \tag{B.24}$$

$$\Leftrightarrow \quad \ln\left(\frac{l\,(\varepsilon_f - \varepsilon_0)}{\varepsilon_0(L-l)}\right) < 0. \tag{B.25}$$

$$\Leftrightarrow \quad \frac{l\,(\varepsilon_f - \varepsilon_0)}{\varepsilon_0(L-l)} < 1. \tag{B.26}$$

One can thus conclude that snap-back instabilities will occur if

$$\frac{l}{L} < \frac{\varepsilon_0}{\varepsilon_f} \tag{B.27}$$

and that they are a structure effect linked to both the damage rate and the relative importance of the localization area.

Appendix C

Discretization and linearization of the variational formulations associated to eikonal-based gradient-type damage and damage-plastic models.

Contents

C.1 Variational formulations associated to the considered nonlocal damage models

In order to implement a given formulation in a finite element code such as OOFEM, one first needs to derive the weak form associated to it. This part will thus present the variational formulations associated to the nonlocal isotropic damage and damage-plastic models presented in Part 3.1, using the general gradient-type formulation (1.29).

While the weak form associated to gradient-type formulations with both fixed [Peerlings et al., 1996, Peerlings et al., 1998] and evolving [Geers et al., 1998, Saroukhani et al., 2013] internal lengths are rather classical, the innovative aspect of this part comes from the use of a function $a \neq 1$.

C.1.1 Pure isotropic damage model

Starting with the pure isotropic damage model, one will first determine the classical weak forms associated to the equilibrium, before moving on to the general gradient-type formulation.

Equilibrium

As pointed out Chapter 1, the equilibrium writes, in the absence of body forces,

$$\nabla \cdot \boldsymbol{\sigma} = \mathbf{0} \tag{C.1}$$

which can be expected to be associated to the classical boundary condition

$$\boldsymbol{\sigma} \cdot \mathbf{n} = \boldsymbol{T} \ , \quad \text{in } \partial\Omega \tag{C.2}$$

where $\boldsymbol{T}$ is the external forces' vector, and $\boldsymbol{\sigma}$ is defined using (4.1) as $\boldsymbol{\sigma} = \tilde{\mathbb{C}} : \boldsymbol{\varepsilon}$.

Considering a virtual displacement field $\boldsymbol{u}^*$, one gets

$$\int_\Omega \left(\nabla \cdot \left(\tilde{\mathbb{C}} : \boldsymbol{\varepsilon} \right) \right) \cdot \boldsymbol{u}^* \ \mathrm{d}V = 0 \ , \quad \forall \ \boldsymbol{u}^* \tag{C.3}$$

which, after an integration by parts gives

$$\int_{\partial\Omega} \boldsymbol{u}^* \cdot \left(\tilde{\mathbb{C}} : \boldsymbol{\varepsilon} \right) \cdot \mathbf{n} \ \mathrm{d}S - \int_\Omega \left(\nabla \cdot \boldsymbol{u}^* \right) : \tilde{\mathbb{C}} : \boldsymbol{\varepsilon} \ \mathrm{d}V = \mathbf{0} \ , \quad \forall \ \boldsymbol{u}^* \tag{C.4}$$

In the end, using both the stress-strain law and boundary condition, this can be written as a classical weak form

$$a_e(\boldsymbol{u}, \boldsymbol{u}^*) = l_e(\boldsymbol{u}^*) \ , \quad \forall \ \boldsymbol{u}^* \tag{C.5}$$

where a_e is a bi-linear and symmetric form defined as

$$a_e : (\boldsymbol{u}, \boldsymbol{u}^*) \mapsto \int_\Omega \nabla \cdot \boldsymbol{u}^* : \tilde{\mathbb{C}} : \nabla \cdot \boldsymbol{u} \ \mathrm{d}V \tag{C.6}$$

and l_e a linear form defined as

$$l_e : \boldsymbol{u}^* \mapsto \int_{\partial\Omega} \boldsymbol{u}^* \cdot \boldsymbol{T} \ \mathrm{d}S \tag{C.7}$$

General gradient-type formulation

Then, one needs to obtain the weak form associated to the general gradient-type formulation (4.5) which writes here

$$\bar{\varepsilon} - a\ \nabla \cdot (b\ \nabla\ \bar{\varepsilon}) = \hat{\varepsilon} \tag{C.8}$$

where a and b are given non-negative functions, function $\hat{\varepsilon}$ is here considered as given, and function $\bar{\varepsilon}$ is the primary unknown. In this case, for lack of a better option, it can be expected that (C.8) is combined with the homogeneous Neumann boundary condition:

$$(\nabla\ \bar{\varepsilon}) \cdot \mathbf{n} = 0\ , \quad \text{in } \partial\Omega \tag{C.9}$$

Starting from (C.8), and considering a virtual nonlocal strain field $\bar{\varepsilon}^*$, one gets:

$$\int_\Omega \bar{\varepsilon}\ \bar{\varepsilon}^*\ \mathrm{d}V - \int_\Omega a\ \nabla \cdot (b\ \ (\nabla\ \bar{\varepsilon}))\ \ \bar{\varepsilon}^*\ \mathrm{d}V = \int_\Omega \hat{\varepsilon}\ \bar{\varepsilon}^*\ \mathrm{d}V\ , \quad \forall\ \bar{\varepsilon}^* \tag{C.10}$$

which, after an integration by parts, gives

$$\begin{aligned} &\int_\Omega \bar{\varepsilon}\ \bar{\varepsilon}^*\ \mathrm{d}V - \int_{\partial\Omega} a\ b\ \bar{\varepsilon}^*\ \ (\nabla\ \bar{\varepsilon}) \cdot \mathbf{n}\ \mathrm{d}S \\ &\quad + \int_\Omega (\nabla\ (a\ \bar{\varepsilon}^*)) \cdot (b\ \ (\nabla\ \bar{\varepsilon}))\ \ \mathrm{d}V = \int_\Omega \hat{\varepsilon}\ \bar{\varepsilon}^*\ \mathrm{d}V\ , \quad \forall\ \bar{\varepsilon}^* \end{aligned} \tag{C.11}$$

Using the boundary condition (C.9), this can be written as

$$\int_\Omega (\bar{\varepsilon}\ \bar{\varepsilon}^* + b\ \bar{\varepsilon}^*\ \ (\nabla\ a) \cdot (\nabla\ \bar{\varepsilon}) + a\ b\ \ (\nabla\ \bar{\varepsilon}) \cdot (\nabla\ \bar{\varepsilon}^*))\, \mathrm{d}V = \int_\Omega \hat{\varepsilon}\ \bar{\varepsilon}^*\ \mathrm{d}V\ , \quad \forall\ \bar{\varepsilon}^* \tag{C.12}$$

It is worth noting that the term $b\ \bar{\varepsilon}^*\ \ (\nabla\ a) \cdot (\nabla\ \bar{\varepsilon})$ in the weak form (C.12) would induce numerical difficulties linked to the computation of the gradient of a. This issue, also observed in [Saroukhani et al., 2013], can be addressed by dividing the gradient equation by the evolving internal length.

Starting again from (C.8) and dividing it by a, one gets:

$$\frac{\bar{\varepsilon}}{a} - \nabla \cdot (b\ \ (\nabla\ \bar{\varepsilon})) = \frac{\hat{\varepsilon}}{a} \tag{C.13}$$

$$\Leftrightarrow \quad \int_\Omega \frac{\bar{\varepsilon}}{a}\ \bar{\varepsilon}^*\ \mathrm{d}V - \int_\Omega \nabla \cdot (b\ \ (\nabla\ \bar{\varepsilon}))\ \ \bar{\varepsilon}^* \mathrm{d}V = \int_\Omega \frac{\hat{\varepsilon}}{a}\ \bar{\varepsilon}^*\ \mathrm{d}V\ , \quad \forall\ \bar{\varepsilon}^* \tag{C.14}$$

which, after an integration by parts, gives

$$\begin{aligned} &\int_\Omega \frac{\bar{\varepsilon}\ \bar{\varepsilon}^*}{a}\ \mathrm{d}V - \int_{\partial\Omega} b\ \bar{\varepsilon}^*\ \ (\nabla\ \bar{\varepsilon}) \cdot \mathbf{n}\ \mathrm{d}S \\ &\quad + \int_\Omega b\ \ (\nabla\ \bar{\varepsilon}) \cdot (\nabla\ \bar{\varepsilon}^*)\ \ \mathrm{d}V = \int_\Omega \frac{\hat{\varepsilon}}{a}\ \bar{\varepsilon}^*\ \mathrm{d}V\ , \quad \forall\ \bar{\varepsilon}^* \end{aligned} \tag{C.15}$$

In the end, using the Neumann boundary condition (C.9), the weak form can be written as

$$\int_\Omega \left(\frac{\bar{\varepsilon}\ \bar{\varepsilon}^*}{a} + b\ \ (\nabla\ \bar{\varepsilon}) \cdot (\nabla\ \bar{\varepsilon}^*) \right) \mathrm{d}V = \int_\Omega \frac{\hat{\varepsilon}}{a}\ \bar{\varepsilon}^*\ \mathrm{d}V\ , \quad \forall\ \bar{\varepsilon}^* \tag{C.16}$$

which remains true so long as a is not equal to 0.

Besides, as far as the classical gradient-type formulation is concerned, its weak form can be obtained by setting $a = 1$ and $b = c^2$, giving

$$\int_\Omega \left(\bar{\varepsilon}\ \bar{\varepsilon}^* + c^2\ (\nabla\ \bar{\varepsilon}) \cdot (\nabla\ \bar{\varepsilon}^*) \right) \mathrm{d}V = \int_\Omega \hat{\varepsilon}\ \bar{\varepsilon}^*\ \mathrm{d}V\ ,\quad \forall\ \bar{\varepsilon}^* \tag{C.17}$$

C.1.2 Isotropic damage-plastic models

As far as the damage-plastic model is concerned, one will, as for the pure damage model, study the weak forms associated to the equilibrium, before moving on to the general gradient-type formulation.

Equilibrium

As before, the equilibrium $\nabla \cdot \boldsymbol{\sigma} = \mathbf{0}$ can still be expected to be associated to the classical boundary condition (C.2), $\boldsymbol{\sigma}$ being now defined using (4.9) as $\boldsymbol{\sigma} = \tilde{\mathbb{C}} : (\boldsymbol{\varepsilon} - \boldsymbol{\varepsilon}^p)$, and the plastic strain tensor $\boldsymbol{\varepsilon}^p$ being considered given here.

Considering a virtual displacement field $\boldsymbol{u}^*$, one gets

$$\int_\Omega \left(\nabla \cdot \left[\tilde{\mathbb{C}} : (\boldsymbol{\varepsilon} - \boldsymbol{\varepsilon}^p) \right] \right) \cdot \boldsymbol{u}^*\ \mathrm{d}V = \int_\Omega \mathbf{0} \cdot \boldsymbol{u}^*\ \mathrm{d}V\ ,\quad \forall\ \boldsymbol{u}^* \tag{C.18}$$

which, following the same steps as before, can be written as a weak form

$$a_e(\boldsymbol{u}, \boldsymbol{u}^*) = l_e(\boldsymbol{u}^*)\ ,\quad \forall\ \boldsymbol{u}^* \tag{C.19}$$

where a_e is a bi-linear and symmetric form defined as

$$a_e : (\boldsymbol{u}, \boldsymbol{u}^*) \mapsto \int_\Omega \nabla \cdot \boldsymbol{u}^* : \tilde{\mathbb{C}} : \nabla \cdot \boldsymbol{u}\ \mathrm{d}V \tag{C.20}$$

and l_e a linear form defined as

$$l_e : \boldsymbol{u}^* \mapsto \int_\Omega (\nabla \cdot \boldsymbol{u}^*) : \tilde{\mathbb{C}} : \boldsymbol{\varepsilon}^p\ \mathrm{d}V + \int_{\partial\Omega} \boldsymbol{u}^* \cdot \boldsymbol{T}\ \mathrm{d}S \tag{C.21}$$

General gradient-type formulation

Then, one needs to obtain the weak form of the general gradient-type formulation (4.18) which writes here

$$\bar{p} - a\ \nabla \cdot (b\ \nabla\ \bar{p}) = p \tag{C.22}$$

where a and b are given non-negative functions, function p is still considered as given, and function $\bar{p}$ is still the primary unknown. As for the previous gradient-type equations, this one can be expected to be combined with the homogeneous Neumann boundary condition:

$$(\nabla\ \bar{p}) \cdot \mathbf{n} = 0\ ,\quad \text{in } \partial\Omega \tag{C.23}$$

Moreover, as for the pure damage model, one should here start by dividing the gradient equation by a to avoid numerical difficulties. Starting from equation (C.22), and considering a virtual nonlocal strain field $\bar{p}^*$, one would get

$$\int_\Omega \frac{\bar{p}}{a}\,\bar{p}^*\,\mathrm{d}V - \int_\Omega \nabla\cdot(b\ (\nabla\ \bar{p}))\ \bar{p}^*\mathrm{d}V = \int_\Omega \frac{p}{a}\,\bar{p}^*\,\mathrm{d}V\ ,\quad \forall\ \bar{p}^* \tag{C.24}$$

Following the same steps as for the pure damage model, this weak form can be written as

$$\int_\Omega \left(\frac{\bar{p}\,\bar{p}^*}{a} + b\ (\nabla\ \bar{p})\cdot(\nabla\ \bar{p}^*)\right)\mathrm{d}V = \int_\Omega \frac{p}{a}\,\bar{p}^*\,\mathrm{d}V\ ,\quad \forall\ \bar{p}^* \tag{C.25}$$

which is true as long as a is not equal to 0.

Regarding the weak form associated to the classical formulation, it can be obtained by setting $a = 1$ and $b = c^2$, giving

$$\int_\Omega \left(\bar{p}\,\bar{p}^* + c^2\ (\nabla\ \bar{p})\cdot(\nabla\ \bar{p}^*)\right)\mathrm{d}V = \int_\Omega p\,\bar{p}^*\,\mathrm{d}V\ ,\quad \forall\ \bar{p}^* \tag{C.26}$$

C.2 Discretization of the considered formulations

At this point, to handle their numerical implementation, one needs to handle the spatial discretization of each equation associated to the considered formulations before linearizing them. This will be done using the notations defined in Part 4.2.1.

C.2.1 Framework and general notations

Following the notations introduced in section 4.2.1, this part will present those used to handle the spatial discretization of the different equations. The following notations will be used for the main degree of freedom, associated to displacement:

- $[\boldsymbol{N}_\mathcal{U}]$ will denote the matrix containing the shape functions for $\boldsymbol{u}$
- $[\boldsymbol{B}_\mathcal{U}]$ will denote the matrix containing the shape functions' gradient for $\boldsymbol{u}$
- $\{\mathcal{U}\}$ will denote the vector containing the solution displacement's projections
- $\{\mathcal{U}^*\}$ will denote the vector containing the virtual displacement's projections

and for the degree of freedom associated to the nonlocal variable:

- $[\boldsymbol{N}_\mathcal{E}]$ will denote the matrix containing the shape functions
- $[\boldsymbol{B}_\mathcal{E}]$ will denote the matrix containing the shape functions' gradient
- $\{\mathcal{E}\}$ will denote the vector containing the solution nonlocal equivalent or cumulative plastic strain's projections
- $\{\mathcal{E}^*\}$ will denote the vector containing the virtual nonlocal equivalent or cumulative plastic strain's projections

The terms linked to both the solution and virtual displacement can then be expressed from $\{\mathcal{U}\}$, $\{\mathcal{U}^*\}$, $[\boldsymbol{N}_\mathcal{U}]$ and $[\boldsymbol{B}_\mathcal{U}]$ as described in Table C.1.

$\boldsymbol{u}$	$\nabla \cdot \boldsymbol{u}$	$\boldsymbol{u}^*$	$\nabla \cdot \boldsymbol{u}^*$
$[\boldsymbol{N}_\mathcal{U}]\{\mathcal{U}\}$	$[\boldsymbol{B}_\mathcal{U}]\{\mathcal{U}\}$	$[\boldsymbol{N}_\mathcal{U}]\{\mathcal{U}^*\}$	$[\boldsymbol{B}_\mathcal{U}]\{\mathcal{U}^*\}$

Table C.1: Expression of the terms linked to displacement

In a similar fashion, the expression of the terms linked to both the solution and virtual nonlocal equivalent strain are detailed in Table C.2, while Table C.3 contains those linked to the solution and virtual nonlocal cumulative plastic strain.

$\bar{\varepsilon}$	$\nabla\ \bar{\varepsilon}$	$\bar{\varepsilon}^*$	$\nabla\ \bar{\varepsilon}^*$
$[\boldsymbol{N}_\mathcal{E}]\{\mathcal{E}\}$	$[\boldsymbol{B}_\mathcal{E}]\{\mathcal{E}\}$	$[\boldsymbol{N}_\mathcal{E}]\{\mathcal{E}^*\}$	$[\boldsymbol{B}_\mathcal{E}]\{\mathcal{E}^*\}$

Table C.2: Expression of the terms linked to nonlocal equivalent strain

$\bar{p}$	$\nabla\ \bar{p}$	$\bar{p}^*$	$\nabla\ \bar{p}^*$
$[\boldsymbol{N}_\mathcal{E}]\{\mathcal{E}\}$	$[\boldsymbol{B}_\mathcal{E}]\{\mathcal{E}\}$	$[\boldsymbol{N}_\mathcal{E}]\{\mathcal{E}^*\}$	$[\boldsymbol{B}_\mathcal{E}]\{\mathcal{E}^*\}$

Table C.3: Expression of the terms linked to nonlocal cumulative plastic strain

The expressions detailed in this section will now be used to determine the discretized expression of the formulations studied in this chapter.

C.2.2 Isotropic damage model

This part will deal with the discretization of the equations associated the nonocal isotropic damage model, namely the equilibrium and the general gradient-type equation. As before, the innovative aspect of this work mainly comes from the use of a state-dependent function b in addition to the evolving internal length a in the general gradient-type formulation.

Equilibrium

The first equation that needs to be discretized is the equilibrium (C.1). Starting from its weak form (C.5) one gets

$$\int_\Omega \left([\boldsymbol{B}_\mathcal{U}]\{\mathcal{U}^*\}\right)^t : \tilde{\mathbb{C}} : \left([\boldsymbol{B}_\mathcal{U}]\{\mathcal{U}\}\right)\ \mathrm{d}V = \int_{\partial\Omega} \left([\boldsymbol{N}_\mathcal{U}]\{\mathcal{U}^*\}\right)^t \cdot \boldsymbol{T}\ \mathrm{d}S\ ,\quad \forall\, \mathcal{U}^* \tag{C.27}$$

which can be written under the classical form

$$\mathbb{K}_\mathcal{U}\ \{\mathcal{U}\} = \{\mathcal{F}_\mathcal{U}\} \tag{C.28}$$

where $\mathbb{K}_\mathcal{U}$ and $\{\mathcal{F}_\mathcal{U}\}$ are defined as

$$\mathbb{K}_\mathcal{U} \quad = \quad \int_\Omega [\boldsymbol{B}_\mathcal{U}]^t : \tilde{\mathbb{C}} : [\boldsymbol{B}_\mathcal{U}]\ \mathrm{d}V \tag{C.29}$$

$$\{\mathcal{F}_{\mathcal{U}}\} \;=\; \int_{\partial\Omega} [\boldsymbol{N}_{\mathcal{U}}]^t \cdot [\boldsymbol{N}_{\mathcal{U}}] \; \mathrm{d}S \tag{C.30}$$

It is worth noting that, in the case of a local formulation, this equation would be nonlinear since $\mathbb{K}$ would depend on D which depends on $\mathcal{U}$. On the other hand, in the case of a nonlocal formulation, this equation would be linear in terms of $\mathcal{U}$, but then $\mathbb{K}_{\mathcal{U}}$ would depend on $\{\mathcal{E}\}$, making the set of equations (equilibrium and nonlocal) nonlinear.

General gradient-type formulation

The next equation that needs to be discretized is the general gradient formulation (C.8). Starting from its weak form (C.16), one can write

$$\begin{aligned} \int_\Omega \left(\frac{([\boldsymbol{N}_{\mathcal{E}}]\{\mathcal{E}^*\})^t \, ([\boldsymbol{N}_{\mathcal{E}}]\{\mathcal{E}\})}{a} + b([\boldsymbol{B}_{\mathcal{E}}]\{\mathcal{E}^*\})^t \, ([\boldsymbol{B}_{\mathcal{E}}]\{\mathcal{E}\}) \right) \mathrm{d}V \\ = \int_\Omega \frac{([\boldsymbol{N}_{\mathcal{E}}]\{\mathcal{E}^*\})^t \; \hat{\varepsilon}}{a} \; \mathrm{d}V \;, \quad \forall \; \mathcal{E}^* \end{aligned} \tag{C.31}$$

which can be written under the classical form

$$\mathbb{K}_{\mathcal{E}} \; \{\mathcal{E}\} = \{\mathcal{F}_{\mathcal{E}}\} \tag{C.32}$$

where $\mathbb{K}_{\mathcal{E}}$ and $\{\mathcal{F}_{\mathcal{E}}\}$ are defined as

$$\mathbb{K}_{\mathcal{E}} \;=\; \int_\Omega \left(\frac{[\boldsymbol{N}_{\mathcal{E}}]^t [\boldsymbol{N}_{\mathcal{E}}]}{a} + b[\boldsymbol{B}_{\mathcal{E}}]^t [\boldsymbol{B}_{\mathcal{E}}] \right) \mathrm{d}V \tag{C.33}$$

$$\{\mathcal{F}_{\mathcal{E}}\} \;=\; \int_\Omega \frac{[\boldsymbol{N}_{\mathcal{E}}]^t \hat{\varepsilon}}{a} \; \mathrm{d}V \tag{C.34}$$

It is worth noting that, since a is a function and not a constant, the problem might not be linear in terms of $\mathcal{E}$ if $\mathbb{K}_{\mathcal{E}}$ depends on $\{\mathcal{E}\}$. Either way, the nonlocal problem is not linear with respect to $\mathcal{U}$, and the complete set of equation (equilibrium and nonlocal) is nonlinear in terms of both $\mathcal{U}$ and $\mathcal{E}$.

As for the weak form, the discretized form associated to the classical gradient-type formulation can be obtained by setting $a = 1$ and $b = c^2$, giving

$$\mathbb{K}_{\mathcal{E}} \;=\; \int_\Omega \left([\boldsymbol{N}_{\mathcal{E}}]^t [\boldsymbol{N}_{\mathcal{E}}] + c^2 [\boldsymbol{B}_{\mathcal{E}}]^t [\boldsymbol{B}_{\mathcal{E}}] \right) \mathrm{d}V \tag{C.35}$$

$$\{\mathcal{F}_{\mathcal{E}}\} \;=\; \int_\Omega [\boldsymbol{N}_{\mathcal{E}}]^t \hat{\varepsilon} \; \mathrm{d}V \tag{C.36}$$

C.2.3 Isotropic damage-plastic models

After dealing with the discretization of the equations associated the nonlocal isotropic damage model, this part will focus on those associated to the nonlocal isotropic damage-plastic model. The discretization of both the equilibrium will first be presented, before moving to the general gradient-type formulation.

Equilibrium

As for the pure damage model, the first equation that needs to be discretized is the equilibrium (C.1). Starting from its weak form (C.19), one gets

$$\begin{aligned}&\int_\Omega ([\boldsymbol{B}_\mathcal{U}]\{\mathcal{U}^*\})^t : \tilde{\mathbb{C}} : ([\boldsymbol{B}_\mathcal{U}]\{\mathcal{U}\}) \ \mathrm{d}V \\ =&\int_\Omega ([\boldsymbol{B}_\mathcal{U}]\{\mathcal{U}^*\})^t : \tilde{\mathbb{C}} : \boldsymbol{\varepsilon}^p \ \mathrm{d}V + \int_{\partial\Omega} ([\boldsymbol{N}_\mathcal{U}]\{\mathcal{U}^*\})^t \cdot \boldsymbol{T} \ \mathrm{d}S \ , \quad \forall\, \mathcal{U}^*\end{aligned} \tag{C.37}$$

which can be written under the classical form

$$\mathbb{K}_\mathcal{U} \ \{\mathcal{U}\} = \{\mathcal{F}_\mathcal{U}\} \tag{C.38}$$

where $\mathbb{K}_\mathcal{U}$ and $\{\mathcal{F}_\mathcal{U}\}$ are defined as

$$\mathbb{K}_\mathcal{U} = \int_\Omega [\boldsymbol{B}_\mathcal{U}]^t : \tilde{\mathbb{C}} : [\boldsymbol{B}_\mathcal{U}] \ \mathrm{d}V \tag{C.39}$$

$$\{\mathcal{F}_\mathcal{U}\} = \int_\Omega [\boldsymbol{B}_\mathcal{U}]^t : \tilde{\mathbb{C}} : \boldsymbol{\varepsilon}^p \ \mathrm{d}V + \int_{\partial\Omega} [\boldsymbol{N}_\mathcal{U}]^t \cdot \boldsymbol{T} \ \mathrm{d}S \tag{C.40}$$

It is worth noting that, here, one considers $\boldsymbol{\varepsilon}^p$ as given, which means that plasticity will require an additional iterative resolution. In this case, as for the pure damage model, this equation would be linear in terms of $\mathcal{U}$ in the case of a nonlocal formulation, and nonlinear in the case of a local one. Moreover, since $\mathbb{K}_\mathcal{U}$ depends on $\{\mathcal{E}\}$ through damage evolution law, the set of equations (equilibrium and nonlocal) will still be nonlinear.

General gradient-type formulation

After the equilibrium, one needs to handle the discretization of the general gradient formulation (C.22) which constitutes the innovative part of this work. Starting with its weak form (C.25), one can write

$$\begin{aligned}\int_\Omega \left(\frac{([\boldsymbol{N}_\mathcal{E}]\{\mathcal{E}^*\})^t \, ([\boldsymbol{N}_\mathcal{E}]\{\mathcal{E}\})}{a} + b([\boldsymbol{B}_\mathcal{E}]\{\mathcal{E}^*\})^t \, ([\boldsymbol{B}_\mathcal{E}]\{\mathcal{E}\}) \right) \mathrm{d}V& \\ = \int_\Omega \frac{([\boldsymbol{N}_\mathcal{E}]\{\mathcal{E}^*\})^t \ p}{a} \ \mathrm{d}V \ , \quad \forall\, \mathcal{E}^*&\end{aligned} \tag{C.41}$$

which can be written as a classical problem:

$$\mathbb{K}_\mathcal{E} \ \{\mathcal{E}\} = \{\mathcal{F}_\mathcal{E}\} \tag{C.42}$$

where $\mathbb{K}_\mathcal{E}$ and $\{\mathcal{F}_\mathcal{E}\}$ are defined as

$$\mathbb{K}_\mathcal{E} = \int_\Omega \left(\frac{[\boldsymbol{N}_\mathcal{E}]^t [\boldsymbol{N}_\mathcal{E}]}{a} + b[\boldsymbol{B}_\mathcal{E}]^t [\boldsymbol{B}_\mathcal{E}] \right) \mathrm{d}V \tag{C.43}$$

$$\{\mathcal{F}_\mathcal{E}\} = \int_\Omega \frac{[\boldsymbol{N}_\mathcal{E}]^t p}{a} \ \mathrm{d}V \tag{C.44}$$

As for the nonlocal formulation with fixed internal length, $\{\mathcal{E}\}$ still denote the cumulative plastic strain p. It is worth noting that the nonlocal equation might

still be nonlinear in terms of $\mathcal{E}$ if $\mathbb{K}_\mathcal{E}$ depends on $\{\mathcal{E}\}$ through the function a. Moreover, as before, the complete set of equation is nonlinear in terms of both $\mathcal{U}$ and $\mathcal{E}$.

As before, the discretized form associated to the classical gradient-type formulation can be obtained by setting $a = 1$ and $b = c^2$, giving

$$\mathbb{K}_\mathcal{E} = \int_\Omega \left([\boldsymbol{N}_\mathcal{E}]^t [\boldsymbol{N}_\mathcal{E}] + c^2 [\boldsymbol{B}_\mathcal{E}]^t [\boldsymbol{B}_\mathcal{E}] \right) \mathrm{d}V \tag{C.45}$$

$$\{\mathcal{F}_\mathcal{E}\} = \left(\int_\Omega [\boldsymbol{N}_\mathcal{E}]^t \; p \; \mathrm{d}V \right) \tag{C.46}$$

C.3 Linearization of the considered formulations

Finally, before moving on to the numerical implementation, one needs to linearize the equations associated to the considered formulations in order to implement them. After defining the associated notations, this part will thus present the ingredients needed to implement the considered nonlocal formulations in OOFEM, and to solve the associated coupled nonlinear problems using Newton-like algorithms.

C.3.1 General idea and notations

Now that the discretized forms of both the equilibrium ((C.28), (C.38)) and gradient-type ((C.32), (C.42)) equation have been determined, one now needs to handle their linarization. The idea here is to determine the internal forces $\Phi_\mathcal{U}$ and $\Phi_\mathcal{E}$, associated respectively to the equilibrium and nonlocal equations, defined as

$$\mathbb{K}_\mathcal{U} \{\mathcal{U}\} = \{\mathcal{F}_\mathcal{U}\} \quad \Leftrightarrow \quad \int_\Omega \Phi_\mathcal{U} \; \mathrm{d}V = \int_{\partial\Omega} [\boldsymbol{N}_\mathcal{U}]^t \cdot \boldsymbol{T} \; \mathrm{d}S \tag{C.47}$$

$$\mathbb{K}_\mathcal{E} \{\mathcal{E}\} = \{\mathcal{F}_\mathcal{E}\} \quad \Leftrightarrow \quad \int_\Omega \Phi_\mathcal{E} \; \mathrm{d}V = 0 \tag{C.48}$$

Their derivatives, $\dfrac{\partial \Phi_\mathcal{U}}{\partial \mathcal{U}}$, $\dfrac{\partial \Phi_\mathcal{U}}{\partial \mathcal{E}}$, $\dfrac{\partial \Phi_\mathcal{E}}{\partial \mathcal{U}}$ and $\dfrac{\partial \Phi_\mathcal{E}}{\partial \mathcal{E}}$, will also be determined here since they will be needed to compute the tangent operators.

It is worth noting that, since the general gradient-type formulation will mainly be used to handle the eikonal-based gradient-type formulations, functions a and b will here be taken as damage-dependent.

C.3.2 Isotropic damage model

This part will present the linearization of the equilibrium and gradient-type equations associated to he nonlocal isotropic damage model. This will give some insight on how the equilibrium and the classical gradient are implemented in OOFEM, which will prepare the implementation of the general gradient.

Equilibrium

First one needs to linearize the equilibrium (C.1). Starting from its discretized form (C.28), one gets

$$\int_\Omega [\boldsymbol{B}_\mathcal{U}]^t : \tilde{\mathbb{C}} : \nabla \boldsymbol{u} \, \mathrm{d}V = \int_{\partial\Omega} [\boldsymbol{N}_\mathcal{U}]^t \cdot \boldsymbol{T} \, \mathrm{d}S \tag{C.49}$$

which is equivalent to the right hand side of (C.47), where $\Phi_\mathcal{U}$ would write

$$\Phi_\mathcal{U} = [\boldsymbol{B}_\mathcal{U}]^t : (1-D)\mathbb{C} : \nabla \boldsymbol{u} \tag{C.50}$$

The derivative of $\Phi_\mathcal{U}$ with respect to the displacement degree of freedom can then be defined as

$$\frac{\partial \Phi_\mathcal{U}}{\partial \mathcal{U}} = [\boldsymbol{B}_\mathcal{U}]^t : (1-D)\mathbb{C} : [\boldsymbol{B}_\mathcal{U}] \tag{C.51}$$

while its with respect to the nonlocal one is given by

$$\frac{\partial \Phi_\mathcal{U}}{\partial \mathcal{E}} = [\boldsymbol{B}_\mathcal{U}]^t \left(-D'(\kappa)\ \kappa'(\bar{\varepsilon})\ \mathbb{C}\ \nabla \boldsymbol{u}\right) [\boldsymbol{N}_\mathcal{E}] \tag{C.52}$$

It is worth noting that these derivatives are only relevant for nonlocal formulations, but they do not depend on the regularization method, so long as the nonlocal variable is the equivalent strain.

General gradient-type formulation

One then needs to address the linearization of the general gradient-type formulation (C.8). Starting from its discretized form (C.32), one can write

$$\int_\Omega \left(\frac{[\boldsymbol{N}_\mathcal{E}]^t\ \bar{\varepsilon}}{a} + [\boldsymbol{B}_\mathcal{E}]^t\ b\ \nabla \bar{\varepsilon} \right) \mathrm{d}V = \int_\Omega [\boldsymbol{N}_\mathcal{E}]^t\ \frac{1}{a}\ \hat{\varepsilon}\ \mathrm{d}V \tag{C.53}$$

which is equivalent to the right hand side of (C.48), where $\Phi_\mathcal{E}$ would be defined as

$$\Phi_\mathcal{E} = [\boldsymbol{N}_\mathcal{E}]^t\ \frac{1}{a}\ (\bar{\varepsilon} - \hat{\varepsilon}) + [\boldsymbol{B}_\mathcal{E}]^t\ b\ \nabla \bar{\varepsilon} \tag{C.54}$$

One thus gets for the derivative of $\Phi_\mathcal{E}$ with respect to the displacement degree of freedom

$$\frac{\partial \Phi_\mathcal{E}}{\partial \mathcal{U}} = [\boldsymbol{N}_\mathcal{E}]^t \left(-\frac{1}{a}\ \frac{\partial \hat{\varepsilon}}{\partial \boldsymbol{\varepsilon}} \right) [\boldsymbol{B}_\mathcal{U}] \tag{C.55}$$

It is worth noting that, except in the 1D case where

$$\frac{\partial \hat{\varepsilon}}{\partial \varepsilon} = \frac{\langle \varepsilon \rangle_+}{\hat{\varepsilon}} \tag{C.56}$$

$\partial \hat{\varepsilon} / \partial \boldsymbol{\varepsilon}$ should be a row matrix.

In a similar fashion, taking into account the dependence of a and b with respect to $\bar{\varepsilon}$, one gets for the derivative of $\Phi_\mathcal{E}$ with respect to the nonlocal degree of freedom

$$\begin{aligned} \frac{\partial \Phi_\mathcal{E}}{\partial \mathcal{E}} = {} & [\boldsymbol{N}_\mathcal{E}]^t \left(\frac{1}{a} + \frac{1}{a^2}\ a'(D)\ D'(\kappa)\ \kappa'(\bar{\varepsilon})\ (\hat{\varepsilon} - \bar{\varepsilon}) \right) [\boldsymbol{N}_\mathcal{E}] \\ & + [\boldsymbol{B}_\mathcal{E}]^t\ b\ [\boldsymbol{B}_\mathcal{E}] + [\boldsymbol{B}_\mathcal{E}]^t \Big(b'(D)\ D'(\kappa)\ \kappa'(\bar{\varepsilon})\ \nabla \bar{\varepsilon} \Big) [\boldsymbol{N}_\mathcal{E}] \end{aligned} \tag{C.57}$$

It is worth noting that the terms associated to the classical gradient-type formulation can again be obtained by setting $a = 1$ and $b = c^2$, giving

$$\Phi_{\mathcal{E}} = [\boldsymbol{N}_{\mathcal{E}}]^t \ (\bar{\varepsilon} - \hat{\varepsilon}) + [\boldsymbol{B}_{\mathcal{E}}]^t \ c^2 \ \nabla\bar{\varepsilon} \tag{C.58}$$

$$\frac{\partial \Phi_{\mathcal{E}}}{\partial \mathcal{U}} = [\boldsymbol{N}_{\mathcal{E}}]^t \left(-\frac{\partial \hat{\varepsilon}}{\partial \boldsymbol{\varepsilon}}\right) [\boldsymbol{B}_{\mathcal{U}}] \tag{C.59}$$

$$\frac{\partial \Phi_{\mathcal{E}}}{\partial \mathcal{E}} = [\boldsymbol{N}_{\mathcal{E}}]^t \ [\boldsymbol{N}_{\mathcal{E}}] + [\boldsymbol{B}_{\mathcal{E}}]^t \ c^2 \ [\boldsymbol{B}_{\mathcal{E}}] \tag{C.60}$$

C.3.3 Isotropic damage-plastic models

Following what was done for the pure damage model, this part will present the linearization of the equilibrium and gradient-type equations associated to he nonlocal isotropic damage-plastic model. Again, the work done on both the equilibrium and the nonlocal treatment with fixed internal length will help understand the way those equations are implemented in OOFEM, which will prepare the implementation of the general gradient-type equation.

Equilibrium

As for the pure damage model, one needs to begin with the linearization of the equilibrium equation (C.1). Starting with the discretized form (C.38) one can write

$$\int_{\Omega} \left([\boldsymbol{B}_{\mathcal{U}}]^t : \tilde{\mathbb{C}} : \nabla \boldsymbol{u} - [\boldsymbol{B}_{\mathcal{U}}]^t : \tilde{\mathbb{C}} : \boldsymbol{\varepsilon}^p \right) \ \mathrm{d}V = \int_{\partial\Omega} [\boldsymbol{N}_{\mathcal{U}}]^t \cdot \boldsymbol{T} \ \mathrm{d}S \tag{C.61}$$

which is equivalent to the right hand side of (C.47) where $\Phi_{\mathcal{U}}$ would be defined as

$$\Phi_{\mathcal{U}} = [\boldsymbol{B}_{\mathcal{U}}]^t : (1 - D)\mathbb{C} : (\boldsymbol{\varepsilon} - \boldsymbol{\varepsilon}^p) \tag{C.62}$$

As for the pure damage model, the derivative of $\Phi_{\mathcal{U}}$ with respect to the displacement degree of freedom can be defined as

$$\begin{aligned} \frac{\partial \Phi_{\mathcal{U}}}{\partial \mathcal{U}} =& [\boldsymbol{B}_{\mathcal{U}}]^t \ (1 - D) \ \mathbb{C} \ [\boldsymbol{B}_{\mathcal{U}}] \\ & - [\boldsymbol{B}_{\mathcal{U}}]^t \ D'(\kappa) \ (1 - m) \ p'(\boldsymbol{\varepsilon}) \ \mathbb{C} : (\boldsymbol{\varepsilon} - \boldsymbol{\varepsilon}^p) \ [\boldsymbol{B}_{\mathcal{U}}] \end{aligned} \tag{C.63}$$

It is worth noting that, here, $p'(\boldsymbol{\varepsilon})$ stands for the numerical derivative of the return mapping algorithm, used to handle plastic evolution.

In a similar fashion, the derivative of $\Phi_{\mathcal{U}}$ with respect to the nonlocal degree of freedom writes

$$\frac{\partial \Phi_{\mathcal{U}}}{\partial \mathcal{E}} = [\boldsymbol{B}_{\mathcal{U}}]^t \left(-D'(\kappa) \ m \ \mathbb{C} : (\boldsymbol{\varepsilon} - \boldsymbol{\varepsilon}^p)\right) [\boldsymbol{N}_{\mathcal{E}}] \tag{C.64}$$

As before, one can note that these derivatives are only relevant for nonlocal formulations, and they do not depend on the regularization method so long as the nonlocal variable is the equivalent strain.

General gradient-type formulation

Finally, one needs to address the linearization of the general gradient formulation (C.22) which constitutes the innovative part of this work. Starting from its discretized form (C.42), one can write:

$$\int_\Omega \left(\frac{[\boldsymbol{N}_\mathcal{E}]^t \ \bar{p}}{a} + [\boldsymbol{B}_\mathcal{E}]^t \ b \ \nabla \bar{p} \right) \mathrm{d}V = \int_\Omega \frac{[\boldsymbol{N}_\mathcal{E}]^t p}{a} \ \mathrm{d}V \tag{C.65}$$

which is equivalent to the right hand side of (C.48), provided $\Phi_\mathcal{E}$ is defined as

$$\Phi_\mathcal{E} = [\boldsymbol{N}_\mathcal{E}]^t \ \frac{1}{a} \ (\bar{p} - p) + [\boldsymbol{B}_\mathcal{E}]^t \ b \ \nabla \bar{p} \tag{C.66}$$

Its derivative with respect to the displacement degree of freedom then writes

$$\begin{aligned} \frac{\partial \Phi_\mathcal{E}}{\partial \mathcal{U}} =& [\boldsymbol{N}_\mathcal{E}]^t \left(-\frac{p'(\boldsymbol{\varepsilon})}{a} + \frac{p - \bar{p}}{a^2} \ a'(D) \ D'(\kappa) \ (1 - m) \ p'(\boldsymbol{\varepsilon}) \right) [\boldsymbol{B}_\mathcal{U}] \\ &+ [\boldsymbol{B}_\mathcal{E}]^t \left(b'(D) \ D'(\kappa) \ (1 - m) \ \nabla \bar{p} \otimes p^{'}(\boldsymbol{\varepsilon}) \right) [\boldsymbol{B}_\mathcal{U}] \end{aligned} \tag{C.67}$$

where $p'(\boldsymbol{\varepsilon})$ still stands for the numerical derivative of the return mapping algorithm.

In a similar fashion, taking into account the dependence of a and b with respect to $\bar{p}$, the derivative of $\Phi_\mathcal{E}$ with respect to the nonlocal degree of freedom writes

$$\begin{aligned} \frac{\partial \Phi_\mathcal{E}}{\partial \mathcal{E}} =& [\boldsymbol{N}_\mathcal{E}]^t \left(\frac{1}{a} + \frac{1}{a^2} \ a'(D) \ D'(\kappa) \ m \, (p - \bar{p}) \right) [\boldsymbol{N}_\mathcal{E}] \\ &+ [\boldsymbol{B}_\mathcal{E}]^t \left(\nabla \bar{p} \ b'(D) \ D'(\kappa) \ m \right) [\boldsymbol{N}_\mathcal{E}] + [\boldsymbol{B}_\mathcal{E}]^t \, (b) \, [\boldsymbol{B}_\mathcal{E}] \end{aligned} \tag{C.68}$$

As for the pure damage model, the terms associated to the classical gradient-type formulation can again be obtained by setting $a = 1$ and $b = c^2$, giving

$$\Phi_\mathcal{E} = [\boldsymbol{N}_\mathcal{E}]^t \ (\bar{p} - p) + [\boldsymbol{B}_\mathcal{E}]^t \ c^2 \ \nabla \bar{p} \tag{C.69}$$

$$\frac{\partial \Phi_\mathcal{E}}{\partial \mathcal{U}} = [\boldsymbol{N}_\mathcal{E}]^t \left(-p^{'}(\boldsymbol{\varepsilon}) \right) [\boldsymbol{B}_\mathcal{U}] \tag{C.70}$$

$$\frac{\partial \Phi_\mathcal{E}}{\partial \mathcal{E}} = [\boldsymbol{N}_\mathcal{E}]^t \ [\boldsymbol{N}_\mathcal{E}] + [\boldsymbol{B}_\mathcal{E}]^t \ c^2 \ [\boldsymbol{B}_\mathcal{E}] \tag{C.71}$$

Bibliography

[ANO, 1998] (1998). Fem 1.001, 3rd edition, rules for the design of hoisting appliances, 8 booklets, english, pages: 305.

[ACA, 2014] (2014). Aviation in europe : A vision for 2050.

[IAT, 2016] (2016). https ://www.iata.org/contentassets/d4b60cceeb4213bb5993d5fa2f358f/frenchpr-2016-10-18-01.pdf. L'iata prevoit que le nombre de passagers va doubler d'ici 20 ans.

[Aifantis, 1987] Aifantis, E. C. (1987). The physics of plastic deformation. International Journal of Plasticity, 3(3):211–247.

[Allix and Deü, 1997] Allix, O. and Deü, J.-F. (1997). Delay-damage modelling for fracture prediction of laminated composites under dynamic loading. Engineering Transactions, 45:29–46.

[Allix et al., 2003] Allix, O., Feissel, P., and Thévenet, P. (2003). A delay damage mesomodel of laminates under dynamic loading: basic aspects and identification issues. Computers & Structures, 81(12):1177–1191.

[Ambrosio and Tortorelli, 1990] Ambrosio, L. and Tortorelli, V. M. (1990). Approximation of functional depending on jumps by elliptic functional via t-convergence. Communications on Pure and Applied Mathematics, 43(8):999–1036.

[Ambrosio and Tortorelli, 1992] Ambrosio, L. and Tortorelli, V. M. (1992). On the approximation of free discontinuity problems.

[Amestoy and Leblond, 1992] Amestoy, M. and Leblond, J. (1992). Crack paths in plane situations—II. detailed form of the expansion of the stress intensity factors. International Journal of Solids and Structures, 29(4):465–501.

[Andrieux et al., 1986] Andrieux, S., Bamberger, Y., and Marigo, J.-J. (1986). Model of microcracked material for concrete and rocks. Journal de Mécanique Théorique et Appliquée, 5.

[Azinpour et al., 2018] Azinpour, E., Ferreira, J. P. S., Parente, M. P. L., and de Sa, J. C. (2018). A simple and unified implementation of phase field and gradient damage models. Advanced Modeling and Simulation in Engineering Sciences, 5(1).

[Bažant and Jirásek, 1994] Bažant, Z. and Jirásek, M. (1994). Damage nonlocality due to microcrack interactions: Statistical determination of crack influence function. Fracture and Damage in Quasibrittle Structures, pages 3–17.

[Bažant et al., 2010] Bažant, Z., Le, J.-L., and Hoover, C. (2010). Nonlocal boundary layer (nbl) model: overcoming boundary condition problems in strength statistics and fracture analysis of quasibrittle materials. In Oh, B., editor, Proceedings, FraMCoS-7, 7th International Conference, pages 135–143. Korea Concrete Institute. Conference date: 01-01-2010.

[Bažant and Oh, 1983] Bažant, Z. P. and Oh, B. H. (1983). Crack band theory for fracture of concrete. Matériaux et Construction, 16(3):155–177.

[Badel et al., 2007] Badel, P., Godard, V., and Leblond, J.-B. (2007). Application of some anisotropic damage model to the prediction of the failure of some complex industrial concrete structure. International Journal of Solids and Structures, 44(18-19):5848–5874.

[Barenblatt, 1962] Barenblatt, G. (1962). The mathematical theory of equilibrium cracks in brittle fracture. In Dryden, H., von Kármán, T., Kuerti, G., van den Dungen, F., and Howarth, L., editors, Advances in Applied Mechanics, volume 7, pages 55 – 129. Elsevier.

[Bažant, 1976] Bažant, Z. P. (1976). Instability, Ductility, and Size Effect in Strain-Softening Concrete. Journal of the Engineering Mechanics Division, 102(2):331–344.

[Bažant, 1991] Bažant, Z. P. (1991). Why continuum damage is nonlocal: Micromechanics arguments. Journal of Engineering Mechanics, 117(5):1070–1087.

[Bažant, 1994] Bažant, Z. P. (1994). Nonlocal damage theory based on micromechanics of crack interactions. Journal of Engineering Mechanics, 120(3):593–617.

[Bažant and Belytschko, 1985] Bažant, Z. P. and Belytschko, T. B. (1985). Wave propagation in a strain-softening bar:exact solution. Journal of Engineering Mechanics, 111(3):381–389.

[Bažant and Jirásek, 2002] Bažant, Z. P. and Jirásek, M. (2002). Nonlocal integral formulations of plasticity and damage: Survey of progress. Journal of Engineering Mechanics, 128(11):1119–1149.

[Belytschko and Black, 1999] Belytschko, T. and Black, T. (1999). Elastic crack growth in finite elements with minimal remeshing. International Journal for Numerical Methods in Engineering, 45(5):601–620.

[Belytschko et al., 1996] Belytschko, T., Krongauz, Y., Organ, D., Fleming, M., and Krysl, P. (1996). Meshless methods: An overview and recent developments. Computer Methods in Applied Mechanics and Engineering, 139(1):3–47.

[Belytschko et al., 1994] Belytschko, T., Lu, Y. Y., and Gu, L. (1994). Element-free Galerkin methods. International Journal for Numerical Methods in Engineering, 37(2):229–256.

[Belytschko et al., 1995] Belytschko, T., Lu, Y. Y., and Gu, L. (1995). Crack propagation by element-free Galerkin methods. Engineering Fracture Mechanics, 51(2):295–315.

[Bender and Orszag, 1978] Bender, C. and Orszag, S. (1978). Advanced Mathematical Methods for Scientists and Engineers. Advanced Book Program - McGraw-Hill Book Company. McGraw-Hill.

[Bischoff and Perry, 1991] Bischoff, P. H. and Perry, S. H. (1991). Compressive behaviour of concrete at high strain rates. Materials and Structures, 24(6):425–450.

[Borino et al., 2003] Borino, G., Failla, B., and Parrinello, F. (2003). A symmetric nonlocal damage theory. International Journal of Solids and Structures, 40(13):3621–3645.

[Bourdin et al., 2000] Bourdin, B., Francfort, G., and Marigo, J.-J. (2000). Numerical experiments in revisited brittle fracture. Journal of the Mechanics and Physics of Solids, 48(4):797–826.

[Bourdin et al., 2008] Bourdin, B., Francfort, G. A., and Marigo, J.-J. (2008). The Variational Approach to Fracture. Journal of Elasticity, 91(1):5–148.

[Brara and Klepaczko, 1997] Brara, A. and Klepaczko, J. (1997). Nouveau dispositif exprimental d'étude de la rupture par écaillage du béton. In Communication-Congres GEO, Aussois, France.

[Brara et al., 1997] Brara, A., Klepaczko, J., and Kruszka, L. (1997). Tensile testing and modeling of concrete under high loading rates. Brandt, Li and Marshall (Eds.), Brittle Matrix Composites, 5:281–290.

[Brillouin, 1926] Brillouin, L. (1926). La mécanique ondulatoire de Schrödinger; une méthode générale de resolution par approximations successives. Compt.Rend.Hebd.Seances Acad.Sci., 183(1):24–26.

[Brünig, 2003] Brünig, M. (2003). An anisotropic ductile damage model based on irreversible thermodynamics. International Journal of Plasticity, 19(10):1679–1713.

[Burlion et al., 2000] Burlion, N., Gatuingt, F., Pijaudier-Cabot, G., and Daudeville, L. (2000). Compaction and tensile damage in concrete: constitutive modelling and application to dynamics. Computer Methods in Applied Mechanics and Engineering, 183(3-4):291–308.

[Cantournet et al., 2009] Cantournet, S., Desmorat, R., and Besson, J. (2009). Mullins effect and cyclic stress softening of filled elastomers by internal sliding and friction thermodynamics model. International Journal of Solids and Structures, 46(11):2255–2264.

[Carol et al., 2001] Carol, I., Rizzi, E., and Willam, K. (2001). On the formulation of anisotropic elastic degradation. i. theory based on a pseudo-logarithmic damage tensor rate. International Journal of Solids and Structures, 38(4):491–518.

[Chaboche, 1984] Chaboche, J. (1984). Anisotropic creep damage in the framework of continuum damage mechanics. Nuclear Engineering and Design, 79(3):309–319.

[Chaboche et al., 1994] Chaboche, J., Lesne, P., and Maire, J. (1994). Phenomenological damage mechanics of brittle materials with description of the unilateral damage effect. In ZP, B. and al., editors, Fracture and damage in quasibrittle structures, pages 75–84. London: E. & F.N. Spon Pubs.

[Chaboche, 1978] Chaboche, J.-L. (1978). Description thermodynamique et phénoménologique de la viscoplasticité cyclique avec endommagement. PhD thesis, Université Paris VI.

[Chaboche, 1979] Chaboche, J.-L. (1979). Le concept de contrainte effective appliqué à l'élasticité et à la viscoplasticité en présence d'un endommagement anisotrope. In Boehler, J.-P., editor, Colloque Int. CNRS 295, Villard de Lans, pages 737–760. Martinus Nijhoff Publishers and Editions du CNRS.

[Chaboche, 1981] Chaboche, J.-L. (1981). Continuous damage mechanics — a tool to describe phenomena before crack initiation. Nuclear Engineering and Design, 64(2):233–247.

[Cordebois and F., 1982] Cordebois, J. and F., S. (1982). Endommagement anisotrope en élasticité et plasticité. J.M.T.A., Special Volume, pages 45–60.

[Cormery and Welemane, 2010] Cormery, F. and Welemane, H. (2010). A stress-based macroscopic approach for microcracks unilateral effect. Computational Materials Science, 47(3):727–738.

[Crisfield, 1991] Crisfield, M. A. (1991). Non-linear finite element analysis of solids and structures. Wiley, Chichester New York.

[de Borst, 1987] de Borst, R. (1987). Computation of post-bifurcation and post-failure behavior of strain-softening solids. Computers & Structures, 25(2):211–224.

[Denoual and Hild, 2000] Denoual, C. and Hild, F. (2000). A damage model for the dynamic fragmentation of brittle solids. Computer Methods in Applied Mechanics and Engineering, 183(3):247–258.

[Desmorat, 2004] Desmorat, R. (2004). Modèle d'endommagement anisotrope avec forte dissymétrie traction/compression. In 5$^{\text{èmes}}$ journées du Regroupement Francophone pour la Recherche et la Formation sur le Béton (RF2B), Liège, Belgium.

[Desmorat, 2006] Desmorat, R. (2006). Positivité de la dissipation intrinsèque d'une classe de modèles d'endommagement anisotropes non standards. Comptes Rendus Mécanique, 334:587–592.

[Desmorat, 2015] Desmorat, R. (2015). Anisotropic damage modeling of concrete materials:. International Journal of Damage Mechanics.

[Desmorat et al., 2010a] Desmorat, R., Chambart, M., Gatuingt, F., and Guilbaud, D. (2010a). Delay-active damage versus non-local enhancement for anisotropic damage dynamics computations with alternated loading. Engineering Fracture Mechanics, 77(12):2294–2315.

[Desmorat et al., 2018] Desmorat, R., Desmorat, B., Olive, M., and Kolev, B. (2018). Micromechanics based framework with second-order damage tensors. European Journal of Mechanics - A/Solids, 69:88–98.

[Desmorat and Gatuingt, 2007] Desmorat, R. and Gatuingt, F. (2007). Introduction of an internal time in nonlocal integral theories. Internal report LMT-Cachan, number 268, year 2007, ENS Cachan/CNRS/Université Paris 6/PRES Universud Paris.

[Desmorat and Gatuingt, 2010] Desmorat, R. and Gatuingt, F. (2010). Introduction of an internal time in nonlocal integral theories. In Computational Modelling of Concrete Structures, Euro-C 2010, page Clé USB, Austria.

[Desmorat et al., 2015] Desmorat, R., Gatuingt, F., and Jirásek, M. (2015). Nonlocal models with damage-dependent interactions motivated by internal time. Engineering Fracture Mechanics, 142:255–275.

[Desmorat et al., 2007a] Desmorat, R., Gatuingt, F., and Ragueneau, F. (2007a). Nonlocal anisotropic damage model and related computational aspects for quasi-brittle materials. Engineering Fracture Mechanics, 74(10):1539–1560.

[Desmorat et al., 2010b] Desmorat, R., Gatuingt, F., and Ragueneau, F. (2010b). Non standard thermodynamics framework for robust computations with induced anisotropic damage. International Journal of Damage Mechanics, 19(1):53–73.

[Desmorat and Otin, 2008] Desmorat, R. and Otin, S. (2008). Cross-identification isotropic/anisotropic damage and application to anisothermal structural failure. Engineering Fracture Mechanics, 75(11):3446–3463.

[Desmorat et al., 2007b] Desmorat, R., Ragueneau, F., and Pham, H. (2007b). Continuum damage mechanics for hysteresis and fatigue of quasi-brittle materials and structures. International Journal for Numerical and Analytical Methods in Geomechanics, 31(2):307–329.

[Dijkstra, 1959] Dijkstra, E. W. (1959). A note on two problems in connexion with graphs. Numerische Mathematik, 1:269–271.

[Dormieux and Kondo, 2016] Dormieux, L. and Kondo, D. (2016). Micromechanics of fracture and damage. John Wiley & Sons.

[Dubé et al., 1996] Dubé, J.-F., Pijaudier-Cabot, G., and Borderie, C. L. (1996). Rate dependent damage model for concrete in dynamics. Journal of Engineering Mechanics, 122(10):939–947.

[Dufour et al., 2008] Dufour, F., Pijaudier-Cabot, G., Choinska, M., and Huerta, A. (2008). Extraction of a crack opening from a continuous approach using regularized damage models. Computers and Concrete, an International Journal, 5(4):375–388.

[Dufour et al., 2010] Dufour, F., Pijaudier-Cabot, G., and Legrain, G. (2010). Nonlocal damage based failure models, extraction of crack opening and transition to fracture. In al. Eds, N. B., editor, EURO-C 2010, Techno Press, pages 301–308, Schladming, Austria.

[Dugdale, 1960] Dugdale, D. S. (1960). Yielding of steel sheets containing slits. Journal of the Mechanics and Physics of Solids, 8(2):100–104.

[Eibl and Schmidt-Hurtienne, 1999] Eibl, J. and Schmidt-Hurtienne, B. (1999). Strain-rate-sensitive constitutive law for concrete. Journal of Engineering Mechanics, 125(12):1411–1420.

[Erdogan and Sih, 1963] Erdogan, F. and Sih, G. C. (1963). On the crack extension in plates under plane loading and transverse shear. Journal of Basic Engineering, 85(4):519–525.

[Eringen et al., 1977] Eringen, A. C., Speziale, C. G., and Kim, B. S. (1977). Crack-tip problem in non-local elasticity. Journal of The Mechanics and Physics of Solids, 25:339–355.

[Feenstra and Borst, 1996] Feenstra, P. H. and Borst, R. D. (1996). A composite plasticity model for concrete. International Journal of Solids and Structures, 33(5):707–730.

[Fichant et al., 1997] Fichant, S., Pijaudier-Cabot, G., and La Borderie, C. (1997). Continuum damage modelling: approximation of crack induced anisotropy. Mechanics Research Communications, 24(2):109–114.

[Francfort and Marigo, 1998] Francfort, G. A. and Marigo, J. J. (1998). Revisiting brittle fracture as an energy minimization problem. Journal of the Mechanics and Physics of Solids, 46(8):1319–1342.

[Frémond and Stolz, 2017] Frémond, M. and Stolz, C. (2017). On alternative approaches for graded damage modelling. In Models, Simulation, and Experimental Issues in Structural Mechanics, pages 87–104. Springer International Publishing, Cham.

[Frémond and Nedjar, 1996] Frémond, M. and Nedjar, B. (1996). Damage, gradient of damage and principle of virtual power. International Journal of Solids and Structures, 33(8):1083–1103.

[Ganghoffer and de Borst, 2000] Ganghoffer, J. F. and de Borst, R. (2000). A new framework in nonlocal mechanics. International Journal of Engineering Science, 38(4):453–486.

[Ganghoffer et al., 1999] Ganghoffer, J. F., Sluys, L. J., and de Borst, R. (1999). A reappraisal of nonlocal mechanics. European Journal of Mechanics - A/Solids, 18(1):17–46.

[Gatuingt and Pijaudier-Cabot, 2001] Gatuingt, F. and Pijaudier-Cabot, G. (2001). Coupled damage and plasticity modelling in transient dynamic analysis of concrete. International Journal for Numerical and Analytical Methods in Geomechanics, 26(1):1–24.

[Gatuingt and Pijaudier-Cabot, 2003] Gatuingt, F. and Pijaudier-Cabot, G. (2003). Gurson ' s plasticity coupled to damage as a cap model for concrete compaction in dynamics. In Constitutive modelling of geomaterials, pages 12–24. CRC Press.

[Geers, 1999a] Geers, M. G. D. (1999a). Enhanced solution control for physically and geometrically non-linear problems. Part II—comparative performance analysis. International Journal for Numerical Methods in Engineering, 46(2):205–230.

[Geers, 1999b] Geers, M. G. D. (1999b). Enhanced solution control for physically and geometrically non-linear problems. Part I—the subplane control approach. International Journal for Numerical Methods in Engineering, 46(2):177–204.

[Geers et al., 1998] Geers, M. G. D., de Borst, R., Brekelmans, W. A. M., and Peerlings, R. H. J. (1998). Strain-based transient-gradient damage model for failure analyses. Computer Methods in Applied Mechanics and Engineering, 160(1):133–153.

[Giry et al., 2011] Giry, C., Dufour, F., and Mazars, J. (2011). Stress-based nonlocal damage model. International Journal of Solids and Structures, 48(25):3431–3443.

[Giry et al., 2010] Giry, C., Dufour, F., Mazars, J., and Kotronis, P. (2010). Stress state influence on nonlocal interactions in damage modelling. In et al., B., editor, EURO-C 2010, Computational Modelling of Concrete Structures, pages 145–152, Rohrmoos/Schladming, Austria. Taylor & Francis Group, London.

[Glacet et al., 2018] Glacet, A., Réthoré, J., Tanguy, A., and Morestin, F. (2018). On the failure resistance of quasi-periodic lattices. Scripta Materialia, 156:23–26.

[Gol'dstein and Salganik, 1974] Gol'dstein, R. V. and Salganik, R. L. (1974). Brittle fracture of solids with arbitrary cracks. International Journal of Fracture, 10(4):507–523.

[Govindjee et al., 1995] Govindjee, S., Kay, G. J., and Simo, J. C. (1995). Anisotropic modelling and numerical simulation of brittle damage in concrete. International Journal for Numerical Methods in Engineering, 38(21):3611–3633.

[Grassl and Jirásek, 2005] Grassl, P. and Jirásek, M. (2005). Plastic model with non-local damage applied to concrete. International Journal for Numerical and Analytical Methods in Geomechanics, 30(1):71–90.

[Grassl and Jirásek, 2006] Grassl, P. and Jirásek, M. (2006). Damage-plastic model for concrete failure. International Journal of Solids and Structures, 43(22-23):7166–7196.

[Griffith, 1921] Griffith, A. A. (1921). Vi. the phenomena of rupture and flow in solids. Philosophical transactions of the royal society of london. Series A, containing papers of a mathematical or physical character, 221(582-593):163–198.

[Guimard et al., 2009] Guimard, J.-M., Allix, O., Pechnik, N., and Thévenet, P. (2009). Characterization and modeling of rate effects in the dynamic propagation of mode-II delamination in composite laminates. International Journal of Fracture, 160(1):55–71.

[Gutiérrez, 2004] Gutiérrez, M. A. (2004). Energy release control for numerical simulations of failure in quasi-brittle solids. Communications in Numerical Methods in Engineering, 20(1):19–29.

[Hall, 2013] Hall, B. C. (2013). Quantum Theory for Mathematicians. Springer New York.

[Halm and Dragon, 1996] Halm, D. and Dragon, A. (1996). A model of anisotropic damage by mesocrack growth; unilateral effect. International Journal of Damage Mechanics, 5(4):384–402.

[Halm and Dragon, 1998] Halm, D. and Dragon, A. (1998). An anisotropic model of damage and frictional sliding for brittle materials. European Journal of Mechanics - A/Solids, 17(3):439–460.

[Herrmann and Kestin, 1988] Herrmann, G. and Kestin, J. (1988). On the thermodynamic fundation of damage theory in elastic solids. In Mazars, J. and Zdeněk P., B., editors, Cracking and damage, strain localization and size effect, pages 228–232.

[Hervé et al., 2005] Hervé, G., Gatuingt, F., and Ibrahimbegović, A. (2005). On numerical implementation of a coupled rate dependent damage-plasticity constitutive model for concrete in application to high-rate dynamics. Engineering Computations, 22(5/6):583–604.

[Hillerborg, 1978] Hillerborg, A. (1978). A model for fracture analysis, volume 3005 of Report TVBM. Division of Building Materials, LTH, Lund University.

[Hillerborg et al., 1976] Hillerborg, A., Modéer, M., and Petersson, P.-E. (1976). Analysis of crack formation and crack growth in concrete by means of fracture mechanics and finite elements. Cement and Concrete Research, 6(6):773–781.

[Häußler-Combe and Kitzig, 2009] Häußler-Combe, U. and Kitzig, M. (2009). Modeling of concrete behavior under high strain rates with inertially retarded damage. International Journal of Impact Engineering, 36(9):1106–1115.

[Irwin, 1957] Irwin, G. R. (1957). Analysis of stresses and strains near the end of a crack traversing a plate. Journal of Applied Mechanics, 24:361–397.

[Irwin, 1958] Irwin, G. R. (1958). Fracture. In Elasticity and Plasticity / Elastizität und Plastizität, pages 551–590. Springer Berlin Heidelberg.

[Jason et al., 2006] Jason, L., Huerta, A., Pijaudier-Cabot, G., and Ghavamian, S. (2006). An elastic plastic damage formulation for concrete: Application to elementary tests and comparison with an isotropic damage model. Computer Methods in Applied Mechanics and Engineering, 195(52):7077–7092.

[Jayet, 2021] Jayet, T.-D. (2021). Modélisation multi-échelle par motifs et phénomènes non linéaires à haute température dans les composites à matrice céramique. PhD thesis.

[Jirásek, 2018] Jirásek, M. (2018). Regularized continuum damage formulations acting as localization limiters. In Computational Modelling of Concrete Structures, pages 25–41. CRC Press.

[Jirásek, 1998] Jirásek, M. (1998). Nonlocal models for damage and fracture: Comparison of approaches. International Journal of Solids and Structures, 35(31):4133–4145.

[Jirásek and Desmorat, 2019] Jirásek, M. and Desmorat, R. (2019). Localization analysis of nonlocal models with damage-dependent nonlocal interaction. International Journal of Solids and Structures, 174-175:1–17.

[Jirásek et al., 2004] Jirásek, M., Rolshoven, S., and Grassl, P. (2004). Size effect on fracture energy induced by non-locality. International Journal for Numerical and Analytical Methods in Geomechanics, 28(7-8):653–670.

[Ju, 1989] Ju, J. (1989). On energy-based coupled elastoplastic damage theories: Constitutive modeling and computational aspects. International Journal of Solids and Structures, 25(7):803–833.

[Kachanov, 1958] Kachanov, L. (1958). On time to rupture in creep conditions. Izv. AN SSSR, OTN, pages 26–31. (in Russian).

[Kachanov, 1993] Kachanov, M. (1993). Elastic solids with many cracks and related problems. In Advances in Applied Mechanics, pages 259–445. Elsevier.

[Kattan and Voyiadjis, 1990] Kattan, P. I. and Voyiadjis, G. Z. (1990). A coupled theory of damage mechanics and finite strain elasto-plasticity—i. damage and elastic deformations. International Journal of Engineering Science, 28(5):421–435.

[Kramers, 1926] Kramers, H. A. (1926). Wellenmechanik und halbzahlige Quantisierung. Zeitschrift für Physik, 39(10):828–840.

[Krayani et al., 2007] Krayani, A., Dufour, F., and Pijaudier-Cabot, G. (2007). Elastoplastic nonlocal damage model for concrete and size effect analysis. In Framcos06.

[Krayani et al., 2009] Krayani, A., Pijaudier-Cabot, G., and Dufour, F. (2009). Boundary effect on weight function in nonlocal damage model. Engineering Fracture Mechanics, 76(14):2217–2231.

[La Borderie, 1991] La Borderie, C. (1991). Phénomènes unilatéraux dans un matériau endommageable: Modélisation et application à l'analyse de structures en béton. PhD thesis, Université Paris 6.

[Ladeveze, 1983] Ladeveze, P. (1983). Sur une théorie de l'endommagement anisotrope. Technical report, internal report 34 of lmt-cachan.

[Ladeveze, 1990] Ladeveze, P. (1990). A Damage Mechanics for Composites Materials, pages 13–24. Springer Netherlands, Dordrecht.

[Ladeveze, 1991] Ladeveze, P. (1991). On a damage mechanics approach. In D, B., editor, Proc. 4th int. MECAMAT seminar on mechanics and mechanisms of damage in composites and multi-materials, pages 119–41. Springer.

[Ladeveze, 1995] Ladeveze, P. (1995). Modelling and simulation of the mechanical behaviour of cmcs. High- Temp. Ceramic-Matrix Compos., 47:53–63.

[Ladeveze, 2002] Ladeveze, P. (2002). An anisotropic damage theory with unilateral effects: Applications to laminate and three- and four-dimensional composites. Continuum Damage Mechanics of Materials and Structures, pages 205–233.

[Ladeveze and Lemaitre, 1984] Ladeveze, P. and Lemaitre, J. (1984). Damage effective stress in quasi-unilateral conditions. The 16th International Cogress of Theoretical and Applied Mechanics, Lyngby, Denmark.

[Le Bellégo et al., 2003] Le Bellégo, C., François Dubé, J., Pijaudier-Cabot, G., and Gérard, B. (2003). Calibration of nonlocal damage model from size effect tests. European Journal of Mechanics - A/Solids, 22(1):33–46.

[Leblond, 2003] Leblond, J. (2003). Mécanique de la rupture fragile et ductile. Études en mécanique des matériaux et des structures. Hermes science publications Lavoisier, Paris.

[Lebon, 2011] Lebon, G. (2011). Analyse de l'endommagement des structures de génie civil : techniques de sous-structuration hybride couplées à un modèle d'endommagement anisotrope. Theses, École normale supérieure de Cachan - ENS Cachan.

[Leckie and Onat, 1981] Leckie, F. A. and Onat, E. T. (1981). Tensorial nature of damage measuring internal variables. In Physical Non-Linearities in Structural Analysis, pages 140–155. Springer Berlin Heidelberg.

[Legrain et al., 2007] Legrain, G., Dufour, F., Huerta, A., and Pijaudier-Cabot, G. (2007). Extraction of Crack Opening from a Nonlocal Damage Field. In COMPLAS 2007, Barcelone, Spain.

[Lemaitre, 1971] Lemaitre, J. (1971). Evaluation of dissipation and damage in metals. In Proc. ICM Kyoto, volume 1.

[Lemaitre, 1985] Lemaitre, J. (1985). Coupled elasto-plasticity and damage constitutive equations. Computer Methods in Applied Mechanics and Engineering, 51(1-3):31–49.

[Lemaitre and Chaboche, 1985] Lemaitre, J. and Chaboche, J. (1985). Mécanique des matériaux solides. Dunod, Paris.

[Lemaitre and Chaboche, 1994] Lemaitre, J. and Chaboche, J. (1994). Mechanics of Solid Materials. Cambridge University Press.

[Lemaitre et al., 2009] Lemaitre, J., Chaboche, J.-L., Benallal, A., and Desmorat, R. (2009). Mécanique des matériaux solides. Dunod, Paris, 3rd edition.

[Lemaitre and Desmorat, 2005] Lemaitre, J. and Desmorat, R. (2005). Engineering Damage Mechanics. Ductile, Creep, Fatigue and Brittle Failure. Springer.

[Lemaitre et al., 2000] Lemaitre, J., Desmorat, R., and Sauzay, M. (2000). Anisotropic damage law of evolution. European Journal of Mechanics - A/Solids, 19(2):187–208.

[Linsbauer et al., 1989a] Linsbauer, H. N., Ingraffea, A. R., Rossmanith, H. P., and Wawrzynek, P. A. (1989a). Simulation of cracking in large arch dam: Part i. Journal of Structural Engineering, 115(7):1599–1615.

[Linsbauer et al., 1989b] Linsbauer, H. N., Ingraffea, A. R., Rossmanith, H. P., and Wawrzynek, P. A. (1989b). Simulation of cracking in large arch dam: Part II. Journal of Structural Engineering, 115(7):1616–1630.

[Lu et al., 1994] Lu, Y. Y., Belytschko, T., and Gu, L. (1994). A new implementation of the element free Galerkin method. Computer Methods in Applied Mechanics and Engineering, 113(3):397–414.

[Marigo, 1981] Marigo, J.-J. (1981). Formulation d'une loi d'endommagement d'un materiau élastique. Comptes Rendus de l'Académie des Sciences. Série II.

[Matallah and Borderie, 2009] Matallah, M. and Borderie, C. L. (2009). Inelasticity–damage-based model for numerical modeling of concrete cracking. Engineering Fracture Mechanics, 76(8):1087–1108.

[Mazars, 1984] Mazars, J. (1984). Application de la mécanique de l'endommagement au comportement non linéaire et à la rupture du béton de structure. PhD thesis, Université Pierre et Marie Curie - Paris 6.

[Mazars et al., 1990] Mazars, J., Berthaud, Y., and Ramtani, S. (1990). The unilateral behaviour of damaged concrete. Engineering Fracture Mechanics, 35(4):629–635.

[Mazars et al., 1989] Mazars, J., Ramtani, S., and Berthaud, Y. (1989). An experimental procedure to delocalize tensile failure and to identify the unilateral effect of distributed damage. In Mazars, J. and Zdeněk P., B., editors, Cracking and damage: strain localization and size effect., pages 55–64. Elsevier, London UK.

[Melenk and Babuška, 1996] Melenk, J. M. and Babuška, I. (1996). The partition of unity finite element method: Basic theory and applications. Computer Methods in Applied Mechanics and Engineering, 139(1):289–314.

[Menzel et al., 2002] Menzel, A., Ekh, M., Steinmann, P., and Runesson, K. (2002). Anisotropic damage coupled to plasticity: Modelling based on the effective configuration concept. International Journal for Numerical Methods in Engineering, 54(10):1409–1430.

[Menzel and Steinmann, 2001] Menzel, A. and Steinmann, P. (2001). A theoretical and computational framework for anisotropic continuum damage mechanics at large strains. International Journal of Solids and Structures, 38(52):9505–9523.

[Meschke et al., 1998] Meschke, G., Lackner, R., and Mang, H. A. (1998). An anisotropic elastoplastic-damage model for plain concrete. International Journal for Numerical Methods in Engineering, 42(4):703–727.

[Michel et al., 2018] Michel, B., Helfer, T., Ramière, I., and Esnoul, C. (2018). A new numerical methodology for simulation of unstable crack growth in time independent brittle materials. Engineering Fracture Mechanics, 188:126–150.

[Miehe et al., 2010a] Miehe, C., Hofacker, M., and Welschinger, F. (2010a). A phase field model for rate-independent crack propagation: Robust algorithmic implementation based on operator splits. Computer Methods in Applied Mechanics and Engineering, 199(45):2765–2778.

[Miehe et al., 2015] Miehe, C., Schänzel, L.-M., and Ulmer, H. (2015). Phase field modeling of fracture in multi-physics problems. Part I. Balance of crack surface and failure criteria for brittle crack propagation in thermo-elastic solids. Computer Methods in Applied Mechanics and Engineering, 294:449–485.

[Miehe et al., 2010b] Miehe, C., Welschinger, F., and Hofacker, M. (2010b). Thermodynamically consistent phase-field models of fracture: Variational principles and multi-field FE implementations. International Journal for Numerical Methods in Engineering, 83(10):1273–1311.

[Mielke, 2003] Mielke, A. (2003). Energetic formulation of multiplicative elasto-plasticity using dissipation distances. Continuum Mechanics and Thermodynamics, 15(4):351–382.

[Moës and Chevaugeon, 2021] Moës, N. and Chevaugeon, N. (2021). Lipschitz regularization for softening material models: the Lip-field approach. Comptes Rendus. Mécanique, 349(2):415–434.

[Molnár and Gravouil, 2017] Molnár, G. and Gravouil, A. (2017). 2D and 3D Abaqus implementation of a robust staggered phase-field solution for modeling brittle fracture. Finite Elements in Analysis and Design, 130:27–38.

[Moës et al., 1999] Moës, N., Dolbow, J., and Belytschko, T. (1999). A finite element method for crack growth without remeshing. International Journal for Numerical Methods in Engineering, 46(1):131–150.

[Moës et al., 2011] Moës, N., Stolz, C., Bernard, P.-E., and Chevaugeon, N. (2011). A level set based model for damage growth: The thick level set approach. International Journal for Numerical Methods in Engineering, 86(3):358–380.

[Moës et al., 2014] Moës, N., Stolz, C., and Chevaugeon, N. (2014). Coupling local and non-local damage evolutions with the thick level set model. Advanced Modeling and Simulation in Engineering Sciences, 1(1).

[Murakami, 1988] Murakami, S. (1988). Mechanical modeling of material damage. Journal of Applied Mechanics, 55(2):280–286.

[Murakami and Kamiya, 1997] Murakami, S. and Kamiya, K. (1997). Constitutive and damage evolution equations of elastic-brittle materials based on irreversible thermodynamics. International Journal of Mechanical Sciences, 39(4):473–486.

[Murakami and Ohno, 1978] Murakami, S. and Ohno, M. (1978). A constitutive equation of creep damage in polycrystalline metals. In IUTAM Coll. Euromech 111 Constitutive Modelling in Inelasticity, Marienbad, Czechoslovakia.

[Nechnech et al., 2002] Nechnech, W., Meftah, F., and Reynouard, J. (2002). An elasto-plastic damage model for plain concrete subjected to high temperatures. Engineering Structures, 24(5):597–611.

[Needleman, 1988] Needleman, A. (1988). Material rate dependence and mesh sensitivity in localization problems. Computer Methods in Applied Mechanics and Engineering, 67(1):69–85.

[Nguyen, 2011] Nguyen, G. D. (2011). A damage model with evolving nonlocal interactions. International Journal of Solids and Structures, 48(10):1544–1559.

[Ortiz, 1985] Ortiz, M. (1985). A constitutive theory for the inelastic behavior of concrete. Mechanics of Materials, 4(1):67–93.

[Papa and Taliercio, 1996] Papa, E. and Taliercio, A. (1996). Anisotropic damage model for the multiaxial static and fatigue behaviour of plain concrete. Engineering Fracture Mechanics, 55(2):163–179.

[Pedersen et al., 2008] Pedersen, R., Simone, A., and Sluys, L. (2008). An analysis of dynamic fracture in concrete with a continuum visco-elastic visco-plastic damage model. Engineering Fracture Mechanics, 75(13):3782–3805.

[Peerlings et al., 1996] Peerlings, R. H. J., Borst, R. D., Brekelmans, W. a. M., and Vree, J. H. P. D. (1996). Gradient Enhanced Damage for Quasi-Brittle Materials. International Journal for Numerical Methods in Engineering, 39(19):3391–3403.

[Peerlings et al., 1998] Peerlings, R. H. J., de Borst, R., Brekelmans, W. A. M., and Geers, M. G. D. (1998). Gradient-enhanced damage modelling of concrete fracture. Mechanics of Cohesive-frictional Materials, 3(4):323–342.

[Peerlings et al., 2001] Peerlings, R. H. J., Geers, M. G. D., de Borst, R., and Brekelmans, W. A. M. (2001). A critical comparison of nonlocal and gradient-enhanced softening continua. International Journal of Solids and Structures, 38(44):7723–7746.

[Pijaudier-Cabot and Bažant, 1987] Pijaudier-Cabot, G. and Bažant, Z. P. (1987). Nonlocal damage theory. Journal of Engineering Mechanics, 113(10):1512–1533.

[Pijaudier-Cabot and Benallal, 1993] Pijaudier-Cabot, G. and Benallal, A. (1993). Strain localization and bifurcation in a nonlocal continuum. International Journal of Solids and Structures, 30(13):1761–1775.

[Pijaudier-Cabot and Dufour, 2010] Pijaudier-Cabot, G. and Dufour, F. (2010). Non local damage model Boundary and evolving boundary effects. European Journal of Environmental and Civil Engineering, 14(1-10):729–749.

[Pijaudier-Cabot et al., 2004] Pijaudier-Cabot, G., Haidar, K., and Dubé, J.-F. (2004). Nonlocal Damage Model with Evolving Internal Length. International Journal for Numerical and Analytical Methods in Geomechanics, 28(7-8):633–652.

[Pijaudier-Cabot et al., 2001] Pijaudier-Cabot, G., Le Bellégo, C., Gérard, B., Haidar, K., and Dubé, J. F. (2001). Scaling of structural strength and non local damage for failure analysis. In Computational Mechanics, ECCM-2001, Cracow, Poland.

[Pons and Karma, 2010] Pons, A. and Karma, A. (2010). Helical crack-front instability in mixed-mode fracture. Nature, 464:85–9.

[Pontiroli, 1995] Pontiroli, C. (1995). Comportement au souffle des structures en béton armé: analyse expérimentale et modélisation. PhD thesis, Cachan, Ecole normale supérieure.

[Rabotnov, 1969] Rabotnov, Y. (1969). Creep Problems in Structural Members. Applied Mathematics and Mechanics Series. Elsevier.

[Ramm, 1981] Ramm, E. (1981). Strategies for tracing the nonlinear response near limit points. In Nonlinear Finite Element Analysis in Structural Mechanics, pages 63–89. Springer Berlin Heidelberg.

[Ramtani et al., 1992] Ramtani, S., Berthaud, Y., and Mazars, J. (1992). Orthotropic behavior of concrete with directional aspects: modelling and experiments. Nuclear Engineering and Design, 133(1):97–111.

[Rastiello et al., 2018a] Rastiello, G., Giry, C., Gatuingt, F., and Desmorat, R. (2018a). From diffuse damage to strain localization from an Eikonal Non-Local (ENL) Continuum Damage model with evolving internal length. Computer Methods in Applied Mechanics and Engineering, 331:650–674.

[Rastiello et al., 2018b] Rastiello, G., Giry, C., Gatuingt, F., Thierry, F., and Desmorat, R. (2018b). Nonlocal damage formulation with evolving internal length: the Eikonal nonlocal approach. In Computational Modelling of Concrete Structures, Euro-C 2018, Bad Hofgastein, Austria.

[Rice and Tracey, 1969] Rice, J. R. and Tracey, D. M. (1969). On the ductile enlargement of voids in triaxial stress fields. Journal of the Mechanics and Physics of Solids, 17(3):201–217.

[Riks, 1979] Riks, E. (1979). An incremental approach to the solution of snapping and buckling problems. International Journal of Solids and Structures, 15(7):529–551.

[Saroukhani et al., 2013] Saroukhani, S., Vafadari, R., and Simone, A. (2013). A simplified implementation of a gradient-enhanced damage model with transient length scale effects. Computational Mechanics, 51(6):899–909.

[Sercombe et al., 1998] Sercombe, J., Ulm, F.-J., and Toutlemonde, F. (1998). Viscous hardening plasticity for concrete in high-rate dynamics. Journal of Engineering Mechanics, 124(9):1050–1057.

[Sethian, 1996] Sethian, J. A. (1996). A fast marching level set method for monotonically advancing fronts. Proceedings of the National Academy of Sciences, 93(4):1591–1595.

[Sethian, 1999] Sethian, J. A. (1999). Level Set Methods and Fast Marching Methods: Evolving Interfaces in Computational Geometry, Fluid Mechanics, Computer Vision, and Materials Science. Cambridge University Press. Google-Books-ID: ErpOoynE4dIC.

[Simo and Ju, 1987a] Simo, J. and Ju, J. (1987a). Strain- and stress-based continuum damage models—i. formulation. International Journal of Solids and Structures, 23(7):821–840.

[Simo and Ju, 1987b] Simo, J. and Ju, J. (1987b). Strain- and stress-based continuum damage models—II. computational aspects. International Journal of Solids and Structures, 23(7):841–869.

[Simo et al., 1986] Simo, J. C., Wriggers, P., Schweizerhof, K. H., and Taylor, R. L. (1986). Finite deformation post-buckling analysis involving inelasticity and contact constraints. International Journal for Numerical Methods in Engineering, 23(5):779–800.

[Simone et al., 2004] Simone, A., Askes, H., and Sluys, L. J. (2004). Incorrect initiation and propagation of failure in non-local and gradient-enhanced media. International Journal of Solids and Structures, 41(2):351–363.

[Simone et al., 2003] Simone, A., Wells, G. N., and Sluys, L. J. (2003). From continuous to discontinuous failure in a gradient-enhanced continuum damage model. Computer Methods in Applied Mechanics and Engineering, 192(41):4581–4607.

[Steinmann and Carol, 1998] Steinmann, P. and Carol, I. (1998). A framework for geometrically nonlinear continuum damage mechanics. International Journal of Engineering Science, 36(15):1793–1814.

[Strömberg and Ristinmaa, 1996] Strömberg, L. and Ristinmaa, M. (1996). FE-formulation of a nonlocal plasticity theory. Computer Methods in Applied Mechanics and Engineering, 136(1-2):127–144.

[Strouboulis et al., 2000] Strouboulis, T., Babuška, I., and Copps, K. (2000). The design and analysis of the Generalized Finite Element Method. Computer Methods in Applied Mechanics and Engineering, 181(1):43–69.

[Strouboulis et al., 2001] Strouboulis, T., Copps, K., and Babuška, I. (2001). The generalized finite element method. Computer Methods in Applied Mechanics and Engineering, 190(32):4081–4193.

[Suaris and Shah, 1984] Suaris, W. and Shah, S. (1984). Test methods for impact resistance of fiber reinforced concrete. American Concrete Institute, pages 247–265.

[Tanné et al., 2018] Tanné, E., Li, T., Bourdin, B., Marigo, J.-J., and Maurini, C. (2018). Crack nucleation in variational phase-field models of brittle fracture. Journal of the Mechanics and Physics of Solids, 110:80–99.

[Taylor et al., 1986] Taylor, L. M., Chen, E.-P., and Kuszmaul, J. S. (1986). Microcrack-induced damage accumulation in brittle rock under dynamic loading. Computer Methods in Applied Mechanics and Engineering, 55(3):301–320.

[Terrien, 1980] Terrien, M. (1980). Emission acoustique et comportement mécanique post-critique d'un béton sollicitéen traction. Bulletin de Liaison du LCPC, (105).

[Tsitsiklis, 1995] Tsitsiklis, J. (1995). Efficient algorithms for globally optimal trajectories. IEEE Transactions on Automatic Control, 40(9):1528–1538.

[Vakulenko and Kachanov, 1971] Vakulenko, A. and Kachanov, M. (1971). Continuum model of medium with cracks. Mech. Solids (Eng. Transl. Izvestia SSSR, Mekhanika Tverdogo Tela) 6, pages 145–151.

[Vandoren and Simone, 2018] Vandoren, B. and Simone, A. (2018). Modeling and simulation of quasi-brittle failure with continuous anisotropic stress-based gradient-enhanced damage models. Computer Methods in Applied Mechanics and Engineering, 332:644–685.

[Verhoosel et al., 2009] Verhoosel, C. V., Remmers, J. J. C., and Gutiérrez, M. A. (2009). A dissipation-based arc-length method for robust simulation of brittle and ductile failure. International Journal for Numerical Methods in Engineering, 77(9):1290–1321.

[Vermeer and Brinkgreve, 1994] Vermeer, P. and Brinkgreve, R. (1994). A new effective non-local strain-measure for softening plasticity. In International workshop on localisation and bifurcation theory for soils and rocks, pages 89–100.

[Voyiadjis and Abu-Lebdeh, 1994] Voyiadjis, G. Z. and Abu-Lebdeh, T. M. (1994). Plasticity model for concrete using the bounding surface concept. International Journal of Plasticity, 10(1):1–21.

[Wangermez et al., 2022] Wangermez, M., Allix, O., Guidault, P.-A., Ciobanu, O., and Rey, C. (2022). Non-intrusive global-local analysis of heterogeneous structures based on a second-order interface coupling. Computational Mechanics, pages 1–17.

[Wentzel, 1926] Wentzel, G. (1926). Eine Verallgemeinerung der Quantenbedingungen für die Zwecke der Wellenmechanik. Z.Phys., 38(6):518–529.

[William and Warnke, 1975] William, K. J. and Warnke, E. (1975). Constitutive model for triaxial behaviour of concrete. In Proc. Concrete and Structures Subjected to Triaxial Stresses, pages 1–30, Zurich. Int. Ass. for Bridge and Structural Engineering.

[Zheng and Collins, 1998] Zheng, Q.-S. and Collins, I. (1998). The relationship between damage variables and their evolution laws and microstructural and physical properties. Proceedings of the Royal Society of London. Series A: Mathematical, Physical and Engineering Sciences, 454(1973):1469–1498.